STRINGQFT

String-Theoretic Construction
of Quantum Field Theory

VOLUME XI

Type IIA Geometric Engineering

Xingyang Yu

StringQFT v1.0 / Source build candidate

Drafted with AI assistance under the supervision of the author.
Manuscript free to read. All rights reserved.

Contents

XI.1 Six-dimensional gauge theory from ALE spaces 1

XI.1.1 A gauge field and something to charge under it 1
XI.1.2 The compact spheres of the resolution 2
XI.1.3 Which gauge fields can propagate? 4
XI.1.4 The charges of the wrapped particles 6
XI.1.5 What controls a wrapped particle's mass? 8
XI.1.6 The normalization of the gauge coupling 11
XI.1.7 The gauge regime and the little-string regime 13
XI.1.8 Exercises 16

XI.2 The four-dimensional local limit 19

XI.2.1 A gauge theory inside a string compactification 19
XI.2.2 What the two spheres measure 20
XI.2.3 From the house Kähler parameter to a worldsheet action 22
XI.2.4 Why the base has a fourth-power trajectory 25
XI.2.5 The hierarchy of masses 28
XI.2.6 Why a vanishing worldsheet weight can leave a finite instanton 31
XI.2.7 Comparing F_0 and F_2 35
XI.2.8 Exercises 37
Status and sources 38
References 39

XI.3 ADE fibrations and the gauge-sector dictionary 40

XI.3.1 What changes when the surface moves 40
XI.3.2 An A2 surface over the sphere 40
XI.3.3 Electric charges and the two Coulomb parameters 44
XI.3.4 Curvature and the adjoint zero modes 46
XI.3.5 The base coupling and the magnetic particles 49
XI.3.6 Two bases and two beta coefficients 52
XI.3.7 Fiber transport and the global gauge group 54
XI.3.8 Exercises 56

XI.4 Matter from enhanced fibers 59

XI.4.1 Matter from a special fiber 59
XI.4.2 A collision of surface singularities 59

XI.4.3 A compact gauge curve and its electric charges . . . 63
XI.4.4 Reading the fundamental from the adjoint . . . 66
XI.4.5 One hypermultiplet at a transverse point . . . 68
XI.4.6 The Kähler mass and the gauge beta function . . . 73
XI.4.7 Two photons resolving one fundamental . . . 76
XI.4.8 A light component and a heavy fundamental . . . 79
XI.4.9 Exercises . . . 82

XI.5 Product gauge theories and conformal engineering 85
XI.5.1 How two gauge sectors share one local geometry . . . 85
XI.5.2 Build the geometry from four columns . . . 85
XI.5.3 Read electric charges from the resolved curves . . . 89
XI.5.4 Separate Coulomb motion, masses, and couplings . . . 92
XI.5.5 Balance the running at both nodes . . . 96
XI.5.6 Change the ranks and rebuild the weights . . . 97
XI.5.7 Follow the six weights into the photon response . . . 99
XI.5.8 Separate finite mixing from logarithmic running . . . 101
XI.5.9 Remove a massive bridge at fixed dynamical scales . . . 103
XI.5.10 Freeze three finite flavor masses . . . 105
XI.5.11 Compare the mass and Coulomb counts at fixed poles . . . 107
XI.5.12 Turn a gauge node into a flavor background . . . 108
XI.5.13 Exercises . . . 111

XI.6 Solving the engineered theory with its mirror 115
XI.6.1 A coupling that depends on the vacuum . . . 115
XI.6.2 From the two rulings to the mirror . . . 116
XI.6.3 Keep the two singularities at finite distance . . . 117
XI.6.4 How fast does the flat period converge? . . . 120
XI.6.5 Which curve contours lift to compact three-cycles? . . . 121
XI.6.6 The cubic and its normalized differential . . . 125
XI.6.7 Electric and magnetic periods at weak coupling . . . 128
XI.6.8 The response carried by the two periods . . . 130
XI.6.9 The two finite monodromies . . . 132
XI.6.10 Two photons from an A_2 fibration . . . 134
XI.6.11 Four periods and a matrix of couplings . . . 136
XI.6.12 Weak coupling and the split discriminant . . . 140
XI.6.13 Recovering a rank-one sector . . . 142
XI.6.14 Exercises . . . 144

XI.7 Worldsheet instantons become gauge instantons 148
XI.7.1 Which degree counts gauge instantons . . . 148
XI.7.2 Connected amplitudes and the fiber factor . . . 150
XI.7.3 Enumerating the first two base sectors . . . 153
XI.7.4 The field theory limit of the fiber sums . . . 155
XI.7.5 How much of the fiber tower survives? . . . 158
XI.7.6 Checking both orders from the periods . . . 160

XI.7.7 Higher genus and the GV trace . . . 162
XI.7.8 A single base wrapping with two fibers . . . 164
XI.7.9 The higher-rank rational function . . . 166
XI.7.10 Reconstructing the coefficient from genus-two periods . . . 168
XI.7.11 Two coupling responses and a heavy eigenvalue . . . 169

XI.8 Atlas of local IIA gauge engineering 176
XI.8.1 What belongs in a construction record? . . . 176
XI.8.2 Two marked geometries for a pure gauge sector . . . 177
XI.8.3 Matching one instanton coefficient . . . 179
XI.8.4 The mirror record and its particle frame . . . 181
XI.8.5 Matter, thresholds and parameter roles . . . 183
XI.8.6 Read the atlas . . . 187
XI.8.7 The two Hirzebruch records . . . 188
XI.8.8 Four ways to compare records . . . 191
XI.8.9 Other local sectors . . . 192
XI.8.10 Choose a higher-rank calculation . . . 194
XI.8.11 Where a record stops . . . 196

Chapter XI.1

Six-dimensional gauge theory from ALE spaces

XI.1.1 A gauge field and something to charge under it

A gauge theory needs both gauge fields and a way to determine their charges. In a non-Abelian theory the gauge bosons themselves carry charges with respect to the Cartan gauge fields. How can a surface in a string compactification supply both kinds of fields? In Type IIA the two roles come from different objects. A normalizable mode of the Ramond–Ramond three-form gives a Cartan gauge field. A D2-brane wrapped on a compact sphere gives a particle charged under it. The sphere can shrink, so the charged particle can become as light as the gauge field.

We will follow this construction on the resolved A_2 surface. The two exceptional spheres specify two independent charges, but there are six charged vectors near enhancement. The intersection pairing explains why there are six. Normalizing the three-form by the charge of a wrapped brane then fixes the normalization of the gauge kinetic term. To follow the calculation, recall that a form potential couples to a brane by integration over its worldvolume, and that the mass of a static wrapped brane includes its tension times its wrapped volume. We will need the refinement of this last statement when the two-form B has a period on the sphere.

We work on the unwarped product of six-dimensional Minkowski spacetime and a complete hyperkähler ALE surface, with constant string coupling g_s. The abbreviation ALE means that the end approaches flat four-space modulo a finite group. We use ordinary massless Type IIA with $H = \mathrm{d}B = 0$, no background Ramond–Ramond field strengths, and no extra flux or discrete data freezing the singularity. Flat B periods can still be nonzero. The frozen variants are discussed in Chapter XIII.10. Here the goal is the localized $(1, 1)$ gauge effective field theory. Finding its gauge algebra and identifying the limit in which it is useful are separate steps.

XI.1.2 The compact spheres of the resolution

Which surfaces can carry wrapped particles without reaching the end of spacetime? Begin with the cyclic action on complex coordinates z_1, z_2. For A_r, let $\xi = \exp(2\pi i/(r+1))$ and take the generator to act as

$$(z_1, z_2) \longmapsto (\xi z_1, \xi^{-1} z_2). \tag{XI.1.1}$$

The determinant is one, so the action preserves the holomorphic two-form. An invariant monomial has an exponent difference divisible by $r+1$. Strip off factors $z_1 z_2$ until only one of the coordinates remains. This expresses each invariant in the three generators

$$x = z_1^{r+1}, \qquad y = z_2^{r+1}, \qquad z = z_1 z_2, \qquad xy = z^{r+1}. \tag{XI.1.2}$$

The relation removes products of x and y, leaving the same monomial basis as the original invariants. The origin of this hypersurface is the singularity that we resolve.

The invariant condition can be used as an explicit reduction procedure. For a monomial $z_1^a z_2^b$, invariance means $a-b$ is a multiple of $r+1$. If $a \geq b$, factor out b copies of $z_1 z_2$; if $b > a$, factor out a copies. The remaining power is a multiple of $r+1$, so

$$z_1^a z_2^b = \begin{cases} x^{(a-b)/(r+1)} z^b, & a \geq b, \\ y^{(b-a)/(r+1)} z^a, & b > a. \end{cases} \tag{XI.1.3}$$

For A_2, the invariant $z_1^7 z_2^4$ is xz^4, whereas $z_1^2 z_2^5$ is yz^2. Multiplying these two descriptions gives $xyz^6 = z^9$, exactly the original monomial $z_1^9 z_2^9$. The quotient equation describes an affine surface, rather than a smooth sphere already sitting inside the covering space. Its singular point has to be replaced by compact geometry before an area or an intersection of exceptional spheres can be assigned.

The A_r resolution can be described by smooth coordinate charts U_i, $i = 0, \ldots, r$, with coordinates (u_i, v_i). Their maps to the original surface are

$$x = u_i^{r+1-i} v_i^{r-i}, \qquad y = u_i^i v_i^{i+1}, \qquad z = u_i v_i. \tag{XI.1.4}$$

Multiplying x by y gives $(u_i v_i)^{r+1}$ in every chart. On the adjacent overlap $u_i \neq 0$, the coordinate change is

$$u_{i+1} = u_i^2 v_i, \qquad v_{i+1} = u_i^{-1}. \tag{XI.1.5}$$

For example, the exponent of u_i in the formula for x from U_{i+1} is

$$2(r-i) - (r-i-1) = r+1-i, \tag{XI.1.6}$$

as in U_i. The powers in y and the product giving z are preserved as well. Away from the origin, at least one of x, y is nonzero. The map is then inverted in one of the two end charts:

$$x \neq 0: \ (u_r, v_r) = (x, z/x), \qquad y \neq 0: \ (u_0, v_0) = (z/y, y). \tag{XI.1.7}$$

Thus the new compact geometry lies over the origin. For A_2 the map in the middle chart U_1 reads

$$x = u_1^2 v_1, \qquad y = u_1 v_1^2, \qquad z = u_1 v_1. \tag{XI.1.8}$$

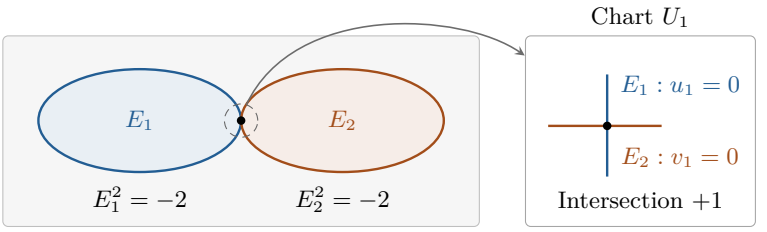


Figure XI.1.1: The exceptional locus of the resolved A_2 surface. The two ovals represent the compact spheres and meet at their common point. The inset magnifies that point and shows the two transverse complex axes in U_1. The point carries intersection $+1$ in the complex orientation; the -2 labels are the self-intersections of the individual spheres. This is an incidence picture, with no metric distances assigned.

Both axes map to the origin. In U_0 the inverse image of the origin is $v_0 = 0$, which the transition glues to $u_1 = 0$ in U_1. Along these axes u_0 and v_1 are inverse coordinates. The two affine lines therefore form the two patches of a single $\mathbb{P}^1$, which we call E_1. The second sphere E_2 is the union of $v_1 = 0$ and $u_2 = 0$ in the next pair of charts. There is one point common to E_1 and E_2, at $u_1 = v_1 = 0$. Since the two local equations are independent complex coordinates, the local intersection multiplicity is one. This is the crossing marked in Figure XI.1.1.

To find a self-intersection, move one sphere in its normal direction. The self-intersection is the degree of that normal line bundle. In (XI.1.5), $u_{i+1} = u_i^2 v_i$ gives its fiber-coordinate transition over the base inversion $v_{i+1} = 1/u_i$. This is the transition of a cotangent line on $\mathbb{P}^1$ up to a constant sign, since $\mathrm{d}v_{i+1} = -u_i^{-2}\mathrm{d}u_i$. The normal degree is -2. To read this degree, distinguish a cotangent basis from the coefficient of a covector in that basis. If $w = 1/u$ on the sphere, a cotangent vector written as $p\,\mathrm{d}u = q\,\mathrm{d}w$ obeys

$$\mathrm{d}w = -u^{-2}\mathrm{d}u, \qquad q = -u^2 p. \tag{XI.1.9}$$

Thus the fiber coefficient changes with u^2, even though the line bundle is $\mathcal{O}(-2)$. In the resolution transition, v_i and u_{i+1} are precisely such normal coefficients. Confusing the coefficient with the local basis would reverse the self-intersection. The compactness has a different origin: the coordinate along the sphere changes by inversion, adding the point at infinity of one affine line from the other chart.

The same sign follows from adjunction. In every chart the two-form

$$\mathrm{d}z \wedge \frac{\mathrm{d}x}{x} = -\mathrm{d}u_i \wedge \mathrm{d}v_i \tag{XI.1.10}$$

extends without a zero or a pole. The canonical bundle of the resolved surface X is therefore trivial. For either exceptional sphere E,

$$2g(E) - 2 = \deg(K_X|_E) + \deg(N_{E/X}) = E \cdot E = -2. \tag{XI.1.11}$$

We obtain the compact intersection matrix Q and its sign-reversed matrix C:

$$Q_{ij} = E_i \cdot E_j = \begin{pmatrix} -2 & 1 \\ 1 & -2 \end{pmatrix}_{ij}, \qquad C = -Q = \begin{pmatrix} 2 & -1 \\ -1 & 2 \end{pmatrix}. \tag{XI.1.12}$$

The compact curve pairing is negative definite. The positive pairing C, which will measure root lengths, uses the opposite sign. The spheres form the finite A_2 chain. There is no extra exceptional sphere for an affine node. The pairing also tests classes that are not individual spheres. For example, bilinearity gives

$$(E_1+E_2)^2 = -2+2(1)-2 = -2, \qquad (2E_1+E_2)^2 = 4(-2)+4(1)-2 = -6. \tag{XI.1.13}$$

The first class has the same self-pairing as a simple sphere, even though its representative at this complex structure is a chain. The second has a different length. This will distinguish a composite root charge from a general integer sum of compact charges. It does not by itself decide which sums have stable brane representatives.

We now use the two actual compact spheres to normalize the fields they can source.

XI.1.3 Which gauge fields can propagate?

A six-dimensional field obtained by expanding a ten-dimensional field must have finite kinetic energy for finite amplitude. Let X have its complete ALE metric and complex orientation. An internal profile ω multiplying an external field contributes the factor

$$\|\omega\|_X^2 = \int_X \omega \wedge *_4\omega \tag{XI.1.14}$$

to the kinetic coefficient. Harmonic profiles solve the internal zero-eigenvalue equation. They describe localized massless modes only if the integral in (XI.1.14) is finite. This extra condition matters because X is noncompact.

On the end of X, the volume element grows as

$$\mathrm{dvol}_X \;\sim\; \rho^3\,\mathrm{d}\rho\,\mathrm{dvol}_{S^3/\Gamma}. \tag{XI.1.15}$$

For a constant scalar profile the radial norm diverges as the fourth power of a large radius cutoff. This excludes a localized graviton from a constant internal metric profile and a localized photon from the Ramond–Ramond one-form with constant internal profile. The parallel hyperkähler two-forms likewise have constant pointwise norm. The noncompact end still supports delocalized waves. The divergence excludes a normalizable six-dimensional zero mode; it does not gap the bulk continuum or turn off its couplings.

A decaying profile can be tested without knowing its exact form in the interior. Suppose its pointwise norm is $c\rho^{-p}$ for large ρ, where $c \neq 0$, and let R be a large radial cutoff. Up to a positive angular factor its tail is

$$\|\omega\|_{\rho>R}^2 \;\sim\; c^2 \int_R^\infty \rho^{3-2p}\,\mathrm{d}\rho = \frac{c^2 R^{4-2p}}{2p-4}, \qquad p > 2. \tag{XI.1.16}$$

The same integral with an upper cutoff L grows as $\log(L/R)$ at $p = 2$, and as a positive power of L at $p < 2$. Smoothness in the interior is assumed in this test. Falloff faster than ρ^{-2} is therefore sufficient for a finite tail, but decay alone does not show that a profile is harmonic. A localized massless field needs both conditions. Conversely, a wave in the continuum need not be a square-integrable zero-eigenvalue profile.

For a complete ALE gravitational instanton the square-integrable harmonic two-forms represent the real middle cohomology. In the complex orientation these forms are anti-self-dual. For the A_2 resolution there are two of them. We choose harmonic representatives ω_i by the period conditions

$$\int_{E_j} \omega_i = \delta_{ij}, \qquad *_4\omega_i = -\omega_i. \tag{XI.1.17}$$

This choice is useful because a particle on E_j will couple with one unit of charge to the field indexed by j.

The period conditions also determine the kinetic metric. Let η_i be the compactly supported Poincaré dual class to E_i. Its period on E_j is the intersection number:

$$\int_{E_j} \eta_i = Q_{ij}, \qquad \int_X \eta_i \wedge \eta_j = Q_{ij}. \tag{XI.1.18}$$

The normalizable classes can be computed with their real compactly supported lifts. In that basis the unit-period condition reads

$$[\omega_i] = \sum_k (Q^{-1})_{ik} [\eta_k]. \tag{XI.1.19}$$

The resulting real pairing is well defined with the ALE boundary conditions. In particular, replacing the classes by their decaying harmonic representatives gives the same integrated pairing. We find

$$\begin{aligned} G_{ij} = \int_X \omega_i \wedge *_4\omega_j &= -\sum_{k,l} (Q^{-1})_{ik}\, Q_{kl}\, (Q^{-1})_{jl} \\ &= -(Q^{-1})_{ij} = \frac{1}{3}\begin{pmatrix} 2 & 1 \\ 1 & 2 \end{pmatrix}_{ij}. \end{aligned} \tag{XI.1.20}$$

The eigenvalues are 1 and 1/3, so both localized kinetic terms have positive norm. The inverse appears because the gauge fields will be labeled by unit periods, rather than by compact Poincaré duals. The real identification does not imply an isomorphism of integral lattices: $\det Q = 3$, and the image of the compactly supported integral classes has index three in the period lattice.

For this example the two real compactly supported lifts are especially concrete:

$$[\omega_1] = -\tfrac{1}{3}(2[\eta_1] + [\eta_2]), \qquad [\omega_2] = -\tfrac{1}{3}([\eta_1] + 2[\eta_2]). \tag{XI.1.21}$$

Integrating the first expression over E_1 gives $-(2(-2)+1)/3 = 1$, while its integral over E_2 is $-(2-2)/3 = 0$. These are unit-period conditions, not orthogonality conditions. For external two-forms F^1, F^2, the corresponding positive quadratic form may be written as

$$\sum_{i,j} G_{ij} F^i \wedge *_6 F^j = \tfrac{1}{2}(F^1 + F^2) \wedge *_6 (F^1 + F^2) + \tfrac{1}{6}(F^1 - F^2) \wedge *_6 (F^1 - F^2). \tag{XI.1.22}$$

For the coefficient vectors $(1,1)$ and $(1,-1)$ the squared internal norms are respectively 2 and $2/3$. Neither combination is absent or has negative norm. The off-diagonal kinetic term expresses the overlap of two independently charge-normalized internal profiles. A real rotation diagonalizes their kinetic energy, but would also change the components used to record integral particle charges.

Let C_3 be the Ramond–Ramond three-form and let μ_2 be the D2 Ramond–Ramond charge. Use the unit-charge potential $\widehat{C}_3 = \mu_2 C_3$. The normalizable vector part and its linearized field strength are

$$\widehat{C}_3 = \sum_i A^i \wedge \omega_i, \qquad \mathrm{d}\widehat{C}_3 = \sum_i F^i \wedge \omega_i, \qquad F^i = \mathrm{d}A^i. \tag{XI.1.23}$$

One index of $\widehat{C}_3$ remains in spacetime and two are absorbed by the internal two-form, so each mode A^i is a vector. These are two relative Cartan fields. No independent overall photon is supplied by the end of the ALE space.

The supersymmetry of these fields follows from the product geometry. The $SU(2)$ holonomy leaves the internal parallel spinors in a single four-dimensional chirality. Label this chirality positive in the product decomposition, so that a product spinor has

$$\Gamma_{(10)} = \Gamma_{(6)}\Gamma_{(4)}, \qquad \Gamma_{(4)}\epsilon_{\mathrm{int}} = +\epsilon_{\mathrm{int}}. \tag{XI.1.24}$$

The two Type IIA supercharges have opposite ten-dimensional chirality. After the internal holonomy restriction their six-dimensional chiralities remain opposite. One minimal supercharge of each chirality gives $(1,1)$, with eight real supercharges of each chirality. For each E_i, the three periods of the metric's hyperkähler forms and the period of B supply four real scalar modes. Together with the four transverse polarizations of a massless vector they give eight bosonic modes per Cartan multiplet. The vector and scalar data now suffice to ask what charges and masses the wrapped particles can have.

XI.1.4 The charges of the wrapped particles

Which charged vectors can join the two Cartan fields? The coupling that measures the charge is independent of the area of the brane. A D2-brane on an oriented compact class $\gamma = \sum_i q_i E_i$ has worldvolume $\mathcal{W}_1 \times \gamma$, where $\mathcal{W}_1$ is its worldline. Its electric coupling to the localized fields is

$$\int_{\mathcal{W}_1 \times \gamma} \widehat{C}_3 = \sum_i \left(\int_\gamma \omega_i \right) \int_{\mathcal{W}_1} A^i = \sum_i q_i \int_{\mathcal{W}_1} A^i. \tag{XI.1.25}$$

We choose the sign of the positive charge by the complex orientation of the sphere and the worldline orientation in this coupling. Reversing the wrapped orientation reverses all the charges. A sum of spheres in a homology class therefore supplies a sum of charges, whether or not a single stable wrapped state realizes that class at arbitrary periods.

The positive pairing on the compact charge lattice is the same as the Euclidean pairing of consecutive differences in $\mathbb{R}^3$. Let e_1, e_2, e_3 be its orthonormal coordinate

vectors. Under

$$E_1 \longleftrightarrow \alpha_1 = e_1 - e_2, \qquad E_2 \longleftrightarrow \alpha_2 = e_2 - e_3, \tag{XI.1.26}$$

we have $\alpha_i \cdot \alpha_j = C_{ij}$. The lattice lies in the plane of triples with zero sum, and the image of γ is

$$q_1\alpha_1 + q_2\alpha_2 = (q_1, q_2 - q_1, -q_2). \tag{XI.1.27}$$

The root condition in the simply laced normalization is

$$q^{\mathsf{T}} C q = 2(q_1^2 - q_1 q_2 + q_2^2) = 2. \tag{XI.1.28}$$

To solve it in integers, multiply the quadratic inside the parentheses by four and complete the square:

$$(2q_1 - q_2)^2 + 3q_2^2 = 4. \tag{XI.1.29}$$

For $q_2 = 0$ the two solutions are $q_1 = \pm 1$. For $q_2 = 1$ the solutions are $q_1 = 0, 1$, and for $q_2 = -1$ they are $q_1 = 0, -1$. No larger $|q_2|$ fits the bound. In particular $E_1 + E_2$ gives a root, but $E_1 - E_2$ has length squared six. Adding classes with different relative signs need not give another charged gauge boson.

The ambient-coordinate map explains the consecutive-chain pattern without guessing roots from a picture. For a general finite A_r chain, set $q_0 = q_{r+1} = 0$. The compact coefficient vector has image

$$\sum_{i=1}^{r} q_i(e_i - e_{i+1}) = \sum_{a=1}^{r+1}(q_a - q_{a-1})e_a, \qquad \sum_{a=1}^{r+1}(q_a - q_{a-1}) = 0. \tag{XI.1.30}$$

An integer zero-sum vector of squared norm two has exactly one entry $+1$, one entry -1 and all other entries zero. Summing its entries from the left recovers a coefficient vector equal to $+1$ on a single interval of spheres and zero elsewhere, or the negative of such a vector. For A_2, the ambient vector $e_1 - e_3$ therefore corresponds to $E_1 + E_2$. A choice of two endpoints in $r + 1$ positions gives one positive interval, so the two orientations give $r(r + 1)$ roots. This counts lattice charges; the wrapped-vector identification supplies the physical content at ordinary enhancement.

It is useful to relate these electric charges to the familiar simple coroot charges. Let $h_1 = \mathrm{diag}(1, -1, 0)$ and $h_2 = \mathrm{diag}(0, 1, -1)$. Evaluation of the root on h_i is $(Cq)_i$. The fields A^i in (XI.1.23) instead couple with charges q_i. Table XI.1.1 keeps these two lists distinct. For example, $E_1 + E_2$ has unit charges $(1, 1)$ and coroot charges $(1, 1)$, but E_1 has charges $(1, 0)$ and coroot charges $(2, -1)$. Agreement for the sum does not identify the two bases.

The two electric descriptions are related by a field transformation, not a change in the physical worldline coupling. Write the same Cartan connection as $A^i H^i = a^i h_i$, with H^i dual to the simple roots and h_i the simple coroots. Since $h_i = \sum_j C_{ij} H^j$, symmetry of C gives

$$A = Ca, \qquad q^{\mathsf{T}} A = (Cq)^{\mathsf{T}} a. \tag{XI.1.31}$$

Here A and a denote columns of one-forms. As a component check, $a = (2, 3)^{\mathsf{T}}\mathcal{A}$ gives $A = (1, 4)^{\mathsf{T}}\mathcal{A}$ for any spacetime one-form $\mathcal{A}$. The E_1 particle couples as $A^1 = \mathcal{A}$ in the

Oriented class	Charges q	Charges Cq	Root generator
E_1	$(1,0)$	$(2,-1)$	e_{12}
E_2	$(0,1)$	$(-1,2)$	e_{23}
E_1+E_2	$(1,1)$	$(1,1)$	e_{13}
$-E_1$	$(-1,0)$	$(-2,1)$	e_{21}
$-E_2$	$(0,-1)$	$(1,-2)$	e_{32}
$-E_1-E_2$	$(-1,-1)$	$(-1,-1)$	e_{31}

Table XI.1.1: The six nonzero A_2 root charges in the two electric bases. The e_{ij} are elementary matrices in the complexified gauge algebra; the two diagonal Cartan generators have zero root charge.

unit-period frame and as $2a^1 - a^2 = \mathcal{A}$ in the coroot frame. Its charge has changed coordinates, while its interaction has stayed the same. The gauge kinetic term must transform with the fields as well, which will be essential for fixing its coefficient.

The wrapped states at ordinary ADE enhancement are massive vector multiplets when moved slightly away from the enhancement locus. The positive roots correspond to consecutive chains with the complex orientation, and the negative roots to the reverse charges. With $e_{ab}e_{cd} = \delta_{bc}e_{ad}$, their algebra has, for example,

$$[e_{12}, e_{23}] = e_{13}, \qquad [e_{12}, e_{21}] = h_1. \tag{XI.1.32}$$

The first bracket combines the two simple charges. The second pairs opposite charges into a neutral diagonal generator. These six generators and the two Cartan generators describe the complexification of $\mathfrak{su}(3)$. Identifying the gauge algebra this way uses the physical wrapped-vector spectrum at the ordinary enhancement locus. An intersection matrix alone specifies a lattice, and a local particle spectrum alone does not select the global form of the gauge group. To see when these vectors are light, we must now compute their masses.

XI.1.5 What controls a wrapped particle's mass?

Does a sphere of zero area always give a massless particle? Start with a smooth holomorphic sphere E_i and the Kähler form J for the complex structure in which the sphere is holomorphic. Its area is $\mathcal{A}_i = \int_{E_i} J > 0$. On this slice the other two hyperkähler periods vanish. We use $\ell_s = \sqrt{\alpha'}$, $M_s = 1/\ell_s$, and the physical D2 tension

$$\tau_2 = \frac{1}{(2\pi)^2 g_s \ell_s^3}, \qquad j_i = \frac{\mathcal{A}_i}{4\pi^2\alpha'}, \qquad b_i = \frac{\int_{E_i} B}{4\pi^2\alpha'}. \tag{XI.1.33}$$

The area has units of length squared, whereas j_i and b_i are dimensionless. The latter is a periodic variable because it enters a worldsheet amplitude as $\exp(2\pi i b_i)$.

The static Dirac–Born–Infeld energy depends on the two-form $\mathcal{F} = B + 2\pi\alpha' F_{\mathrm{wv}}$ on the brane, where F_{wv} is the worldvolume gauge curvature. With $H = 0$ on this spin sphere the flux is integral. Write it as

$$n = \frac{1}{2\pi}\int_{E_i} F_{\mathrm{wv}} \in \mathbb{Z}, \qquad \int_{E_i} \mathcal{F} = 4\pi^2\alpha'(b_i + n). \tag{XI.1.34}$$

Even on a smooth sphere the energy must include this term. In an oriented orthonormal frame on the curve, $\mathcal{F} = f\,\mathrm{dvol}_{E_i}$ adds the off-diagonal entries $f, -f$ to the induced spatial metric. Thus

$$\frac{\det(g+\mathcal{F})}{\det g} = \det\begin{pmatrix} 1 & f \\ -f & 1 \end{pmatrix} = 1 + f^2, \qquad M^{\mathrm{DBI}}_{i,n} = \tau_2 \int_{E_i} \sqrt{1+f^2}\,\mathrm{dvol}_{E_i}. \tag{XI.1.35}$$

We can minimize this integral at fixed flux. The function $\sqrt{1+f^2}$ is strictly convex, so its average over the sphere is at least its value at the average f. Equality requires constant f. More explicitly, for $h(f) = \sqrt{1+f^2}$ one has

$$h''(f) = (1+f^2)^{-3/2} > 0, \qquad \overline{f} = \frac{1}{\mathcal{A}_i}\int_{E_i} \mathcal{F}, \qquad \frac{1}{\mathcal{A}_i}\int_{E_i} h(f)\,\mathrm{dvol}_{E_i} \geq h(\overline{f}). \tag{XI.1.36}$$

The minimization is over the flux distribution, with the metric and the total flux fixed. It therefore includes a possibly nonuniform pullback of B: the worldvolume curvature can compensate its varying part. This is why the minimum depends on its integral and on the area rather than on a chosen coordinate expression for B.

The curvature needed to make f constant has the prescribed integral flux, so it can be realized by a connection on the same line bundle. At the minimum, $f = \int_{E_i}\mathcal{F}/\mathcal{A}_i$ and

$$\begin{aligned} M^{\mathrm{DBI}}_{i,n} &= \tau_2\sqrt{\mathcal{A}_i^2 + \left(\int_{E_i}\mathcal{F}\right)^2} \\ &= \frac{M_s}{g_s}\sqrt{j_i^2 + (b_i+n)^2}. \end{aligned} \tag{XI.1.37}$$

The prefactor has units of mass, as a wrapped D2 now has only a time direction on its worldvolume. Area and flux contribute in quadrature, so reducing the first contribution leaves the second in place. This derivation uses the smooth-curve action at leading derivative order.

In the ordinary unframed local sector a shift of the B lift by an integer changes the flux label of the same state:

$$b_i \longmapsto b_i + k, \qquad n \longmapsto n - k, \qquad b_i + n \longmapsto b_i + n. \tag{XI.1.38}$$

For example, $(b_i, n) = (2/3, -1)$ and $(-1/3, 0)$ have the same residual period $-1/3$. At $j_i = 0$ the dimensionless period combination $j_i^2 + (b_i+n)^2$ has the formal value $1/9$. Shifting b_i while holding the integer label fixed would instead compare different states. An integral b_i can be removed with a relabeling that gives $b_i + n = 0$. A nonintegral period cannot be canceled by any integer flux.

We use the protected wrapped-vector identification near the ordinary enhancement point to interpret these periods when the curves approach zero size. The smooth determinant calculation does not control the curvature at the singularity. The wrapped-vector description says that an ordinary root can become massless when its metric periods vanish and its B period is zero modulo the allowed integer relabeling. On the A_2 resolution slice, full enhancement requires this for both simple roots. If only E_1 shrinks with zero residual B period while E_2 has positive area, the first pair of root vectors can become massless but the other two pairs cannot. If both areas vanish and the simple-root B periods have small nonzero lifts, the geometry may have the singular metric while the gauge bosons are still massive. The collapsed metric and the full gauge enhancement locus are distinct data.

Near enhancement we can compute the relative masses using the gauge effective field theory. Choose a common lift near $b_i = 0$ and take the zero-flux branch. Let Φ^I be the four adjoint scalars in unrescaled mass units, with $I = 1, \ldots, 4$. On the Cartan branch they are diagonal, $\Phi^I = \mathrm{diag}(\phi_1^I, \phi_2^I, \phi_3^I)$ and traceless. The vector mass operator from the covariant scalar kinetic term gives

$$[\Phi^I, e_{ab}] = (\phi_a^I - \phi_b^I) e_{ab}, \tag{XI.1.39}$$

$$\sum_I [\Phi^I, [\Phi^I, e_{ab}]] = M_{ab}^2 e_{ab}, \qquad M_{ab}^2 = \sum_I (\phi_a^I - \phi_b^I)^2. \tag{XI.1.40}$$

We match the simple-root differences to the local mass coordinates. On the resolution slice they have two active components,

$$\boldsymbol{m}_1 = \frac{M_s}{g_s}(j_1, b_1), \qquad \boldsymbol{m}_2 = \frac{M_s}{g_s}(j_2, b_2). \tag{XI.1.41}$$

The diagonal scalars can be reconstructed from these differences, which makes the tracelessness condition and the mass calculation compatible. Write $\boldsymbol{\phi}_a = (\phi_a^1, \ldots, \phi_a^4)$. Solving $\boldsymbol{\phi}_1 - \boldsymbol{\phi}_2 = \boldsymbol{m}_1$, $\boldsymbol{\phi}_2 - \boldsymbol{\phi}_3 = \boldsymbol{m}_2$ and $\sum_a \boldsymbol{\phi}_a = 0$ gives

$$\boldsymbol{\phi}_1 = \frac{2\boldsymbol{m}_1 + \boldsymbol{m}_2}{3}, \qquad \boldsymbol{\phi}_2 = \frac{-\boldsymbol{m}_1 + \boldsymbol{m}_2}{3}, \qquad \boldsymbol{\phi}_3 = -\frac{\boldsymbol{m}_1 + 2\boldsymbol{m}_2}{3}. \tag{XI.1.42}$$

For any two such differences the third root mass obeys

$$M_{13}^2 = M_{12}^2 + M_{23}^2 + 2\boldsymbol{m}_1 \cdot \boldsymbol{m}_2, \qquad |M_{12} - M_{23}| \le M_{13} \le M_{12} + M_{23}. \tag{XI.1.43}$$

The cross term measures alignment in scalar space and vanishes for orthogonal differences. The mass M_{13} reaches its upper bound when the differences are parallel with the same orientation. The same formula is valid for four active scalar components; the resolution slice restricts us to the two components already specified.

Their sum gives the difference between the first and third scalar eigenvalues. For example, if $(j_1, b_1) = \lambda(3, 4)$ and $(j_2, b_2) = \lambda(1, 0)$, choose $\lambda > 0$ small enough that all three charged vectors lie well below the string scale. Then

$$(M_{12}, M_{23}, M_{13}) = \frac{\lambda M_s}{g_s}\big(5, 1, 4\sqrt{2}\big), \qquad \boldsymbol{m}_1 + \boldsymbol{m}_2 = \frac{\lambda M_s}{g_s}(4, 4). \tag{XI.1.44}$$

Adding the two scalar masses would have given 6 in the last slot. The gauge theory adds the two vectors of scalar differences before taking the norm. This calculation concerns the light root vectors in the common local lift. It does not predict a bound-state spectrum at arbitrary B periods. To change the input, take $(j_1, b_1) = \lambda(2, 1)$ and $(j_2, b_2) = \lambda(1, -1)$, with $\lambda/g_s \ll 1$. The sum has vanishing B component although each simple root has a nonzero one. The local scalar calculation gives

$$(M_{12}, M_{23}, M_{13}) = \frac{\lambda M_s}{g_s}(\sqrt{5}, \sqrt{2}, 3), \qquad \boldsymbol{m}_1 \cdot \boldsymbol{m}_2 = \left(\frac{\lambda M_s}{g_s}\right)^2 . \tag{XI.1.45}$$

The positive areas keep every root massive in this example. Cancellation of the B component of the combined root does not cancel its area component. As another limit, send both components of $\boldsymbol{m}_1$ to zero while holding $\boldsymbol{m}_2 \neq 0$ small and fixed. Then $M_{12} = 0$ and $M_{13} = M_{23} = |\boldsymbol{m}_2|$: the first two scalar eigenvalues coincide, while the third remains separate. In this local gauge description the unbroken algebra is $\mathfrak{su}(2) \oplus \mathfrak{u}(1)$, generated by the first root pair and the two Cartan directions. The other four charged generators remain massive. This is the gauge meaning of a partial collapse.

For $t_i = b_i + ij_i$ and $T_i = -2\pi i t_i$, the weight is $e^{-T_i} = e^{2\pi i t_i} = e^{2\pi i b_i - 2\pi j_i}$. At $b_i = 0$ in the zero-flux branch, $T_i = 2\pi j_i$ and $M_i = M_s T_i/(2\pi g_s)$. This is the zero-B normalization used in the four-dimensional local limit in Chapter XI.2.

XI.1.6 The normalization of the gauge coupling

Does turning down g_s turn off the interactions of the localized gauge fields? The answer depends on the normalization of the field that carries one unit of electric charge. We can determine it by reducing the Ramond–Ramond kinetic term in the same basis as the particle coupling (XI.1.25).

At leading two-derivative order the string-frame normalization of the four-form term is

$$S_{\mathrm{RR}} = -\frac{1}{4\kappa_0^2}\int_{\mathbb{R}^{1,5}\times X} \mathrm{d}C_3 \wedge *_{10}\mathrm{d}C_3, \qquad 2\kappa_0^2 = (2\pi)^7 \ell_s^8. \tag{XI.1.46}$$

Here $H = 0$ as in the background specified above. In these variables the Ramond–Ramond term has no factor of g_s^{-2}. The physical coefficient for graviton exchange will be $\kappa_{10}^2 = g_s^2\kappa_0^2$ instead. The D2 charge is $\mu_2 = g_s\tau_2$, so changing to $\widehat{C}_3 = \mu_2 C_3$ puts the kinetic term in the form

$$S_{\mathrm{RR}} = -\frac{1}{2e_2^2}\int \mathrm{d}\widehat{C}_3 \wedge *_{10}\mathrm{d}\widehat{C}_3, \qquad e_2^2 = 2\kappa_0^2\mu_2^2 = (2\pi)^3\alpha'. \tag{XI.1.47}$$

The coefficient e_2^2 pertains to the unit-charge ten-dimensional potential. Inserting (XI.1.23) separates the internal integral and gives the Cartan kinetic action

$$S_{\mathrm{Cartan}} = -\frac{1}{2e_2^2}\sum_{i,j} G_{ij}\int_{\mathbb{R}^{1,5}} F^i \wedge *_6 F^j. \tag{XI.1.48}$$

Both the normalization of the potential and the matrix G matter. A comparison in a basis with different electric charges would change the coefficient multiplying its component fields.

The generators H^i dual to the simple roots have unit evaluation on one simple root and zero on the other:

$$H^1 = \tfrac{1}{3}\,\mathrm{diag}(2,-1,-1), \qquad H^2 = \tfrac{1}{3}\,\mathrm{diag}(1,1,-2), \qquad \alpha_j(H^i) = \delta^i_j. \tag{XI.1.49}$$

For instance the difference of the first two entries of H^1 is one and the difference of its last two entries is zero. Thus the connection $\sum_i A^i H^i$ has exactly the unit electric charges of the wrapped particles. Its trace Gram matrix is

$$\mathrm{Tr}_f(H^i H^j) = \frac{1}{3}\begin{pmatrix} 2 & 1 \\ 1 & 2 \end{pmatrix}_{ij} = G_{ij}. \tag{XI.1.50}$$

The coroot description gives a useful independent way to organize this matrix comparison. The diagonal matrices satisfy

$$h_1 = 2H^1 - H^2, \qquad h_2 = -H^1 + 2H^2, \qquad \mathrm{Tr}_f(h_i h_j) = C_{ij}. \tag{XI.1.51}$$

At the linearized Cartan level let $f^i = \mathrm{d}a^i$, so that $F = Cf$. Then the same kinetic energy is

$$F^{\mathsf{T}} G \wedge *_6 F = f^{\mathsf{T}} C^{\mathsf{T}} C^{-1} C \wedge *_6 f = f^{\mathsf{T}} C \wedge *_6 f. \tag{XI.1.52}$$

The matrix is inverse Cartan in one frame and Cartan in the other. Using the first matrix with coroot charges, or the second with unit simple-root charges, would compare two different normalizations of the connection. The unit-charge brane coupling removes this ambiguity.

With generators T^a normalized by $\mathrm{Tr}_f(T^a T^b) = \delta^{ab}/2$, the Yang–Mills action is

$$S_{\mathrm{YM}} = -\frac{1}{g_6^2}\int \mathrm{Tr}_f(F \wedge *_6 F) = -\frac{1}{4g_6^2}\int \mathrm{d}^6x\, F^a_{\mu\nu} F^{a\mu\nu}. \tag{XI.1.53}$$

Restricting to $F = \sum_i F^i H^i$ and comparing with (XI.1.48) now fixes the leading coupling:

$$g^2_{6,\mathrm{lead}} = 2e_2^2 = 2(2\pi)^3\alpha'. \tag{XI.1.54}$$

An A_1 sphere provides a check on the factor of two. Its inverse Cartan entry is $1/2$. The unit-charge generator is $\mathrm{diag}(1,-1)/2$, with trace square $1/2$. The Cartan action then has coefficient $1/(4e_2^2)$, while the Yang–Mills form in this same generator has coefficient $1/(2g_6^2)$. The coefficients agree precisely at (XI.1.54). The match comes from a closed-string kinetic term. It is not the Yang–Mills coupling on a D2-brane probe. It fixes the leading coefficient in the smooth reduction; it does not establish an all-orders statement about the singular string background.

In the electric normalization the covariant derivative contains A with no factor of g_6. In mass units this gives $[A] = 1$ and $[F] = 2$. Requiring the six-dimensional action to be dimensionless gives

$$[g_6^2] = -2, \qquad g_6^2 E^2 \quad \text{dimensionless.} \tag{XI.1.55}$$

The dimension of the coupling can also be read from a canonically normalized field. In the component action let $A^a_\mu = g_6 \mathcal{A}^a_\mu$, and denote the Lie algebra structure constants by f^{abc}. The field strength then has the form

$$F^a_{\mu\nu} = g_6(\partial_\mu \mathcal{A}^a_\nu - \partial_\nu \mathcal{A}^a_\mu) + g_6^2 f^{abc}\mathcal{A}^b_\mu \mathcal{A}^c_\nu, \qquad [\mathcal{A}] = 2, \qquad [g_6] = -1. \tag{XI.1.56}$$

Thus a cubic interaction brings a coupling with inverse mass dimension. The dimensionless size of a process grows with $g_6 E$, consistent with (XI.1.55). This statement concerns the fixed-rank low-energy expansion; it is not an extrapolation of Yang–Mills theory to energies where string excitations have become important.

At fixed rank the gauge interactions become weak toward low energy. Equation (XI.1.54) also shows why decreasing g_s at fixed α' does not remove the gauge interaction scale. This is the reason that two ways of suppressing gravity have different outcomes.

XI.1.7 The gauge regime and the little-string regime

Which scales must be separated to isolate the gauge theory? Choose a simple-root state in a lift near the gauge origin. Write its complex period as $t_i = b_i + ij_i$ and its mass scale as $M_{W,i}$. For a local root vector with fixed residual period the matching above gives

$$M_{W,i} = \frac{M_s}{g_s}|t_i + n_i|, \qquad M_{\mathrm{D0}} = \frac{M_s}{g_s}, \qquad 2\kappa_{10}^2 = (2\pi)^7 g_s^2 \ell_s^8. \tag{XI.1.57}$$

The second scale is the bulk D0 mass, given by the D0 tension. It is useful for comparison with the first: the wrapped mass is smaller by the small dimensionless period. The last coefficient is the physical ten-dimensional Newton normalization in asymptotic string-frame units. There is no localized six-dimensional graviton to which we can assign a finite Newton constant on the complete ALE space.

At nonzero, small root masses, an observer below all of them needs only the Cartan fields. An observer above those masses but sufficiently below the string scale can describe the charged vectors in the non-Abelian Yang–Mills effective field theory. For a weakly coupled gauge calculation at fixed rank the useful window satisfies

$$\max_{\gamma\,\mathrm{root}} M_\gamma \ll E \ll M_s, \qquad g_6^2 E^2 \ll 1, \tag{XI.1.58}$$

where M_γ is the mass of the vector of charge γ. At exact enhancement there is no lower mass threshold. The inequalities specify a parametric region, not sharp thresholds. The coupling scale $1/g_6$ is proportional to M_s at fixed rank, but the strength of a particular gauge process also depends on group and loop factors. Figure XI.1.2 depicts the ordering for a resolved vacuum in which the root masses are well below M_s.

First hold ℓ_s fixed and send g_s to zero. At the enhancement locus the charged root vectors are massless. To stay slightly away from that locus with a fixed finite root mass, hold a complex quantity z_i with units of mass fixed and tune the residual dimensionless period as

$$t_i + n_i = \frac{g_s}{M_s}\, z_i. \tag{XI.1.59}$$

This gives $M_{W,i} = |z_i|$. Holding a nonzero residual dimensionless period fixed instead would make that vector heavy. The dimensionless gravity measure at a fixed external energy E behaves as

$$\kappa_{10}^2 E^8 \propto g_s^2 (\ell_s E)^8 \longrightarrow 0, \qquad g_{6,\mathrm{lead}}^2 \text{ fixed}. \tag{XI.1.60}$$

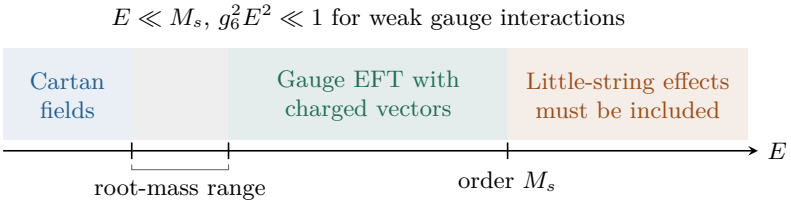


Figure XI.1.2: Schematic energy axis for the localized sector at fixed M_s and small nonzero root masses. Below the lightest root the gauge fields are Cartan fields; the root-mass range may contain several thresholds. Above the largest such mass, but well below the string scale, the charged vectors belong in the gauge effective theory. At energies of order M_s, the local little-string dynamics requires more than the Yang–Mills degrees of freedom. Distances and the colored boundaries on the axis are schematic.

A vanishing Newton coupling does not prove factorization from every bulk mode. We use the ordinary localized ALE decoupling limit, in which the bulk continuum decouples from the sector at the singularity as $g_s \to 0$. At fixed M_s that sector retains finite-tension string excitations. It is the $(1,1)$ little-string theory, whose low-energy description at the gauge origin is six-dimensional $(1,1)$ Yang–Mills. A fixed nonzero z_i describes a deformation away from that origin in the same limit. Noncompactness, which ruled out the constant graviton mode, is a distinct statement from this interacting-sector limit.

Now send $\ell_s \to 0$ at fixed external energy and fixed rank, with bounded weak g_s. Keep the simple-root masses finite by the same tuning (XI.1.59). The gauge and gravity interaction measures then behave as

$$M_s \to \infty, \qquad g_6^2 E^2 \propto \ell_s^2 E^2 \to 0, \qquad \kappa_{10}^2 E^8 \to 0, \qquad M_{\mathrm{D0}} \to \infty. \tag{XI.1.61}$$

The local gauge interaction weakens in this fixed-energy limit. Attempting to keep $g_6^2 E^2$ nonzero by increasing E as $1/\ell_s$ keeps E/M_s nonzero, so it does not remove the string scale relative to the process. The two trajectories do not construct an interacting six-dimensional $(1,1)$ superconformal fixed point.

The scales used in these comparisons are summarized in Table XI.1.2. As a check, let $\ell_s = \epsilon \ell_{s0}$, with fixed positive ℓ_{s0} and g_s, and choose $j_i = \epsilon j_0$ with fixed $j_0 > 0$ and $b_i = n_i = 0$. The physical area then behaves as ϵ^3. Using the area and D2 tension in (XI.1.33) gives

$$\mathcal{A}_i = 4\pi^2 \ell_{s0}^2 j_0 \epsilon^3, \qquad \tau_2 \mathcal{A}_i = \frac{j_0}{g_s \ell_{s0}}. \tag{XI.1.62}$$

The tension grows as ϵ^{-3}, leaving the root mass fixed in the local matching. The dimensionless period scales as ϵ even though the physical area scales as ϵ^3.

One can diagnose both trajectories without selecting the powers in advance. Let $\ell_s = \epsilon^a \ell_{s0}$, $g_s = \epsilon^c g_{s0}$ and $j = \epsilon^d j_0$, with nonzero fixed positive coefficients, $b = n = 0$, and fixed external energy. The leading scales have powers

quantity	M_s	M_W	g_6^2	κ_{10}^2	$\mathcal{A}$
power of ϵ	$-a$	$d-a-c$	$2a$	$8a+2c$	$2a+d$

(XI.1.63)

Quantity	Scale or measure	Mass dim.	Role
Root-vector mass	$(M_s/g_s)\lvert t_i + n_i\rvert$	1	Retained by tuning the residual period.
String scale	$M_s = 1/\ell_s$	1	Finite in the little-string limit.
Bulk D0 mass	M_s/g_s	1	Diverges in both trajectories above.
Gauge coupling squared	$g_6^2 \propto \ell_s^2$	-2	Sets the size of $g_6^2 E^2$.
Bulk Newton coefficient	$\kappa_{10}^2 \propto g_s^2 \ell_s^8$	-8	Suppresses gravity at fixed E when it goes to zero.

Table XI.1.2: Mass dimensions and the roles of the scales in the ordinary local Type IIA construction. The root row uses a simple root in the local period lift. A mass dimension is the exponent of mass in the corresponding quantity.

Retaining a finite nonzero root mass therefore imposes $d = a + c$. The corresponding area exponent is $3a + c$. For example, shrinking the string length and the coupling together, $a = c = 1$, requires $j \propto \epsilon^2$ and $\mathcal{A} \propto \epsilon^4$. The root mass stays finite, the D0 mass grows as ϵ^{-2}, and the Newton coefficient decreases as ϵ^{10}. Choosing $j \propto \epsilon$ on that same path instead would make the root mass grow as ϵ^{-1}. Each path has to tune the period in relation to both the tension and the coupling.

The weak-coupling and low-energy requirements can now be compared in one ratio. At the displayed leading normalization,

$$g_{6,\mathrm{lead}}^2 E^2 = 2(2\pi)^3 (E/M_s)^2, \qquad \frac{M_W}{M_s} = \frac{|t+n|}{g_s}. \tag{XI.1.64}$$

The first condition constrains the energy in string units, and the second constrains how close the vacuum lies to enhancement. Sending g_s to zero improves neither ratio unless the residual periods are also tuned. Once they are tuned, decreasing g_s can suppress bulk gravity while leaving the localized gauge interaction unchanged. This explains why the finite-string-scale limit and the fixed-energy limit with vanishing string length answer different physical questions.

The IIB contrast can be seen by counting the dimensions of the unwrapped objects. On the same kind of surface the two IIB supercharges have equal ten-dimensional chirality and give a chiral $(2,0)$ theory. The IIB four-form with two internal legs gives a chiral two-form in six dimensions. A D3 wrapped on the sphere still has a spatial direction outside X, so it gives a string. On a smooth geometric slice at zero background periods other than the area, its tension scales as

$$T_{\text{wrapped D3}} \;\propto\; \tau_3 \mathcal{A}, \tag{XI.1.65}$$

and it becomes tensionless at the ordinary collapse locus. The low-energy singular point of the localized IIB construction is the interacting $(2,0)$ superconformal theory, with a tensor branch. Chapter XII.1 treats that construction. The IIA construction

here supplies gauge fields and charged particles that will be the starting point for the separate four-dimensional limit in Chapter XI.2.

XI.1.8 Exercises

The calculations below extend the worked A_2 example. Give the reasoning even when the requested result is a matrix or a number.

E1. From the A_3 chain to root charges. Use the chart transitions in (XI.1.5) with $r = 3$ to find the intersection matrix in the ordered basis (E_1, E_2, E_3). In particular, explain why E_1 and E_3 do not intersect. Map the classes to consecutive differences of coordinate vectors in $\mathbb{R}^4$. Use this map to find all the squared-length-two charges as coefficient triples in the ordered sphere basis. Include both orientations. Why does having three compact spheres not give only three positive roots?

E2. Falloff and kinetic mixing. Suppose a smooth internal form has pointwise norm proportional to ρ^{-p} on the end. Of $p = 1, 2, 3$, which powers give a finite tail for its norm squared? Check the borderline power explicitly. In A_2, express the two unit-period forms in the compact Poincaré dual basis and recompute their Hodge metric. Explain why a delocalized wave of the ten-dimensional Ramond–Ramond one-form is compatible with the absence of a localized six-dimensional photon from that one-form.

E3. Follow a flux sector through a change of lift. Start with $j_i = 1/3$, $b_i = 3/4$ and $n = -1$. If the same state is described in the lift $b_i = -1/4$, what is its new flux label? Use the smooth leading-order expression to compute its mass squared in units of $(M_s/g_s)^2$ at $j_i = 1/3$. Then give the formal value of the same dimensionless period combination at $j_i = 0$. Explain whether any integer choice of flux can cancel the residual B term there and what the smooth determinant can establish about the wrapped spectrum at zero area.

E4. Keep the particle, change the string scale. Fix the external energy $E > 0$ and rank. In both trajectories set $b = n = 0$ and $j = \epsilon j_0$ with fixed $j_0 > 0$, as $\epsilon \to 0^+$. In the first trajectory take $g_s = \epsilon$ and hold $\ell_s > 0$ fixed. In the second take $\ell_s = \epsilon \ell_{s0}$ with fixed $\ell_{s0} > 0$ and hold $g_s > 0$ fixed and weak. For each trajectory give the four powers of ϵ, in order, for $(M_s, M_W, g_6^2, \kappa_{10}^2)$. Interpret them at fixed E. Which trajectory retains a finite little-string scale, and why is $\kappa_{10}^2 E^8 \to 0$ by itself insufficient to identify the interacting local theory?

The following written problems practice changes of description. They do not add numerical submissions to E1–E4.

W1. Starting from the two unit-period forms, find the internal norms of their sum and difference. Explain why diagonalizing the kinetic term does not produce a third localized photon or remove the integral normalization of brane charge.

W2. In the local scalar frame set $\boldsymbol{m}_1 = \nu(1,2)$ and $\boldsymbol{m}_2 = \nu(2,-1)$, with $\nu > 0$ a mass much smaller than M_s. Reconstruct the three traceless scalar eigenvalue vectors and compare all three root masses. Which geometric periods must vanish to turn the first simple-root pair massless while retaining the other two pairs at finite mass?

W3. On a path with $\ell_s \propto \epsilon^2$ and $g_s \propto \epsilon$, choose a period scaling that retains a nonzero finite root mass. Derive the physical area scaling and distinguish the gauge, gravitational and string scales at fixed energy.

Status and sources

§XI.1.2 The compact spheres. [MATH] The chart calculation gives the compact curve matrix (XI.1.12). See Douglas and Moore 1996, arXiv:hep-th/9603167v1, §2.1, for the ADE pairing and geometry.
§XI.1.3 The localized modes. [MATH] The complete ALE case of Hausel et al. 2004, arXiv:math/0207169v2, §7.1.1, gives the L^2 cohomology used in (XI.1.17). For anti-self-duality in the complex orientation see Douglas and Moore 1996, arXiv:hep-th/9603167v1, §2.1. The matrices (XI.1.20) and (XI.1.22) use real period duality. [SUGRA] The mode (XI.1.23), the absence of constant localized profiles, and the scalar partners follow from the unwarped reduction without background flux in Douglas and Moore 1996, §§2.2–2.3.
§XI.1.4 The root charges. [MATH] The compact length calculation (XI.1.28) enumerates the A_2 charges. [GEO-X] The ordinary wrapped-vector identification at ADE enhancement uses the ordinary ALE construction; see Katz et al. 1996, arXiv:hep-th/9601108v2, §2.1, and Aharony et al. 2004, arXiv:hep-th/0310197v3, §§3.1–3.2.
§XI.1.5 The mass calculation. [SUGRA] The smooth disk calculation (XI.1.37) uses Polchinski et al. 1996, arXiv:hep-th/9602052v2, eqs. (2.19)–(2.20). [GEO-X] Enhancement at vanishing metric and residual B periods is the protected identification, distinct from the smooth determinant. See Aspinwall 1995, arXiv:hep-th/9507012v1, §§3–4, eqs. (5)–(6), and Aharony et al. 2004, arXiv:hep-th/0310197v3, §§3.1–3.2 and §4. [MATH] The relative masses from (XI.1.39) use the local matching of simple-root scalar differences to the periods. The reconstruction and the second example in (XI.1.42)– (XI.1.45) are consequences in that same local EFT, including its partial-enhancement limit.
§XI.1.6 The gauge coupling. [SUGRA] The leading coefficient (XI.1.54) uses the RR kinetic and physical Newton coefficients of Castellano et al. 2023, published Appendix D, eqs. (D.1)–(D.3), printed p. 110, and the charge normalization ratio of Polchinski 1995, arXiv:hep-th/9510017v3, eqs. (12)–(13). Chang et al. 2014, arXiv:1407.7511v3, eqs. (1.1) and (4.2), supplies an independent tension normalization.
§XI.1.7 The two limits. [MATH] The scale algebra in (XI.1.60) and (XI.1.61) follows from the leading coefficients and the local mass matching; (XI.1.63) organizes the same conditional scaling for general exponents. [DEC] The finite-M_s localized little-string limit uses Giveon and Kutasov 1999, arXiv:hep-th/9909110v2, §1, and Aharony 2000, arXiv:hep-th/9911147v1, §1.1. [GEO-E] The IIB comparison uses the D3-brane construction of Witten 1995, arXiv:hep-th/9507121v1, §1, the opposite reduction of Douglas and Moore 1996, arXiv:hep-th/9603167v1, §2.4, and the low-energy $(2,0)$

interpretation in Aharony 2000, §1.1.

The calculation uses mostly-plus signature and the spinor and brane-action conventions of the preceding volumes. The cyclic action, finite exceptional graph and complexified Kähler period are specified above. The displayed coupling uses a potential with unit D2 electric charge and the stated fundamental trace. The accompanying checks reproduce the geometry, root charges, normalization, masses and limits. The four exercise checks cover only the numerical and algebraic parts of the answers.

Aharony, O. (2000). “A brief review of little string theories”. In: *Class. Quant. Grav.* 17, pp. 929–938. DOI: 10.1088/0264-9381/17/5/302. arXiv: hep-th/9911147.

Aharony, O. et al. (2004). “Little string theory and heterotic/Type II duality”. In: *Nucl. Phys. B* 679, pp. 3–65. DOI: 10.1016/j.nuclphysb.2003.11.041. arXiv: hep-th/0310197.

Aspinwall, P. S. (1995). “Enhanced gauge symmetries and K3 surfaces”. In: *Phys. Lett. B* 357, pp. 329–334. DOI: 10.1016/0370-2693(95)00957-M. arXiv: hep-th/9507012.

Castellano, A., A. Herráez, and L. E. Ibáñez (2023). “The emergence proposal in quantum gravity and the species scale”. In: *JHEP* 06, p. 047. DOI: 10.1007/JHEP06(2023)047. arXiv: 2212.03908 [hep-th].

Chang, C.-M. et al. (2014). “Little string amplitudes (and the unreasonable effectiveness of 6D SYM)”. In: *JHEP* 12, p. 176. DOI: 10.1007/JHEP12(2014)176. arXiv: 1407.7511 [hep-th].

Douglas, M. R. and G. W. Moore (1996). “D-branes, quivers, and ALE instantons”. In: arXiv preprint; not published in a journal. arXiv: hep-th/9603167.

Giveon, A. and D. Kutasov (1999). “Little string theory in a double scaling limit”. In: *JHEP* 10, p. 034. DOI: 10.1088/1126-6708/1999/10/034. arXiv: hep-th/9909110.

Hausel, T., E. Hunsicker, and R. Mazzeo (2004). “Hodge cohomology of gravitational instantons”. In: *Duke Math. J.* 122.3, pp. 485–548. DOI: 10.1215/S0012-7094-04-12233-X. arXiv: math/0207169.

Katz, S., D. R. Morrison, and M. R. Plesser (1996). “Enhanced gauge symmetry in Type II string theory”. In: *Nucl. Phys. B* 477, pp. 105–140. DOI: 10.1016/0550-3213(96)00331-8. arXiv: hep-th/9601108.

Polchinski, J. (1995). “Dirichlet branes and Ramond–Ramond charges”. In: *Phys. Rev. Lett.* 75, pp. 4724–4727. DOI: 10.1103/PhysRevLett.75.4724. arXiv: hep-th/9510017.

Polchinski, J., S. Chaudhuri, and C. V. Johnson (1996). *Notes on D-branes*. arXiv: hep-th/9602052.

Witten, E. (1995). *Some comments on string dynamics*. arXiv: hep-th/9507121.

Chapter XI.2

The four-dimensional local limit

XI.2.1 A gauge theory inside a string compactification

A vanishing two-sphere in type IIA string theory can produce a light charged particle. If the sphere belongs to an A_1 surface singularity, its two orientations give the pair of states expected at an $SU(2)$ enhancement. Fibering this singularity over a second two-sphere offers a route to a four-dimensional $\mathcal{N} = 2$ gauge theory. Yet the resulting string model also contains string excitations, motion on the base, gravity in a compact completion, and perhaps other bulk states. To obtain a field theory, one must say which masses remain finite and which go to infinity in the same units.

Our example is the canonical bundle of $F_0 = \mathbb{P}^1_b \times \mathbb{P}^1_f$. The fiber sphere carries the wrapped D2 W state; the base sphere controls the coupling. We will keep the W mass and a gauge-theory scale finite while raising the string scale. The fiber and base must approach this limit at correlated rates. A vanishing base-instanton weight can then multiply a divergent fiber sum to give a finite gauge-instanton contribution.

The six-dimensional starting point is the $(1, 1)$ gauge effective theory of Chapter 1. In the ordinary genus-zero setup used here, the base supplies no adjoint hypermultiplet, leaving the intended pure four-dimensional $\mathcal{N} = 2$ sector. Our first task is to define its mass and area units. We then find the scaling trajectory, test the unwanted local masses, and calculate the surviving one-instanton term. The geometry-to-gauge identification and the isolation from a possible bulk sector will be stated at the steps where each is used.

XI.2.2 What the two spheres measure

The compact surface F_0 has two curve classes b and f, with

$$b^2 = f^2 = 0, \qquad b \cdot f = 1, \qquad K_{F_0} = -2b - 2f. \tag{XI.2.1}$$

The total space $X = \mathrm{Tot}(K_{F_0})$ is a noncompact Calabi–Yau threefold. A point on the base $\mathbb{P}^1_b$ labels a fiber $\mathbb{P}^1_f$. Contracting the latter gives the local A_1 geometry along the base. Geometrically the two rulings are symmetric, but the engineering construction selects which one contracts and which one controls the coupling. We keep that choice fixed below.

The local toric description makes the two parameters independent at the starting point. Ordering the five relevant divisors so that the first is the compact surface, two belong to one ruling and two to the other, the two curve-relation vectors can be written

$$\ell_f = (-2, 1, 1, 0, 0), \qquad \ell_b = (-2, 0, 0, 1, 1), \qquad \sum_i \ell_{f,i} = \sum_i \ell_{b,i} = 0. \tag{XI.2.2}$$

The zero sums are the local Calabi–Yau charge condition. The vectors also show why one should expect two independent Kähler actions before imposing a field-theory limit. Their labels f, b describe our selected engineering frame; interchanging the two rulings would exchange the roles, not produce a new intersection form. The correlated scaling introduced later is a trajectory through this two-parameter space, not an intrinsic equality of its coordinates.

A D2-brane can wrap f with either orientation. The resulting pair has opposite electric charge. At vanishing fiber B period and zero worldvolume flux, its BPS mass is measured in the chosen string-frame normalization by the D2 tension times the physical fiber area $J_f = \int_f J$:

$$T_{D2} = \frac{1}{(2\pi)^2 g_s \alpha'^{3/2}}, \qquad M_W = T_{D2} J_f = \frac{J_f}{(2\pi)^2 g_s \alpha'^{3/2}}. \tag{XI.2.3}$$

This fixes the physical mass variable $a_W := M_W$ used in the limit. The precise relation of a_W to a chosen Seiberg–Witten electric period depends on the normalization of electric charge and of the central charge. We do not silently identify them. At a sub-stringy fiber size, the classical wrapped brane picture is used through its protected BPS charge and central-charge continuation. It is not a semiclassical estimate of every excitation on the small sphere.

The base plays a different role. Compactifying the six-dimensional gauge sector over it makes its area control a bare four-dimensional coupling. A fundamental string wrapping the base has an action proportional to that area. A degree-n wrapping has weight Q_b^n. The field-theory interpretation of n as the gauge instanton number will be made explicit in Section XI.2.6. The parameter table separates physical areas and masses from dimensionless Kähler variables.

The dimensional reduction is simple enough to display without choosing a microscopic six-dimensional coupling normalization. In a product-metric zero-mode approximation with a constant six-dimensional kinetic coefficient, a gauge field that is approximately

constant on a base of physical area J_b has

$$\begin{aligned} &-\frac{1}{4g_6^2}\int_{M_4\times\mathbb{P}^1_b} F_{MN}F^{MN} \\ &\longrightarrow -\frac{J_b}{4g_6^2}\int_{M_4} F_{\mu\nu}F^{\mu\nu}, \\ &\frac{1}{g_4^2}=\frac{J_b}{g_6^2} \qquad \text{(at this zero-mode level).} \end{aligned} \tag{XI.2.4}$$

Because g_6^2 has dimensions of area, the ratio is dimensionless. This calculation explains why the base, rather than the small fiber, is the coupling control. It does not fix the exact coefficient between the worldsheet action A_b and $8\pi^2/g_4^2$: that coefficient needs the string normalization and threshold matching, not merely the zero-mode integral. Warping or a varying kinetic coefficient would replace J_b by a weighted integral. The example assumes the zero mode remains the selected light gauge field as the base and fiber parameters approach their correlated limit.

Object	Geometric or string variable	Four-dimensional role
Fiber f	$J_f=\int_f J$; $T_f=J_f/(2\pi\alpha')$ at $B_f=0$	$a_W=M_W=T_fM_s/(2\pi g_s)$
Base b	$J_b=\int_b J$; $A_b=J_b/(2\pi\alpha')$	Bare instanton action along the calibrated local trajectory
Base phase	$\theta_b=B_b/(2\pi\alpha')$ and $Q_b=e^{-A_b+i\theta_b}$	Gauge-instanton phase in the chosen orientation
String scale	$M_s=\alpha'^{-1/2}$, g_s fixed	$\epsilon=2\pi g_s/M_s$ is a length
Strong scale	Λ held finite	$Q_b=Ce^{i\theta_b}(\epsilon\Lambda)^4$, with finite $C>0$

Table XI.2.1: The local F_0 parameter dictionary. The real T_f and A_b are worldsheet areas divided by $2\pi\alpha'$; they are not physical areas. The finite constant C reflects a matching convention and cannot absorb a change in the power of ϵ.

The distinction in the first row is already decisive. Solving the wrapped-brane mass formula for its area gives

$$J_f=(2\pi)^2 g_s a_W M_s^{-3}, \qquad \frac{J_f}{\alpha'}=(2\pi)^2 g_s\frac{a_W}{M_s}. \tag{XI.2.5}$$

At fixed g_s and a_W, doubling M_s divides the physical area by eight and its area in string units by two. These two changes keep the product of tension and area fixed. If J_f were held fixed while M_s rose, (XI.2.3) would send M_W to infinity. If the dimensionless ratio J_f/α' were held fixed, the mass would still grow like M_s/g_s. The finite-W limit needs $J_f\propto M_s^{-3}$ at fixed g_s, a more rapid physical shrinkage than one would infer by saying only that the fiber "becomes small."

The same dictionary can be used in reverse. Suppose the desired charged particle has mass a_W, and a regulator has been chosen by specifying M_s and g_s. The physical area, dimensionless action and worldsheet weight are then determined in that order:

$$a_W \;\longmapsto\; J_f = \frac{4\pi^2 g_s a_W}{M_s^3} \;\longmapsto\; T_f = \frac{M_s^2 J_f}{2\pi} = \frac{2\pi g_s a_W}{M_s} \;\longmapsto\; Q_f = e^{-2\pi g_s a_W/M_s}. \tag{XI.2.6}$$

The first arrow uses the wrapped D2, while the last uses a fundamental worldsheet. Their tensions have different powers of g_s and α'. A small worldsheet action can therefore coexist with a finite particle mass. Equating the action T_f directly to a mass would discard precisely the regulator factor that makes this possible.

For example, change the target Coulomb mass by a finite factor $\lambda > 0$ while keeping the regulator fixed. Equations (XI.2.3) and (XI.2.6) give

$$a'_W = \lambda a_W, \qquad J'_f = \lambda J_f, \qquad T'_f = \lambda T_f, \qquad Q'_f = Q_f^{\lambda}. \tag{XI.2.7}$$

This operation moves along the gauge theory's Coulomb branch. By contrast, raising M_s at fixed a_W improves the separation from string excitations without changing that physical point. If $M'_s = \eta M_s$, with g_s fixed, then

$$\alpha'' = \eta^{-2}\alpha', \qquad J'_f = \eta^{-3} J_f, \qquad T'_f = \eta^{-1} T_f, \qquad Q'_f = Q_f^{1/\eta}. \tag{XI.2.8}$$

Doubling the Coulomb mass doubles both area measures at a fixed cutoff; doubling the cutoff at a fixed mass changes the two area measures by different factors. These are different directions in the parameter space, even though both alter the fiber worldsheet weight.

There is also a useful dimensional check on the reduction formula. Since J_b and g_6^2 both have dimensions of length squared, a small physical base does not by itself imply strong four-dimensional coupling. The microscopic six-dimensional coefficient varies along the string limit as well. The reduction only compares their ratio:

$$g_4^{-2} = J_b/g_6^2, \qquad J_b \to 0 \quad \text{does not determine} \quad \lim g_4^{-2} \text{ without the behavior of } g_6^2. \tag{XI.2.9}$$

The worldsheet action, whose denominator is α', will instead grow on the base. The next sections track that dimensionless quantity and its calibrated instanton interpretation.

XI.2.3 From the house Kähler parameter to a worldsheet action

A physical two-cycle area has dimensions of length squared. The Kähler parameter used in a string instanton expansion is dimensionless and complex. For an oriented curve C, our convention is

$$t_C = \frac{1}{4\pi^2\alpha'}\int_C (B + iJ), \qquad q_C = e^{2\pi i t_C}. \tag{XI.2.10}$$

The real part records the B period, while the imaginary part measures area. It is useful to introduce the Euclidean action

$$T_C := -2\pi i t_C = \frac{1}{2\pi\alpha'}\int_C (J - iB), \qquad e^{-T_C} = q_C. \tag{XI.2.11}$$

For $B_C = 0$, T_C is positive and real. Its exponential is suppressed for a large curve. A source that writes $q_C = e^{-t_C^{\text{source}}}$ uses a variable of the T_C type, up to its stated normalization; its t_C^{source} is not the complex t_C of (XI.2.10). This is the translation needed when reading the local-limit formula of Katz, Klemm and Vafa.

A shift $B_C \mapsto B_C + 4\pi^2\alpha'$ sends $t_C \mapsto t_C + 1$ and $T_C \mapsto T_C - 2\pi i$. It therefore leaves $q_C = e^{-T_C}$ unchanged. For the base we write

$$A_b = \operatorname{Re} T_b = \frac{J_b}{2\pi\alpha'}, \qquad \theta_b = \frac{B_b}{2\pi\alpha'}, \qquad T_b = A_b - i\theta_b, \qquad Q_b = e^{-T_b} = e^{-A_b + i\theta_b}. \tag{XI.2.12}$$

The theta phase appears once. An expression $e^{-T_b + i\theta_b}$ would count it twice when T_b is complex. In the scale estimates we set $\theta_b = 0$; in instanton terms of degree n we restore its factor $e^{in\theta_b}$.

At $B_f = 0$, (XI.2.11) makes $J_f = 2\pi\alpha' T_f$. Substituting this into (XI.2.3) gives the promised relation

$$a_W = \frac{T_f M_s}{2\pi g_s}, \qquad \epsilon := \frac{2\pi g_s}{M_s}, \qquad T_f = \epsilon a_W. \tag{XI.2.13}$$

The dimensions are transparent: T_f and g_s are dimensionless, whereas a_W and M_s have mass dimension one, so ϵ has length dimension. The source's schematic $t_f \sim \epsilon a$ becomes an equality in these declared variables. Another choice of electric charge normalization would rescale a period and the inverse charge used to represent the same state, leaving the physical mass a_W unchanged. It would not change the fourth power of the local trajectory.

As a check, take fixed $g_s = 1/2$, $a_W = 1$ in an arbitrary mass unit, and $M_s = 100$ in the same unit. Then $\epsilon = \pi/100$ in inverse mass units and $T_f = \pi/100$. The fiber worldsheet weight is $Q_f = e^{-\pi/100}$, close to one, while the wrapped D2 mass remains exactly the chosen unit in the normalization of (XI.2.13). The example does not assign a macroscopic radius to the fiber: it only tracks its BPS mass and its dimensionless action.

The fiber B period is part of the limit, not an optional decoration. At nonzero B_f, write $T_f = A_f - i\theta_f$ with $A_f = J_f/(2\pi\alpha')$ and $\theta_f = B_f/(2\pi\alpha')$. If $A_f \to 0$ while θ_f approaches a fixed value not equal to zero modulo 2π, then

$$Q_f = e^{-A_f + i\theta_f} \longrightarrow e^{i\theta_f}, \qquad |1 - Q_f| \longrightarrow |1 - e^{i\theta_f}| > 0. \tag{XI.2.14}$$

The fiber pole used in the instanton calculation would not appear. For example, $\theta_f = \pi$ sends $Q_f \to -1$, whereas the desired limit has $Q_f \to 1$. We choose the zero-period branch and scale the fiber action to zero there. This is also the branch on which the selected wrapped-D2 central charge can vanish at the enhancement point. A different flux or charge frame would need its own translation; it cannot be inferred from the area limit alone.

This example clarifies the distinct jobs of B and J. J_f sets the positive exponential suppression and the wrapped-brane area in our chosen frame. B_f gives a phase in the worldsheet weight and can obstruct the $Q_f \to 1$ singular limit unless it is tuned. The base B_b instead survives as the four-dimensional instanton phase even while its real action grows. Keeping both parts of the complexified Kähler parameter visible prevents a misleading statement that "both areas are taken to zero or infinity" fully specifies the limit.

The inverse complex-coordinate map is equally practical. If a worldsheet weight has been specified as $q_C = e^{-A_C + i\theta_C}$ on a chosen branch, then

$$t_C = \frac{\theta_C}{2\pi} + i\frac{A_C}{2\pi}, \qquad J_C = 2\pi\alpha' A_C, \qquad B_C = 2\pi\alpha'\theta_C. \tag{XI.2.15}$$

The branch ambiguity $\theta_C \mapsto \theta_C + 2\pi k$ is exactly the integer shift of t_C. Thus the phase determines B_C modulo its period; it does not determine a unique real representative of B_C. A fixed angle and a fixed physical B period are also different instructions when α' changes.

For the base trajectory we hold θ_b fixed. Its representative physical period then shrinks with the regulator,

$$B_b = \frac{2\pi\theta_b}{M_s^2}, \qquad \operatorname{Re} t_b = \frac{\theta_b}{2\pi}, \qquad \operatorname{Im} t_b = \frac{A_b}{2\pi} \longrightarrow \infty. \tag{XI.2.16}$$

The diminishing physical period has a finite effect because a wrapped worldsheet measures B_b/α'. This is how a finite instanton angle survives while the base shrinks in physical units. For the fiber at $B_f = 0$, the corresponding trajectory goes toward the origin of the chosen complex coordinate:

$$t_f = i\frac{g_s a_W}{M_s}, \qquad T_f = \epsilon a_W \to 0, \qquad Q_f \to 1. \tag{XI.2.17}$$

The two paths approach different boundaries of Kähler parameter space. They are not specified by a common instruction to shrink all physical periods. The action and the phase must each be tracked in units of α'.

To make the branch sensitivity quantitative without changing the BPS mass convention, consider only the worldsheet weight along a path $\theta_f = \nu\epsilon a_W$, with fixed real ν. Its small-action behavior would be

$$T_f^{\text{complex}} = (1 - i\nu)\epsilon a_W, \qquad \frac{1 - Q_f}{\epsilon a_W} \longrightarrow 1 - i\nu. \tag{XI.2.18}$$

A fourth-order fiber pole would retain a factor $(1 - i\nu)^{-4}$. This calculation concerns the complex worldsheet coordinate; assigning a physical charged-particle mass away from the zero-period branch requires the corresponding central-charge map. Our mass trajectory continues to use $\nu = 0$. The exercise shows why tuning a phase merely to zero, without specifying its rate relative to the area, does not automatically reproduce the same complex limiting coupling.

XI.2.4 Why the base has a fourth-power trajectory

An asymptotically free four-dimensional theory remembers its strong scale even when its ultraviolet coupling tends to zero. For pure $\mathcal{N} = 2$ $SU(2)$, decompose the vector multiplet into an $\mathcal{N} = 1$ vector and an adjoint chiral multiplet. In a convention where $C_A = h^\vee = 2$, their one-loop contributions give

$$b_0 = 3C_A - T(\text{adj}) = 3(2) - 2 = 4. \tag{XI.2.19}$$

There are no hypermultiplets in this example. In a pure four-dimensional regime, with $\tau = \theta/(2\pi) + 4\pi i/g_4^2$, the leading running is

$$\frac{8\pi^2}{g_4^2(\mu)} = 4\log\frac{\mu}{\Lambda} + \text{finite scheme term}, \qquad \mu \gg \Lambda. \tag{XI.2.20}$$

A unit gauge instanton carries the familiar exponential $e^{-8\pi^2/g_4^2+i\theta}$, so the exponent four is the natural scale power of its weight. Equation (XI.2.20) is a four-dimensional statement at scales where unwanted KK modes have already left the effective theory.

The geometric base weight is $Q_b = e^{-A_b+i\theta_b}$. The local construction calibrates a unit base wrapping to a unit gauge instanton. With that dictionary, the trajectory proposed for the field-theory limit is

$$Q_b = Ce^{i\theta_b}(\epsilon\Lambda)^4, \qquad T_f = \epsilon a_W, \qquad \epsilon \to 0, \tag{XI.2.21}$$

where C is a finite nonzero real matching factor. It can be shifted by a finite definition of Λ; it cannot hide a different power of ϵ. This is a calibrated geometric trajectory: pure four-dimensional running does not by itself cross the base KK threshold. Set $x := M_s/M_0$ with a fixed reference mass M_0. In the real $B_b = 0$ slice,

$$A_b = -\log|Q_b| = 4\log\frac{1}{\epsilon\Lambda} - \log C = 4\log\frac{M_s}{2\pi g_s\Lambda} - \log C. \tag{XI.2.22}$$

Thus A_b grows only logarithmically while T_f falls linearly with $1/M_s$. This correlated pair is the content of the local limit.

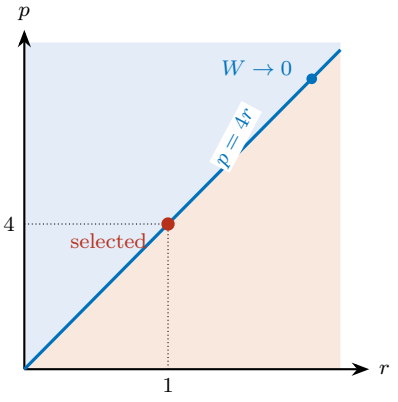
One can see why the power must be four before calculating any instanton coefficient. The leading one-instanton correction to a dimensionless gauge coupling has the form Λ^4/a_W^4, up to the normalization of the Coulomb variable. The geometric expression that can produce it is

$$\frac{Q_b}{T_f^4} = Ce^{i\theta_b}\left(\frac{\Lambda}{a_W}\right)^4. \tag{XI.2.23}$$

If one instead used $Q_b \propto \epsilon^p$ with the same $T_f = \epsilon a_W$, the ratio would scale as ϵ^{p-4}. For $p = 3$ it diverges; for $p = 5$ it vanishes. The two wrong limits lose the finite one-instanton coupling in opposite ways. The same reasoning gives $Q_b^n/T_f^{4n} \to C^n e^{in\theta_b}(\Lambda/a_W)^{4n}$ at each fixed instanton number n.

The power count can be turned into a diagnostic for any proposed trajectory. Suppose a candidate takes $T_f \propto \epsilon^r$ and $|Q_b| \propto \epsilon^p$, with positive exponents. The coupling ratio scales as ϵ^{p-4r}, so its finite nonzero locus is the line $p = 4r$. But that line alone is

not enough: from (XI.2.13) the wrapped-D2 mass behaves as $M_W \propto M_s T_f \propto \epsilon^{r-1}$ at fixed g_s. Keeping a nonzero finite W mass forces $r = 1$ and therefore $p = 4$. A point such as $(r, p) = (2, 8)$ lies on the finite-instanton line but sends the W mass to zero; $(r, p) = (1, 8)$ keeps the W finite but erases the one-instanton term. The selected point is the intersection of two independent requirements, not merely a dimensional guess.



Above $p = 4r$: the fixed-order instanton term vanishes.

At $(1, 4)$: finite W mass and finite instanton ratio.

Below $p = 4r$: the same ratio diverges.

Figure XI.2.1: A proposed scaling $T_f \propto \epsilon^r$ and $|Q_b| \propto \epsilon^p$ retains a finite fixed-order gauge-coupling instanton only on $p = 4r$. A finite nonzero wrapped-D2 W mass requires $r = 1$, selecting $(r, p) = (1, 4)$. Above the line the instanton vanishes; below it the term diverges. This power test does not supply the geometric unit-instanton matching premise.

There is a necessary matching qualification. The base radius calculated in Section XI.2.5 produces a KK threshold below M_s. One must not run the pure four-dimensional beta function in (XI.2.20) all the way to M_s and then declare $A_b = 8\pi^2/g_4^2(M_s)$ by algebra alone. For example, evaluating the pure-four-dimensional logarithm at a base KK scale proportional to $M_s/\sqrt{\log x}$ changes it by $-2 \log\log x$ relative to evaluation at M_s. That is not a finite scheme constant. The unit-instanton dictionary and its threshold matching are physical inputs to the geometric trajectory. The beta coefficient explains the fourth power in the four-dimensional theory; it does not compute the complete string threshold matching.

It is instructive to isolate the mismatch algebraically. Write the controlled base estimate as $M_{KK,b} = \kappa M_s/\sqrt{\log x}$, where κ tends to a nonzero constant. Pure four-dimensional running evaluated just below that threshold would give

$$q_{4d}(M_{KK,b}) \propto \left(\frac{\Lambda}{M_{KK,b}}\right)^4 \asymp \frac{(\log x)^2}{\kappa^4} \left(\frac{\Lambda}{M_s}\right)^4 . \tag{XI.2.24}$$

By contrast the geometric trajectory has $|Q_b| \propto (\Lambda/M_s)^4$ at fixed g_s. Equating these two expressions without a threshold factor would leave an unwanted $(\log x)^2$. No finite constant C removes it. The local string calculation must be read as supplying a matching prescription across the KK regime, not as a derivation from (XI.2.20) alone.

This is why the phrase "the base area is the bare gauge coupling" is useful at the level of roles but insufficient as a normalized equality.

A compact way to use the result is to keep three levels visible: $\mathcal{N} = 2$ field content fixes b_0; the local construction maps base wrapping to instanton number; and the matching prescription selects the fourth-power Q_b trajectory. Confusing these levels would make a formal scale identity appear to prove more than it does.

For actual calculations it helps to separate the regulator from the physical ratio that controls the instanton expansion. At a chosen nonzero Coulomb mass define

$$\delta := \epsilon a_W, \qquad \rho := \frac{\Lambda}{a_W}, \qquad T_f = \delta, \qquad |Q_b| = C\rho^4\delta^4. \tag{XI.2.25}$$

Taking the field-theory limit decreases δ while holding ρ fixed. Choosing a weakly coupled Coulomb point instead decreases ρ. These are independent operations. In particular, sending the string scale to infinity does not force a_W/Λ to infinity. The coefficient-by-coefficient instanton limit below can be studied at fixed ρ without asserting convergence at every such point.

The base remains in its positive-area chamber when

$$A_b = -\log(C\rho^4\delta^4) > 0 \quad \Longleftrightarrow \quad \delta < C^{-1/4}\rho^{-1}. \tag{XI.2.26}$$

At fixed positive finite C, ρ, this condition holds for sufficiently small δ. It is a condition on a finite representative of the trajectory, rather than an extra exponent in its asymptotic law. For $C = 1$, $\rho = 1/4$ and $\delta = 1/100$, one obtains

$$|Q_b| = (1/400)^4 = 3.90625 \times 10^{-11}, \qquad A_b = 4\log 400 \simeq 23.9659, \qquad \frac{Q_b}{T_f^4} = \frac{e^{i\theta_b}}{256}. \tag{XI.2.27}$$

Reducing δ by a factor ten makes the base weight smaller by 10^4 and the leading fiber pole larger by the same factor. The instanton ratio stays fixed. This is a useful finite-cutoff test: small Q_b alone says little about the retained correction.

Now change the physical input to $a'_W = 2a_W$ while keeping $M_s, g_s, \Lambda, C, \theta_b$ fixed. The geometry of the base is unchanged, but the fiber area doubles. The variables in (XI.2.25) become

$$\delta' = 2\delta, \qquad \rho' = \rho/2, \qquad Q'_b = Q_b, \qquad \frac{Q'_b}{T_f'^4} = \frac{1}{16}\frac{Q_b}{T_f^4}. \tag{XI.2.28}$$

The factor $1/16$ is the physical suppression of the leading instanton coupling further out on the Coulomb branch. Alternatively, doubling Λ at fixed a_W multiplies Q_b and that ratio by 16 and reduces A_b by $4\log 2$. These changes follow from the same trajectory; none can be absorbed by changing the cutoff alone.

XI.2.5 The hierarchy of masses

The base is large in string units but small in physical units. At fixed g_s, a_W, Λ and with $x = M_s/M_0 \to \infty$ as defined above, equations (XI.2.13) and (XI.2.22) give

$$T_f \asymp M_s^{-1}, \qquad A_b \asymp 4\log x, \qquad J_f = 2\pi\alpha' T_f \asymp M_s^{-3}, \qquad J_b = 2\pi\alpha' A_b \asymp \frac{\log x}{M_s^2}. \tag{XI.2.29}$$

The symbols $\asymp$ here suppress finite positive factors, not a change of power. In particular, J_b tends to zero as a physical area even though $A_b = J_b/(2\pi\alpha')$ diverges. This is possible because α' goes to zero faster than J_b.

If the base has a controlled ordinary metric with a single radius scale, its physical radius obeys $R_b \asymp \sqrt{J_b}$ up to the shape-dependent factor of order one. Its KK threshold is therefore

$$\frac{R_b}{\ell_s} \asymp \sqrt{\log x} \to \infty, \qquad R_b \asymp \frac{\sqrt{\log x}}{M_s} \to 0, \qquad M_{KK,b} \asymp \frac{M_s}{\sqrt{\log x}} \to \infty, \qquad \ell_s = \sqrt{\alpha'}. \tag{XI.2.30}$$

For any fixed finite a_W and Λ, this gives $a_W, \Lambda \ll M_{KK,b} \ll M_s$ at sufficiently large x. The base KK tower leaves the finite-energy gauge sector while remaining below the string oscillator scale. This is precisely the ordering that made the threshold qualification in the previous section necessary.

Other simple scales can be read from their tensions. A D2-brane wrapping the base has

$$M_{D2,b} = \frac{A_b M_s}{2\pi g_s} \asymp \frac{M_s \log x}{g_s} \to \infty, \qquad M_{D0} \asymp \frac{M_s}{g_s} \to \infty, \qquad M_{\rm osc} \asymp M_s \to \infty. \tag{XI.2.31}$$

The ratio of the base-wrapped D2 mass to the first base KK scale is

$$\frac{M_{D2,b}}{M_{KK,b}} \asymp \frac{(\log x)^{3/2}}{g_s}, \qquad \frac{M_{\rm osc}}{M_{KK,b}} \asymp \sqrt{\log x}. \tag{XI.2.32}$$

Both ratios diverge. A brane wrapping the base and a mode moving on the base therefore leave at different rates, despite referring to the same sphere. These comparisons use a fixed nonzero g_s and one string-frame mass unit. Letting g_s run would require a new correlated analysis; the present trajectory has no need for that extra freedom. Higher wrapped branes and winding sectors require the same kind of charge-by-charge check if a proposed completion brings them near finite energy.

The fiber behaves differently from the base. Its radius would be below ℓ_s if one assigned it a naive smooth-sphere area scale: $R_f/\ell_s \asymp \sqrt{T_f} \to 0$. The formula $M_{KK,f} \sim 1/R_f$ is not a reliable semiclassical spectrum calculation there. The relevant finite object is the wrapped D2 state whose BPS mass was fixed in (XI.2.13). The claim that no additional unwanted finite-energy states appear is a condition on the local singularity and its spectrum, not a deduction from the inverse-radius formula. In particular, the local A_1 enhancement and the pure-gauge content are part of the physical construction.

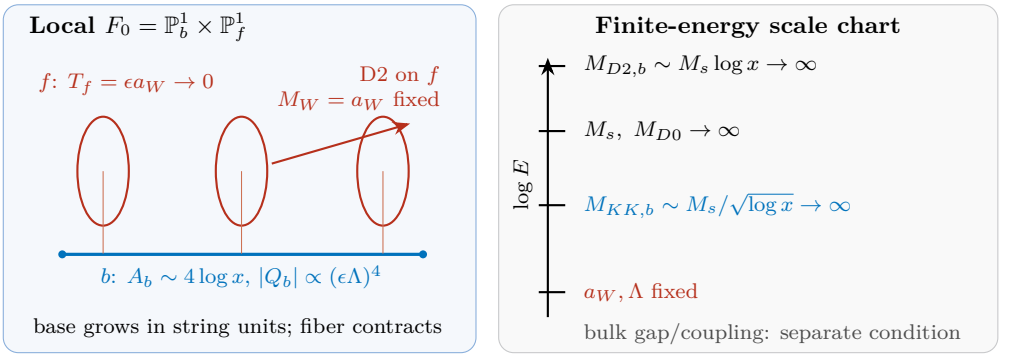


Figure XI.2.2: The two roles of local F_0 and the resulting mass hierarchy. The horizontal base line is a schematic projection of $\mathbb{P}^1_b$. The fiber f contracts in string units and retains the wrapped-D2 W mass; the base b grows logarithmically in string units but its physical KK threshold rises. The right-hand scale chart is asymptotic, not drawn to metric scale. The bulk/gravity condition requires the separate completion or boundary assumptions described in the text.

The figure makes the point that one geometric word, "large," can refer to two distinct ratios. $A_b \to \infty$ means the base is large relative to α' and suppresses a fundamental worldsheet wrapping. It does not mean that the physical base radius stays large. The latter shrinks, so its ordinary KK excitations become heavy in the field-theory mass unit. The fiber does the converse job: its worldsheet weight tends to one, and the wrapped D2 remains at finite mass.

A more explicit base metric is useful for testing these estimates. Assume, only for this illustration, that the base is a round sphere of radius R_b and area $J_b = 4\pi R_b^2$. Define the characteristic inverse radius $\widehat{M}_{KK,b} := 1/R_b$; exact spherical harmonic eigenmasses supply fixed factors such as $\sqrt{\ell(\ell+1)}$. Then

$$R_b = \frac{1}{M_s}\sqrt{\frac{A_b}{2}}, \qquad \widehat{M}_{KK,b} = M_s\sqrt{\frac{2}{A_b}}, \qquad \frac{R_b}{\ell_s} = \sqrt{\frac{A_b}{2}}. \tag{XI.2.33}$$

The same A_b increases the radius in string units and decreases the KK threshold relative to M_s. Yet the threshold relative to the retained mass increases because M_s/a_W grows more rapidly:

$$\frac{\widehat{M}_{KK,b}}{a_W} = \frac{2\pi g_s}{\delta}\sqrt{\frac{2}{A_b}}, \qquad \frac{M_s}{a_W} = \frac{2\pi g_s}{\delta}, \qquad \frac{M_{D2,b}}{a_W} = \frac{A_b}{\delta}. \tag{XI.2.34}$$

These ratios test decoupling by increasing masses. For states removed in this way, each mass must become large relative to a fixed external gauge-theory energy, not merely relative to another regulator-dependent scale. Vanishing couplings provide a separate route, discussed below.

For an illustrative numerical path choose mass units with $a_W = 1$, and set $\Lambda = 1/4$, $g_s = 1/(2\pi)$ and $C = 1$. In this case $\epsilon = 1/M_s$, $\delta = 1/M_s$ and $A_b = 4\log(4M_s)$. The round-base formulas give

M_s	T_f	A_b	R_b/ℓ_s	$\widehat{M}_{KK,b}$	$M_{D2,b}$
100	0.01	23.9659	3.4616	28.888	2396.59
1000	0.001	33.1762	4.0728	245.528	33176.2

(XI.2.35)

The base grows by a modest factor in string radii while its physical radius falls and its KK mass rises. The string scale rises by ten, whereas the KK scale rises by about 8.5. This slower growth is still sufficient to remove the KK tower at fixed external energy. The table uses a chosen ordinary metric to illustrate the conditional hierarchy; it does not approximate the contracting fiber by a smooth round sphere.

Another instructive ratio compares the two physical curve areas:

$$\frac{J_b}{J_f} = \frac{A_b}{T_f} = \frac{A_b}{\delta} \longrightarrow \infty, \qquad J_b \to 0, \qquad J_f \to 0. \tag{XI.2.36}$$

Both physical areas shrink, but the base is much larger than the fiber. Its ordinary metric description improves relative to the string length, while the fiber is described by the protected singularity physics. This difference is why the two curves require different spectrum arguments even though their intersection data are symmetric.

What about gravity? If the local neighborhood is embedded in a compact six-dimensional internal space of volume V_6, define its dimensionless volume $v_6 = V_6/\ell_s^6$. The parametric four-dimensional Planck relation is

$$M_{\mathrm{Pl},4}^2 \asymp \frac{V_6}{g_s^2 \alpha'^4} = \frac{v_6 M_s^2}{g_s^2}. \tag{XI.2.37}$$

At fixed g_s, the required condition is $v_6 M_s^2 \to \infty$. A positive lower bound on v_6 is sufficient, but it is not necessary. This formula depends on a compact completion and a common frame; the noncompact local model by itself has no finite four-dimensional Planck mass to compute.

The Planck condition is also insufficient to remove every bulk state. Suppose a compact completion has a bulk radius that remains fixed in physical units while $M_s \to \infty$. Its KK mass $1/R_{\mathrm{bulk}}$ stays finite even if (XI.2.37) diverges. If that mode couples to the local gauge sector with a nonvanishing strength, it can affect a finite-energy observable. More generally, a fixed positive spectral gap is not decoupling: exchange of a field of mass m_0 and coupling h contains, in a simple Euclidean exchange model,

$$\mathcal{A}_{\mathrm{bulk}}(p) \propto \frac{h^2}{p^2 + m_0^2}, \qquad \lim_{M_s \to \infty} \frac{h_0^2}{p^2 + m_0^2} = \frac{h_0^2}{p^2 + m_0^2} \neq 0 \tag{XI.2.38}$$

when $h_0 \neq 0$ and m_0 remain fixed. The unwanted effect disappears if its gap tends to infinity at bounded coupling, or its coupling tends to zero at fixed gap. The Planck formula alone imposes neither change. The same question applies to possible bulk zero modes or continua in a noncompact formulation. Noncompactness can remove a

normalizable four-dimensional graviton under appropriate boundary conditions; it does not settle their couplings automatically.

The exchange test can also distinguish a vanishing coupling from a large gap. To keep this statement within the same simple exchange model, take a fixed nonzero Euclidean momentum p, and suppose

$$m(x) = m_0 x^r, \qquad h(x) = h_0 x^{-u}, \qquad \mathcal{A}(x;p) \propto \frac{h_0^2 x^{-2u}}{p^2 + m_0^2 x^{2r}}. \tag{XI.2.39}$$

For $r > 0$, the denominator is asymptotically the mass term, giving $\mathcal{A} \propto x^{-2(u+r)}$. At bounded coupling, $u \geq 0$, this tends to zero. For $r = 0$, it tends to zero precisely when the coupling does, $u > 0$. If $r < 0$, the mass falls to zero; at the stated nonzero momentum the denominator tends to p^2, and $u > 0$ again suppresses the exchange:

$$\mathcal{A}(x;p) \asymp \begin{cases} (h_0^2/m_0^2) x^{-2(u+r)}, & r > 0, \\ [h_0^2/(p^2 + m_0^2)] x^{-2u}, & r = 0, \\ (h_0^2/p^2) x^{-2u}, & r < 0. \end{cases} \tag{XI.2.40}$$

For instance, $(r, u) = (-1, 1)$ gives a light mode whose exchange at this fixed momentum vanishes, whereas $(-1, 0)$ leaves a finite exchange. The zero-momentum limit of a massless field needs separate infrared care. This calculation tests one mode; a tower or continuum also requires control of its summed spectral weight. It explains the two mechanisms allowed in the decoupling condition without inferring them from the Planck scale.

Thus the local trajectory supplies a calculable base/string hierarchy and a finite charged gauge sector. A fully decoupled four-dimensional theory requires a compatible completion or local boundary prescription that also controls the gravitational and bulk spectrum. This condition is a part of the construction, not a conclusion smuggled into the word "local."

XI.2.6 Why a vanishing worldsheet weight can leave a finite instanton

The base weight Q_b tends to zero. If it occurred only as an ordinary power series with coefficients bounded as $T_f \to 0$, every nonzero base degree would disappear. The fiber degeneration changes that conclusion. Its worldsheet sums develop poles in T_f, and the fourth-power base scaling can cancel them. This is the local mechanism by which the four-dimensional instanton expansion remains visible after the string scale has gone to infinity.

First, why does base degree count gauge instanton number? In the six-dimensional type-IIA setup, a field equation relates the dual three-form flux to gauge and gravitational characteristic densities. Suppressing normalization conventions, the relation used by Katz, Klemm and Vafa has the structure

$$d\big[*\big(e^{-2\phi} H\big)\big] \;\sim\; \operatorname{tr} R \wedge R - \operatorname{tr} F \wedge F. \tag{XI.2.41}$$

A worldsheet wrapped n times around the base is pointlike in the remaining four dimensions. Surround that point by an S^3. The integral of the left-hand flux counts the wrapping number n; through the gauge term on the right it supplies instanton number n in the local gauge sector. The gravitational term is omitted only in the decoupling regime where its effect on the selected gauge observable has disappeared. The equation establishes the charge-matching picture in the stated setup; it does not, by itself, calculate every threshold or prove the existence of a global compact completion.

The quantitative question is whether a term with fixed n survives when $Q_b \to 0$. Let $d_{n,m}$ denote the primitive worldsheet data at base degree n and fiber degree m. In the source's flat Kähler coordinates, the relevant instanton contribution to the second fiber derivative of the prepotential has the form

$$\mathcal{G}_f^{\mathrm{ws}} = \sum_{n,m} \sum_{k\geq 1} d_{n,m}\, m^2\, \frac{Q_b^{nk} Q_f^{mk}}{k}, \qquad Q_f = e^{-T_f} \quad (B_f = 0). \tag{XI.2.42}$$

We use $\mathcal{G}_f$ for this source-normalized coupling derivative. Its numerical conversion to a chosen physical τ involves the normalization of the Coulomb coordinate and the usual polynomial ambiguity of a prepotential. The factor m^2 is essential: two fiber derivatives insert two powers of fiber degree. Without it the pole order would be wrong.

The degree weight and the cover factor can be reconstructed directly. For this purpose introduce the dimensionless worldsheet prepotential sum whose second fiber derivative is used above:

$$\mathcal{F}^{\mathrm{ws}}(T_b, T_f) = \sum_{n,m} d_{n,m}\, \mathrm{Li}_3(Q_b^n Q_f^m) = \sum_{n,m} \sum_{k\geq 1} d_{n,m} \frac{e^{-k(nT_b + mT_f)}}{k^3}. \tag{XI.2.43}$$

At positive real actions the derivative can first be taken in a region where these series converge. One fiber derivative brings down $-km$; the second brings a second such factor. Thus

$$\partial_{T_f} \frac{e^{-k(nT_b+mT_f)}}{k^3} = -\frac{m}{k^2} e^{-k(nT_b+mT_f)}, \qquad \partial_{T_f}^2 \frac{e^{-k(nT_b+mT_f)}}{k^3} = \frac{m^2}{k} e^{-k(nT_b+mT_f)}. \tag{XI.2.44}$$

This recovers (XI.2.42). Taking a field-theory limit of this derivative is a different operation from taking a limit of $\mathcal{F}^{\mathrm{ws}}$ itself. In particular, a pole of order four in the coupling sum cannot be assigned to the undifferentiated prepotential. The Coulomb-coordinate conversion must also be supplied when a physical prepotential is wanted.

The term with no base wrapping is a useful warm-up. The local F_0 data have $d_{0,1} = -2$ and $d_{0,m} = 0$ for primitive $m > 1$. Summing the multicovers in (XI.2.42) gives

$$\mathcal{G}_{f,\mathrm{pert}}^{\mathrm{ws}} = -2 \sum_{k\geq 1} \frac{Q_f^k}{k} = 2\log(1 - Q_f) = 2\log(\epsilon a_W) + O(\epsilon a_W). \tag{XI.2.45}$$

For a fixed reference mass M_0, write $2\log(\epsilon a_W) = 2\log(\epsilon M_0) + 2\log(a_W/M_0)$. The first dimensionless logarithm diverges and is common to different finite Coulomb masses.

Taking a difference at a_W and a fixed reference mass $a_{W,0}$ removes it:

$$\lim_{\epsilon\to 0} 2\log\frac{1-e^{-\epsilon a_W}}{1-e^{-\epsilon a_{W,0}}} = 2\log\frac{a_W}{a_{W,0}}. \tag{XI.2.46}$$

This is the geometric logarithm behind the perturbative running. The displayed coefficient is in the source's fiber-coordinate normalization. Equation (XI.2.19) supplies the independently normalized four-dimensional beta coefficient; the two should not be identified without the electric-period map.

At one base wrapping, F_0 provides an explicit nontrivial check. Its primitive data are $d_{1,m}^{F_0} = -(2m+2)$ for positive fiber degree. The leading $k=1$ contribution to the coupling is

$$S_{F_0}(Q_f) := \sum_{m\geq 1} d_{1,m}^{F_0} m^2 Q_f^m = -2\sum_{m\geq 1}(m^3+m^2)Q_f^m \tag{XI.2.47}$$

$$= -\frac{4Q_f(1+2Q_f)}{(1-Q_f)^4}. \tag{XI.2.48}$$

The last equality follows from differentiating the geometric series. To reproduce the rational function, let $D_q = q\,d/dq$ and begin with $\sum_{m\geq 0} q^m = (1-q)^{-1}$ for $|q|<1$. Each application of D_q inserts one power of m:

$$\sum_{m\geq 1} mq^m = \frac{q}{(1-q)^2}, \qquad \sum_{m\geq 1} m^2 q^m = \frac{q(1+q)}{(1-q)^3}, \qquad \sum_{m\geq 1} m^3 q^m = \frac{q(1+4q+q^2)}{(1-q)^4}. \tag{XI.2.49}$$

Combining the last two with coefficient -2 gives (XI.2.47). Near $q=1$ their pole orders differ by one. The linear growth of $d_{1,m}$, multiplied by the m^2 from the derivatives, produces the fourth-order pole. Omitting those derivatives would give only a second-order pole, which the fourth-power Q_b trajectory would suppress completely.

Since $1-Q_f = \epsilon a_W + O(\epsilon^2)$, the base-weighted expression has a finite limit,

$$\lim_{\epsilon\to 0} Q_b S_{F_0}(Q_f) = -12Ce^{i\theta_b}\left(\frac{\Lambda}{a_W}\right)^4. \tag{XI.2.50}$$

The factor -12 is the coefficient in this source-normalized worldsheet coupling, not a declaration of the normalized first Seiberg–Witten prepotential coefficient. The lesson is the finite fourth-order pole cancellation. Setting $Q_b = 0$ before taking the fiber limit would miss it.

The exact expression also controls how the limit is approached. Set $z = T_f = \epsilon a_W > 0$ and expand the rational function at $q = e^{-z}$. Keeping the first finite-cutoff terms gives

$$z^4 S_{F_0}(e^{-z}) = -12 - 4z - \frac{z^4}{60} + O(z^5), \tag{XI.2.51}$$

so the calibrated one-base term is

$$Q_b S_{F_0}(e^{-\epsilon a_W}) = Ce^{i\theta_b}\left(\frac{\Lambda}{a_W}\right)^4\left[-12 - 4\epsilon a_W + O((\epsilon a_W)^4)\right]. \tag{XI.2.52}$$

For the earlier $\rho = 1/4$, $C = 1$, $\theta_b = 0$ example, $z = 0.01$ gives $z^4 S_{F_0} \simeq -12.0400000002$, whereas $z = 0.001$ gives -12.0040000000. The common limiting coefficient is already visible, and the leading error falls linearly with the regulator. These are corrections in the selected source coordinate, not a claim about a normalized physical higher-derivative interaction.

The divergent sum has a useful physical interpretation. At every fixed fiber degree m, the base-weighted term vanishes:

$$Q_b[-2(m^3 + m^2)]e^{-m\epsilon a_W} = O(\epsilon^4) \longrightarrow 0 \qquad (m \text{ fixed}). \tag{XI.2.53}$$

A fixed finite truncation of the fiber sum would therefore give zero. The surviving contribution comes from fiber degrees increasing as the fiber contracts. Write $y = mz$, so adjacent values of y are separated by z. Then

$$z^4 \sum_{m\geq 1} m^3 e^{-mz} = z \sum_{m\geq 1} (mz)^3 e^{-mz} \longrightarrow \int_0^\infty y^3 e^{-y}\, dy = 6. \tag{XI.2.54}$$

The function $y^3 e^{-y}$ peaks at $y = 3$. Thus the leading term samples degrees of order $m \sim 3/z$, rather than a fixed small set of curves. When z decreases from 0.01 to 0.001, this characteristic degree increases from about 300 to about 3000. The m^2 part of the sum has one fewer inverse power of z and supplies the $-4z$ correction. This explains the noncommuting operations: summing the fiber degrees before taking the limit captures an expanding range of curves that a fixed-degree limit removes.

For a fixed higher instanton number n, the same mechanism can be stated without claiming all coefficients. Suppose the primitive data have the large-m behavior found in the local calculation, $d_{n,m} \sim \gamma_n m^{4n-3}$. The m^2 in (XI.2.42) gives m^{4n-1}. A Riemann-sum limit then shows

$$\lim_{T_f\to 0^+} T_f^{4n} \sum_{m\geq 1} m^{4n-1} e^{-mT_f} = \int_0^\infty y^{4n-1} e^{-y}\, dy = \Gamma(4n). \tag{XI.2.55}$$

Consequently, at each fixed n,

$$Q_b^n \sum_m m^2 d_{n,m} Q_f^m \sim C^n e^{in\theta_b} \gamma_n \Gamma(4n) \left(\frac{\Lambda}{a_W}\right)^{4n}. \tag{XI.2.56}$$

Why was the $k = 1$ term sufficient in this fixed-n estimate despite the full sum in (XI.2.42)? For a fixed positive primitive base degree $n \geq 1$ and cover number k, the same Riemann-sum step gives

$$\frac{Q_b^{nk}}{k} \sum_m m^2 d_{n,m} e^{-kmT_f} \sim \frac{\gamma_n \Gamma(4n)}{k^{4n+1}} Q_b^{nk} T_f^{-4n} \propto \epsilon^{4n(k-1)}. \tag{XI.2.57}$$

For each fixed $n \geq 1$, every $k > 1$ term therefore vanishes in this scaling. At a fixed positive total base degree $N = nk \geq 1$, only finitely many divisors k occur, so this is a coefficient-by-coefficient statement. The $n = 0$ multicovers instead supply the perturbative logarithm in (XI.2.45); they are not suppressed by this positive-degree

argument. It does not establish convergence after summing over all $N \geq 1$. The distinction matters: a finite limit for each coefficient need not yield a convergent series at arbitrary Λ/a_W. One can see the distinction already at total base degree two. The coefficient of Q_b^2 receives both primitive degree $(n,k) = (2,1)$ and a double cover $(n,k) = (1,2)$. For the primitive degree-two data with the stated asymptotic growth, the scaling is

$$Q_b^2 \sum_m m^2 d_{2,m} e^{-mT_f} \sim \gamma_2 \Gamma(8) \frac{Q_b^2}{T_f^8} = \gamma_2 \Gamma(8) C^2 e^{2i\theta_b} \left(\frac{\Lambda}{a_W}\right)^8. \tag{XI.2.58}$$

The double cover uses degree-one primitive data, so its fiber pole is still fourth order. Its factor $1/k$ also remains:

$$\frac{Q_b^2}{2} \sum_m m^2 d_{1,m} e^{-2mT_f} \sim -\frac{12}{32} \frac{Q_b^2}{T_f^4} = -\frac{3}{8} C^2 e^{2i\theta_b} \epsilon^4 \frac{\Lambda^8}{a_W^4} \longrightarrow 0. \tag{XI.2.59}$$

Both terms have the same total base degree and theta phase. Their fiber singularities distinguish them. This example makes explicit why total instanton number alone does not determine the pole order of each intermediate multicover term.

This checks the powers and the phase of the surviving term. Determining the exact physical coupling in a specified electric frame still requires the period calculation of the later mirror chapter.

XI.2.7 Comparing F_0 and F_2

The surface F_2 gives a useful comparison because it is not globally the same ruled surface as F_0, while it can realize the same local pure-$SU(2)$ field-theory limit. Write s for its negative section and f for a fiber. Their intersections and canonical class are

$$s^2 = -2, \qquad s \cdot f = 1, \qquad f^2 = 0, \qquad K_{F_2} = -2s - 4f. \tag{XI.2.60}$$

The contracting fiber still has the local A_1 role. The section structure changes the coordinates in which a base area and the effective curve cone are described. In particular, the formal class $s + f$ has $(s+f)^2 = 0$ and $(s+f) \cdot f = 1$, so in the basis $(s+f, f)$ the intersection matrix resembles that of F_0. But $(s+f) \cdot s = -1$; this basis change does not identify the effective cones or the finite-area enumerative data. An intersection matrix by itself is too small a dictionary for a complete string compactification.

We can compare a more physical output without solving the full mirror problem. The explicit one-base-wrapping data in the local calculation are

$$d_{1,m}^{F_0} = -(2m+2), \qquad d_{1,m}^{F_2} = -2m. \tag{XI.2.61}$$

The data differ at every fixed m. Nevertheless, both have leading large-m behavior $-2m$, the part selected by the field-theory scaling. For F_2 the weighted sum is

$$S_{F_2}(Q_f) = -2 \sum_{m \geq 1} m^3 Q_f^m = -\frac{2Q_f(1 + 4Q_f + Q_f^2)}{(1-Q_f)^4}, \qquad \lim_{Q_f \to 1^-} (1-Q_f)^4 S_{F_2} = -12. \tag{XI.2.62}$$

Equation (XI.2.47) has the same leading coefficient. Subtracting the two exact sums makes the lost information visible:

$$S_{F_0}(q) - S_{F_2}(q) = -2\sum_{m\geq 1} m^2 q^m = -\frac{2q(1+q)}{(1-q)^3}. \tag{XI.2.63}$$

The difference has only a third-order pole. On the real fiber branch, $1-q \sim \epsilon a_W$, whereas $Q_b \sim \epsilon^4$. Consequently

$$Q_b\big[S_{F_0}(Q_f) - S_{F_2}(Q_f)\big] \sim -4Ce^{i\theta_b}\epsilon\frac{\Lambda^4}{a_W^3} \longrightarrow 0. \tag{XI.2.64}$$

For example, the first primitive fiber degree has values -4 and -2; that finite-degree discrepancy is real. The limit keeps the leading large-degree contribution while suppressing this lower pole. Thus the selected one-instanton coupling term agrees at leading order after the appropriate local-limit normalization, while the unscaled worldsheet counts do not. This is the level of comparison needed here. The full equality of engineered physical periods, including frame and finite-coordinate choices, belongs to the mirror calculation. No claim of a unique compact embedding or unique path through Kähler moduli space follows from these leading terms.

The exact sums quantify the information discarded by this limit. Their relative difference on the real fiber branch is

$$\frac{S_{F_0}(q) - S_{F_2}(q)}{S_{F_2}(q)} = \frac{1-q^2}{1+4q+q^2} = \frac{z}{3} + O(z^3), \qquad q = e^{-z}. \tag{XI.2.65}$$

At $z = 0.01$ the discrepancy is about one part in 300 even though the primitive $m = 1$ counts differ by a factor two. The sum at small z emphasizes large fiber degree; relative agreement of these sums therefore need not imply agreement of their first few coefficients.

Indeed, the finite-cutoff expansions are

$$\begin{aligned} z^4 S_{F_0}(e^{-z}) &= -12 - 4z - \frac{z^4}{60} + O(z^5), \\ z^4 S_{F_2}(e^{-z}) &= -12 - \frac{z^4}{60} + O(z^6). \end{aligned} \tag{XI.2.66}$$

The linear correction distinguishes the two realizations before the limit, while the limiting fourth-order residue agrees. The absence of a linear correction in the second expression follows from these specific degree-one data; it is not a statement about all corrections to a physical F_2 gauge coupling.

The geometric basis comparison can also be checked directly. With $u = s + f$ one finds

$$u^2 = s^2 + 2s\cdot f + f^2 = 0, \qquad u\cdot f = 1, \qquad K_{F_2} = -2u - 2f, \qquad u\cdot s = -1. \tag{XI.2.67}$$

The first three expressions have the F_0 form, yet the last detects the negative section of F_2. It prevents treating u as an interchangeable movable ruling of a product surface. The local limit has selected particular gauge observables and discarded some finite

geometric data. Agreement of those observables is therefore compatible with distinct effective cones and distinct finite-area curve counts.

The two examples also show what the word "pure" does and does not mean. The genus-zero base and the local singularity identify the intended four-dimensional gauge content. They do not forbid all massive matter or bulk states at finite string scale. The correlated limit sends the identified unwanted local scales away, and an environmental condition must handle the remaining coupled bulk sector. The resulting pure gauge theory is the finite-energy endpoint under those conditions.

XI.2.8 Exercises

The numerical and symbolic parts of these exercises have bounded domains given in the questions. Use `benchmark/tasks.json` to find the question IDs and `benchmark/PROTOCOL.md` for submission. A short physical explanation is also required where indicated; it is assessed as written reasoning rather than as a numerical field.

1. **A scaling that loses the instanton.** Let $Q_b = (\epsilon\Lambda)^p$ and $T_f = \epsilon a_W$ with $\epsilon \to 0^+$ and fixed positive a_W, Λ. Determine the unique $p > 0$ for which Q_b/T_f^4 has a finite nonzero limit. Calculate the ratio and classify the limits for $p = 3$ and $p = 5$. Explain in one sentence what each wrong power does to the one-instanton coupling. For the symbolic submission, use an expression defined for all positive a_W, Λ.

2. **Gravity and a bulk KK tower.** Set $x = M_s/M_0 \to \infty$ with fixed positive M_0, R_0, v_0, g_s. Suppose $A_b = c \log x$ for $c > 0$, while a hypothetical compact completion has $R_{\text{bulk}} = R_0 x^{-r}$ and $v_6 = v_0 x^{-s}$ for real r, s. Find the powers of x and $\log x$ in the base KK mass. Give the separate conditions on r and s for bulk KK masses and the Planck mass to diverge. Work through $(r, s) = (0, 0)$ and $(r, s) = (1/2, 3)$ and explain why neither "noncompact" nor "large Planck mass" replaces these two separate conditions. The power-law completion is a scale model, not an asserted explicit Calabi–Yau embedding.

3. **From area to mass and instanton phase.** Use $J_f = 4$, $B_f = 1$, $g_s = 1/2$, and $\alpha' = 2$ in a common unit system. Compute the real and imaginary parts of the house t_f, the source-style $T_f = -2\pi i t_f$, and $Q_f = e^{-T_f}$. Repeat Q_f after $B_f \mapsto B_f + 4\pi^2\alpha'$, and compute the wrapped-D2 mass at $B_f = 0$. Explain why the phase is periodic while the mass formula contains $1/g_s$. The machine-checking domain is $0.1 \le J_f, g_s, \alpha' \le 10$, $|B_f| \le 10$, and $J_f/\alpha' \le 20$; the shifted B_f need not lie in that input interval.

4. **Two surfaces, one leading limit.** In the ordered bases (b, f) for F_0 and (s, f) for F_2, write both intersection matrices, identify the class of self- intersection -2, and name the contracting A_1 fiber. Verify the common pure-$SU(2)$ beta coefficient. Using (XI.2.61), decide whether the unscaled one-instanton data agree and compute their leading m coefficient as part of the written calculation. Explain why this comparison supports a common local-limit behavior without proving equality of the finite-volume theories.

Written transfer practice. The following tasks extend the reasoning above and do not add numerical fields to the preceding four questions.

1. At fixed M_s, g_s, C, θ_b, change a_W by a factor 3 and Λ by a factor 2. Track J_f, T_f, Q_b, A_b and the limiting one-instanton coupling. Explain which changes move a physical gauge parameter and which could be produced by raising the cutoff alone.

2. For the ordinary round-base model, start with the numerical path in (XI.2.35) and derive the ratio of the KK thresholds at M_s and $10M_s$ without treating A_b as constant. Explain why a decreasing ratio $M_{KK,b}/M_s$ is compatible with $M_{KK,b}/a_W \to \infty$.

3. Derive (XI.2.49) using D_q. Then compare a fiber sum truncated at a fixed $m_{\max}$ with one whose cutoff is $m_{\max} = \lfloor L/T_f \rfloor$ for fixed $L > 0$. Show which finite part of the fourth-order residue this keeps, then explain why taking $L \to \infty$ recovers the full residue. Identify the missing large-degree window for a fixed cutoff.

4. Use the fixed-total-degree-two example to compare the roles of n, k and $N = nk$. State which terms vanish and which may survive, and explain why this argument cannot establish convergence of the sum over every instanton number.

Status and sources

The local construction and source-native scaling are those of (Katz et al. 1997, Secs. 2–3, Eq. (2.1)). The source identifies the wrapped D2 orientations with the W pair, relates base area to a bare gauge coupling, and argues for the base-wrapping/gauge-instanton map with its six-dimensional flux equation. These are physical inputs to the local engineering dictionary. The conversion $T = -2\pi i t$, the displayed D2 tension factors, the correlated power limits, and the base KK hierarchy are calculations in the conventions stated here. Continuation of the wrapped BPS mass into the sub-stringy fiber region is assumed, rather than established by a classical radius estimate.

The one-loop coefficient $b_0 = 4$ follows from the declared pure $\mathcal{N} = 2$ $SU(2)$ field content. Identifying one base wrapping with a unit gauge instanton fixes the kind of matching needed for $Q_b \sim (\epsilon\Lambda)^4$. The source's schematic bare coupling does not determine the exact house-normalized coefficient across the base KK threshold. The threshold lies below M_s and prevents an unqualified use of pure-four-dimensional running up to the string scale. The finite matching constant and the physical electric-period normalization remain separate.

The worldsheet data and coupling sums in Section XI.2.6 come from (Katz et al. 1997, Sec. 5, Eqs. (5.1)–(5.2), pp. 12–15). Their fixed-instanton-number pole gives a controlled asymptotic statement, not convergence of the entire instanton series or a full Seiberg–Witten period solution. The F_0 Mori description appears before Eq. (4.11) of the same source; its F_2 intersection data and the explicit F_0/F_2 one-instanton formulas support the limited comparison in Section XI.2.7. The broad fiber-degree shift printed on p. 14 does not agree under a literal same-coordinate substitution with the explicit

formulas there. Its coordinate or range interpretation is left open and it is not needed for this chapter's comparison.

The base KK, string oscillator and base-wrapped D2 scales leave the finite-energy spectrum along the displayed trajectory, subject to a controlled base metric and the specified local light spectrum. A complete gravity and bulk-sector decoupling statement additionally requires a compact completion or noncompact boundary prescription for which unwanted coupled modes acquire an unbounded mass gap or vanishing coupling. Equation (XI.2.37) gives only the gravitational scale condition in a compact completion; noncompactness alone is not a substitute for the bulk condition. The local calculation does not select a unique completion.

The additional inverse parameter maps, finite-input comparisons, round-base illustration, single-mode exchange power test, degree-moment derivation and finite-T_f expansions are algebraic developments of those same inputs. The round-base calculation assumes its explicitly stated ordinary metric; the exchange calculation concerns a single mode at fixed nonzero Euclidean momentum. The phase-rate example concerns the worldsheet coordinate and does not assign a new nonzero-B_f physical mass formula. The degree-two cover example uses the same fixed-degree asymptotic premise as the general instanton estimate. No full-series convergence, new period normalization or new compact completion is inferred from these calculations.

The full local engineering and instanton-matching inputs carry [GEO-E]. The convention identities and the conditional scaling, series, and beta-coefficient calculations carry [MATH]; their physical starting assumptions remain as specified above. Isolation of gravity and every unwanted coupled sector carries [DEC].

References

Katz, S. H., A. Klemm, and C. Vafa (1997). "Geometric engineering of quantum field theories". In: *Nucl. Phys. B* 497, pp. 173–195. DOI: 10.1016/S0550-3213(97)00282-4. arXiv: hep-th/9609239.

Chapter XI.3

ADE fibrations and the gauge-sector dictionary

XI.3.1 What changes when the surface moves

A vanishing sphere in an ALE surface supplies a charged particle in the six-dimensional type IIA gauge theory. Suppose the same sphere is available at every point of a compact curve. A four-dimensional observer sees the zero modes of the particle fields along that curve. The question is then which zero modes survive. Knowing the intersection matrix of a single fiber answers the charge question, but it leaves this second question open.

We will carry out the reduction for a family of A_2 surfaces. Over the sphere the result is the local pure $\mathcal{N} = 2$ theory of algebra $\mathfrak{su}(3)$. The same A_2 surface times a flat elliptic curve, with periodic spinors and trivial holonomies, gives a vector and an adjoint hypermultiplet, making up $\mathcal{N} = 4$. The two base curves differ in their harmonic forms. We will see why the fields that become adjoint matter are sensitive to those forms, while the gauge field is sensitive to the volume of the base.

We use the type IIA ALE gauge effective theory and the local-limit distinction between a geometric period and a physical mass from the preceding chapters. We recall the few toric and cohomological facts needed in the calculation. The question here is the uniform gauge sector. A fiber that enhances only at an isolated point of the base requires a different calculation.

XI.3.2 An A2 surface over the sphere

How can we tell that a fiber singularity persists over an entire compact curve? A local equation at one point cannot distinguish a uniform family from one with exceptional fibers elsewhere. We will build a model with two charts that cover the base. On each chart the fan displays the same resolved surface, and the overlap identifies the two exceptional curves in the same order.

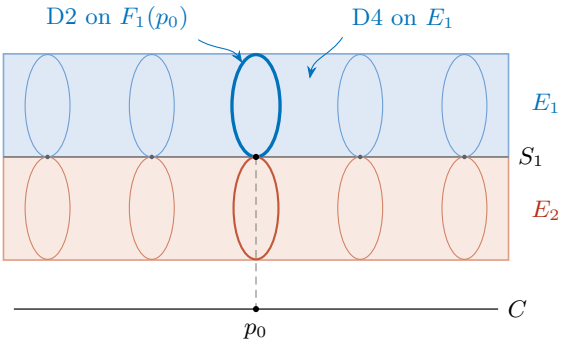


Figure XI.3.1: A schematic view of the two families of exceptional spheres. At each $p \in C$, the two spheres meet at one point. These points sweep out the section S_1, where the surfaces E_1 and E_2 meet. The blue sphere at p_0 supports an electric D2. A magnetic D4 wraps the whole blue surface E_1. The two-dimensional drawing represents fibers and their incidence, rather than an embedding of the surfaces.

Take the lattice $N = \mathbb{Z}^3$ and the rays generated by

$$v_\pm = (\pm 1, 0, 1), \qquad d_k = (0, k, 1), \qquad k = 0, 1, 2, 3. \tag{XI.3.1}$$

Here a ray is specified by its primitive lattice vector. Let D_k also denote the corresponding toric divisor, and write $E_1 = D_1$, $E_2 = D_2$. The six maximal cones, including their faces, are

$$\langle v_\pm, d_k, d_{k+1} \rangle, \qquad k = 0, 1, 2. \tag{XI.3.2}$$

To see that they fit together, intersect the cones with the plane of height one. The d_k lie on the segment from d_0 to d_3. Coning the three subsegments to v_+ and to v_- triangulates the triangle shown in Figure XI.3.2. Each determinant has magnitude one, as follows by replacing the last column by $d_{k+1} - d_k = (0, 1, 0)$. The cones are therefore smooth. Moreover the height functional takes the value one on every ray. The corresponding toric character has divisor the sum of the toric divisors, so the canonical class of this smooth threefold is trivial.

The map to the base is induced by the lattice projection

$$\pi_N(x, y, z) = x, \qquad \pi_N(v_\pm) = \pm 1, \qquad \pi_N(d_k) = 0. \tag{XI.3.3}$$

Over the positive base chart, the vector v_+ splits off from the vertical lattice $\ker \pi_N$, and the cones over that chart are products with the ray generated by v_+. The same argument on the negative chart uses v_-. In the vertical lattice the cone with endpoints d_0, d_3 has index three. Both endpoints have height one, and d_1, d_2 give its minimal smooth subdivision. This is the A_2 surface resolution. The two charts cover $\mathbb{P}^1$. On the overlap a torus translation preserves the toric divisors, so one globally labeled sphere F_i sweeps out each E_i. Removing the interior rays contracts the same pair over every base point. The labeling is split even though the total space is not a global product.

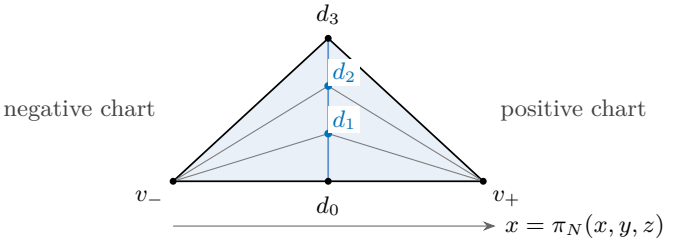


Figure XI.3.2: The plane of height one for the six cones in (XI.3.2). Blue points give the two interior rays of the resolved surface fan. The projection to the horizontal coordinate gives the two charts of the sphere.

We can make the overlap explicit. This also tells us what the nontrivial fibration changes. Let χ^m denote the torus character with exponent $m \in M = \mathrm{Hom}(N, \mathbb{Z})$; its order on a ray v is $\langle m, v\rangle$. On the dense torus, choose a base coordinate and two vertical coordinates by

$$z = \chi^{(1,0,0)}, \qquad u = \chi^{(0,1,0)}, \qquad h_+ = \chi^{(-1,0,1)}. \tag{XI.3.4}$$

The exponents of u, h_+ annihilate v_+. They are therefore fiber coordinates in the positive splitting. In the negative splitting use $w = \chi^{(-1,0,0)}$ and $h_- = \chi^{(1,0,1)}$. On the overlap of the base charts,

$$w = z^{-1}, \qquad u_- = u_+ = u, \qquad h_- = z^2 h_+. \tag{XI.3.5}$$

The torus coordinates need not themselves be regular at the exceptional curves. To reach those curves, use the dual basis to the three rays of each maximal cone. For the cone $\langle v_+, d_k, d_{k+1}\rangle$, the three regular affine coordinates are

$$z, \qquad x_{k,+} = \chi^{(-k-1,-1,k+1)} = u^{-1} h_+^{k+1}, \qquad y_{k,+} = \chi^{(k,1,-k)} = u h_+^{-k}. \tag{XI.3.6}$$

For example the exponent of $x_{k,+}$ pairs with (v_+, d_k, d_{k+1}) as $(0, 1, 0)$. Negative powers of u or h_+ in the torus expression consequently cause no singularity in this affine chart. The monomial is regular on the cone because all three pairings are nonnegative. The same construction with v_- gives coordinates $w, x_{k,-}, y_{k,-}$, and their overlap is

$$x_{k,-} = z^{2(k+1)} x_{k,+}, \qquad y_{k,-} = z^{-2k} y_{k,+}, \qquad x_{k,\pm} y_{k,\pm} = h_\pm. \tag{XI.3.7}$$

These are invertible coordinate changes whenever $z \neq 0$. They multiply each fiber coordinate by a nonzero number and never exchange its zero divisor. Thus the overlap transports each exceptional curve to itself even though it changes its normal coordinates.

For fixed k, the curve $x_{k,\pm} = y_{k,\pm} = 0$ is the section $S_k = D_k \cap D_{k+1}$ over the base. A normal coordinate for $\mathcal{O}(d)$ on $\mathbb{P}^1$ transforms as $\xi_- = z^{-d}\xi_+$. Hence the two normal degrees of this section in the threefold are

$$N_{S_k/X} = \mathcal{O}\big(-2(k+1)\big) \oplus \mathcal{O}(2k), \qquad \deg N_{S_k/X} = -2. \tag{XI.3.8}$$

Here the direct sum follows from the explicit diagonal transition of this toric model. The total degree is the same as $\deg K_{\mathbb{P}^1}$, as adjunction in a Calabi–Yau threefold requires. In particular the compact surfaces swept out by the exceptional curves need not be products with the base. We will see this twisting again in their magnetic volumes.

It is useful to retain the integral ray relations. In the order $(v_+, v_-, d_0, d_1, d_2, d_3)$, they are

$$\begin{pmatrix} 1 & 1 & -2 & 0 & 0 & 0 \\ 0 & 0 & 1 & -2 & 1 & 0 \\ 0 & 0 & 0 & 1 & -2 & 1 \end{pmatrix}. \tag{XI.3.9}$$

For example, $v_+ + v_- = 2d_0$ is a base relation, while the second and third rows use only vertical rays. To see that the rows generate all integral relations, first use the horizontal coordinate to equate the two coefficients of $v_\pm$, and subtract a multiple of the first row to remove both. Subtract multiples of the third and second rows in that order to remove the coefficients at d_3, d_2. Independence of d_0, d_1 then forces the remaining coefficients to vanish.

There is a useful way to use these relations without confusing them with electric charges. Introduce homogeneous coordinates $(p_+, p_-, x_0, x_1, x_2, x_3)$ for the six rays. A basis of their three quotient rescalings can be written

$$\begin{aligned} &(p_+, p_-, x_0, x_1, x_2, x_3) \\ &\quad \longmapsto (\rho_b p_+, \rho_b p_-, \rho_b^{-2}\rho_1 x_0, \rho_1^{-2}\rho_2 x_1, \rho_1\rho_2^{-2} x_2, \rho_2 x_3). \end{aligned} \tag{XI.3.10}$$

The stable open sets are those of the fan in (XI.3.2). This expression records its integral coordinate weights; it does not choose a different geometric phase. If V is the matrix of ray columns and Q the relation matrix, then

$$VQ^{\mathsf{T}} = 0, \qquad Q(1,1,1,1,1,1)^{\mathsf{T}} = 0, \qquad QV^{\mathsf{T}} m = 0. \tag{XI.3.11}$$

The last identity says that the monomial representing any torus character has zero quotient weight: its exponents on the homogeneous coordinates are $\langle m, v_a \rangle$. It explains why the affine coordinates just constructed descend through the quotient. The row sums vanish because all rays have height one. These three rows encode relations among six rays; the electric root sector instead has rank two and will use the compact divisor–fiber pairing.

In each fiber, $d_{i-1} + d_{i+1} = 2d_i$ gives self-intersection -2 for F_i, and the two adjacent spheres meet once. Restricting E_i to a fiber gives F_i, so the intersection needed by a particle wrapping that fiber is

$$E_i \cdot F_j = F_i \cdot F_j = -\mathsf{C}_{ij}, \qquad \mathsf{C} = \begin{pmatrix} 2 & -1 \\ -1 & 2 \end{pmatrix}. \tag{XI.3.12}$$

The first equality uses the geometry of the whole family; the last uses just one transverse surface. This is why the charge computation can begin with the ALE theory while the four-dimensional matter count will require information about the base.

XI.3.3 Electric charges and the two Coulomb parameters

A type IIA D2 can wrap a fiber curve and leave a worldline in the noncompact spacetime. To compute the charge of that worldline, choose two-form modes ω_i on the ALE fiber with unit periods, so $\int_{F_j} \omega_i = \delta_{ij}$. The reduction of the RR three-form contains the terms $A^i \wedge \omega_i$, where A^i are the unit-period gauge potentials. If the wrapped class is Σ, its coupling to the potentials is proportional to

$$\Sigma = \sum_j n_j F_j, \qquad \int_{\mathbb{R}_{\mathrm{wl}} \times \Sigma} C_3 = \sum_i n_i \int_{\mathbb{R}_{\mathrm{wl}}} A^i. \tag{XI.3.13}$$

A common RR charge normalization is understood in this equation. This frame makes the simple D2 charges unit vectors.

To compare with the gauge algebra, use the simple coroots $H_1 = \mathrm{diag}(1, -1, 0)$ and $H_2 = \mathrm{diag}(0, 1, -1)$. If A_H is the vector of components along these coroots, then

$$A = \mathsf{C} A_H, \qquad q = \mathsf{C} n, \qquad q_i = -E_i \cdot \Sigma. \tag{XI.3.14}$$

Indeed the unit-period kinetic form is C^{-1}. Applying the change of basis gives the trace form of the simple coroots:

$$\mathsf{C}^{\mathsf{T}} \mathsf{C}^{-1} \mathsf{C} = \mathsf{C}, \qquad \mathrm{Tr}_f \, H_i H_j = \mathsf{C}_{ij}. \tag{XI.3.15}$$

The sign of q relative to the divisor pairing is fixed here by the positive coroot convention. For an independent Lie algebra calculation, write $H_i = \mathrm{diag}(\alpha_i)$ where $\alpha_i = e_i - e_{i+1}$ and e_i is a standard basis vector. The matrix unit U_{jk} then obeys

$$[H_i, U_{jk}] = \big((\alpha_i)_j - (\alpha_i)_k\big) U_{jk}. \tag{XI.3.16}$$

For example U_{13} has charges $(1, 1)$, the sum of those of U_{12} and U_{23}. Its homology class is the chain $F_1 + F_2$. This describes one root charge; it does not require a third smooth exceptional sphere in the resolved fiber. The identification of these charged states as the ordinary ALE root sector is the same physical input as in the six-dimensional construction. Write a_i for the local central-charge period of the simple class F_i; the table uses the signed additive period $Z(\sum_i n_i F_i) = \sum_i n_i a_i$. The mass calibration is specified in (XI.3.17) below.

The two independent periods give two mass parameters. With vanishing fiber B in a common local lift, positive curve areas $A_{f,i}$, and no worldvolume flux, define

$$A_{f,i} = \int_{F_i} J, \qquad a_i = \tau_2 A_{f,i} = \frac{M_s}{g_s} \frac{A_{f,i}}{4\pi^2 \alpha'}, \qquad \tau_2 = \frac{1}{(2\pi)^2 g_s (\alpha')^{3/2}}. \tag{XI.3.17}$$

Here $M_s = 1/\sqrt{\alpha'}$. In the same phase convention the complex period is $a_i = (M_s/g_s) t_{F_i}/i$, where $t_{F_i} = \int_{F_i} (B + iJ)/(4\pi^2 \alpha')$. This local relation uses the ordinary charged-state continuation discussed for ALE spaces. Integer flux and large B transformations must be treated in the same common lift. These a_i measure simple-root

Root	D2 class	n	q	Z
α_1	F_1	$(1,0)$	$(2,-1)$	a_1
α_2	F_2	$(0,1)$	$(-1,2)$	a_2
$\alpha_1+\alpha_2$	F_1+F_2	$(1,1)$	$(1,1)$	a_1+a_2
$-\alpha_1$	$-F_1$	$(-1,0)$	$(-2,1)$	$-a_1$
$-\alpha_2$	$-F_2$	$(0,-1)$	$(1,-2)$	$-a_2$
$-\alpha_1-\alpha_2$	$-F_1-F_2$	$(-1,-1)$	$(-1,-1)$	$-a_1-a_2$

Table XI.3.1: The six oriented A_2 root classes. The charge is shown in the unit-period frame n and the coroot frame q. The final column is the local electric central charge in the chosen phase.

differences, without assigning an absolute normalization to an exact Seiberg–Witten period.

The same basis conversion must be made for the scalar in the gauge multiplet. Expand the traceless diagonal field in the coroot basis, $\Phi = \phi_H^1 H_1 + \phi_H^2 H_2$. Evaluating each simple root on Φ gives

$$\begin{pmatrix} a_1 \\ a_2 \end{pmatrix} = \mathsf{C} \begin{pmatrix} \phi_H^1 \\ \phi_H^2 \end{pmatrix}, \qquad \begin{pmatrix} \phi_H^1 \\ \phi_H^2 \end{pmatrix} = \frac{1}{3} \begin{pmatrix} 2 & 1 \\ 1 & 2 \end{pmatrix} \begin{pmatrix} a_1 \\ a_2 \end{pmatrix}. \tag{XI.3.18}$$

A state with unit-period coefficients n consequently has exactly the same central charge in either frame:

$$Z = n^{\mathsf{T}} a = (\mathsf{C}n)^{\mathsf{T}} \phi_H = q^{\mathsf{T}} \phi_H. \tag{XI.3.19}$$

Using q with the simple periods a would change the answer. For F_1, for instance, the correct coroot-frame expression is $2\phi_H^1 - \phi_H^2 = a_1$. This equality joins the charge normalization fixed by the RR coupling to the scalar normalization fixed by the D2 mass.

For an explicit comparison with the classical gauge theory, take $\Phi = \mathrm{diag}(\lambda_1, \lambda_2, \lambda_3)$ with $\mathrm{Tr}\,\Phi = 0$. A field proportional to U_{jk} sees the difference $\lambda_j - \lambda_k$. Thus

$$\lambda_1 - \lambda_2 = a_1, \qquad \lambda_2 - \lambda_3 = a_2, \qquad (\lambda_1, \lambda_2, \lambda_3) = \frac{1}{3}(2a_1 + a_2, -a_1 + a_2, -a_1 - 2a_2). \tag{XI.3.20}$$

If $a_1 = m$ and $a_2 = 2m$ with $m > 0$, the three positive root masses are $m, 2m, 3m$. Reversing an orientation reverses the central charge without changing the mass. Even at $a_1 = a_2 = m$ the first two charges are distinct. Their equality in mass does not give an unbroken nonabelian generator.

One can diagnose an enhancement without relying on a mass degeneracy. Keep $a_2 = 2m$ fixed and send $a_1 = \delta$ to zero within the real chamber. The eigenvalues and positive-root central charges are

$$\lambda = \frac{1}{3}(2\delta + 2m, -\delta + 2m, -\delta - 4m), \qquad (Z_{12}, Z_{23}, Z_{13}) = (\delta, 2m, 2m + \delta). \tag{XI.3.21}$$

At $\delta = 0$, $\lambda_1 = \lambda_2$, so the pair of oppositely charged states for F_1 becomes massless. The remaining two positive roots have equal nonzero masses. The classical unbroken algebra is $\mathfrak{su}(2) \oplus \mathfrak{u}(1)$, the centralizer of this diagonal matrix in $\mathfrak{su}(3)$. At $a_1 = a_2 = m$, in contrast, the eigenvalues are $(m, 0, -m)$ and the centralizer is only $\mathfrak{u}(1)^2$. This test uses zero root evaluations, rather than equality between two positive ones. It concerns the classical gauge chart; quantum singular loci of the pure theory require its corrected periods.

The Weyl group permutes the λ_i. For coordinates on the classical quotient, set $u_2 = \frac{1}{2}\operatorname{Tr}\Phi^2$ and $u_3 = \frac{1}{3}\operatorname{Tr}\Phi^3$. The trace condition gives the characteristic polynomial $z^3 - u_2 z - u_3$, hence

$$4u_2^3 - 27u_3^2 = \prod_{j<k}(\lambda_j - \lambda_k)^2 = a_1^2 a_2^2 (a_1 + a_2)^2. \tag{XI.3.22}$$

The invariants can also be computed directly from the two input periods:

$$u_2 = \frac{a_1^2 + a_1 a_2 + a_2^2}{3}, \qquad u_3 = \frac{(2a_1 + a_2)(a_1 - a_2)(a_1 + 2a_2)}{27}. \tag{XI.3.23}$$

For $(a_1, a_2) = (m, 2m)$, these give $u_2 = 7m^2/3$, $u_3 = -20m^3/27$; substituting in the left side of (XI.3.22) gives $36m^6$, the square of the product $m(2m)(3m)$. The degree of each term also checks the mass calibration: u_2 has mass dimension two, u_3 dimension three and the discriminant dimension six.

The zero of each factor is an eigenvalue coincidence. The equation is classical and will not be used as a quantum discriminant of the pure theory. We have now accounted for the Cartan fields and the possible root charges. The next step is to find the multiplets in which these gauge degrees of freedom appear after the reduction.

XI.3.4 Curvature and the adjoint zero modes

Which components of a six-dimensional vector multiplet can be massless in four dimensions? A flat-space decomposition of field components will not suffice on a curved base. A component with spin on the curve is a section of a bundle, and its kinetic operator can have no zero mode even if the same component is massless before compactification.

Let C be compact and connected of genus g, with a uniform split A-type fiber. Take the gauge and residual flat holonomies to be trivial. In the local reduction of the six-dimensional $(1, 1)$ gauge effective theory, choose the twist in which the generator of frame rotations on the base is replaced by

$$J' = J_L - J_3^{(1)} - J_3^{(2)}. \tag{XI.3.24}$$

Here J_L is the original frame generator, and $J_3^{(1,2)}$ are the two Cartans of the six-dimensional R-symmetry, each with doublet weights $\pm\frac{1}{2}$. Geometrically, this is the choice in which two real adjoint scalar components remain scalars, while the other two supply the real and imaginary parts of a complex one-form. A brane description in a dual frame motivates this choice. The underlying smooth normal bundle splits into

one trivial complex line and one with the canonical-bundle transformation law. This argument does not require a holomorphic splitting. Requiring eight supercharges alone would not suffice to select the twist.

To see the cancellation locally, denote the base frame connection by ω_C. After turning on the specified R background, the connection term acting on a component of weights (j, r_1, r_2) is proportional to

$$D_C = d + i\omega_C(j - r_1 - r_2), \qquad j' = j - r_1 - r_2. \tag{XI.3.25}$$

This formula describes the frame and R part of the derivative; the gauge connection is trivial at the background where we count modes. For the representative supercharge with $j = +\frac{1}{2}$ and $r_2 = +\frac{1}{2}$, the two terms cancel. Its other doublet component has $j' = 1$ and transforms as a one-form. The second supercharge row supplies a neutral representative with $j = -\frac{1}{2}$, $r_1 = -\frac{1}{2}$. The neutral representatives and their reality partners can be constant on the sphere. Thus the twist supplies globally defined supersymmetries in the presence of curvature, without requiring a parallel spinor for the original untwisted spin connection.

A component with $J' = 0$ has no net coupling to the base frame connection. A component of weight $+1$ has the transformation law of a section of the canonical bundle K_C, and a component of weight -1 has its conjugate law. For example the scalars are $(\mathbf{2}, \mathbf{2})$ under the two R-symmetry factors and have $J_L = 0$. The possible subtracted R weights are $1, 0, 0, -1$. The gauge field has no R weight, so its two internal components already have weights $+1$ and -1.

Field components	J_L	R representations	J' weights
A_μ	0	$(\mathbf{1}, \mathbf{1})$	0
$A_z, A_{\bar{z}}$	$+1, -1$	$(\mathbf{1}, \mathbf{1})$	$+1, -1$
Four real scalars, complexified	0	$(\mathbf{2}, \mathbf{2})$	$-1, 0, 0, +1$
ψ	$+\frac{1}{2}$	$(\mathbf{2}, \mathbf{1})$	$0, +1$
λ	$-\frac{1}{2}$	$(\mathbf{1}, \mathbf{2})$	$-1, 0$
Q	$+\frac{1}{2}$	$(\mathbf{1}, \mathbf{2})$	$0, +1$
$\bar{Q}$	$-\frac{1}{2}$	$(\mathbf{2}, \mathbf{1})$	$-1, 0$

Table XI.3.2: Weights in the twisted reduction. The fermion rows use four-dimensional Weyl representatives with the conjugate fields understood. The two weight-zero supercharge entries and their reality partners give eight real supercharges on the curved base.

We can now find the zero modes at zero adjoint background. For a scalar component, integration by parts on the compact curve gives

$$\Delta f = 0 \quad \Longrightarrow \quad 0 = \langle f, \Delta f \rangle = \int_C |df|^2, \qquad h^0(C, \mathcal{O}_C) = 1. \tag{XI.3.26}$$

There is just the constant internal wavefunction. In particular A_μ has one such wavefunction for every generator. For the connection along C, linearized gauge transformations

remove the exact part. In a transverse gauge, the Maxwell zero modes are harmonic one-forms:

$$dA_C = d^* A_C = 0, \qquad A_C = \sum_{r=1}^{h^0(K_C)} \big(c_r \eta_r + \bar{c}_r \bar{\eta}_r\big). \tag{XI.3.27}$$

Here the η_r form a basis of holomorphic differentials; the display is for real Lie algebra components before grouping them into four-dimensional fields. Hodge theory supplies this basis and its conjugate. In particular a harmonic form need not be covariantly constant on a curved base.

The twisted scalar and fermion operators use the Dolbeault differential and its adjoint. For a positive weight component s of type $(1,0)$, the zero-mode condition is

$$\bar{\partial} s = 0, \qquad s \in H^0(C, K_C). \tag{XI.3.28}$$

One can see the kernel by taking the squared norm of $\bar{\partial} s$; the conjugate weight has the conjugate kernel. The neutral fermion components have the constant kernel. By Riemann–Roch for $\mathcal{O}_C$ and duality on the curve,

$$h^0(C, \mathcal{O}_C) - h^0(C, K_C) = 1 - g, \qquad h^0(C, K_C) = g. \tag{XI.3.29}$$

The supersymmetric pairing is now explicit. The constant gauge field, two real scalar modes and two Weyl species comprise a four-dimensional vector multiplet. For each η_r, the connection gives one complex scalar and the twisted six-dimensional scalars give another. The nonzero-weight fermions give two Weyl species per form. Thus the additional matter is

$$n^{\text{matter}}_{\text{real scalars}} = 4g, \qquad n^{\text{matter}}_{\text{Weyl}} = 2g, \qquad n_{\text{full adjoint hypers}} = g. \tag{XI.3.30}$$

Counting the conjugate differential as a second independent hypermultiplet would double the result.

An explicit expansion makes this reality condition visible. For a single real Lie algebra generator, write the connection modes and the complex twisted scalar modes as

$$A_C = \sum_{r=1}^{g} (c_r \eta_r + \bar{c}_r \bar{\eta}_r), \qquad \varphi_C = \sum_{r=1}^{g} d_r \eta_r, \qquad \bar{\varphi}_C = \sum_{r=1}^{g} \bar{d}_r \bar{\eta}_r. \tag{XI.3.31}$$

The variables c_r, d_r are independent complex spacetime fields; the barred coefficients are their conjugates. There are two complex, or four real, scalars for each r. All coefficients take values in the adjoint because the parent fields do, while the differential only labels an internal wavefunction. The one-form inner products

$$G_{r\bar{s}} = \int_C \eta_r \wedge * \bar{\eta}_s, \qquad \sum_{r,s} \bar{c}_s G_{r\bar{s}} c_r > 0 \quad (c \neq 0) \tag{XI.3.32}$$

provide finite kinetic norms on the compact base. Changing this positive matrix changes field normalizations, not the number of coefficients. The common constant mode is similarly normalized by $\int_C 1 \, \mathrm{vol}_C = V_C$. This is where a continuous metric parameter

enters a calculation whose multiplicities were fixed by topology. The count gives full adjoint multiplets before choosing a Coulomb background. An off-diagonal component then feels the commutator with Φ.

For $C = \mathbb{P}^1$, $K_C = \mathcal{O}(-2)$ has no holomorphic section. Concretely, under $w = 1/z$, a differential $f(z)\,dz$ has coefficient $-w^{-2}f(1/w)$. Regularity at $w = 0$ together with holomorphy at all finite z forces $f = 0$. There are no adjoint hypers in this example. For the comparison choose the actual product of the resolved A_2 surface and $E = \mathbb{C}/(\mathbb{Z} + \tau_E\mathbb{Z})$. The constant differential dz spans $H^0(E, K_E)$. On this torus, write $z = x + \tau_E y$ with x, y of period one. The two real harmonic one-forms can be taken as dx, dy, and

$$dz = dx + \tau_E dy, \qquad A_C = A_x\,dx + A_y\,dy = c\,dz + \bar{c}\,d\bar{z}. \tag{XI.3.33}$$

The two real numbers A_x, A_y are equivalent to one complex coefficient c, not two independent complex fields. A globally holomorphic function on the compact torus is constant, so any holomorphic differential $f(z)dz$ has constant f. This gives one complex differential directly. On the sphere the overlap $dz = -w^{-2}dw$ instead obstructed a nonzero global differential. The difference arises even if the two base metrics have the same area.

With the flat base metric, periodic spinors, trivial gauge and R-symmetry holonomies, and no mass deformation, there is also a direct untwisted count:

$$(A_\mu,\ 4 + 2 \text{ real scalars},\ 4 \text{ Weyl species}) \quad \text{and} \quad 16 \text{ real supercharges}. \tag{XI.3.34}$$

Here the two extra real scalars are the constant components of the gauge field along the two directions of the torus. All sixteen supercharges have constant representatives. The vector and massless adjoint hyper therefore assemble into $\mathcal{N} = 4$ in this product model. Genus one supplies a holomorphic differential; the additional supersymmetry uses the trivial background just specified.

XI.3.5 The base coupling and the magnetic particles

The gauge zero mode is constant on the base. What changes if we increase the size of that base while keeping the two fiber periods fixed? The field must now fill a larger internal volume. This costs more kinetic action for the same four-dimensional field strength and therefore increases the inverse bare coupling.

Use the fundamental trace with $\mathrm{Tr}_f(T_aT_b) = \frac{1}{2}\delta_{ab}$. In the unwarped leading reduction, the spacetime component of the gauge field contributes

$$-\frac{1}{2g_6^2}\int_{\mathbb{R}^{1,3}\times C} \mathrm{Tr}_f\, F_{\mu\nu}F^{\mu\nu} = -\frac{V_C}{2g_6^2}\int_{\mathbb{R}^{1,3}} \mathrm{Tr}_f\, F_{\mu\nu}F^{\mu\nu}, \qquad \frac{1}{g_4^2} = \frac{V_C}{g_6^2}. \tag{XI.3.35}$$

The integration measures are those of the common string-frame metric. This factorization holds for the constant product mode. We use it to leading order for the A_2 family with a controlled adiabatic base metric near fiber collapse. Let $S_0 = D_0 \cap E_1$ be the

base section, and define $A_b = \int_{S_0} J$. In this limit the base area V_C equals A_b at leading order. The leading ALE normalization gives

$$g_6^2 = 2(2\pi)^3\alpha', \qquad \frac{8\pi^2}{g_4^2} = \frac{A_b}{2\pi\alpha'}. \tag{XI.3.36}$$

Both g_6^2 and A_b have units of length squared. The four-dimensional inverse coupling is dimensionless, as required.

The base also has a B-period. In the weak-coupling local identification it supplies the gauge instanton phase. Write

$$t_b = \frac{1}{4\pi^2\alpha'}\int_{S_0}(B + iJ), \qquad T_b = -2\pi i t_b, \qquad \theta_b = \frac{1}{2\pi\alpha'}\int_{S_0} B. \tag{XI.3.37}$$

Thus the leading local dictionary reads

$$Q_b = e^{-T_b} = \exp\left(-\frac{8\pi^2}{g_4^2} + i\theta_b\right). \tag{XI.3.38}$$

The area determines the classical suppression and the B-period determines the phase once. Equation (XI.3.38) is a relation to the bare parameter in this frame. It leaves room for threshold matching and for the Coulomb-dependent effective coupling. Nothing in the kinetic reduction computes the latter.

The independent geometric variations are now clear in the leading frame. Keep α', g_s, B and both fiber areas fixed, and multiply the base area by $\kappa > 0$. Then

$$a_i \longmapsto a_i, \qquad g_4^{-2} \longmapsto \kappa g_4^{-2}, \qquad |Q_b| \longmapsto |Q_b|^{\kappa}. \tag{XI.3.39}$$

The theta phase is held fixed here, so this is a statement about the absolute value of the instanton weight. The W masses are unchanged while instantons are more suppressed for $\kappa > 1$. Holding the base fixed and varying a fiber area instead changes a simple W mass. Neither operation changes the number of zero modes in the specified uniform family. A change of genus changes that count even at fixed area, as the elliptic comparison demonstrated.

There is a second way to see why a magnetic quantity involves the base. A D4 wrapped on the entire swept divisor E_i has a worldline in four dimensions, just as a D2 wrapped on F_i does. The D4 couples to C_5, the magnetic dual potential of C_3. The compact electric-magnetic pairing is the intersection of a curve and a divisor. With orientation $-E_i$ for the positive magnetic coroot it is

$$\langle F_j, -E_i\rangle = -E_i \cdot F_j = \mathsf{C}_{ij}. \tag{XI.3.40}$$

This orientation changes the charge sign and does not change the wrapped volume. Figure XI.3.1 distinguishes the sphere at one point, available to the D2, from the surface over the entire base, available to the D4.

We can compute the latter volume without approximating the swept divisor by a product. The section $S_k = D_k \cap D_{k+1}$ corresponds to the wall generated by d_k, d_{k+1}.

The maximal cones on its two sides have added rays v_+, v_-. The wall relation, with both added-ray coefficients equal to one, follows by inserting the coordinates:

$$v_+ + v_- - 2(k+1)d_k + 2kd_{k+1} = 0. \tag{XI.3.41}$$

In a smooth toric fan the coefficients of the two wall rays give the intersections of their divisors with the wall curve. Here they are

$$D_k \cdot S_k = -2(k+1), \qquad D_{k+1} \cdot S_k = 2k. \tag{XI.3.42}$$

For example, S_0 inside E_1 is cut out by D_0. Its self-intersection there is $D_0 \cdot S_0 = -2$. The other section of E_1, S_1, has self-intersection $+2$ there, since it is cut out by D_2. Inside E_2, the same S_1 is cut out by D_1, giving self-intersection -4. The other section, S_2, has self-intersection $+4$ in E_2. The ruled surfaces are consequently $\mathbb{F}_2$ and $\mathbb{F}_4$. In E_1, the two disjoint sections satisfy $S_1 = S_0 + 2F_1$ numerically, as follows by intersecting both sides with S_0 and F_1.

To compute a volume on $\mathbb{F}_n$, let S denote its negative section and F its fiber. The area parameters A_s and A_f are their integrals of J. Identifying the curve classes with their Poincaré duals on the surface gives

$$S^2 = -n, \quad S \cdot F = 1, \quad F^2 = 0, \qquad J|_{\mathbb{F}_n} = A_f S + (A_s + nA_f)F. \tag{XI.3.43}$$

The first coefficient follows by intersecting with F; the second restores the desired area on S. Squaring this expression gives

$$\mathrm{Vol}(\mathbb{F}_n) = \frac{1}{2}\int_{\mathbb{F}_n} J \wedge J = A_f A_s + \frac{n}{2}A_f^2. \tag{XI.3.44}$$

The two bases for this calculation are S_0 of area A_b and S_1 of area $A_b + 2A_{f,1}$, respectively. Hence

$$V_{E_1} = A_{f,1}(A_b + A_{f,1}), \qquad V_{E_2} = A_{f,2}(A_b + 2A_{f,1} + 2A_{f,2}). \tag{XI.3.45}$$

The correction involving $A_{f,1}$ in V_{E_2} comes from the change of section. Using the same area for both negative sections would miss it. By comparison, in the elliptic product the swept surface is $F_i \times E$; integrating the square of the sum of the two Kähler forms gives exactly $A_{f,i}V_C$.

For vanishing B, $H = dB$, and worldvolume flux, the leading DBI contribution for a smooth wrapped D4 in the weak-curvature regime is $\tau_4 V_{E_i}$. The ruled surfaces have even index, so the first Chern class $2S + (n+2)F$ is even and there is no spin obstruction forcing half-integral flux in this slice. In the small-fiber-to-base-area expansion, the leading ratio is

$$\frac{M_{D4(E_i)}}{M_{D2(F_i)}} \longrightarrow \frac{\tau_4}{\tau_2}A_b = \frac{A_b}{4\pi^2\alpha'} = \frac{4\pi}{g_4^2}, \qquad \tau_4 = \frac{1}{(2\pi)^4 g_s(\alpha')^{5/2}}. \tag{XI.3.46}$$

The ratio here compares the leading volume terms and agrees with the weak-coupling magnetic slope. A D4 samples a whole surface and can also receive worldsheet-instanton

corrections to its central charge. The classical calculation does not give an exact monopole mass at sub-stringy fiber size.

Within the stated classical volume calculation one can retain the first correction rather than immediately taking the small-fiber limit. Define the ratios of the leading wrapped-volume terms by

$$R_i^{\mathrm{vol}} = \frac{\tau_4 V_{E_i}}{\tau_2 A_{f,i}}, \qquad R_1^{\mathrm{vol}} = \frac{A_b + A_{f,1}}{4\pi^2\alpha'}, \qquad R_2^{\mathrm{vol}} = \frac{A_b + 2A_{f,1} + 2A_{f,2}}{4\pi^2\alpha'}. \tag{XI.3.47}$$

Their fractional corrections to the common leading slope are

$$\frac{R_1^{\mathrm{vol}}}{A_b/(4\pi^2\alpha')} - 1 = \frac{A_{f,1}}{A_b}, \qquad \frac{R_2^{\mathrm{vol}}}{A_b/(4\pi^2\alpha')} - 1 = \frac{2A_{f,1} + 2A_{f,2}}{A_b}. \tag{XI.3.48}$$

Thus $A_{f,2} \ll A_b$ alone is insufficient to approximate the second swept volume by a product: its negative section also remembers $A_{f,1}$. For example, the positive areas

$$A_b = 12\pi^2\alpha', \qquad A_{f,1} = \tfrac{1}{2}\pi^2\alpha', \qquad A_{f,2} = \tfrac{1}{4}\pi^2\alpha' \quad \Longrightarrow \quad (R_1^{\mathrm{vol}}, R_2^{\mathrm{vol}}) = (25/8, 27/8) \tag{XI.3.49}$$

replace the common leading value 3. Doubling the base area with the fibers fixed adds 3 to both ratios; it leaves the difference $(A_{f,1} + 2A_{f,2})/(4\pi^2\alpha')$ unchanged. This isolates the volume correction due to the ruled geometry from the leading coupling dependence. These numbers evaluate the classical Kähler polynomial. Their interpretation as physical masses additionally requires the smooth weak-curvature DBI regime already stated.

XI.3.6 Two bases and two beta coefficients

Suppose we arrange the same leading inverse coupling for two different bases. Do the gauge couplings then run in the same way? The one-loop coefficient is set by the multiplets of the four-dimensional gauge description below the compactification scales. We can compute it from the adjoint zero modes without varying the fiber geometry.

Let $T(R)$ denote the index of a representation, with $\mathrm{Tr}_R\, T_a T_b = T(R)\delta_{ab}$. For a traceless diagonal $H = \mathrm{diag}(h_i)$ in $\mathfrak{su}(N)$, the adjoint weights are $h_i - h_j$ together with the zero Cartan weights. It follows that

$$\mathrm{Tr}_{\mathrm{ad}}\, H^2 = \sum_{i,j}(h_i - h_j)^2 = 2N\sum_i h_i^2 - 2\left(\sum_i h_i\right)^2 = 2N\,\mathrm{Tr}_f\, H^2. \tag{XI.3.50}$$

Since $T(f) = \frac{1}{2}$, this gives $T(\mathrm{ad}) = N$. With the convention

$$\mu\,\frac{dg_4}{d\mu} = -\frac{b_0}{16\pi^2} g_4^3 + \cdots, \tag{XI.3.51}$$

an $\mathcal{N} = 1$ vector contributes $3T(\mathrm{ad})$ and each adjoint chiral contributes $-T(\mathrm{ad})$. The $\mathcal{N} = 2$ vector contains one such chiral, and each full adjoint hyper contains two. Therefore

$$b_0 = (3 - 1 - 2g)T(\mathrm{ad}) = 2N(1 - g). \tag{XI.3.52}$$

For example, at $N = 3$ the vector contributes $9 - 3 = 6$ and one full adjoint hyper contributes -6. The two reductions give different matter even when their areas are equal.

Base and background	$h^0(K_C)$	Local multiplets	b_0 for A_2
Sphere, selected twist	0	$\mathcal{N} = 2$ vector	6
Flat elliptic product	1	Vector and adjoint hyper	0

Table XI.3.3: The same fiber and the same index $T(\mathrm{ad}) = 3$ give different one-loop coefficients. The elliptic entry is for the periodic, trivial-holonomy product.

On the sphere, the pure theory is asymptotically free. In its four-dimensional gauge regime the beta equation gives

$$\frac{d}{d\log\mu}\left(\frac{8\pi^2}{g_4^2}\right) = b_0 \qquad \text{at one loop.} \tag{XI.3.53}$$

For $b_0 = 6$, the exponentiated action scales with the sixth power of the ratio of the strong scale to the reference scale.

Integrating within the four-dimensional one-loop regime between scales μ_1 and μ_2 gives

$$S(\mu_2) - S(\mu_1) = b_0 \log\frac{\mu_2}{\mu_1}, \qquad S(\mu) = \frac{8\pi^2}{g_4^2(\mu)}, \qquad \mu^{b_0} e^{-S(\mu)} = \text{constant}. \tag{XI.3.54}$$

For the pure A_2 sector, raising a reference scale by a factor of two raises S by $6\log 2$. The instanton magnitude at that reference scale decreases by 2^{-6}; the invariant is unchanged. For the elliptic product, the right side of the first relation is zero because the vector and adjoint hyper cancel. The base area specifies a bare starting parameter, while this equation describes running only after the four-dimensional effective theory has been matched. The local geometric matching of the pure rank-two model uses

$$1 - Q_{f,i} \sim \epsilon a_i, \qquad Q_b \sim C_{\mathrm{match}} e^{i\theta_b} (\epsilon\Lambda)^6, \qquad \epsilon = \frac{2\pi g_s}{M_s}. \tag{XI.3.55}$$

Here $Q_{f,i} = e^{-T_{f,i}}$ and $T_{f,i} = -2\pi i t_{F_i}$. In the real period lift, $T_{f,i} = \epsilon a_i$, so the first relation follows by expansion. The finite matching constant C_{match} and the second relation refer to the selected local limit. Agreement of the exponent with the four-dimensional coefficient is a check of the matching. It does not justify running a pure four-dimensional coupling across the base Kaluza–Klein threshold to the string scale.

The fiber relation also has a controlled error estimate in the real chamber. Since $T_{f,i} = \epsilon a_i$,

$$\frac{1 - Q_{f,i}}{\epsilon a_i} = 1 - \frac{\epsilon a_i}{2} + \frac{(\epsilon a_i)^2}{6} + O\big((\epsilon a_i)^3\big). \tag{XI.3.56}$$

Both simple periods must satisfy $|\epsilon a_i| \ll 1$ to use their linear scaling. Their sum then scales as the period of the composite root. The base relation has a different form. For

positive C_{match} in the magnitude convention, taking its logarithm and using the leading area identification gives

$$\frac{A_b}{2\pi\alpha'} \sim 6\log\frac{1}{\epsilon\Lambda} - \log C_{\mathrm{match}}. \tag{XI.3.57}$$

At fixed a_i, Λ, shrinking ϵ by a factor of two therefore increases this dimensionless base area by $6\log 2$, while the dimensionless fiber areas decrease. This is an algebraic consequence of the selected local matching. It identifies which parameters must move together; it is not a derivation of isolation of bulk or Kaluza–Klein modes. The physical base area contains the additional factor α', so the logarithm alone also does not say that its size in physical units diverges.

For the elliptic product, $b_0 = 0$ and there is a marginal coupling rather than the asymptotically free logarithm. Its enhanced supersymmetry follows from the flat reduction, not from the numerical cancellation. If $g > 1$ in the same ordinary twist, the formula gives an infrared-free gauge description; it does not supply a four-dimensional ultraviolet completion. In both worked models we use energies below the unwanted Kaluza–Klein masses. For an autonomous sector the other unwanted modes must also become heavy or cease to couple in the local limit.

XI.3.7 Fiber transport and the global gauge group

The charge table uses labels F_i that return to themselves when transported in the base. What information changes if they do not? This is one question about global geometry. A different question is which Wilson lines exist in a four-dimensional theory once its algebra is fixed. The two questions can have different answers for the same local root data.

Consider a change of gluing for an A_3 algebra that uses its diagram reversal. We specify the lift, since a permutation of nodes alone does not specify an action on all root generators. Write $e_i = U_{i,i+1}$ and $h_i = [e_i, e_i^{\mathsf{T}}]$ in $\mathfrak{sl}_4$, and set

$$J_{\mathrm{sp}} = U_{14} - U_{23} + U_{32} - U_{41}, \qquad \sigma(X) = -J_{\mathrm{sp}}^{-1} X^{\mathsf{T}} J_{\mathrm{sp}}. \tag{XI.3.58}$$

Inserting e_i and h_i shows that σ exchanges $1 \leftrightarrow 3$ with positive signs on these generators and fixes 2. In the projected algebra the simple generators and coroots can be taken as

$$X_s = e_1 + e_3, \quad X_l = e_2, \qquad K_s = h_1 + h_3, \quad K_l = h_2. \tag{XI.3.59}$$

The subscripts give the short and long root in this order. For example, both h_1 and h_3 act on e_2 with eigenvalue -1, whereas h_2 acts on e_1 and e_3 with eigenvalue -1 on each. Thus the two off-diagonal actions are unequal:

$$[K_i, X_j] = A_{ij} X_j, \qquad A = \begin{pmatrix} 2 & -2 \\ -1 & 2 \end{pmatrix}. \tag{XI.3.60}$$

The fixed matrices satisfy $X^{\mathsf{T}} J_{\mathrm{sp}} + J_{\mathrm{sp}} X = 0$. Equivalently $J_{\mathrm{sp}} X$ is symmetric, giving ten independent entries and identifying the complex fixed algebra as $\mathfrak{sp}_4$. The example

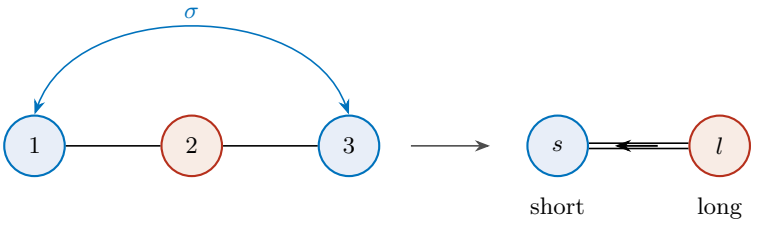


Figure XI.3.3: The stated lift of the A_3 reversal identifies the end-node orbit and preserves the middle node. In the projected algebra their coroot actions differ as in (XI.3.60). The drawing labels the two orbits; the arrow points toward the short root. The matrix is obtained from the commutators.

computes an invariant algebra for a specified lift and presupposes compatible gluing. It does not classify non-split fibrations or determine their matter.

A Weyl reflection on the Coulomb branch is a different operation. In the split theory it sends a root α to

$$s_i(\alpha) = \alpha - \alpha(H_i)\alpha_i. \tag{XI.3.61}$$

It permutes the complete root system. The two choices of Coulomb labeling give the same gauge algebra.

For example, reflecting in the first simple root exchanges λ_1 and λ_2. The simple-period coordinates change by

$$(a_1, a_2) \longmapsto (-a_1, a_1 + a_2), \qquad s_1^2 = 1. \tag{XI.3.62}$$

The three positive-root expressions $a_1, a_2, a_1 + a_2$ become $-a_1, a_1 + a_2, a_2$. Including the negative roots, the same six central charges remain. The explicit polynomials (XI.3.23) are unchanged. This calculation merely changes coordinates on the same Weyl quotient; it discards no generator. Projection under an outer transport, by contrast, selects invariant generators because the others have no constant global mode in that example.

Return to the split A_2 model. Its D2 roots span the root lattice Q. The weight lattice P has the fundamental weights as a basis, and the two columns of C generate Q in this basis. The character

$$(p, q) \;\longmapsto\; p + 2q \pmod 3 \tag{XI.3.63}$$

vanishes on the columns and maps $(1, 0)$ to 1. Because $\det \mathsf{C} = 3$, it induces $P/Q \simeq \mathbb{Z}_3$. For a highest weight with Dynkin labels (p, q), the corresponding center phase is $\exp(2\pi i(p + 2q)/3)$. The representation descends to PSU(3) precisely when this phase is one, or equivalently when the class in (XI.3.63) is zero. The center element $e^{2\pi i/3}\mathbb{1}$ acts on a fundamental as a nontrivial phase. It acts trivially on every adjoint weight. A fundamental Wilson line is therefore a test that distinguishes the simply connected SU(3) from its quotient PSU(3). The local W-bosons and the beta coefficient are the same for these choices.

The root-lattice criterion can be checked without enumerating representations. For a weight with Dynkin labels (p, q), its coordinates in the simple-root basis are

$$\mathsf{C}^{-1}\begin{pmatrix} p \\ q \end{pmatrix} = \frac{1}{3}\begin{pmatrix} 2p+q \\ p+2q \end{pmatrix}. \tag{XI.3.64}$$

Both entries are integral exactly when $p + 2q = 0 \pmod 3$: modulo three, $2p + q = 2(p + 2q)$. Thus $(1, 1)$ lies in Q, while $(1, 0)$ does not. The local root charges test this integrality condition but supply no fundamental particle that would force a choice of global group. The admissibility of a fundamental Wilson line is additional information about the four-dimensional theory.

An absolute four-dimensional gauge theory must also specify a mutually local spectrum of genuine magnetic and dyonic lines. The compact D2–D4 pairing alone gives the charges of the particles just constructed, and does not make that selection. We will use the name pure SU(3) for the local gauge dynamics in the ordinary rational example, with the choice of allowed lines left to additional boundary data. The next chapter changes the fiber at a point of the base and asks which charged modes become localized there.

XI.3.8 Exercises

Use `benchmark/tasks.json` to find the question IDs and `benchmark/PROTOCOL.md` for submission. Every written explanation is assessed separately by a reader or instructor.

E1. For A_3, let H_i be the three simple coroots in $\mathfrak{sl}_4$. Use $[H_i, U_{jk}]$ to find the three coroot charges of each of the six positive roots. Report each triple in order of increasing coroot label, and label its row by the pair jk with $j < k$. Explain how to obtain the negative root charges and why the Cartan generators are absent from this table.

E2. Take the same uniform A_2 twist on a genus-two curve, with trivial holonomies. Determine the number of vector multiplet species, the number of full adjoint hypermultiplet species and b_0, in that order. Count each adjoint multiplet as one species. Explain the role of conjugation in the scalar and fermion counts. What does the sign of b_0 tell you about the low-energy gauge description?

E3. Set $A_b = 12\pi^2\alpha'$ in the leading reduction and take $B = 0$. Compute $4\pi/g_4^2$ and the leading classical ratio $M_{D4(E_2)}/M_{D2(F_2)}$ in the expansion in the fiber areas divided by A_b. Give the two numbers in this order. What correction to the second number would the non-product volume give at finite $A_{f,1}$ and $A_{f,2}$? Explain why that correction does not determine a quantum monopole mass.

E4. Using the stated lift of the A_3 reversal, work out all four commutators from the generators in (XI.3.59), including its definitions of K_s, K_l. Present the result with coroots in the rows and short root first. Explain which generators can have constant modes after the projection and why changing the Coulomb Weyl chamber of the split theory would not impose this projection.

E5. Find the center charges modulo three of the representations with Dynkin labels $(1,0),(0,1),(1,1),(3,0)$, in this order. Which representations can be used to define Wilson lines for PSU(3)? Explain why this calculation leaves a magnetic and dyonic line choice.

The following transfer problems have written solutions only. They extend the calculations without changing the five numerical submissions.

T1. Starting with the three rays v_+, d_k, d_{k+1}, derive the dual characters in (XI.3.6). Repeat with v_-, derive the overlap powers and recover the normal degrees of S_1. Explain why these powers preserve fiber labels.

T2. At fixed $a_2 = 2m$, compare the limits $a_1 \to 0$ and $a_1 \to 2m$. Compute the classical eigenvalues and centralizers. Use the charge-period pairing to explain why equal positive W masses and vanishing W masses answer different questions.

T3. Keep A_b and $A_{f,2}$ fixed and vary $A_{f,1}$. Derive the changes of both swept volumes and both ratios R_i^{vol}. Which term in the second ratio would disappear if one incorrectly used S_0 as the negative section of E_2?

T4. At fixed Λ, replace ϵ by $\epsilon/3$ in the stated pure-model matching. Find the leading change in $A_b/(2\pi\alpha')$, the leading ratio of the two $|Q_b|$ and the first relative correction to each linear fiber scaling. State which further scale conditions are needed before interpreting this motion as an autonomous four-dimensional limit.

Status and sources

§§ 3.2–3.3. The fan in (XI.3.1)–(XI.3.12) uses S. H. Katz et al. (1997, §6.1, (6.3)), with the chart and integral relation derivations given here [MATH].

The explicit dual-cone coordinates, overlap, normal degrees and quotient neutrality in (XI.3.4)–(XI.3.8) and (XI.3.10)–(XI.3.11) are algebraic consequences of that same fan [MATH]. The charge basis and classical Coulomb algebra in (XI.3.13)–(XI.3.22) reuse the XI.1 frame [MATH]. The ordinary six-dimensional ALE gauge and electric root-sector interpretation uses the ordinary ALE enhancement and S. Katz et al. (1996, §2, pp. 5–6 of arXiv v2) [GEO-X]. The four-dimensional reduction requires the additional twisting and isolation premises described above.

§ 3.4. The geometric identification with the twisted gauge effective theory follows S. Katz et al. (1996, §2.1, (2.1)–(2.2)). Their D-brane argument, (2.13)–(2.18), motivates the choice of twist through a smooth normal-bundle splitting, without requiring a holomorphic splitting [GEO-E]. Equations (XI.3.24)–(XI.3.34) derive the linear mode multiplicities in the stated bundle and holonomy frame [MATH]. The four-dimensional ordinary IIA gauge interpretation, including the flat product comparison, is scoped to the selected models [GEO-E].

§§ 3.5–3.6. The leading gauge kinetic reduction (XI.3.35) uses the XI.1 normalization and agrees with S. H. Katz et al. (1997, §2, arXiv v2) [SUGRA]. The base complex weight and the pure rank-two matching, (XI.3.38) and (XI.3.55), follow the weak-coupling identification in S. H. Katz et al. (1997, §§2 and 6.1, (6.1)) with the XI.2 period conventions [GEO-E]. The magnetic particle identification uses S. Katz et al. (1996, §2, note 6 of arXiv v2) [GEO-E]. The ruled volumes and classical tension ratio (XI.3.41)–(XI.3.46) use the stated chamber and the

standard brane tensions [MATH]. Equation (XI.3.52) is the trace calculation conditional on the multiplet count and one-loop index formula [MATH]. Isolation of the desired local sector, including its light-state continuation and unwanted-sector separation, has the hypotheses of the local-limit discussion [DEC].

§ 3.7. Equations (XI.3.58)–(XI.3.60) compute a particular algebraic projection [MATH]; S. H. Katz et al. (1997, §1) discusses the use of outer automorphisms, while S. Katz et al. (1996, §3.3, (3.14)) discusses a reflection of the split model. The center character (XI.3.63) is a calculation in the weight lattice [MATH]. The local particle lattice does not select the full line spectrum; see Aharony et al. (2013, §§1.1 and 2.1, (1.4) and (2.1), arXiv v5) for the line distinction [GEO-E].

§ 3.8. The five exercises have submitted-answer checks for the charge table, multiplet counts, two numbers in the leading coupling comparison, folded matrix, and center residues. Written explanations are assessed separately.

The additional transfer problems are written practice. The expanded charge-period, Weyl-invariant, volume-ratio and scaling calculations are consequences of the previously stated classical model and matching, with their respective regimes unchanged [MATH].

References

Aharony, O., N. Seiberg, and Y. Tachikawa (2013). "Reading between the lines of four-dimensional gauge theories". In: *JHEP* 08, p. 115. DOI: 10.1007/JHEP08(2013)115. arXiv: 1305.0318 [hep-th].

Katz, S., D. R. Morrison, and M. R. Plesser (1996). "Enhanced gauge symmetry in Type II string theory". In: *Nucl. Phys. B* 477, pp. 105–140. DOI: 10.1016/0550-3213(96)00331-8. arXiv: hep-th/9601108.

Katz, S. H., A. Klemm, and C. Vafa (1997). "Geometric engineering of quantum field theories". In: *Nucl. Phys. B* 497, pp. 173–195. DOI: 10.1016/S0550-3213(97)00282-4. arXiv: hep-th/9609239.

Chapter XI.4

Matter from enhanced fibers

XI.4.1 Matter from a special fiber

In the previous chapter, the same two exceptional spheres occurred over every point of a rational base. Wrapped D2-branes supplied the charged gauge bosons of the resulting $\mathfrak{su}(3)$ theory. Now let a third sphere appear at just one point. It can carry charge under the gauge fields from the first two spheres. Its support along the base is different, however, so it need not belong to another gauge multiplet.

We will separate three questions. Which charges does the new geometry allow? How many multiplets carry those charges? Which geometric parameter becomes their mass? The answer in the split, transverse example is one full fundamental hypermultiplet. To derive it we will resolve the special fiber, use the resulting intersections to compute the weights, and count the charged modes near the point. The intersection calculation determines the representation. The localization calculation supplies its multiplicity. We then follow that same fundamental onto the Coulomb branch and calculate its full matrix of electric thresholds, including a limit with just one light component.

We use ordinary Type IIA without flux or discrete data that freeze the vanishing curves. We work in the local four-dimensional gauge regime with eight supercharges. Recall that a compact sphere carries an oriented D2 charge and that its area, in the smooth zero-flux regime, sets a wrapped mass. We will distinguish the holomorphic separation that locates the extra degeneration from the Kähler periods that set the particle masses.

XI.4.2 A collision of surface singularities

Which curves exist throughout the base, and which exist only at the special point? Let s be a local holomorphic coordinate along the base. We use the family of surfaces

$$X_f : \qquad xy = z^3\big(z - f(s)\big). \tag{XI.4.1}$$

The triple root of the right-hand side is at $z = 0$. If $f(s) \neq 0$, the factor $z - f(s)$ is a unit near that root and

$$y_{\text{loc}} = \frac{y}{z - f(s)}, \qquad xy_{\text{loc}} = z^3. \tag{XI.4.2}$$

This is the generic A_2 surface. The simple root at $z = f(s)$ gives a smooth point of the surface, since the derivative of $z^3(z - f(s))$ at that root is $f(s)^3 \neq 0$. At $f(s) = 0$ the equation becomes $xy = z^4$, the A_3 surface. A nonzero constant f would give no enhancement. For $f(s) = s$, the two root positions meet transversely at $s = 0$.

The variable s labels a surface before we resolve it. The total space has complex dimension three, since one equation constrains the four coordinates (x, y, z, s). Resolving just the surface at $s = 0$ would exhibit an A_3 chain, but would not show whether each sphere moves with s. We therefore keep s throughout the resolution. In particular, the two useful questions about an exceptional curve are whether it contracts to $(x, y, z) = (0, 0, 0)$ at a fixed s, and whether it can move to neighboring values of s. The first is a statement about the contraction map. The second uses the resolved threefold, rather than the Dynkin diagram of one slice.

We resolve the family by ordering the three factors z before the last factor $z - f(s)$. At each step resolve the ratio between a variable and the next factor z. The first step is the closure of the graph of $[x : z]$. The chart $z = xr_1$ is smooth, because substitution gives $y = r_1 z^2(z - f)$. In the other chart $x = zu_2$ the remaining equation is $u_2 y = z^2(z - f)$. To see why this gives a resolution rather than a substitution that loses the exceptional curve, introduce homogeneous coordinates $[p : q] = [x : z]$. The graph equation is $xq = zp$. In the patch $p = 1$ write $q = r_1$, and in the patch $q = 1$ write $p = u_2$. The equations on the two proper transforms are

$$z = xr_1, \qquad y = r_1 z^2(z - f(s)), \tag{XI.4.3}$$

$$x = zu_2, \qquad u_2 y = z^2(z - f(s)). \tag{XI.4.4}$$

The first patch has free coordinates (x, r_1, s). The second still has a surface singularity to resolve. Cancelling a factor of x or z here selects the proper transform, the closure of the part where the original ratio was defined. Keeping the projective coordinate also keeps the limiting directions at the origin. In particular, setting $x = z = 0$ does not force either p or q to vanish.

The next two steps repeat this operation, each removing one factor of z from the continuing equation. With $u_j = x/z^{j-1}$ on the dense overlap, the first three smooth charts are

$$(u_j, r_j, s): \qquad z = u_j r_j, \quad x = u_j z^{j-1}, \quad y = r_j z^{3-j}(z - f(s)), \qquad j = 1, 2, 3. \tag{XI.4.5}$$

For example, the middle step has $u_2 = x/z$ and $z = u_2 r_2$. Putting this into the remaining equation gives

$$u_2 y = (u_2 r_2)^2(u_2 r_2 - f), \qquad y = r_2 z(z - f). \tag{XI.4.6}$$

At the third step $u_3 = x/z^2$ and the remaining equation is $u_3 y = z(z - f)$. Its two patches are particularly simple,

$$z = u_3 r_3, \quad y = r_3(u_3 r_3 - f), \qquad \text{or} \qquad u_3 = bz, \quad by = z - f. \tag{XI.4.7}$$

In the first patch (u_3, r_3, s) are free. In the second, z can be eliminated, leaving (b, y, s) free. These formulas make the smoothness visible without dividing by a function at its zero.

The last chart has coordinates (b, y, s), with

$$b = x/z^3, \qquad z = f(s) + by. \tag{XI.4.8}$$

The division in the definitions describes the gluing on dense open sets; the graph construction supplies the missing points at $z = 0$. On overlaps, the next chart takes the reciprocal of the ratio in the preceding one:

$$u_{j+1} = 1/r_j, \qquad r_{j+1} = zr_j \quad (j = 1, 2), \qquad b = 1/r_3. \tag{XI.4.9}$$

One can check the overlap without guessing which ratio is inverted. Using $u_j = x/z^{j-1}$ and $r_j = z/u_j$ on their common open set gives

$$\frac{x}{z^j} = \frac{u_j}{z} = \frac{1}{r_j}, \qquad \frac{z}{u_{j+1}} = zr_j. \tag{XI.4.10}$$

Thus the two affine coordinates along a given exceptional sphere are reciprocals, just as for the two standard patches of $\mathbb{P}^1$. The expressions using quotients are only a way to compute the transition. The regular patch coordinates, including $r_j = 0$ or $u_{j+1} = 0$, define its extension.

The resolution is crepant. For example, the residue on the dense locus with $x \neq 0$ extends across the first three charts without a zero or pole. Using the equation of X_f gives an equivalent expression for the last chart:

$$\frac{dx \wedge dz \wedge ds}{x} = du_j \wedge dr_j \wedge ds, \qquad j = 1, 2, 3, \tag{XI.4.11}$$

$$-\frac{dy \wedge dz \wedge ds}{y} = db \wedge dy \wedge ds. \tag{XI.4.12}$$

For clarity, the first residue calculation can be done once for all three charts. Since $x = u_j^j r_j^{j-1}$ and $z = u_j r_j$,

$$\det \frac{\partial(x, z)}{\partial(u_j, r_j)} = ju_j^j r_j^{j-1} - (j-1)u_j^j r_j^{j-1} = x. \tag{XI.4.13}$$

The factor x cancels the denominator of the residue. The resulting form in (XI.4.11) is regular and nowhere zero even where the displayed quotient in the singular coordinates was not defined. This is the local reason the resolution preserves the Calabi–Yau form.

Now fix s. For $j = 1, 2$, the branch $u_j = 0$ in chart j and the branch $r_{j+1} = 0$ in the next chart glue to a sphere C_j. The two branches through the origin of chart 2 meet transversely. The spheres are labeled throughout the family by the order of the factors. This is the split case: transport does not exchange the gauge curve labels. The candidate third sphere would have $u_3 = 0$ in chart 3. There

$$u_3 = 0: \qquad x = z = 0, \qquad y = -r_3 f(s). \tag{XI.4.14}$$

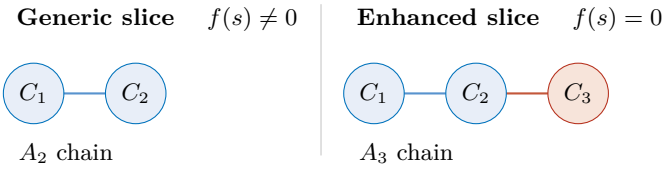


Figure XI.4.1: Compact exceptional curves in the resolved s slices of (XI.4.1). Each vertex is a sphere and each edge is a transverse intersection in the surface. The red endpoint C_3 exists as an exceptional curve only at the enhancement.

The whole branch lies over the singular point only when $f(s) = 0$. At that value it glues to $y = 0$ in chart 4 and defines C_3. It meets C_2 at $u_3 = r_3 = 0$ and misses C_1. Figure XI.4.1 records the resulting chains.

At $f = 0$, the two descriptions of the last sphere can be written as equations inside smooth coordinate spaces,

$$C_3 \cap U_3 = \{u_3 = s = 0\}, \quad r_3 \in \mathbb{C}, \qquad C_3 \cap U_4 = \{y = s = 0\}, \quad b \in \mathbb{C}, \qquad b = r_3^{-1}. \tag{XI.4.15}$$

Here we have specialized to $f = s$. The point $r_3 = \infty$ is present as $b = 0$ in the second chart. At nonzero s, the equation $u_3 = 0$ instead maps to a line with varying $y = -r_3 s$. It therefore fails to contract to a point. This distinguishes a line drawn in one chart from an exceptional compact sphere of the contraction.

The normal bundle of C_3 in the threefold gives a further distinction. At a simple zero we can use $f(s)$ as a local coordinate. Write $u = x/z^2$ and $w = z - f(s)$ after the first two steps. The remaining contraction and the last chart change are

$$uy = zw, \tag{XI.4.16}$$

$$b = r_3^{-1}, \qquad (z, y) = r_3(u, w). \tag{XI.4.17}$$

The coordinate change from (z, s) to (z, w) is invertible because $w = z - f(s)$ and $f'(0) \neq 0$. In particular, when $f = s$ its inverse is $s = z - w$. In the first of the two remaining patches, (u, w) are transverse coordinates to the curve, while r_3 is its coordinate. In the other, (z, y) are transverse and b is its coordinate. This gives an actual coordinate interpretation of the two entries in (XI.4.17).

Equation (XI.4.16) is the ordinary threefold node. In (XI.4.17) the base coordinates r_3, b cover the exceptional $\mathbb{P}^1$. Each normal coordinate has the $\mathcal{O}(-1)$ transition. Consequently,

$$N_{C_3/X} = \mathcal{O}(-1) \oplus \mathcal{O}(-1), \qquad H^0(C_3, N_{C_3/X}) = 0, \tag{XI.4.18}$$

where X denotes the resolved threefold. We use the convention that fiber coordinates of $\mathcal{O}(-1)$ obey $v_b = r_3 v_r$ on $b = r_3^{-1}$. A global section would have $v_r(r_3)$ holomorphic on the finite plane and $v_b(b) = b^{-1} v_r(b^{-1})$ regular at $b = 0$. A power series in r_3 then produces only negative powers of b, so regularity forces every coefficient to vanish. Each of the two normal components in (XI.4.17) obeys this condition. Figure XI.4.2 shows the coordinate roles.

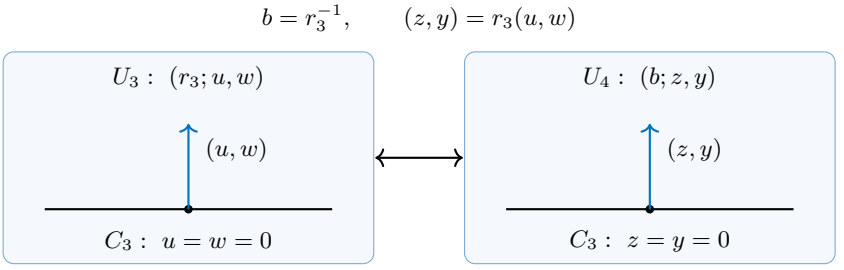


Figure XI.4.2: The two affine patches of the isolated sphere C_3. The horizontal coordinates r_3 and b are related by inversion. The blue arrows depict the pair of normal fiber coordinates, not extra curves. Both normal components are multiplied by r_3 on the overlap. The equations distinguish a coordinate along the sphere from a displacement away from it.

Thus C_3 has no infinitesimal motion in X. Its self-intersection in the resolved A_3 *surface* is -2, as for the other exceptional spheres of that surface. These are different statements: the surface self-intersection measures a line normal to the curve inside a surface, while (XI.4.18) describes both normal directions in the threefold.

XI.4.3 A compact gauge curve and its electric charges

A small disk suffices to analyze the collision. To measure a four-dimensional charge, we also want a model in which the gauge curves sweep out compact divisors. We will build one over $\mathbb{P}^1$, then use a wall relation in its fan to compute each charge. The construction uses the same height-one convention as the split fibration of the previous chapter.

Use planar coordinates for rays of height one in the toric lattice:

$$P = (1, 0), \quad L = (-1, 0), \quad E = (-1, 1), \qquad D_k = (0, k) \quad (k = 0, 1, 2, 3). \tag{XI.4.19}$$

A ray in these formulas means the vector $(a, b, 1)$ in a three-dimensional lattice when its planar label is (a, b). The last component is important. For example, the planar identity $D_0 + D_2 = 2D_1$ also holds for the lifted vectors because both sides have height two. A character $m = (A, B, C)$ is a monomial on the algebraic torus. Its vanishing order on the ray $(a, b, 1)$ is

$$\langle m, (a, b, 1) \rangle = Aa + Bb + C. \tag{XI.4.20}$$

Nonnegative pairings mean the monomial extends over that affine toric patch. This criterion will connect the fan to the polynomial equation of the collision.

The smooth fan has seven maximal cones. Six come from joining each segment $D_k D_{k+1}$ to P and to L. The last cone fills the triangle LED_3:

$$(P, D_k, D_{k+1}), \quad (L, D_k, D_{k+1}) \quad (k = 0, 1, 2), \qquad (L, E, D_3). \tag{XI.4.21}$$

The triangles have disjoint interiors and fill the polygon bounded by P, L, E, D_3. The determinants of their lifted ray triples have absolute value one: for the first six, this uses the unit separation of adjacent D_k and the first coordinate ± 1; for the last it uses the unit length of LE and the unit horizontal distance to D_3. All rays have height one, so the subdivision is crepant. Projecting the first coordinate gives the fan of $\mathbb{P}^1$. The divisors of the interior rays D_1, D_2 are compact and map onto that base.

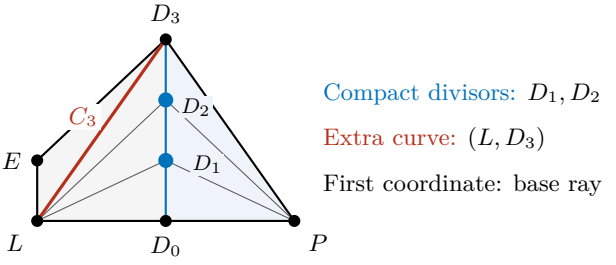


Figure XI.4.3: Height-one slice of the fan in (XI.4.21). The shaded triangles on the right give the positive base chart. The compact gauge divisors are the two interior vertices. The red internal edge is the compact curve C_3, although its two endpoints correspond to noncompact divisors.

To connect this fan to the local collision, contract the subdivision in the negative base chart. The dual lattice characters, written as integer triples, are

$$x = (0, 1, 0), \quad y = (2, -1, 3), \quad z = (1, 0, 1), \quad w = (-1, 0, 0). \tag{XI.4.22}$$

A dual lattice point (A, B, C) pairs nonnegatively with L, E, D_0, D_3 precisely when $C \geq 0$, $C + 3B \geq 0$, $A \leq C$ and $A \leq C + B$. For $B \geq 0$ it is $Bx + Cz + (C - A)w$. For $B = -d < 0$ it is $dy + (C - 3d)z + (C - d - A)w$. In each expression all coefficients are nonnegative. The relation of the four exponents gives the single equation of the contracted patch:

$$x + y = 3z + w \quad \text{in the character lattice,} \qquad xy = z^3 w \quad \text{in the affine coordinates.} \tag{XI.4.23}$$

For instance, on the cone (L, D_2, D_3) the three smooth coordinates are x/z^2, z^3/x and w. Their exponents pair as a basis with the cone generators. This is the chart (u_3, r_3, w) of the small resolution in (XI.4.17). The adjacent cone (L, E, D_3) has coordinates y, b, z with $b = x/z^3$, the other chart of that resolution.

The base projection on the negative chart is the character w. The dual inequalities on the contracted positive cone are $A + C \geq 0$, $C \geq 0$ and $C + 3B \geq 0$. Now use the characters

$$W = (1, 0, 0), \quad X = (0, 1, 0), \quad Y = (-3, -1, 3), \quad Z = (-1, 0, 1). \tag{XI.4.24}$$

An allowed exponent with $B \geq 0$ is $(A + C)W + BX + CZ$. For $B = -d < 0$ it is $(A + C)W + dY + (C - 3d)Z$. This gives the product patch $XY = Z^3$. On the overlap

the coordinate functions satisfy

$$W = w^{-1}, \qquad (X, Y, Z) = (x, w^5 y, w^2 z), \qquad XY = w^5 xy = w^6 z^3 = Z^3. \quad \text{(XI.4.25)}$$

The singular gauge lines therefore glue to a rational curve with a split A_2 family away from the exceptional point. To recover the local ALE collision on the negative chart, use $s = z - w$. This coordinate equals $-w$ on the singular gauge line. Away from the line it gives a different slicing: $s = 0$ has $xy = z^4$, whereas $w = 0$ has $xy = 0$. There is no second enhancement on the positive product patch.

A compact toric wall curve meets two neighboring maximal cones. If their opposite rays are R_+, R_- and the two wall rays are U, V, write the integral relation as

$$R_+ + R_- + d_U U + d_V V = 0. \quad \text{(XI.4.26)}$$

We use the ray labels for their divisors as well. The coefficients are the intersections of the corresponding divisors with the curve. The opposite divisors each meet it once, at the two ends of the toric $\mathbb{P}^1$. Intersecting a principal divisor from a lattice character with the curve then fixes the other two coefficients. The two gauge fibers over the negative chart are the walls $(L, D_1), (L, D_2)$, and C_3 is (L, D_3). In order, their relations are

$$D_0 + D_2 - 2D_1 = 0, \quad \text{(XI.4.27)}$$

$$D_1 + D_3 - 2D_2 = 0, \quad \text{(XI.4.28)}$$

$$E + D_2 - L - D_3 = 0. \quad \text{(XI.4.29)}$$

For example, C_3 is the common face (L, D_3) of the two cones (L, D_2, D_3) and (L, E, D_3). The opposite divisors are D_2 and E. Their intersections with C_3 are $+1$. Let the two remaining intersections be d_L, d_3. Intersecting principal divisors with a compact curve gives zero. Requiring this for every lattice character is equivalent to

$$(0, 2, 1) + (-1, 1, 1) + d_L(-1, 0, 1) + d_3(0, 3, 1) = 0. \quad \text{(XI.4.30)}$$

The first component gives $d_L = -1$, the second gives $d_3 = -1$, and the height equation is then satisfied. Neither compactness of E nor compactness of L was used. The compact curve C_3 is the orbit closure of the internal wall (L, D_3) joining those two cones; E and D_2 are their opposite vertices. The compact gauge divisors are the surfaces D_1, D_2. Intersecting the wall with D_2 already shows how a curve at an endpoint can carry gauge charge.

These relations also check that the three curve areas can vary independently in a common Kähler chamber. Assign positive bending parameters p_1, p_2, p_3, h by taking heights

$$\eta_L = \eta_{D_0} = \eta_{D_1} = 0, \qquad (\eta_{D_2}, \eta_{D_3}, \eta_E, \eta_P) = (p_1,\ 2p_1 + p_2,\ p_1 + p_2 + p_3,\ h). \quad \text{(XI.4.31)}$$

The three wall rows in (XI.4.29) evaluate to p_1, p_2, p_3. The corresponding positive-side fiber rows evaluate to p_1, p_2. Across the three central walls $D_k D_{k+1}$ the bends are h, $h + 2p_1$ and $h + 2p_1 + 4p_2$. All eight are positive, so these heights give a strictly convex subdivision.

Choose the signed coroot convention $q_i(C) = -D_i \cdot C$. This turns the first two columns of the curve pairing into the positive A_2 Cartan matrix. The extra boundary divisor E provides a third linear functional $\ell(C) = E \cdot C$:

Curve	q_1	q_2	ℓ
C_1	2	-1	0
C_2	-1	2	0
C_3	0	-1	1

(XI.4.32)

The full charge computation can now be used without the fan. For an oriented class $C = n_1C_1 + n_2C_2 + n_3C_3$, linearity gives

$$\begin{pmatrix} q_1(C) \\ q_2(C) \\ \ell(C) \end{pmatrix} = \begin{pmatrix} 2 & -1 & 0 \\ -1 & 2 & -1 \\ 0 & 0 & 1 \end{pmatrix} \begin{pmatrix} n_1 \\ n_2 \\ n_3 \end{pmatrix}. \tag{XI.4.33}$$

For example, $n = (0, 1, 1)$ gives $(-1, 1; 1)$. Reversing the orientation changes n to $-n$ and reverses every charge. The three rows of this matrix are measurements on a curve class. They should not be interpreted as three compact gauge fields. The third measurement will be the charge under the fixed flavor background.

Thus C_3 carries gauge charge even though it does not add a third compact gauge divisor. In this noncompact model we fix the extra flavor value at the boundary. The intersections themselves make no assertion about normalizability in another embedding.

There is another useful chamber for this same ray set. Starting from (XI.4.21), replace the internal diagonal (L, D_3) by (E, D_2), then (L, D_2) by (E, D_1). The two curves on (L, D_1) and (E, D_1) in that chamber have wall relations

$$D_0 + E - L - D_1 = 0, \qquad L + D_2 - E - D_1 = 0. \tag{XI.4.34}$$

Adding them gives the original generic C_1 row. This is the description in which one fiber of the first ruled surface splits. The end-node picture in Figure XI.4.1 instead uses the chamber of (XI.4.21). The same ray set can describe different effective curves; comparing these wall rows does not compare the full BPS spectra of the two chambers.

XI.4.4 Reading the fundamental from the adjoint

How do we recognize the matter representation from the charges? At the enhanced point the ordinary ALE root system is A_3. In an ordered basis of four coordinate vectors e_i, the simple roots are $\alpha_j = e_j - e_{j+1}$. They label C_j. The root $e_i - e_j$ for $i < j$ therefore has the oriented class $C_i + \cdots + C_{j-1}$. The generic gauge algebra uses the first three coordinates. Its six roots $e_i - e_j$ with $1 \le i \ne j \le 3$ already occur in the generic fiber. The six additional roots are $\pm(e_i - e_4)$ for $i = 1, 2, 3$.

To compute how they transform, work in the complex Lie algebra. Write a traceless parent matrix in blocks:

$$\mathcal{X} = \begin{pmatrix} A + \varphi I_3 & v \\ \widetilde{v} & -3\varphi \end{pmatrix}, \qquad \operatorname{Tr} A = 0, \qquad H = \operatorname{diag}(1, 1, 1, -3). \tag{XI.4.35}$$

Commuting with a gauge generator $\mathrm{diag}(G,0)$ sends v to Gv and $\widetilde{v}$ to $-\widetilde{v}G$. Thus v is a fundamental column and $\widetilde{v}$ a dual row. The diagonal block A is an adjoint and φH is a singlet. For a matrix unit E_{ij} and a diagonal matrix h the commutator is

$$[h, E_{ij}] = (h_{ii} - h_{jj})E_{ij}. \tag{XI.4.36}$$

In particular, $[H, E_{i4}] = 4E_{i4}$ and $[H, E_{4i}] = -4E_{4i}$. The factor four comes from the difference $1-(-3)$, not from the number of components of v. With the integral generator H the decomposition is

$$\mathbf{15} = \mathbf{8}_0 \oplus \mathbf{1}_0 \oplus \mathbf{3}_4 \oplus \overline{\mathbf{3}}_{-4}. \tag{XI.4.37}$$

One may use $H/4$ as a Lie algebra generator with unit matter charge. This rescales the coefficient of the generator in a background field; it does not prescribe a global gauge group.

The dimension count provides a useful first check on the branching. A traceless 3×3 matrix has eight components, the centralizer has one, and the two off-diagonal blocks have three each,

$$15 = 8 + 1 + 3 + 3. \tag{XI.4.38}$$

This count says how many generators transform in each block. It does not yet say how many wave functions of a given block are localized along the base. One could have the same block transformation law with several independent transverse wave functions. The next section determines that remaining number for a simple point.

For the two gauge charges use $h_1 = \mathrm{diag}(1,-1,0,0)$ and $h_2 = \mathrm{diag}(0,1,-1,0)$. Apply (XI.4.36) to E_{14}, E_{24}, E_{34}. The three results must also follow from the divisor pairing, which is additive on the curve classes. In order, they give

Root	Oriented class	$(q_1, q_2; q_H)$
$e_1 - e_4$	$C_1 + C_2 + C_3$	$(1, 0; 4)$
$e_2 - e_4$	$C_2 + C_3$	$(-1, 1; 4)$
$e_3 - e_4$	C_3	$(0, -1; 4)$

(XI.4.39)

where $q_H = 4\ell$. For example, adding the C_2 and C_3 rows of (XI.4.32) gives $(-1,2;0) + (0,-1;4) = (-1,1;4)$ in the H normalization. The opposite orientations negate all charges. The rows are different weights of one representation. In the matrix basis, the simple gauge raising operators act by

$$[E_{23}, E_{34}] = E_{24}, \qquad [E_{12}, E_{24}] = E_{14}. \tag{XI.4.40}$$

In the curve basis these steps add C_2 and then C_1 to the class of the extra endpoint. Thus the three entries in (XI.4.39) belong to a single connected weight diagram. A class such as $C_2 + C_3$ need not be represented by an individual smooth sphere. The root and divisor calculations tell us its charge, not the stability of a separate wrapped state on a reducible curve.

We can practice the charge calculation in a different integral basis while staying in this same geometry. Define

$$B_1 = C_1, \qquad B_2 = C_2, \qquad B_3 = C_2 + C_3, \qquad C_3 = B_3 - B_2. \tag{XI.4.41}$$

The change of basis has determinant one, so it preserves the integral lattice spanned by these three classes. Its point is to make the middle weight, rather than the lowest weight, a basis vector. Apply (XI.4.33) to the new basis,

Class	$(q_1, q_2; \ell)$
B_1	$(2, -1; 0)$
B_2	$(-1, 2; 0)$
B_3	$(-1, 1; 1)$

(XI.4.42)

The extra roots $e_1 - e_4, e_2 - e_4, e_3 - e_4$ now have the classes

$$(B_1 + B_3,\ B_3,\ B_3 - B_2). \tag{XI.4.43}$$

For instance, the charge of the last entry is $(-1, 1; 1) - (-1, 2; 0) = (0, -1; 1)$, exactly the charge of C_3. The other two give $(1, 0; 1)$ and $(-1, 1; 1)$. Thus the apparent subtraction in the lowest weight has changed no electric charge. An integral basis need not consist of generators of the effective cone. In particular, this re-expression establishes no new stability statement about B_3 as a wrapped particle.

The same exercise explains how the sequence of charges operates. The gauge operator E_{23} adds the root of B_2 to the lowest weight $B_3 - B_2$, producing B_3. Then E_{12} adds B_1, producing $B_1 + B_3$. A weight string is therefore a sequence of gauge-related components. Counting its three entries as three fundamentals would count the color index three times.

The neutral summand in (XI.4.37) describes the parent centralizer direction. It does not count a neutral hypermultiplet at the special point. To count matter we still need to determine how many normalizable charged modes are supported there.

XI.4.5 One hypermultiplet at a transverse point

Why does one special point contribute one copy of the fundamental? The extra charged fields acquire a mass as one moves away from the enhancement. In the local Type IIA description this mass comes from the separation of the fourth root position from the other three. The charged zero-mode equation in the transverse plane is of Dirac type, with the holomorphic mass proportional to $f(s)$. At a simple zero we translate its position to the origin and retain the linear mass. We will solve this flat local problem on the complex plane. It counts the modes in the linear approximation, rather than the zero modes of an operator on a complete compactification.

Write $s = x_1 + ix_2$ and $\partial = (\partial_{x_1} - i\partial_{x_2})/2$, $\bar\partial = (\partial_{x_1} + i\partial_{x_2})/2$. After absorbing the phase of the slope into the components and rescaling the local coordinates, a representative of the linear problem, with flat measure $d^2 s$, is

$$\mathcal{D} = \begin{pmatrix} \bar\partial & \kappa s \\ \kappa \bar s & \partial \end{pmatrix}, \qquad \mathcal{D}^\dagger = \begin{pmatrix} -\partial & \kappa s \\ \kappa \bar s & -\bar\partial \end{pmatrix}, \qquad \kappa > 0. \tag{XI.4.44}$$

The adjoint signs follow from integration by parts in the flat measure. For fields that decay at infinity,

$$\bar\partial^\dagger = -\partial, \qquad (\kappa s)^\dagger = \kappa \bar s. \tag{XI.4.45}$$

The derivatives and multiplication terms act on the wave function to their right. When multiplying the matrices one must therefore use the product rule. Treating s as a number that commutes with ∂ would remove the term that permits the zero mode.

A direct solution of two first-order equations could find a Gaussian. Squaring gives a way to check whether there are any other solutions. In $\mathcal{D}^\dagger\mathcal{D}$, the upper off-diagonal entry acts as $-\kappa\partial(s\psi) + \kappa s\partial\psi = -\kappa\psi$. The reverse product has an upper off-diagonal derivative $\bar\partial s = 0$. The lower entries follow by conjugation. Writing $\sigma_1 = \left(\begin{smallmatrix} 0 & 1 \\ 1 & 0 \end{smallmatrix}\right)$ and I for the two-component identity gives

$$\mathcal{D}^\dagger\mathcal{D} = H_{\rm osc} I - \kappa\sigma_1, \qquad \mathcal{D}\mathcal{D}^\dagger = H_{\rm osc} I, \tag{XI.4.46}$$

$$H_{\rm osc} = -\frac{1}{4}(\partial_{x_1}^2 + \partial_{x_2}^2) + \kappa^2(x_1^2 + x_2^2). \tag{XI.4.47}$$

Here is a direct way to see both the oscillator gap and its cancellation. For one real coordinate define

$$A_i = \frac{1}{2}\partial_{x_i} + \kappa x_i, \qquad A_i^\dagger = -\frac{1}{2}\partial_{x_i} + \kappa x_i, \qquad [A_i, A_i^\dagger] = \kappa. \tag{XI.4.48}$$

Then the two-coordinate oscillator satisfies

$$H_{\rm osc} = A_1^\dagger A_1 + A_2^\dagger A_2 + \kappa. \tag{XI.4.49}$$

Both $A_i^\dagger A_i$ are nonnegative in this domain. The plus eigenvector of σ_1 subtracts exactly the last κ in (XI.4.49), while the minus eigenvector adds another κ. A possible zero mode must therefore satisfy $A_1\psi = A_2\psi = 0$ and lie in the plus spinor direction. This is also a uniqueness argument.

For each coordinate, set $\xi = \sqrt{2\kappa}\, x_i$. The operator in that coordinate becomes $\kappa(-\partial_\xi^2 + \xi^2)/2$, with levels $\kappa(n_i + \frac{1}{2})$. The two eigenvalues of σ_1 are ± 1, and the resulting squared levels in its two channels are

$$E_+ = \kappa(n_1 + n_2), \qquad E_- = \kappa(n_1 + n_2 + 2). \tag{XI.4.50}$$

Only the ground state of the plus channel can vanish. The reverse product has a gap κ, so the adjoint has no zero mode. The normalized solution of the original linear equation is

$$\Psi_0(s) = \sqrt{\frac{\kappa}{\pi}}\, e^{-\kappa|s|^2} \begin{pmatrix} 1 \\ 1 \end{pmatrix}. \tag{XI.4.51}$$

The Gaussian can be verified before normalizing it. If $g = e^{-\kappa s\bar s}$, then

$$\bar\partial g = -\kappa s g, \qquad \partial g = -\kappa \bar s g, \qquad \mathcal{D}\begin{pmatrix} g \\ g \end{pmatrix} = 0. \tag{XI.4.52}$$

The two components have equal sign because the zero mode is in the plus eigenspace of σ_1. Their equal norm is essential for the prefactor in (XI.4.51).

The normalization follows from $\int_{\mathbb{C}} e^{-2\kappa|s|^2} d^2 s = \pi/(2\kappa)$. There is one transverse wave function per independent color component, not one flavor per component.

The spatial extent of this solution is useful for interpreting the word localized. From the probability density $\Psi_0^\dagger \Psi_0 = (2\kappa/\pi) e^{-2\kappa|s|^2}$ one finds

$$\int d^2 s \, \Psi_0^\dagger \Psi_0 = 1, \qquad \langle |s|^2 \rangle = \frac{1}{2\kappa}. \tag{XI.4.53}$$

The scale $\kappa^{-1/2}$ is a width in the chosen flat local coordinate. When the linear approximation models a small patch of a curved base, its use requires that the wave function be supported where that approximation is adequate. For a transverse zero, the phase of the nonzero slope can be absorbed in the fields. Its magnitude, together with the local normalization of the kinetic and mass terms, sets κ. This slope controls localization; it is not yet a four-dimensional quark mass.

We can keep the center and phase explicit instead of removing them. This makes it possible to compare two ordinary enhancement points without confusing their positions, widths and multiplicities. Put $\xi = s - s_0$, and let the coefficient of the linear mass be $\eta = \kappa e^{i\theta}$ with θ real. In the same flat measure,

$$\mathcal{D}_\eta = \begin{pmatrix} \bar{\partial} & \eta\xi \\ \bar{\eta}\bar{\xi} & \partial \end{pmatrix}, \qquad \Psi_{s_0,\theta} = \sqrt{\frac{\kappa}{\pi}} \, e^{-\kappa|\xi|^2} \begin{pmatrix} 1 \\ e^{-i\theta} \end{pmatrix}. \tag{XI.4.54}$$

The phase appears in the relative components, rather than in the probability density. For example, the upper equation gives

$$\bar{\partial} e^{-\kappa|\xi|^2} + \eta\xi e^{-i\theta} e^{-\kappa|\xi|^2} = (-\kappa + \eta e^{-i\theta}) \xi e^{-\kappa|\xi|^2} = 0. \tag{XI.4.55}$$

The lower equation uses $\bar{\eta} = \kappa e^{-i\theta}$ and vanishes as well. Translation and a constant unitary rotation of the two components take this problem to (XI.4.44). They preserve the norm and the dimension of the kernel. In particular a negative real slope corresponds to $\theta = \pi$, not to a lost Gaussian or an extra matter copy.

Both components enter the norm. Writing $r = |\xi|$ gives the normalization and centered variance directly,

$$\|\Psi_{s_0,\theta}\|^2 = \frac{2\kappa}{\pi} \int_0^\infty e^{-2\kappa r^2} \, 2\pi r \, dr = 1, \tag{XI.4.56}$$

$$\langle s \rangle = s_0, \qquad \ell^2 := \langle |s - s_0|^2 \rangle = \frac{2\kappa}{\pi} \int_0^\infty r^2 e^{-2\kappa r^2} \, 2\pi r \, dr = \frac{1}{2\kappa}. \tag{XI.4.57}$$

Thus the two points at $s_0 = 1$ and $s_0 = -1$ in the later example have different centers, even when their linearized slopes have the same magnitude and their probability profiles have the same width. The three color entries multiply this transverse solution. They do not multiply its normalization constant or change its transverse width.

The Gaussian on the whole plane is an exact solution of a linear operator. To use it as a local model on the actual base, we must check where the nonlinear terms become significant. At an ordinary zero, expand the holomorphic separation as

$$f(s_0 + \xi) = A\xi + B\xi^2 + \sum_{n \geq 3} b_n \xi^n, \qquad A = f'(s_0) \neq 0, \quad B = \tfrac{1}{2} f''(s_0). \tag{XI.4.58}$$

After a phase choice take $A > 0$. Fixing the local kinetic and mass normalizations so that $\kappa = A$, the ratio of the quadratic term to the linear term at one width is

$$\frac{|B|\ell^2}{A\ell} = \frac{|B|}{\sqrt{2A^3}}, \qquad \ell = \frac{1}{\sqrt{2A}}. \tag{XI.4.59}$$

This is a leading diagnostic, not a sufficient condition for a general analytic f. A controlled use of a patch requires a small remainder throughout the region where most probability lies. For a chosen fixed $L > 1$, a useful pair of conditions is

$$\sup_{0<|\xi|\le L\ell} \left| \frac{f(s_0+\xi) - A\xi}{A\xi} \right| \ll 1, \qquad L\ell \ll L_{\text{metric}}. \tag{XI.4.60}$$

Here L_{metric} is the coordinate scale over which the flat kinetic approximation changes substantially. The omitted Gaussian probability outside the disk is

$$\int_{|\xi|>L\ell} d^2\xi\, \Psi^\dagger \Psi = e^{-2\kappa L^2 \ell^2} = e^{-L^2}. \tag{XI.4.61}$$

These estimates explain the role of the local approximation without assigning an exact compact zero-mode count to the truncated operator.

For example, in fixed flat units let $f(\xi) = \xi + 100\xi^3$. The quadratic coefficient vanishes, but the cubic term at the linear width is large,

$$f''(0) = 0, \qquad \kappa = 1, \qquad \ell = \frac{1}{\sqrt{2}}, \qquad \left| \frac{100\ell^3}{\ell} \right| = 50. \tag{XI.4.62}$$

The linear Gaussian therefore supplies no controlled approximation across that width. By contrast, for a purely linear $f = A\xi$ all the Taylor corrections vanish. Changing A then changes the width while preserving one transverse solution. Neither operation specifies the Kähler period of the wrapped sphere. We turn to those periods after identifying the full matter multiplet.

At the gauge enhancement, the same transverse equation acts on each entry of the fundamental column. If e_i is a color basis, the solutions in that charged block have the form

$$\Psi(s) = \Psi_0(s) \otimes \sum_{i=1}^{3} v_i e_i, \qquad \ker \mathcal{D} \otimes \mathbf{3} \simeq \mathbb{C} \otimes \mathbf{3}. \tag{XI.4.63}$$

There is one coefficient vector v transforming as a $\mathbf{3}$. Three independent vectors of this kind, rather than its three entries, would constitute three flavors.

For the ordinary split Type IIA enhancement, the localized mode is identified with the charged matter from the new vanishing cycle. The local calculation provides one copy of the fundamental and its conjugate. Reversing D2 orientation gives the opposite charges. In four-dimensional $\mathcal{N} = 1$ notation the fields of one full $\mathcal{N} = 2$ hypermultiplet are

$$Q \in \mathbf{3}_4, \qquad \widetilde{Q} \in \overline{\mathbf{3}}_{-4}. \tag{XI.4.64}$$

The complex scalar space of the pair has a commuting antilinear map $(Q, \widetilde{Q}) \mapsto (-\widetilde{Q}^\dagger, Q^\dagger)$ whose square is -1. This supplies the quaternionic structure of a hypermultiplet. A single $\mathbf{3}$ does not admit such a map: the center acts by conjugate eigenvalues

on $\mathbf{3}$ and $\overline{\mathbf{3}}$, so the two representations are inequivalent. Thus the conjugate charges in (XI.4.37) are needed for a full hypermultiplet; they are not a second flavor.

This distinction can also be counted in scalar components. Write $Q = (q_1, q_2, q_3)$ and $\widetilde{Q} = (\widetilde{q}^1, \widetilde{q}^2, \widetilde{q}^3)$. The scalar space of one full fundamental has

$$\dim_{\mathbb{C}}(\mathbf{3} \oplus \overline{\mathbf{3}}) = 6, \qquad \dim_{\mathbb{H}} = 3. \tag{XI.4.65}$$

Its quaternionic dimension equals the color dimension of the representation. The flavor multiplicity is still one. Conjugating the oriented D2 charge selects the partner representation inside this pair. It does not create an independent transverse solution of the same charge block.

Two separated simple zeros can give two such local problems. For example take $f(s) = s^2 - 1$ on a disk containing both roots. The expansions are

$$f(1+\delta) = 2\delta + \delta^2, \qquad f(-1+\delta) = -2\delta + \delta^2. \tag{XI.4.66}$$

For example, denote the centered coordinate in either patch by $\delta = s - s_0$. The linear coordinate in the local node model is $f(s)$, and the two inverse expansions begin as

$$\delta = \tfrac{1}{2} f + O(f^2) \quad (s_0 = 1), \qquad \delta = -\tfrac{1}{2} f + O(f^2) \quad (s_0 = -1). \tag{XI.4.67}$$

The sign changes a coordinate phase, not the number of normalizable ground states. No such coordinate exists at a double zero because the inverse derivative would diverge.

Each has a nonzero linear slope. With the same split gauge embedding at both points and no projection identifying them, the two local contributions add. Figure XI.4.4 shows what the two local wave functions mean. The calculation compares two neighborhoods; it does not require a second compact model with a specified global metric.

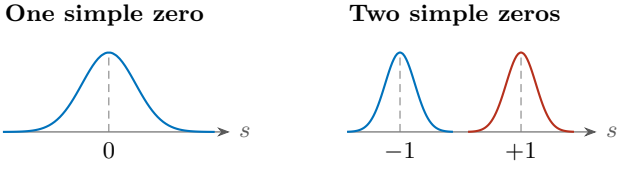


Figure XI.4.4: Profiles of the local Gaussian amplitudes on a real slice through the enhancement points. For $f = s$ there is one linear problem centered at zero. For $f = s^2 - 1$ the two profiles represent separate linear problems near -1 and $+1$, with widths shown schematically. The right panel is not a solution of a single nonlinear Dirac problem over the whole base.

When the zeros coalesce, the linear argument changes. Take $f = s^2$ and return to the equation after the first two graph steps. The term zs^2 has no quadratic part:

$$uy - z(z - s^2) = uy - z^2 + zs^2. \tag{XI.4.68}$$

The quadratic form now has rank three rather than four. The change is visible in the normal directions as well. Keeping s as a coordinate, the last transition has

$y = r_3^2 u - r_3 f(s)$. At $f'(0) = 0$ its linearization on the normal coordinates is

$$\begin{pmatrix} y \\ s \end{pmatrix}_{\text{lin}} = \begin{pmatrix} r_3^2 & 0 \\ 0 & 1 \end{pmatrix} \begin{pmatrix} u \\ s \end{pmatrix}_{\text{lin}}. \tag{XI.4.69}$$

It gives $\mathcal{O}(-2) \oplus \mathcal{O}$, with one first-order section. That section need not extend to an actual motion of the curve. Neither the ordinary node calculation nor the flat linear oscillator applies to this double zero. The surface still has the A_3 type at $s = 0$, which is why the branching alone cannot count its states. A genuine outer monodromy would introduce a different issue: it would prevent us from transporting the gauge curve labels globally as in Figure XI.4.1.

XI.4.6 The Kähler mass and the gauge beta function

Which physical parameter controls the mass, and how does the one full fundamental affect the gauge coupling? The coordinate s and the function $f(s)$ tell us where the enhancement is located in the holomorphic model. To set a D2 mass we resolve the vanishing cycles and measure their Kähler periods instead. Let J be the Kähler form, B the two-form potential, and $M_s = 1/\sqrt{\alpha'}$. In a common local period and integer-flux lift write

$$t_C = \frac{1}{4\pi^2\alpha'} \int_C (B + iJ), \qquad T_C = -2\pi i\, t_C, \qquad a_C = \frac{M_s}{g_s}\, \frac{t_C}{i}. \tag{XI.4.70}$$

Here t_C, T_C are dimensionless and a_C has mass dimension one. We fix the smooth leading mass at small curvature in string units, at $B = 0$ and with vanishing worldvolume flux. The D2 tension is $\tau_2 = 1/((2\pi)^2 g_s \alpha'^{3/2})$, and for an effective smooth calibrated sphere

$$M_C^{\text{smooth}} = \tau_2 \int_C J = \frac{M_s}{g_s}\, \frac{1}{4\pi^2\alpha'} \int_C J = a_C. \tag{XI.4.71}$$

The use of these periods for the light charged sector near collapse invokes the protected wrapped-state continuation. The smooth tension formula alone is not a derivation at sub-stringy curve area.

There are now two geometric calculations in play, with different purposes. The roots of f are points in the complex-structure description. The integrals of $B + iJ$ are periods on resolved curves. Even on the real $B = 0$ slice, multiplying the area by a brane tension is needed to obtain mass units,

$$[\alpha'] = \text{length}^2, \quad \left[\int_C J\right] = \text{length}^2, \quad [t_C] = 1, \quad [\tau_2 \int_C J] = \text{mass}. \tag{XI.4.72}$$

A coordinate separation such as $f'(s_0)\delta$ has no prescribed mass normalization until a metric and kinetic normalization have been supplied. The period formula is the mass convention we use for the selected charged states.

Let $(a_1, a_2, c) = (a_{C_1}, a_{C_2}, a_{C_3})$. The chamber of the fan allows all three positive. Use Coulomb eigenvalues λ_i in the mass convention, so

$$\lambda_1 - \lambda_2 = a_1, \quad \lambda_2 - \lambda_3 = a_2, \quad \lambda_1 + \lambda_2 + \lambda_3 = 0. \tag{XI.4.73}$$

The first two equations give $\lambda_2 = \lambda_3 + a_2$ and $\lambda_1 = \lambda_3 + a_2 + a_1$. The trace condition then gives

$$(\lambda_1, \lambda_2, \lambda_3) = \frac{1}{3}(2a_1 + a_2,\ -a_1 + a_2,\ -a_1 - 2a_2). \tag{XI.4.74}$$

To find the mass parameter, include the flavor scalar coefficient φ in the parent diagonal matrix of (XI.4.35). Its first three entries are $\lambda_i + \varphi$ and the last is -3φ. Therefore the oriented extra root $e_i - e_4$ evaluates to

$$Z_i = (\lambda_i + \varphi) - (-3\varphi) = \lambda_i + m, \qquad m = 4\varphi. \tag{XI.4.75}$$

Using $Z_3 = a_{C_3} = c$ from (XI.4.39) and additivity gives

$$m = c + \frac{a_1 + 2a_2}{3}, \qquad (Z_1, Z_2, Z_3) = (a_1 + a_2 + c,\ a_2 + c,\ c). \tag{XI.4.76}$$

The mass map can be inverted without any geometric guess. Take differences of the three signed periods and then their mean,

$$a_1 = Z_1 - Z_2, \qquad a_2 = Z_2 - Z_3, \qquad m = \frac{Z_1 + Z_2 + Z_3}{3}, \qquad c = Z_3. \tag{XI.4.77}$$

The mean removes the traceless gauge scalar. This identifies the common shift of all three weights with the flavor mass. It also shows why the signed periods, before taking absolute values, are the appropriate variables for a linear charge map.

In the integral basis (XI.4.41), put $d = a_{B_3} = a_2 + c$. The same map becomes

$$(Z_1, Z_2, Z_3) = (a_1 + d,\ d,\ d - a_2), \qquad m = d + \frac{a_1 - a_2}{3}. \tag{XI.4.78}$$

The original positive chamber has $a_1, a_2, c > 0$, so here it requires $d > a_2$, in addition to $a_1, a_2 > 0$. Arbitrarily imposing only positivity of the new basis periods would enlarge that chamber. This is the period counterpart of the warning that an integral basis does not specify an effective cone.

The masses in the weak electric description are $|Z_i|$ in this normalization. For example, if $a_1 = a_2 = 3\mu_0$ and $c = 2\mu_0$ with $\mu_0 > 0$, then

$$\lambda = (3, 0, -3)\mu_0, \qquad m = 5\mu_0, \qquad (M_1, M_2, M_3) = (8, 5, 2)\mu_0. \tag{XI.4.79}$$

The lightest mass c is not the flavor parameter m: moving on the Coulomb branch at fixed m changes $c = m + \lambda_3$. Varying the flavor background at fixed a_1, a_2 changes all three signed Z_i by the same amount. In the model here, the flavor vector is fixed at the noncompact boundary. In an embedding with a normalizable flavor vector mode that is kept dynamical, its scalar would instead be integrated over as part of a gauge multiplet. The adjoint branching by itself does not decide between these prescriptions.

A small variation makes the independent parameters concrete. At fixed flavor mass, differentiate (XI.4.76),

$$\delta m = 0 \quad \Longrightarrow \quad \delta c = -\frac{\delta a_1 + 2\delta a_2}{3}, \qquad \delta Z_i = \delta\lambda_i. \tag{XI.4.80}$$

For the numerical example above, increasing a_1 by $\epsilon\mu_0$ at fixed a_2 and m gives

$$c = (2 - \epsilon/3)\mu_0, \qquad Z = (8 + 2\epsilon/3,\ 5 - \epsilon/3,\ 2 - \epsilon/3)\mu_0. \tag{XI.4.81}$$

For sufficiently small ϵ the same positive chamber persists and the mean remains $5\mu_0$. Conversely, varying m at fixed a_1, a_2 gives $\delta Z = (1, 1, 1)\delta m$. Moving a zero of f along the base asks a third question, where the mode is supported. It cannot be substituted for either of these period variations.

Now take a perturbative scale μ_{RG} above the relevant W and matter thresholds but below the base Kaluza–Klein and string scales. This is the window in which to read the coefficient of the non-Abelian gauge description. We use the sign convention

$$\mu_{\mathrm{RG}} \frac{dg}{d\mu_{\mathrm{RG}}} = -\frac{b_0}{16\pi^2} g^3 + \cdots, \qquad \mathrm{Tr}_{\mathrm{f}}(T_a T_b) = \tfrac{1}{2}\delta_{ab}. \tag{XI.4.82}$$

The index of a fundamental is $T(\mathrm{f}) = 1/2$. For a traceless diagonal matrix h with entries h_i, use (XI.4.36) to sum the squared charges in the adjoint:

$$\mathrm{Tr}_{\mathrm{ad}}\, h^2 = \sum_{i,j} (h_i - h_j)^2 = 2N \sum_i h_i^2 - 2\Big(\sum_i h_i\Big)^2 = 2N\, \mathrm{Tr}_{\mathrm{f}}\, h^2. \tag{XI.4.83}$$

The cross term in this trace sum vanishes precisely because the generator is traceless. To check the normalization in our actual rank-two frame, take $h = h_1 = \mathrm{diag}(1, -1, 0)$. The six ordered root charges have squares $4, 4, 1, 1, 1, 1$, whereas the fundamental entries have squares $1, 1, 0$,

$$\mathrm{Tr}_{\mathrm{ad}}\, h_1^2 = 12, \qquad \mathrm{Tr}_{\mathrm{f}}\, h_1^2 = 2, \qquad \frac{T(\mathrm{ad})}{T(\mathrm{f})} = 6. \tag{XI.4.84}$$

The fundamental trace already sums over all three colors. Adding another factor of three when computing a fundamental's contribution to the beta function would count that sum twice.

It follows that $T(\mathrm{ad}) = N$. An $\mathcal{N} = 1$ vector contributes $3T(\mathrm{ad})$ to b_0 and a chiral in R contributes $-T(R)$. The extra chiral in the $\mathcal{N} = 2$ vector is in the adjoint. Each full fundamental contains two chirals of equal index, by (XI.4.64). With N_f such fundamentals and no adjoint hypers,

$$b_0 = 3N - N - N_f\left(\tfrac{1}{2} + \tfrac{1}{2}\right) = 2N - N_f. \tag{XI.4.85}$$

There are no adjoint hypers from the rational gauge base. For $\mathfrak{su}(3)$, the pure value is 6, the single-enhancement value is 5, and the two-point comparison with no other charged matter gives 4. The beta function is sensitive to the multiplicity of the representation, not to the number of weights written in the table.

We can also see the removal of one flavor at a heavy threshold. Take $|m| \gg |\lambda_i|$ and a weak regime in which the common quark threshold $|m|$ is well above the strong scale and still below the unwanted modes. At this accuracy the three quark masses can be matched at the same threshold. The one-loop running of $8\pi^2/g^2$ is $b_0 \log(\mu_{\mathrm{RG}}/\Lambda)$.

Matching the $b_0 = 5$ and $b_0 = 6$ descriptions at $|m|$ in the same real threshold scheme gives

$$6 \log \frac{|m|}{\Lambda_{\text{pure}}} = 5 \log \frac{|m|}{\Lambda_1}, \qquad \Lambda_{\text{pure}}^6 = |m| \Lambda_1^5. \tag{XI.4.86}$$

Changing the threshold convention can introduce a finite factor. Below the quark threshold and above the W thresholds the effective coefficient is the pure one. Equation (XI.4.86) is real one-loop matching, without a prescription for an exact holomorphic scale or quantum periods.

The field-theory interpretation uses the local limit of Chapter 2: retain the selected light charged fields, put the base Kaluza–Klein and string scales above the observation window, and require unwanted bulk modes to have divergent gaps or vanishing couplings to this sector. The local geometry determines the charges and degeneration in that setup. It does not prove isolation of the bulk. We can now resolve the contribution of this fundamental into the two electric couplings on its Coulomb branch.

XI.4.7 Two photons resolving one fundamental

The coefficient $b_0 = 5$ describes the non-Abelian theory above its charged thresholds. What can we calculate after moving to a generic Coulomb vacuum, where the two Cartan photons remain light? The three color components now have different masses. A charged component screens the photon combination to which its weight couples, so a single scalar coupling no longer displays the full response. We will calculate the resulting two-by-two matrix for the same fundamental already constructed from the resolved fiber.

The first step is to choose electric scalar coordinates dual to the charges in (XI.4.39). Using the same coroot generators, write

$$\begin{aligned} \Phi &= v_1 h_1 + v_2 h_2 = \operatorname{diag}(v_1, -v_1 + v_2, -v_2), \\ h_1 &= \operatorname{diag}(1, -1, 0), \qquad h_2 = \operatorname{diag}(0, 1, -1). \end{aligned} \tag{XI.4.87}$$

A fundamental component has eigenvalue $w_i \cdot v$, with $v = (v_1, v_2)^T$. Thus its electric weights and central charges are

$$w_1 = \begin{pmatrix} 1 \\ 0 \end{pmatrix}, \quad w_2 = \begin{pmatrix} -1 \\ 1 \end{pmatrix}, \quad w_3 = \begin{pmatrix} 0 \\ -1 \end{pmatrix}, \qquad Z_i = m + w_i \cdot v. \tag{XI.4.88}$$

These are exactly the charges of the three suffix classes of the exceptional chain. In particular the last component is the primitive end-curve charge, with $Z_3 = m - v_2 = c$. The root periods used earlier are differences of eigenvalues,

$$\begin{pmatrix} a_1 \\ a_2 \end{pmatrix} = C \begin{pmatrix} v_1 \\ v_2 \end{pmatrix}, \qquad C = \begin{pmatrix} 2 & -1 \\ -1 & 2 \end{pmatrix}, \qquad v = C^{-1} a = \frac{1}{3} \begin{pmatrix} 2a_1 + a_2 \\ a_1 + 2a_2 \end{pmatrix}. \tag{XI.4.89}$$

The distinction matters when differentiating. A derivative with respect to v_1 measures the integer charges in (XI.4.88); a derivative with respect to a_1 does not. The original

example $a_1 = a_2 = 3\mu_0$ corresponds to $v_1 = v_2 = 3\mu_0$, but equality of their numerical values at that symmetric point does not identify the two coordinate systems.

We now use a field-theory input. In the weak electric regime, the one-loop contribution of one full fundamental to the holomorphic Wilsonian prepotential can be written

$$\mathcal{F}_{\rm h}(v,m) = -\frac{i}{8\pi}\sum_{i=1}^{3} Z_i^2 \log\frac{Z_i^2}{\mu_*^2}, \qquad Z_i = m + w_i\cdot v. \tag{XI.4.90}$$

The reference μ_* has mass dimension one. We use electric mass units with precisely these arguments of the logarithms. A common change of mass unit changes the reference scale, while a local quadratic polynomial fixes the coupling convention. We keep that polynomial fixed when comparing two vacua. Equation (XI.4.90) already includes the two conjugate chiral multiplets of a full hypermultiplet. Adding a second identical contribution for the reversed D2 orientation would double its threshold incorrectly.

The Hessian of the prepotential gives the holomorphic coupling matrix in the chosen electric chart,

$$(\tau_{\rm h})_{ab} = \left.\frac{\partial^2\mathcal{F}_{\rm h}}{\partial v_a \partial v_b}\right|_m, \qquad a,b = 1,2. \tag{XI.4.91}$$

The scalar m is a fixed background in these derivatives. Each entry refers to this basis of two gauge fields; an individual entry need not be a separate non-Abelian coupling. We are isolating the matter contribution to the weak theory. The bare coupling and W-boson contributions can be added in the same frame.

The required differentiation is elementary but fixes the coefficient and the finite term. For $g(Z) = Z^2\log(Z^2/\mu_*^2)$,

$$g'(Z) = 2Z\left(\log\frac{Z^2}{\mu_*^2} + 1\right), \qquad g''(Z) = 2\log\frac{Z^2}{\mu_*^2} + 6. \tag{XI.4.92}$$

Since $\partial_{v_a} Z_i = w_{ia}$, the Hessian is

$$\tau_{\rm h} = -\frac{i}{4\pi}\sum_i w_i w_i^T\left(\log\frac{Z_i^2}{\mu_*^2} + 3\right). \tag{XI.4.93}$$

The outer product records the two gauge couplings of the same component. It is why a component with two nonzero charges also changes the mixed gauge kinetic term. All Z_i must be nonzero when that component is omitted from the low-energy action.

For two parameter choices in a common weak patch, let $L_i = \log Z_i' - \log Z_i$ be the difference continued along the chosen path. The finite matter response has no constant term,

$$\Delta\tau_{\rm h} = -\frac{i}{2\pi}\sum_i w_i w_i^T L_i. \tag{XI.4.94}$$

On a positive-real path $L_i = \log(Z_i'/Z_i)$ with the real logarithm. For a complex path that notation must retain the continued difference. Choosing a new principal logarithm of each ratio independently can discard a winding and change the electric shear. A

further derivative also removes the local quadratic ambiguity without comparing two points,

$$\partial_{v_c}(\tau_{\mathrm{h}})_{ab} = -\frac{i}{2\pi}\sum_i \frac{w_{ia}w_{ib}w_{ic}}{Z_i}. \tag{XI.4.95}$$

Thus the residue of the response near a light component directly measures its electric charge tensor.

For the actual weight set, the three outer products are

$$w_1 w_1^T = \begin{pmatrix} 1 & 0 \\ 0 & 0 \end{pmatrix}, \quad w_2 w_2^T = \begin{pmatrix} 1 & -1 \\ -1 & 1 \end{pmatrix}, \quad w_3 w_3^T = \begin{pmatrix} 0 & 0 \\ 0 & 1 \end{pmatrix}. \tag{XI.4.96}$$

The middle component couples to the difference of the two photon fields. Summing gives both a useful normalization check and the explicit finite answer,

$$\sum_i w_i w_i^T = C, \qquad \Delta\tau_{\mathrm{h}} = -\frac{i}{2\pi}\begin{pmatrix} L_1+L_2 & -L_2 \\ -L_2 & L_2+L_3 \end{pmatrix}. \tag{XI.4.97}$$

The three entries of the fundamental have produced three rank-one contributions to one response matrix. The matrix is not three independent copies of the fundamental's non-Abelian index.

We can now complete a finite calculation using the original resolved-curve example. Hold $v = (3,3)\mu_0$ fixed and change the background mass from $5\mu_0$ to $7\mu_0$. The periods and masses at the two endpoints are

$$\lambda = (3,0,-3)\mu_0, \qquad Z = (8,5,2)\mu_0 \longrightarrow Z' = (10,7,4)\mu_0, \qquad c : 2\mu_0 \longrightarrow 4\mu_0. \tag{XI.4.98}$$

Both endpoints remain in the original positive curve chamber. Substituting the three ratios gives

$$\Delta\tau_{\mathrm{h}} = -\frac{i}{2\pi}\begin{pmatrix} \log(7/4) & -\log(7/5) \\ -\log(7/5) & \log(14/5) \end{pmatrix}. \tag{XI.4.99}$$

For example, the upper-left entry contains $\log(10/8) + \log(7/5) = \log(7/4)$, while the lower-right contains $\log(7/5) + \log(4/2) = \log(14/5)$. The off-diagonal entry survives because the second color component carries both charges. Omitting it would change the response to a generic linear combination of photons.

The sign of screening is a statement about the quadratic form, not about each matrix entry. For a real photon direction $p = (p_1, p_2)^T$ and the real symmetric matrix R inside (XI.4.97),

$$p^T R p = \sum_i L_i (w_i \cdot p)^2 = L_1 p_1^2 + L_2(p_2 - p_1)^2 + L_3 p_2^2. \tag{XI.4.100}$$

All three L_i in this example are positive and the weights span the two charge directions. Therefore R is positive definite and raising the masses decreases the imaginary matter coupling. Reversing the path increases it in every nonzero photon direction, as expected when the charged matter can screen down to a lower scale. The off-diagonal entry alone has the opposite sign from the diagonal entries and cannot decide this question.

Finally we can express the same calculation in the earlier root periods without changing any charge physics. The chain rule gives

$$\tau_a = C^{-T}\tau_v C^{-1}, \qquad \Delta\tau_a = C^{-T}\Delta\tau_v C^{-1}. \tag{XI.4.101}$$

One must transform the entire matrix. Treating a_1, a_2 as if they were the scalars dual to the integer weights would change its normalization and its mixing. This is the differential version of the earlier statement that changing an integral curve basis does not change the physical charges.

XI.4.8 A light component and a heavy fundamental

How does the response know that only the end curve is becoming small, and when can all three components instead be removed at one common threshold? These are two regimes of the same localized fundamental. We first identify its electric mass locus, then take the two limits with the relevant scales stated.

At fixed Coulomb eigenvalues a component becomes massless at $m = -\lambda_i$. Introduce the two Weyl-invariant Coulomb polynomials

$$u = \frac{1}{2}\sum_i \lambda_i^2, \qquad v_{\mathrm{inv}} = \lambda_1\lambda_2\lambda_3, \qquad \sum_i \lambda_i = 0. \tag{XI.4.102}$$

Since $\sum_{i<j}\lambda_i\lambda_j = -u$, the product of the three signed electric masses is

$$\prod_i (m + \lambda_i) = m^3 - um + v_{\mathrm{inv}}. \tag{XI.4.103}$$

The right side is a single equation on the Weyl quotient. It assembles the three color components into a gauge-invariant mass locus; it does not count their flavor multiplicity. The sign of the last term follows directly from expanding the product. For example $\lambda = (1, 2, -3)\mu_0$ gives

$$u = 7\mu_0^2, \quad v_{\mathrm{inv}} = -6\mu_0^3, \qquad \prod_i (m + \lambda_i) = m^3 - 7\mu_0^2 m - 6\mu_0^3. \tag{XI.4.104}$$

Its roots are $m = (-1, -2, 3)\mu_0$, as required by the individual masses. In the symmetric example used for the threshold matrix,

$$u = 9\mu_0^2, \qquad v_{\mathrm{inv}} = 0, \qquad \prod_i (m + \lambda_i) = m(m^2 - 9\mu_0^2). \tag{XI.4.105}$$

This is a perturbative electric mass condition. It is not an exact quantum discriminant expressed in microscopic geometric moduli. The latter would require the quantum periods and their relation to those moduli.

There are now two distinct uses of a zero that must remain clear. A zero of $f(s)$ in the holomorphic surface family marks a support point on the base. A zero of $m + \lambda_i$ marks a charged component becoming light as periods vary. Even with one ordinary

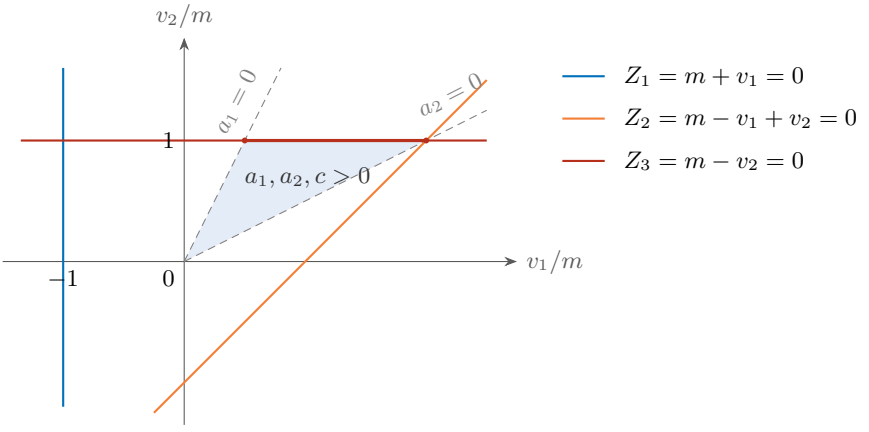


Figure XI.4.5: A real electric scalar slice at fixed $m > 0$, with axes v_1/m and v_2/m. The three straight lines are $Z_1 = 0$ (blue), $Z_2 = 0$ (orange) and $Z_3 = 0$ (red). The shaded region is the chosen chamber $a_1 = 2v_1 - v_2 > 0$, $a_2 = -v_1 + 2v_2 > 0$, $c = m - v_2 > 0$. Its sloping boundaries have a massless W boson. On the upper red edge away from its endpoints, only the third matter component becomes light. These lines are loci in scalar parameters, not three enhancement points on the geometric base.

enhancement point, three such mass loci occur on the electric cover of Coulomb and mass parameters. Figure XI.4.5 shows how the selected positive curve chamber meets just one of them away from a W-boson wall.

Return to the resolved geometry and keep a_1, a_2 fixed and positive. Approach its end-curve boundary with $c = \epsilon > 0$. The full vector of signed masses is then

$$Z_1 = a_1 + a_2 + \epsilon, \qquad Z_2 = a_2 + \epsilon, \qquad Z_3 = \epsilon, \qquad m = v_2 + \epsilon. \tag{XI.4.106}$$

The first two remain finite as the end sphere shrinks. The approach has $\delta m = \delta\epsilon$ and fixed v; it is not a Hessian taken at fixed c. The Hessian was already differentiated at fixed background mass in (XI.4.91), and is only now evaluated along this path.

Take a weak hierarchy in which the unwanted modes are above the charged gauge-theory scales and

$$E_{\mathrm{obs}} \ll \epsilon, \qquad \Lambda_{\mathrm{strong}} \ll \epsilon \ll a_1, a_2. \tag{XI.4.107}$$

Here E_{obs} is the external energy of the Wilsonian process, and $\Lambda_{\mathrm{strong}}$ marks the scale below which the perturbative expansion is inadequate. In this window the third component can still be integrated out. Its dominant extra logarithm is

$$\tau_{\mathrm{h}} = -\frac{i}{2\pi}\begin{pmatrix} 0 & 0 \\ 0 & 1 \end{pmatrix} \log\frac{\epsilon}{\mu_*} + \tau_{\mathrm{reg}}(a_1, a_2, \epsilon), \tag{XI.4.108}$$

where the remaining terms are regular at $\epsilon = 0$ in the formal one-loop expression. The coefficient is $w_3 w_3^T$, of rank one. Only the photon combination measured by $w_3 = (0, -1)$ receives this singular threshold. Replacing that matrix by C would incorrectly let the other two color components become light at the same rate.

The coefficient can be read without any convention-dependent constant by differentiating along the path,

$$\lim_{\epsilon\to 0^+} \epsilon \frac{d\tau_{\mathrm{h}}}{d\epsilon} = -\frac{i}{2\pi}\begin{pmatrix} 0 & 0 \\ 0 & 1 \end{pmatrix}. \tag{XI.4.109}$$

This limit extracts a coefficient of a perturbative function. It does not extend the omitted-particle action to the massless point. Once ϵ is comparable to E_{obs}, the light charged component must be retained as a field. If the strong scale is approached first, the perturbative computation must also be replaced. The divergent logarithm identifies these limits of the chosen effective description.

There is a useful analytic check on the charge normalization. Under a formal positive loop of Z_3 around zero, its continued logarithm changes by $2\pi i$, so the one-loop matrix changes by

$$\Delta_{\mathrm{loop}}\tau_{\mathrm{h}} = -\frac{i}{2\pi} w_3 w_3^T (2\pi i) = \begin{pmatrix} 0 & 0 \\ 0 & 1 \end{pmatrix}. \tag{XI.4.110}$$

This unit electric shear follows from the primitive end-curve charge. It is a property of the continued perturbative logarithm; it supplies neither a global quantum monodromy group nor a continuation of this resolution chamber through its boundary.

At the other extreme, take a heavy common flavor mass with $|m| \gg |\lambda_i|$, and stay on a branch where the expansion in λ_i/m is valid. Then

$$\log\frac{m+\lambda_i}{\mu_*} = \log\frac{m}{\mu_*} + \frac{\lambda_i}{m} - \frac{\lambda_i^2}{2m^2} + \cdots, \tag{XI.4.111}$$

$$\sum_i w_i w_i^T \log\frac{m+\lambda_i}{\mu_*} = C\log\frac{m}{\mu_*} + \frac{S_1}{m} + O\!\left(\frac{\lambda^2}{m^2}\right), \tag{XI.4.112}$$

where λ in the error denotes the largest eigenvalue magnitude and the finite matrix S_1 is obtained from the same three outer products,

$$S_1 = \sum_i \lambda_i w_i w_i^T = \begin{pmatrix} \lambda_1+\lambda_2 & -\lambda_2 \\ -\lambda_2 & \lambda_2+\lambda_3 \end{pmatrix} = \begin{pmatrix} -\lambda_3 & -\lambda_2 \\ -\lambda_2 & -\lambda_1 \end{pmatrix}. \tag{XI.4.113}$$

The leading tensor C gives a common threshold for the full fundamental. The next tensor records the mass splitting that this approximation omits. For $\lambda = (3,0,-3)\mu_0$,

$$\begin{aligned} S_1 &= 3\mu_0 \begin{pmatrix} 1 & 0 \\ 0 & -1 \end{pmatrix}, \\ \tau_{\mathrm{h}} &= -\frac{i}{2\pi}\left[C\log\frac{m}{\mu_*} + \frac{3\mu_0}{m}\begin{pmatrix} 1 & 0 \\ 0 & -1 \end{pmatrix} + O\!\left(\frac{\mu_0^2}{m^2}\right)\right] + \tau_{\mathrm{local}}. \end{aligned} \tag{XI.4.114}$$

The constant matrix τ_{local} includes the fixed local quadratic convention. The first correction has opposite signs for the two diagonal responses, although their leading heavy logarithm is proportional to the same C. Approximating the three masses by $|m|$ is justified at leading order, but not for this splitting correction.

We can recover the non-Abelian coefficient without selecting a single Cartan generator. The six ordered roots are $\alpha_{ij} = w_i - w_j$, $i \neq j$, and $\sum_i w_i = 0$ gives

$$\sum_{i\neq j} \alpha_{ij}\alpha_{ij}^T = 2(3)\sum_i w_i w_i^T - 2\Big(\sum_i w_i\Big)\Big(\sum_i w_i\Big)^T = 6C. \tag{XI.4.115}$$

The vector logarithm has the opposite sign to the fundamental term. In the same prepotential convention it is

$$\mathcal{F}_{\mathrm{vec}}^{1\,\mathrm{loop}} = \frac{i}{8\pi}\sum_{i\neq j}(\lambda_i-\lambda_j)^2\log\frac{(\lambda_i-\lambda_j)^2}{\mu_*^2}. \tag{XI.4.116}$$

Under a common positive rescaling $(v,m)\mapsto(tv,tm)$, its Hessian and the matter Hessian therefore have the combined shift

$$\tau^{1\,\mathrm{loop}}(tv,tm)-\tau^{1\,\mathrm{loop}}(v,m) = \frac{i}{2\pi}(6C-C)\log t = \frac{5i}{2\pi}C\log t. \tag{XI.4.117}$$

The same coefficient 5 multiplies the full rank-two metric rather than just its value on one generator. This is the $2N-N_f$ result already derived by trace indices, now seen in the complete electric response. The common heavy term removes one fundamental tensor C, consistently with the earlier real matching $\Lambda_{\mathrm{pure}}^6 = |m|\Lambda_1^5$. The remaining powers in (XI.4.112) resolve the thresholds within that one multiplet.

All of these responses belong to the four-dimensional window specified earlier. The local geometry fixes the charged curve classes, while the imported weak gauge-theory prepotential gives their perturbative effect on the electric couplings. An exact quantum period calculation is a further task. The next chapter extends the geometric charge calculation to matter charged under more than one gauge factor.

XI.4.9 Exercises

Use the charge and period conventions of this chapter. Give the charge arrays and numbers in the stated order. Use `benchmark/tasks.json` to find the question IDs and `benchmark/PROTOCOL.md` for submission. Written derivations and explanations are assessed by a human reader.

E1. Repeat the branching in rank one. Use the split $A_1\to A_2$ enhancement with $h=\mathrm{diag}(1,-1,0)$ and $H=\mathrm{diag}(1,1,-2)$. Decompose the parent adjoint under the gauge algebra and H. Give the two upper-right block weights as unordered $[h,H]$ pairs. Let the gauge and extra curve periods be $a=4\mu_0$ and $c=3\mu_0$. Compute m/μ_0 in unit flavor normalization. Explain how the opposite H charges distinguish the two chiral partners in the full doublet.

E2. Two separated points. Let $f(s)=s^2-1$ on a disk with the same split gauge embedding at each zero and no projection identifying the two neighborhoods. Assume there are no other charged hypers or adjoint hypers in the four-dimensional window. Give the two enhancement positions, the fundamental multiplicity and the $\mathfrak{su}(3)$ one-loop coefficient. Explain what property of the two zeros the local argument uses.

E3. Hold the mass fixed on the Coulomb branch. At $B=0$ begin with $(a_1,a_2,c)=(3,2,1)\mu_0$. Give m/μ_0. Now change a_1 to $2\mu_0$, holding a_2 and m fixed. What is the new c/μ_0? Explain how changing the fixed flavor background would differ from varying a dynamical vector-multiplet scalar in another embedding.

E4. Remove a hypothesis. Replace $f(s) = s$ by $f(s) = s^2$. Find the rank of the residual Hessian at the origin and $h^0(N_{C_3/X})$ from the linearized normal transition. Which step of the one-hyper argument no longer applies? Separately, explain why an outer monodromy exchanging the two gauge Dynkin labels would require checking which charges transport globally. Distinguish it from a change of Weyl labeling in a split model.

As further written practice, repeat the charge and mass calculation in (XI.4.41) with $a_1 = 2\mu_0$, $a_2 = \mu_0$ and $d = 4\mu_0$. Recover c, m and all three signed Z_i, and verify the chamber inequality. Then explain why three color components of the resulting localized mode still give one contribution of -1 to b_0. This practice has no additional numerical submission contract.

Two further written calculations practice the resolved threshold matrix. First keep $v = (3, 3)\mu_0$ and vary m from $7\mu_0$ back to $5\mu_0$. Derive the change of the quadratic coupling for $p = (1, 1)^T$ and for $p = (1, -1)^T$, retaining the mixed entry. Then approach $c = \epsilon$ at fixed positive a_1, a_2 and explain which charged field must return to the effective action when E_{obs} reaches ϵ. In a separate heavy-mass example take $\lambda = (1, 2, -3)\mu_0$. Compute S_1 and its off-diagonal entry, and state the expansion parameter. These are written exercises with no additional numerical submission contract.

Status and sources

§XI.4.2 The transverse collision. [MATH] The coordinate choice in (XI.4.1) is the ordered $n = k = 3$ example of S. Katz and Vafa (1997), arXiv:hep-th/9606086v1, §3 eq. (3.1) and §4.1 eq. (4.1), after a translation of the root positions and a sign change in one coordinate. The chart maps, residue and normal bundle in (XI.4.5)–(XI.4.18) are computed in the text.

§XI.4.3 The compact-base example. [MATH] The fan, two patch descriptions, and wall relations are (XI.4.19)–(XI.4.34). The alternate triangulation realizes the first ruled-fiber split described in S. H. Katz et al. (1997), arXiv:hep-th/9609239v2, §6.2, printed pp. 22–23. This comparison uses the rank-two fiber rows and does not require equality of spectra across the flops.

§XI.4.4 The extra weights. [MATH] The matrix units and the curve intersections give the same charges in (XI.4.39). For the general root-sum convention see S. Katz and Vafa (1997), §3 and §4.1. [GEO-X] The oriented wrapped-D2 root correspondence uses the ordinary unfrozen ALE setting of XI.1.

§XI.4.5 Multiplicity. [MATH] Equations (XI.4.44)–(XI.4.51) solve the specified flat linear model. The scalar pairing in (XI.4.64) has a quaternionic structure; (XI.4.68)–(XI.4.69) are local calculations for the double zero. [GEO-E] The use of the single transverse mode, together with its charge conjugate, as one full fundamental hypermultiplet of localized IIA matter follows S. Katz and Vafa (1997), §2 eq. (2.1) and the discussion of polynomial separation, and S. H. Katz et al. (1997), §§1, 6.2. The separated-point comparison assumes a common split gauge embedding and no additional projection.

§XI.4.6 Periods and running. [MATH] The additive map (XI.4.76) uses the common period conventions of XI.1 and XI.2. The conditional one-loop arithmetic in (XI.4.85)

and (XI.4.86) can be compared to the rank-one coefficient and threshold in Seiberg and Witten (1994), arXiv:hep-th/9408099v1, §4.1 and §12.2 eq. (12.5). [GEO-E] The smooth wrapped-D2 calibration is distinct from the protected light-mass interpretation; the flavor background is fixed by the boundary prescription. [DEC] The four-dimensional interpretation retains the scale and isolation premises of XI.2.

§XI.4.5 Local width and approximation. [MATH] Equations (XI.4.54)–(XI.4.62) solve and normalize the translated complex-slope flat linear operator, and test its local Taylor approximation. The Gaussian tail and remainder criteria do not compute a global compact zero-mode spectrum. The physical localized-matter identification remains the ordinary split Type IIA input of S. Katz and Vafa (1997), §2 eq. (2.1), printed pp. 2–3.

§XI.4.7 The full electric response. [MATH] The coroot-to-root-period map, outer products, Hessian, third derivatives and finite matrix in (XI.4.87)–(XI.4.101) are explicit calculations in the stated electric chart. [MATH] The conditional Hessian calculation takes its weak one-loop Wilsonian prepotential and coupling definition from D'Hoker et al. (1996), arXiv:hep-th/9609041v1, §II, printed pp. 4–5, especially eq. (2.1) and the preceding Wilsonian action. One full fundamental is counted once. The response uses fixed flavor mass, a fixed local quadratic convention and consistently continued logarithms. No exact geometric quantum-period map is inferred.

§XI.4.8 Light and heavy regimes. [MATH] The electric mass polynomial, rank-one logarithmic coefficient, formal perturbative electric shear, heavy expansion and root-tensor calculation are (XI.4.102)–(XI.4.117). The polynomial is not an exact quantum discriminant; the loop calculation is not a global monodromy theorem. [GEO-E] Application to the engineered charged sector uses the same sourced weak prepotential. The light-particle omission requires (XI.4.107), while the heavy expansion requires $|\lambda_i/m| \ll 1$ on a consistent branch. [DEC] The field-theory scale and isolation assumptions remain those of XI.2; a local fan and a perturbative prepotential do not supply a bulk-decoupling proof.

D'Hoker, E., I. M. Krichever, and D. H. Phong (1996). *The Effective Prepotential of N=2 Supersymmetric SU(Nc) Gauge Theories*. arXiv: hep-th/9609041.

Katz, S. and C. Vafa (1997). "Matter from geometry". In: *Nucl. Phys. B* 497, pp. 146–154. DOI: 10.1016/S0550-3213(97)00280-0. arXiv: hep-th/9606086.

Katz, S. H., A. Klemm, and C. Vafa (1997). "Geometric engineering of quantum field theories". In: *Nucl. Phys. B* 497, pp. 173–195. DOI: 10.1016/S0550-3213(97)00282-4. arXiv: hep-th/9609239.

Seiberg, N. and E. Witten (1994). "Monopoles, duality and chiral symmetry breaking in N=2 supersymmetric QCD". In: *Nucl. Phys. B* 431, pp. 484–550. DOI: 10.1016/0550-3213(94)90214-3. arXiv: hep-th/9408099.

Chapter XI.5

Product gauge theories and conformal engineering

XI.5.1 How two gauge sectors share one local geometry

A curve that shrinks over an entire compact base can supply a gauge sector. A curve that shrinks only at a special fiber can supply matter. How can the same local threefold supply matter charged under *two* gauge sectors, and still let us choose their gauge couplings independently? We will construct the geometry for two $SU(2)$ gauge factors, one full bifundamental hypermultiplet, and two fundamental hypers at each end. We will also change the ranks to $SU(2) \times SU(3)$ and use its six bridge periods to calculate finite photon mixing. Following that same bridge to large mass, or holding it finite while a node becomes a flavor background, will distinguish the two limits.

The starting point is the ordinary six-dimensional $(1,1)$ gauge theory near an ALE surface, as in Chapter 1. We use the genus-zero gauge reduction from Chapter 3 and the transverse matter construction from Chapter 4. The new step is to fit their inputs into one noncompact Calabi–Yau threefold. We will use the toric rays and their intersection relations to read off which curves supply the gauge roots, which curve couples to both sectors, and which combinations of periods can be changed while all the background parameters stay fixed.

XI.5.2 Build the geometry from four columns

Which part of the geometry lets two gauge bases meet at a point? Start with four columns of three points each. Label the points by (i, j) and lift them to rays at height one:

$$v_{i,j} = (i, j, 1), \qquad 0 \le i \le 3, \qquad 0 \le j \le 2. \tag{XI.5.1}$$

Write $D_{i,j}$ for the corresponding divisors. In each strip between neighboring columns, denote the projected points on its left and right by L_j and R_j. Take the cones over

these four triangles and all their faces:

$$(L_0, L_1, R_0), \quad (L_1, L_2, R_0), \quad (L_2, R_0, R_1), \quad (L_2, R_1, R_2). \tag{XI.5.2}$$

Each triangle has a vertical edge of unit length and its third vertex is one column away. Its lifted determinant is therefore ± 1. This makes each affine chart smooth. The height character takes value one on every ray, so the canonical divisor, minus the sum of the toric divisors, is principal.

For example, the first two cones of the middle strip use the columns $x = 1, 2$. Their determinants can be read without a general toric calculation. Subtract the first ray from the other two; the vertical edge becomes $(0, 1, 0)$ and the horizontal displacement has first component one. Thus

$$\left|\det\left(v_{1,0}, v_{1,1}, v_{2,0}\right)\right| = 1, \qquad \left|\det\left(v_{1,1}, v_{1,2}, v_{2,0}\right)\right| = 1. \tag{XI.5.3}$$

The same subtraction works for the triangles with their vertical edge on the right. There are four triangles per strip and three strips, with total normalized area twelve. Smoothness concerns these small triangles; the singular geometry used for gauge enhancement will appear when we contract their interior walls.

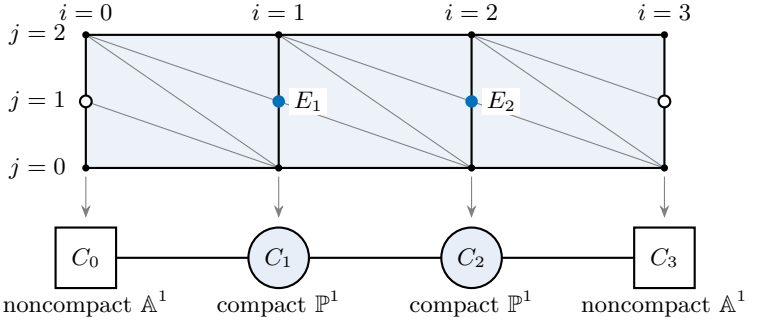


Figure XI.5.1: The complete height-one rectangle and its projected base. The filled blue middle points give the compact divisors E_1, E_2. The open middle points give noncompact divisors. Projection forgets j; the four columns map to four base curves, and each line between base symbols denotes a single intersection.

The triangles cover the whole rectangle. One can also see that they come from a strict lower hull: assign height

$$h(x, y) = 1000x^2 + y^2 + 10xy \tag{XI.5.4}$$

to the projected lattice points. Within the strip at $x = i, i+1$, the slopes along successive vertical segments at $x = i$ are $10i + 1, 10i + 3$; at $x = i + 1$ they are $10i + 11, 10i + 13$. The two triangles with an edge on the left therefore come first. For example, the plane through L_j, L_{j+1}, R_0 has y slope $q = 10i + 2j + 1$. The height minus the plane is

$$\begin{cases} (y - j)(y - j - 1), & x = i, \\ y(y + 9 - 2j), & x = i + 1. \end{cases} \tag{XI.5.5}$$

Both are positive at the other points on those two columns. For the plane through L_2, R_j, R_{j+1} the right-column gap is $(y-j)(y-j-1)$ and the left-column gap is $(y-2)(y-9-2j)$, again positive off the triangle. At a nonadjacent column the quadratic in x contributes a gap $1000(x-i)(x-i-1) \geq 2000$. The remaining terms in the gap have absolute value less than 1000 on the rectangle: their point heights are at most 64, the y slopes are at most 33, and interpolating the plane from the two columns uses coefficients whose absolute values sum to at most 5. Thus these triangles indeed give a regular subdivision of one affine cone.

The two strictly interior rays are $(1,1,1)$ and $(2,1,1)$. The star of each in the quotient by the ray is complete: the triangles go all the way around its point. These are the only compact toric divisors:

$$E_1 = D_{1,1}, \qquad E_2 = D_{2,1}. \tag{XI.5.6}$$

No triangle contains both points. The divisors E_1 and E_2 are disjoint in this resolution. We will find a compact curve that intersects each of them.

It is useful to see compactness directly in this drawing. A toric divisor inherits its fan by taking all cones containing its ray and quotienting by that ray. Around an interior point the neighboring triangles fill every angular direction. Around a boundary point there is an uncovered direction, extending to infinity. In the present rectangle this gives

$$\#\{\text{rays}\} = 12, \qquad \#\{\text{compact divisor rays}\} = 2, \qquad \operatorname{rank}\ker(\mathbb{Z}^{12} \longrightarrow \mathbb{Z}^3) = 9. \tag{XI.5.7}$$

These three numbers count different objects. The last number counts relations and hence independent curve periods. It does not say that nine scalar fields fluctuate in the local four-dimensional theory. The two compact divisor variations will select its two Coulomb directions.

To identify the base of the fibration, we now project the threefold fan. Project the lattice by $(i,j,1) \mapsto w_i = (i,1)$. Every strip maps to the cone on w_i, w_{i+1}. These adjacent rays have determinant -1, so they give a smooth toric surface. Write C_i for the base curve of w_i. For $i = 1, 2$, both adjacent cones are present and project to the two opposite rays in the quotient by w_i. For $i = 0, 3$, only one cone is present. Thus

$$C_1, C_2 \simeq \mathbb{P}^1, \qquad C_0, C_3 \simeq \mathbb{A}^1, \qquad C_i \cap C_{i+1} = \{p_i\}. \tag{XI.5.8}$$

The three points p_i are distinct, and the non-neighboring curves do not intersect. Figure XI.5.1 shows the projection. The curve C_i lives in this base surface. A curve in the threefold that maps onto C_i will be called a section lift and will get a different symbol.

The projection also lets us find the singularity over each intersection of base curves. Forget the subdivision inside each strip while keeping its four corners. The smooth fan refines this coarser fan with the same support, so there is a toric contraction. To read its local equation, work over one base cone and translate the left column to $x = 0$. Allow the left and right column heights to be h and k for this step. A dual lattice vector (p,q,r) belongs to the dual cone if its pairings with the four corners are nonnegative:

$$r \geq 0, \quad p + r \geq 0, \quad r + hq \geq 0, \quad p + r + kq \geq 0. \tag{XI.5.9}$$

The characters for the two base coordinates are $S = (-1, 0, 1)$ and $T = (1, 0, 0)$. Introduce $U = (0, 1, 0)$ and $V = (k - h, -1, h)$. Every dual lattice vector has a nonnegative integral expression, using U or V according to the sign of q:

$$(p, q, r) = \begin{cases} rS + (p + r)T + qU, & q \geq 0, \\ (r + hq)S + (p + r + kq)T - qV, & q \leq 0. \end{cases} \tag{XI.5.10}$$

The equality $U + V = hS + kT$ reduces any product containing both fiber characters to one of the two expressions. The two expressions agree at $q = 0$. Hence, calling the functions s, t, u, v, respectively, we obtain the full affine chart

$$uv = s^h t^k. \tag{XI.5.11}$$

The two cases above also explain why this single equation is enough. Every monomial can be reduced by replacing a pair uv with $s^h t^k$. The reduced monomial contains either u or v, and its exponent vector determines which of the two cases applies. For instance, when $h = k = 2$, the dual vector $(p, q, r) = (1, -2, 4)$ has

$$(r + 2q,\ p + r + 2q,\ -q) = (0, 1, 2), \qquad (1, -2, 4) = T + 2V. \tag{XI.5.12}$$

Its function is tv^2. No extra generator or further polynomial relation is hidden in this negative-q part of the dual cone.

We can make the gluing equally explicit for the height-two rectangle. Return to the global lattice and add a strip index. The base characters and the common height character are

$$S_i = (-1, 0, i + 1), \qquad T_i = (1, 0, -i), \qquad W = S_i + T_i = (0, 0, 1). \tag{XI.5.13}$$

The fiber characters are the same in each strip: $U = (0, 1, 0)$ and $V = (0, -1, 2)$. On the overlap with strip $i + 1$, the character s_i is invertible, since it pairs to zero with the common column and to one with the column omitted on that overlap. The change of coordinates follows by adding characters:

$$S_{i+1} = 2S_i + T_i, \quad T_{i+1} = -S_i, \qquad s_{i+1} = s_i^2 t_i, \quad t_{i+1} = s_i^{-1}. \tag{XI.5.14}$$

In particular $s_{i+1}t_{i+1} = s_i t_i$. Therefore the two equations $uv = s_i^2 t_i^2$ and $uv = s_{i+1}^2 t_{i+1}^2$ agree on the overlap. This is one threefold with three affine base patches, rather than three unrelated collision equations. The inverse transformation uses $t_{i+1}^{-1} = s_i$ on the same overlap.

In the rectangle, $h = k = 2$. Away from $t = 0$, the factor t^2 is a unit and a transverse surface to the $s = 0$ curve has type A_1. The same holds along $t = 0$ away from $s = 0$. To see the change at their intersection, take surface slices $s = z$, $t = z + \delta$:

$$uv = z^2(z + \delta)^2. \tag{XI.5.15}$$

For $\delta \neq 0$, the two double roots give two A_1 singularities; for $\delta = 0$, the fourth-order root gives A_3. The threefold maps to a surface with a one-dimensional conic fiber. The ALE

surfaces just used are *transverse slices* in the threefold, rather than two-dimensional fibers of that map.

The distinction can be checked in coordinates. On the open set $t \neq 0$, replace v by $\widetilde{v} = v/t^2$ and hold t fixed. Then

$$uv = s^2t^2 \quad \Longrightarrow \quad u\widetilde{v} = s^2, \qquad t \in \mathbb{C}^*. \tag{XI.5.16}$$

The last equation is the transverse A_1 surface. At a generic point of the two-dimensional base, s, t are fixed and uv is a nonzero constant, leaving a one-dimensional fiber. At the junction one must keep both vanishing factors; setting one of them to a unit would discard the extra roots in (XI.5.15).

The same collision occurs at all three p_i, but their roles depend on which base curves carry dynamical fields. With the ordinary genus-zero twist on the compact split A_1 sectors, C_1 and C_2 supply the two four-dimensional vectors. At the ends we take fixed flavor backgrounds on the noncompact curves. It remains to determine the representation and its masses at each junction. The walls of the resolved fan give a direct calculation.

XI.5.3 Read electric charges from the resolved curves

Which curve couples to both gauge groups if their divisors do not intersect? A wall shared by two smooth three-cones gives a compact torus-invariant curve. The two rays outside the wall give divisors that meet the curve transversely, once each. The two wall coefficients then follow from the relation among the four lifted rays. We write the curve's intersection vector using $e_{i,j}$ for the unit vector at $D_{i,j}$; its coefficient at $D_{i,j}$ is $D_{i,j} \cdot \Gamma$ for a curve Γ.

The wall (L_1, R_0) in (XI.5.2) has outside rays L_0, L_2. Since $v_{i,0} + v_{i,2} = 2v_{i,1}$, its row is

$$F_i = e_{i,0} - 2e_{i,1} + e_{i,2}. \tag{XI.5.17}$$

The wall (L_2, R_1) gives F_{i+1} by the same computation in the right column. The generic root over C_i has the same class F_i: away from its junction, the transverse subdivision in the column is the standard A_1 resolution with the vertical relation (XI.5.17). In the middle strip, each root curve is contained in one compact divisor.

Now use the wall (L_2, R_0), whose outside rays are L_1, R_1. The sums of lifted rays agree, $v_{i,1} + v_{i+1,1} = v_{i,2} + v_{i+1,0}$, so the middle curve is

$$G_i = e_{i,1} + e_{i+1,1} - e_{i,2} - e_{i+1,0}. \tag{XI.5.18}$$

For the central strip this reads

$$v_{1,1} + v_{2,1} - v_{1,2} - v_{2,0} = (1,1,1) + (2,1,1) - (1,2,1) - (2,0,1) = 0. \tag{XI.5.19}$$

The positive coefficients are at the two outside rays. The negative coefficients are at the two divisors containing the wall curve. This fixes the sign before we apply the electric-charge convention. In particular, G_1 meets E_1 and E_2 once each. It is contained in neither. Its two normal degrees are $-1, -1$, from the two wall divisors that contain

it. The adjacent triangles form a primitive parallelogram, so contracting just that wall locally gives the ordinary conifold chart, while the two root curves remain distinguished. The three compact components over p_1 occur in the order F_1, G_1, F_2; Figure XI.5.2 also shows the two noncompact tails.

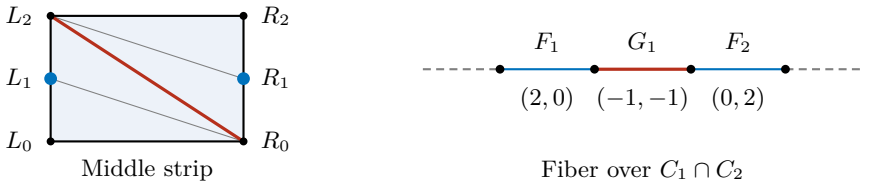


Figure XI.5.2: The central bridge and its compact charges. The highlighted wall on the left gives G_1; the two blue points are its outside rays, so both divisor intersections are $+1$. On the right, the solid segments are the three compact curve components; the dashed tails are noncompact. The charge pairs use $q_i = -E_i \cdot \Gamma$. This chain of curves joins the two sectors even though E_1 and E_2 themselves are disjoint.

The remaining compact walls are vertical, in columns $1, 2$. Take $(v_{i,0}, v_{i,1})$ in one of these columns. Its outside rays are $v_{i-1,2}, v_{i+1,0}$, so the relation gives

$$B_i = e_{i-1,2} + e_{i+1,0} - 2e_{i,1}, \qquad i = 1, 2. \tag{XI.5.20}$$

The upper wall $(v_{i,1}, v_{i,2})$ has the same row. These walls give sections over C_i: the two rays of the wall project to w_i and the neighboring rays project to primitive generators on either side of it. The two base lattices at the ends of C_i are unimodular, so the map has degree one along the section. We use B_i for this class upstairs, distinct from C_i downstairs.

We can now count the independent curve periods without choosing a gauge-theory interpretation. The four F_i, three G_i, and two B_i generate the integral relation lattice of the fan. To see why they give an integral basis, consider any row $c = (c_{i,j})$ with $\sum_{i,j} c_{i,j} v_{i,j} = 0$. Set $S_i = \sum_j c_{i,j}$ and $J_i = \sum_j j c_{i,j}$. Then

$$\sum_i S_i = \sum_i i S_i = \sum_i J_i = 0. \tag{XI.5.21}$$

In the column sums the two section rows are $(1, -2, 1, 0)$ and $(0, 1, -2, 1)$. Subtracting $S_0 B_1 + S_3 B_2$ sets S_0, S_3 to zero. The first two constraints then give $S_1 = S_2 = 0$. With these sums removed, the bridge rows shift the J values by consecutive differences:

$$(J_i, J_{i+1})_{G_i} = (-1, 1), \qquad \big(S_i, J_i\big)_{F_i} = (0, 0). \tag{XI.5.22}$$

The consecutive differences span the integer vectors of zero total sum. After subtracting the bridges, the row in each column has both its sum and its j moment zero, so it is an integer multiple of $(1, -2, 1)$. This proves generation; reversing the steps proves uniqueness. It explains why there are nine curve periods to organize, before we ask which are Coulomb variables.

The column reduction is also a practical way to decompose a new curve relation. For a row with zero column sum, the two conditions inside a single height-two column are

$$c_0 + c_1 + c_2 = 0, \qquad c_1 + 2c_2 = 0 \quad \Longrightarrow \quad (c_0, c_1, c_2) = c_2(1, -2, 1). \tag{XI.5.23}$$

For example, after the section rows remove the column sums, a residual moment vector $(J_0, J_1, J_2, J_3) = (2, -1, -1, 0)$ is removed by $-2G_0 - G_1$. Its moments are

$$-2(-1, 1, 0, 0) - (0, -1, 1, 0) = (2, -1, -1, 0). \tag{XI.5.24}$$

Only the four vertical fiber rows then remain. The reduction uses integer subtraction throughout. Thus it establishes an integral relation basis, stronger than a count of nine linearly independent real periods. The later half-fiber combinations used for masses will be a different, rational change of coordinates.

The wall relations determine the gauge charges of the bridge and its root shifts. Use the coroot charges $q_i(\Gamma) = -E_i \cdot \Gamma$. The central wall relations give

$$q(F_1) = (2, 0), \qquad q(G_1) = (-1, -1), \qquad q(F_2) = (0, 2). \tag{XI.5.25}$$

Adding either simple root raises its corresponding charge by two. The four resulting weights are those of a doublet under each $SU(2)$:

$$q(G_1 + \ell F_1 + r F_2) = (-1 + 2\ell, -1 + 2r), \qquad \ell, r \in \{0, 1\}. \tag{XI.5.26}$$

Here is the charge calculation with all four rows displayed:

Γ	$E_1 \cdot \Gamma$	$E_2 \cdot \Gamma$	q_1	q_2
G_1	1	1	-1	-1
$G_1 + F_1$	-1	1	1	-1
$G_1 + F_2$	1	-1	-1	1
$G_1 + F_1 + F_2$	-1	-1	1	1

(XI.5.27)

The root has coroot charge two, while a doublet weight has charge one. This is why a unit root shift connects the two doublet weights. The bridge is charged under both compact divisors even though those divisors do not meet: intersecting a connecting curve is a different incidence condition from intersecting one another. We can check the representation directly in the enhanced algebra. Separate the four eigenvalues into two pairs and use the coroot matrices $H_1 = \mathrm{diag}(1, -1, 0, 0)$ and $H_2 = \mathrm{diag}(0, 0, 1, -1)$. The weight of an off-block matrix unit E_{ab}, $a \in \{1, 2\}$ and $b \in \{3, 4\}$, is

$$\big((H_1)_{aa} - (H_1)_{bb}, (H_2)_{aa} - (H_2)_{bb}\big). \tag{XI.5.28}$$

This gives all four weights in (XI.5.26). The reverse block is the conjugate orientation.

The enhanced algebra makes the division between gauge roots and matter weights transparent. The two diagonal 2×2 blocks contain the two $\mathfrak{su}(2)$ adjoints and the relative abelian generator. The two off-diagonal blocks each contain four matrix units. At the level of dimensions,

$$15 = (3 + 3 + 1) + 4 + 4. \tag{XI.5.29}$$

The two groups of four are conjugate, not two independent copies of the local collision. The geometric intersection table establishes their weights; the localization rule determines how they enter a four-dimensional multiplet.

The weights fix the representation. The ordinary IIA localization rule for the simple transverse collision supplies the multiplicity: one *full* hypermultiplet in $(\mathbf{2},\mathbf{2})$. A full hyper has the two conjugate chiral components. Reversing the orientation above accounts for the conjugate component, so it does not double the hyper count. The product of the two doublets is real; this is not a half hyper. The argument uses the local matter dictionary and does not require each effective sum of curves to remain an isolated stable brane at arbitrary moduli.

At an outer strip, the same off-block representation has one doublet index for a fixed end sector. For the neighboring gauge group it is a pair of full fundamental hypers, one for each end eigenvalue. Thus the middle junction gives a single bifundamental and each outside junction gives two fundamentals. Their charge shifts are already visible in the curve sums. We now evaluate the periods of those same sums.

XI.5.4 Separate Coulomb motion, masses, and couplings

Which periods must stay fixed when we change a gauge eigenvalue? The bridge period itself is not a bare mass. Its curve carries gauge charge, so part of its central charge comes from the Coulomb expectation values. We first separate that contribution, then apply the same test to each gauge base.

We begin by fixing the normalization and sign of these periods. Use the complexified Kähler period t_Γ and action T_Γ of Chapter 2:

$$t_\Gamma = \frac{\int_\Gamma (B + iJ)}{4\pi^2\alpha'}, \qquad T_\Gamma = -2\pi i\, t_\Gamma, \qquad Q_\Gamma = e^{-T_\Gamma}. \tag{XI.5.30}$$

Here B is the two-form potential, distinct from a section class B_i, and J is the Kähler form. On the aligned real slice with zero B and zero flux, a calibrated D2 on a curve of physical area A_Γ has mass $A_\Gamma/[(2\pi)^2 g_s(\alpha')^{3/2}]$. Since $A_\Gamma = 2\pi\alpha' T_\Gamma$ on this slice, define the signed, mass-normalized periods by

$$\epsilon = \frac{2\pi g_s}{M_s}, \qquad Z(\Gamma) = \frac{T_\Gamma}{\epsilon}, \qquad 2a_i = Z(F_i), \qquad M_s = (\alpha')^{-1/2}. \tag{XI.5.31}$$

In a common local complex lift we keep the same linear relation. The continuation of the selected charged masses to shrinking curves is the protected input used in Chapter 2. For $i = 1, 2$, the eigenvalues are $+a_i, -a_i$ and the root has central charge $2a_i$. For $i = 0, 3$, the same notation records fixed end splittings.

Write m_i for the midpoint of the four signed periods in the ith strip. Additivity and (XI.5.26) give

$$m_i := Z(G_i) + a_i + a_{i+1}, \qquad (m_0, m_1, m_2) = (m_L, m, m_R). \tag{XI.5.32}$$

The period of each charged class is then

$$Z(G_i + \ell F_i + r F_{i+1}) = m_i + (2\ell - 1)a_i + (2r - 1)a_{i+1}. \tag{XI.5.33}$$

The midpoint can be recovered from the four charged periods without knowing which one was called the bridge. Averaging over the two root shifts cancels both electric charges:

$$\frac{1}{4}\sum_{\ell,r=0}^{1} Z(G_i + \ell F_i + r F_{i+1}) = m_i, \qquad \frac{1}{4}\sum_{\ell,r=0}^{1}(-1 + 2\ell, -1 + 2r) = (0, 0). \tag{XI.5.34}$$

This explains the use of a signed midpoint. A physical BPS mass is the magnitude of the relevant central charge. Taking absolute values before averaging would lose its linear dependence on the bare mass and Coulomb variables. We use one common additive lift for this calculation, and take magnitudes only when discussing threshold sizes. At the middle strip the last two terms both depend on the vacuum. At the left strip, the term $(2\ell - 1)a_0$ instead distinguishes two masses for doublets at node 1. The right strip works the same way. Thus the five signed bare masses, in a local frame that orders the end eigenvalues, are

$$m_L + a_0, \quad m_L - a_0, \quad m, \quad m_R + a_3, \quad m_R - a_3. \tag{XI.5.35}$$

For example the four left-junction periods are

$$(m_L - a_0) - a_1, \quad (m_L - a_0) + a_1, \quad (m_L + a_0) - a_1, \quad (m_L + a_0) + a_1. \tag{XI.5.36}$$

Regrouping them into the two pairs with the same parenthesis gives two doublets of node 1. Each pair changes with a_1 in precisely the manner required by its electric weights, while its parenthesis stays fixed. At the center there is no external doublet splitting to hold fixed: both a_1 and a_2 are vacuum coordinates and only the common midpoint m is a bare mass. The holomorphic root separation δ in (XI.5.15) locates the collision. These Kähler combinations are the parameters that move the charged masses.

For a real chamber, take $a_0, a_1, a_2, a_3 = (1, 2, 3, 4)$ and $m_L, m, m_R = (11, 13, 17)$ in a common mass unit. In particular

$$(Z(G_0), Z(G_1), Z(G_2)) = (8, 8, 10), \qquad (m_L \pm a_0,\ m,\ m_R \pm a_3) = (12, 10, 13, 21, 13). \tag{XI.5.37}$$

Every root and bridge period is positive. With positive section actions this is inside the real Kähler chamber of the chosen fan. Although one left mass and the right masses enter different sectors, the test for all of them is the same: their midpoint and fixed splitting, not a raw bridge period.

The section periods need the same separation between gauge motion and fixed boundary data. The charges of F_j and B_j under the two compact divisors are both $2\delta_{ij}$, by (XI.5.17) and (XI.5.20). Thus the section alone has a compact variation. Choose instead the action of the class

$$K_i = B_i - F_i, \qquad E_j \cdot K_i = 0 \quad (i, j = 1, 2). \tag{XI.5.38}$$

This difference is a period coordinate; we do not need an effective representative of K_i. The masses in (XI.5.35) have the same property. For example the two charges of the middle mass combination cancel:

$$q\big(G_1 + \tfrac{1}{2}(F_1 + F_2)\big) = (-1,-1) + \tfrac{1}{2}\big((2,0) + (0,2)\big) = (0,0). \tag{XI.5.39}$$

The outside combinations cancel the one compact charge at that junction. The extra half-fiber terms involving F_0 or F_3 change only the fixed end splitting.

The compact variations change the root periods with diagonal pairing $E_i \cdot F_j = -2\delta_{ij}$. The five masses and the two T_{K_i} are independent complementary coordinates: the change from (m_L, a_0) to $(m_L + a_0, m_L - a_0)$ has determinant -2, and the right pair contributes another factor of -2. The remaining transformations only reorder or shift variables. In particular, vary a_1 by Δ at fixed a_2 and fixed backgrounds. The raw periods move as

$$\Delta Z(F_1) = 2\Delta, \qquad \Delta Z(G_0) = \Delta Z(G_1) = -\Delta, \qquad \Delta T_{B_1} = 2\epsilon\Delta. \tag{XI.5.40}$$

The mass and T_{K_1} shifts cancel. One can also invert the entire map, which shows explicitly that the two coupling coordinates do not impose a relation among the five masses. Write $\mu_{L\pm} = m_L \pm a_0$ and $\mu_{R\pm} = m_R \pm a_3$. Then

$$a_0 = \frac{\mu_{L+} - \mu_{L-}}{2}, \qquad m_L = \frac{\mu_{L+} + \mu_{L-}}{2}, \tag{XI.5.41}$$

$$a_3 = \frac{\mu_{R+} - \mu_{R-}}{2}, \qquad m_R = \frac{\mu_{R+} + \mu_{R-}}{2}, \tag{XI.5.42}$$

$$Z(F_i) = 2a_i, \qquad Z(G_i) = m_i - a_i - a_{i+1}, \tag{XI.5.43}$$

$$T_{B_i} = T_{K_i} + 2\epsilon a_i, \qquad i = 1,2. \tag{XI.5.44}$$

The end eigenvalue ordering chooses a local cover of the mass space. Exchanging the two eigenvalues exchanges μ_{L+} and μ_{L-}, or their right counterparts. The factors of one half in this inverse map are appropriate for continuous parameter coordinates; they do not identify a primitive integral charge basis.

For a simultaneous Coulomb motion, keep all backgrounds fixed and take $(\delta a_1, \delta a_2) = (1/2, -1/3)$ in a common mass unit. The raw periods respond as follows:

$$(\delta Z(F_0), \delta Z(F_1), \delta Z(F_2), \delta Z(F_3)) = (0, 1, -2/3, 0), \tag{XI.5.45}$$

$$(\delta Z(G_0), \delta Z(G_1), \delta Z(G_2)) = (-1/2, -1/6, 1/3), \tag{XI.5.46}$$

$$(\delta T_{B_1}, \delta T_{B_2}) = \epsilon(1, -2/3). \tag{XI.5.47}$$

For the central mass the cancellation is $-1/6 + (1 - 2/3)/2 = 0$; at each end the analogous cancellation uses the adjacent half-fiber. The section and root changes also cancel in T_K. These are tangent directions to the linear parameter chart; when used for an actual motion in the chosen real resolution, their amplitude must keep its effective wall areas positive.

A change of a single bare mass looks different. At fixed Coulomb variables, choose $\delta m_L = \delta a_0 = \eta$ and keep the other backgrounds unchanged. Then

$$\delta\mu_{L+} = 2\eta, \qquad \delta\mu_{L-} = 0, \qquad \delta Z(F_0) = 2\eta, \qquad \delta Z(G_0) = 0. \tag{XI.5.48}$$

The lower left bridge period happens to stay fixed while one physical bare mass changes. Together with (XI.5.40), this gives two reasons not to identify a raw bridge area with a bare mass: it can move under a pure Coulomb variation and can stay fixed under a mass variation. A compact curve period can therefore enter a background parameter: the distinction is which combinations pair with compact divisor variations. We use the ordinary local gauge sector in which the two compact directions give retained normalizable Coulomb modes and the other seven coordinates are prescribed boundary data. The intersection calculation identifies the variations, without an analytic classification of normalizable modes on the threefold.

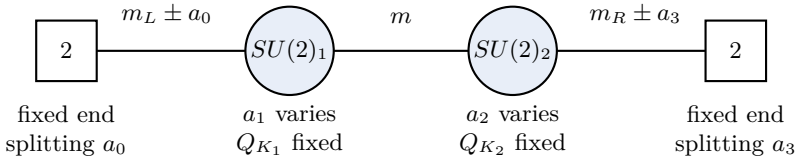


Figure XI.5.3: The same four-column geometry written as an engineered gauge quiver. Circles denote the two gauge sectors; squares denote the end doublets held as flavor backgrounds. The three edges come from the three junctions. The masses above the edges stay fixed under the two compact variations. Each circle has its own Coulomb variable and its own independently chosen bare coordinate.

We can now compare these neutral coordinates with the weak gauge couplings. In the leading reduction of Chapter 3, the inverse squared coupling is the physical area of the base divided by g_6^2. Using a section B_i to measure the base in the collapse metric and the fundamental trace convention gives

$$\begin{aligned} A_i &= 2\pi\alpha' \operatorname{Re} T_{B_i}, \qquad g_6^2 = 2(2\pi)^3\alpha', \\ \frac{8\pi^2}{g_i^2} &= \frac{8\pi^2 A_i}{g_6^2} = \frac{A_i}{2\pi\alpha'} = \operatorname{Re} T_{B_i}. \end{aligned} \tag{XI.5.49}$$

The theta angle in this lift is $\theta_i = -\operatorname{Im} T_{B_i}$. Thus the leading bare coordinate has the action and phase

$$Q_{B_i} = e^{i\theta_i - 8\pi^2/g_i^2}, \qquad \tau_i = \frac{\theta_i}{2\pi} + \frac{4\pi i}{g_i^2}. \tag{XI.5.50}$$

At this order $Q_{B_i} = e^{2\pi i \tau_i}$; finite weak matching can change the coordinates. It is not a formula for the effective photon period matrix.

Keep the seven finite fiber quantities in mass units and take $\epsilon \to 0$. The two independently adjustable base actions can stay large and fixed, so both gauge couplings stay weak and finite. The shift from the effective section to the fixed boundary coordinate vanishes in this limit:

$$T_{B_i} = T_{K_i} + T_{F_i}, \qquad Q_{K_i} = Q_{B_i} e^{T_{F_i}}, \qquad T_{F_i} = 2\epsilon a_i \to 0. \tag{XI.5.51}$$

At nonzero ϵ the distinction is already measurable in the coordinates. A Coulomb

variation with fixed T_{K_i} gives

$$\delta \log Q_{K_i} = 0, \qquad \delta \log Q_{B_i} = -2\epsilon\, \delta a_i, \qquad \frac{Q_{K_i}}{Q_{B_i}} = 1 + 2\epsilon a_i + O(\epsilon^2 a_i^2). \tag{XI.5.52}$$

The correction is small at fixed mass-normalized a_i because ϵ has units of inverse mass. In contrast, the base action can remain a fixed positive dimensionless number. For two arbitrary weak choices $L_1, L_2 \gg 1$ in the real slice,

$$\operatorname{Re} T_{K_1} = L_1, \quad \operatorname{Re} T_{K_2} = L_2 \quad \Longrightarrow \quad \operatorname{Re} T_{B_i} = L_i + 2\epsilon a_i, \qquad |Q_{B_i}| \longrightarrow e^{-L_i}. \tag{XI.5.53}$$

Neither equation constrains the other base action or the five masses. This is the local independence required to turn off one gauge interaction while preserving the other. Figure XI.5.3 summarizes the two Coulomb variables, five masses, and two couplings. The physical area A_i tends to zero for a fixed action, even if that action is numerically large in string units. For an isolated four-dimensional theory, we still require the controlled base metric and heavy or decoupled unwanted modes of the local limit. These scale conditions are distinct from counting the adjustable periods. We can now check which couplings may remain finite without introducing a strong scale.

XI.5.5 Balance the running at both nodes

Why does a single bifundamental supply two flavors to each node? The gauge field at one end acts on one index of the hypermultiplet, while the other index gives a multiplicity. The one-loop calculation measures this multiplicity with a trace, so the same weight table that fixed the masses also fixes the screening.

Take the one-loop convention

$$\mu \frac{dg_i}{d\mu} = -\frac{b_i g_i^3}{16\pi^2}, \qquad b_i = 2T(\text{adj}) - \sum_{\text{full hypers } R} 2T(R), \qquad T(\text{fund}) = \tfrac{1}{2}. \tag{XI.5.54}$$

In $SU(2)$, the fundamental coroot is $H = \operatorname{diag}(1, -1)$, so $T(R) = \operatorname{tr}_R H^2/4$. For the vector multiplet, the roots ± 2 and the zero Cartan weight give $\operatorname{tr}_{\text{adj}} H^2 = 8$. The four bridge weights in (XI.5.26) have charge of magnitude one at either node, so they give $\operatorname{tr}_{(\mathbf{2},\mathbf{2})} H_i^2 = 4$. A fundamental contributes $\operatorname{tr}_{\mathbf{2}} H^2 = 2$. Therefore

$$b_i = \frac{8}{2} - \frac{4}{2} - 2\frac{2}{2} = 4 - 2 - 2 = 0, \qquad i = 1, 2. \tag{XI.5.55}$$

There is one central edge in Figure XI.5.3, but its trace contribution equals that of two fundamental hypers for each node. The two chiral components of each full hyper are already accounted for in (XI.5.54).

For $SU(N_1) \times SU(N_2)$ with one full bifundamental, H_1 acts as $H_1 \otimes 1$ on the representation. Its trace square factors:

$$\operatorname{tr}_{\mathbf{N}_1 \otimes \overline{\mathbf{N}}_2} (H_1 \otimes 1)^2 = N_2 \operatorname{tr}_{\mathbf{N}_1} H_1^2. \tag{XI.5.56}$$

With f_1, f_2 full end fundamentals and $T(\mathrm{adj}_{SU(N_i)}) = N_i$, the general two-node calculation is

$$b_1 = 2N_1 - N_2 - f_1, \qquad b_2 = 2N_2 - N_1 - f_2. \tag{XI.5.57}$$

Two changes illustrate what balance requires. First give one left fundamental a mass above the observation scale while the other hypers remain light there. The central edge still supplies two flavors on each side. The left count falls to three and the right count remains four, so $(b_1, b_2) = (1, 0)$ in this energy window. A related fan comparison lowers the outer left column height from two to one, giving $(1, 2, 2, 2)$. The first junction now has $uv = st^2$ and only one end weight on the height-one side. This is a separate geometry with the smaller matter content. In the one-loop weak description, a positive b means that increasing the observation scale decreases the bare fugacity:

$$\mu \frac{d}{d\mu} \frac{8\pi^2}{g^2} = b, \qquad |Q(\mu)| \;\propto\; (\Lambda/\mu)^b \qquad (b > 0). \tag{XI.5.58}$$

This fixes the sign of the suppression without identifying the threshold matching between the two string geometries.

The energy window matters in this comparison. Let M_H be the heavy left mass, and suppose the observation scale is above all the other charged thresholds and well below M_H, inside a weak four-dimensional regime. Above M_H the original four-flavor count applies. Below it the left node has lost one unit of screening:

weak energy window	b_1	b_2
$\mu \gg M_H$	0	0
other thresholds $\ll \mu \ll M_H$	1	0

(XI.5.59)

The inequalities refer to threshold magnitudes, not signed central charges. Choose two scales $\mu_1 < \mu_2$ inside the second window. Integrating the stated one-loop equation gives

$$\frac{8\pi^2}{g_1^2(\mu_2)} - \frac{8\pi^2}{g_1^2(\mu_1)} = \log \frac{\mu_2}{\mu_1}, \qquad \frac{|Q_1(\mu_2)|}{|Q_1(\mu_1)|} = \frac{\mu_1}{\mu_2}. \tag{XI.5.60}$$

The second node has zero logarithmic running in this window. These equations compare two scales of the same weak effective theory. A finite-mass threshold trajectory has more information than lowering a column height, which specifies a second local geometry. The common index is the quantity established by this comparison.

Changing the neighbor rank changes this same trace multiplicity. We next reconstruct such a geometry and follow its additional root.

XI.5.6 Change the ranks and rebuild the weights

Next take $N_1 = 2$, $N_2 = 3$. Keeping two end fundamentals on each side would give $(b_1, b_2) = (-1, 2)$. To keep both nodes balanced, (XI.5.57) instead requires

$$f_1 = 4 - 3 = 1, \qquad f_2 = 6 - 2 = 4. \tag{XI.5.61}$$

The heights $(1,2,3,4)$ give these numbers in the same grouped strip construction. This is a useful transfer of the method: both the root system at the second node and the end multiplicities change. We can follow the geometry before using the quiver index.

Use the rays $(i,j,1)$ with $0 \le j \le i+1$. For a strip with left height h and right height k, the triangles are (L_j, L_{j+1}, R_0) for $0 \le j < h$ and (L_h, R_j, R_{j+1}) for $0 \le j < k$. Hence this finite example has

$$\#\{\text{rays}\} = 2+3+4+5 = 14, \qquad \#\{\text{triangles}\} = 3+5+7 = 15. \tag{XI.5.62}$$

The triangles are again unimodular and are lower faces of the same lifting function used above, evaluated on these points. Only the vertical points strictly inside the polygon give compact divisors:

$$D_{1,1}, \quad D_{2,1}, \quad D_{2,2}, \qquad \dim \mathcal{C} = (2-1)+(3-1) = 3. \tag{XI.5.63}$$

Here $\mathcal{C}$ denotes the Coulomb parameter space in the ordinary gauge-sector boundary choice. The two interior base curves remain compact. The root ranks have changed, rather than the number of gauge factors.

The semigroup derivation of (XI.5.11) works strip by strip. Its three equations now read

$$uv = st^2, \qquad uv = s^2t^3, \qquad uv = s^3t^4, \tag{XI.5.64}$$

where s,t are local coordinates in each respective base patch. For example the middle transverse slice is $uv = z^2(z+\delta)^3$. Away from the collision its two root clusters have types A_1 and A_2; at the collision the combined type is A_4. The off-block roots carry a doublet index of the first factor and a three-valued index of the second.

It is instructive to recover those six weights from the resolved curves. Call the left simple-root row F, the two right rows R_1, R_2, and the bridge row G. Against the three compact divisors, with the same sign convention as before,

$$q(F) = (2,0,0), \quad q(R_1) = (0,2,-1), \quad q(R_2) = (0,-1,2), \quad q(G) = (-1,-1,0). \tag{XI.5.65}$$

The six off-block classes and weights are therefore

	G	$G+R_1$	$G+R_1+R_2$
q	$(-1,-1,0)$	$(-1,1,-1)$	$(-1,0,1)$
$q(\cdot + F)$	$(1,-1,0)$	$(1,1,-1)$	$(1,0,1)$

(XI.5.66)

The three right pairs $(-1,0),(1,-1),(0,1)$ sum to zero and are connected by the A_2 simple roots. The first charge is ± 1 independently. This recovers the off-block $(\mathbf{2},\overline{\mathbf{3}})$ weight set, up to a choice of which conjugate orientation is named first.

The mass calculation has the same midpoint interpretation. Let $c = Z(R_1)$ and $d = Z(R_2)$, and choose the ordered right eigenvalues

$$\lambda_0 = -\frac{2c+d}{3}, \qquad \lambda_1 = \frac{c-d}{3}, \qquad \lambda_2 = \frac{c+2d}{3}. \tag{XI.5.67}$$

Their sum is zero and their successive differences are c, d. With $2a = Z(F)$, define the middle mass by $Z(G) = m - a + \lambda_0$. The six periods become

$$Z(G+\ell F+\text{right root shifts}) = m+(2\ell-1)a+\lambda_r, \qquad \ell = 0,1, \quad r = 0,1,2. \tag{XI.5.68}$$

Their average is m. The extra right root therefore adds a Coulomb coordinate and a third weight, without adding a second bifundamental bare mass.

Finally evaluate the index in this changed representation. For the $SU(2)$ coroot, the six squared charges sum to six; for either simple $SU(3)$ coroot they sum to four. Since the corresponding fundamental trace is two in each case, the full bifundamental contributes three units of screening at node 1 and two at node 2. The end heights supply one and four full fundamentals, respectively, so

$$b_1 = 4 - 3 - 1 = 0, \qquad b_2 = 6 - 2 - 4 = 0, \qquad n_{\text{mass}} = 1 + 1 + 4 = 6. \tag{XI.5.69}$$

The last sum counts the left end mass, one middle mass, and four right end masses. This worked comparison shows which geometric inputs must change to rebalance the ranks. It establishes the finite construction and its conditional index arithmetic, without classifying other rank assignments. We can now follow these six bridge periods into the weak Coulomb response of the same theory.

XI.5.7 Follow the six weights into the photon response

The changed-rank example gives more than a new flavor count. A bridge particle couples to photons from both gauge factors. How does its mass change the response of those photons when we move either Coulomb expectation value? We can answer this in the same $SU(2) \times SU(3)$ theory, using the six periods we have just constructed. The calculation retains one left end hypermultiplet and four right end hypermultiplets.

Work in a weak electric Coulomb patch where all charged particles to be removed from the photon action have nonzero masses. The external photon momentum must be below those masses. We calculate the perturbative two-derivative response; instanton corrections remain small in the chosen patch and are not included here. The geometry has already supplied the linear charges and mass parameters. The further physical input is the one-loop determinant of a charged full hypermultiplet. Its dependence on a central charge z is proportional to $z^2 \log z^2$. Differentiating twice measures how the charged particle changes the photon kinetic term.

Use the dimension-one electric coordinates

$$X = (a, c, d), \qquad \lambda_0 = -\frac{2c + d}{3}, \quad \lambda_1 = \frac{c - d}{3}, \quad \lambda_2 = \frac{c + 2d}{3}, \qquad z_{sr} = m + sa + \lambda_r, \tag{XI.5.70}$$

where $s = \pm 1$ and $r = 0, 1, 2$. The parameters c, d are simple-root periods of the right node. They are not its components along the two fundamental coroots. If these components are b_1, b_2, then

$$\begin{pmatrix} c \\ d \end{pmatrix} = \begin{pmatrix} 2 & -1 \\ -1 & 2 \end{pmatrix} \begin{pmatrix} b_1 \\ b_2 \end{pmatrix}, \qquad (\lambda_0, \lambda_1, \lambda_2) = (-b_1, b_1 - b_2, b_2). \tag{XI.5.71}$$

Thus the integral charges displayed in (XI.5.66) become rational gradients when the

independent variables are c, d. Define

$$v_0 = \frac{1}{3}(-2,-1), \qquad v_1 = \frac{1}{3}(1,-1), \qquad v_2 = \frac{1}{3}(1,2), \qquad w_{sr} = \partial_X z_{sr} = (s, v_r). \tag{XI.5.72}$$

These gradients specify a coordinate response. The primitive charge normalization is still the integral coroot normalization used earlier.

To fix the finite quadratic convention, let μ be a positive reference mass and use the local holomorphic function

$$f(z) = z^2\left[\log\frac{z^2}{\mu^2} - 3\right], \qquad f'(z) = 2z\left[\log\frac{z^2}{\mu^2} - 2\right], \qquad f''(z) = 2\log\frac{z^2}{\mu^2}. \tag{XI.5.73}$$

Choose logarithm branches on a simply connected patch that excludes the charged thresholds. The subtraction differs from $z^2\log(z^2/\mu^2)$ by a quadratic term. Its advantage is that the second derivative contains only the logarithm. We count one full hypermultiplet over the six weights of its representation. Adding the conjugate weights a second time would double its screening contribution.

We can place this bridge term inside the complete weak theory. Call the left end mass M_L, and choose orientations of the four right end masses M_A, $A = 1, \dots, 4$, so that their periods are $M_A + \lambda_r$. The vector root periods and hypermultiplet periods are

$$\begin{aligned} &\mathcal{R} = \{\pm 2a,\ \pm c,\ \pm d,\ \pm(c+d)\}, \\ &\mathcal{H} = \{M_L \pm a\} \ \cup\ \{z_{sr}\}_{s,r} \ \cup\ \{M_A + \lambda_r\}_{A,r}. \end{aligned} \tag{XI.5.74}$$

With τ_i^{UV} the weak nonabelian couplings, the perturbative prepotential in this convention is

$$\mathcal{F}_{\mathrm{pert}} = \tau_1^{\mathrm{UV}} a^2 + \frac{\tau_2^{\mathrm{UV}}}{2}\sum_r \lambda_r^2 - \frac{1}{8\pi i}\sum_{\rho\in\mathcal{R}} f(\rho) + \frac{1}{8\pi i}\sum_{h\in\mathcal{H}} f(h). \tag{XI.5.75}$$

The root sum includes both signs. The hypermultiplet sum includes each representation weight once. The Coulomb photon matrix is $\tau_{IJ}^{\mathrm{eff}} = \partial_I\partial_J\mathcal{F}$. Already the tree term gives $\tau_{aa}^{\mathrm{tree}} = 2\tau_1^{\mathrm{UV}}$, so the three-coordinate Hessian is not the pair of bare nonabelian couplings.

Only the bridge can give a mixed derivative between a and the right coordinates. Its contribution follows directly:

$$\mathcal{F}_{\mathrm{br}} = \frac{1}{8\pi i}\sum_{s,r} f(z_{sr}), \qquad \tau_{IJ}^{\mathrm{br}} = \frac{1}{4\pi i}\sum_{s,r} w_{sr,I}\, w_{sr,J}\log\frac{z_{sr}^2}{\mu^2}. \tag{XI.5.76}$$

This is a contribution to the full kinetic matrix, rather than a positive metric on its own. In a sufficiently weak patch the positive tree inverse couplings dominate the full metric.

For an explicit matrix, introduce the sum and difference of the two logarithms associated with each right weight:

$$L_r^{\pm} = \log\frac{(m \pm a + \lambda_r)^2}{\mu^2}, \qquad S_r = L_r^+ + L_r^-, \qquad A_r = L_r^+ - L_r^-. \tag{XI.5.77}$$

Writing $D = 4\pi i\,\tau^{\mathrm{br}}$, the three first-row entries are

$$D_{aa} = S_0 + S_1 + S_2, \qquad D_{ac} = \frac{-2A_0 + A_1 + A_2}{3}, \qquad D_{ad} = \frac{-A_0 - A_1 + 2A_2}{3}. \tag{XI.5.78}$$

The remaining symmetric block is

$$\begin{pmatrix} D_{cc} & D_{cd} \\ D_{cd} & D_{dd} \end{pmatrix} = \frac{1}{9}\begin{pmatrix} 4S_0 + S_1 + S_2 & 2S_0 - S_1 + 2S_2 \\ 2S_0 - S_1 + 2S_2 & S_0 + S_1 + 4S_2 \end{pmatrix}. \tag{XI.5.79}$$

For example, the coefficient $-2/3$ in D_{ac} is the c-gradient of the period of the first bridge weight. The matrix therefore keeps the specific curve information that was lost when we reduced the same representation to a single flavor multiplicity. We next ask which part of this matrix can run with a common reference scale.

XI.5.8 Separate finite mixing from logarithmic running

The beta coefficients vanished at both nodes. Does this make their Coulomb photons independent? The response above shows why it does not. A beta coefficient measures the coefficient of a common scale logarithm. The finite logarithms also compare six different particle masses.

The useful trace is now a matrix of second moments. Regard v_r as a column vector and set

$$V = \sum_{r=0}^{2} v_r v_r^T = \frac{1}{3}\begin{pmatrix} 2 & 1 \\ 1 & 2 \end{pmatrix}, \qquad \sum_r v_r = 0. \tag{XI.5.80}$$

For the six bridge gradients, the sum over $s = \pm 1$ gives

$$G_{\mathrm{br}} = \sum_{s,r} w_{sr} w_{sr}^T = \begin{pmatrix} 6 & 0 & 0 \\ 0 & 4/3 & 2/3 \\ 0 & 2/3 & 4/3 \end{pmatrix}, \qquad \mu\partial_\mu D = -2G_{\mathrm{br}}. \tag{XI.5.81}$$

In particular the mixed common-scale terms vanish. The factor s in w_a cancels between the two left weights at each fixed r. This cancellation does not require the right trace constraint. Tracelessness will instead remove a subleading mixed term in the large-mass limit below.

For comparison, taking gradients of the root and end periods in (XI.5.74) yields

$$G_{\mathrm{vec}} = \begin{pmatrix} 8 & 0 & 0 \\ 0 & 4 & 2 \\ 0 & 2 & 4 \end{pmatrix}, \qquad G_{\mathrm{end}} = \begin{pmatrix} 2 & 0 & 0 \\ 0 & 8/3 & 4/3 \\ 0 & 4/3 & 8/3 \end{pmatrix}. \tag{XI.5.82}$$

The upper entry of G_{end} comes from one left fundamental. Its right block is $4V$, from four right fundamentals. Thus the complete scale-dependent Coulomb response cancels:

$$G_{\mathrm{vec}} - G_{\mathrm{br}} - G_{\mathrm{end}} = 0, \qquad \mu\partial_\mu \tau_{IJ}^{1-\mathrm{loop}} = 0. \tag{XI.5.83}$$

This is the matrix form of $b_1 = 4 - 3 - 1 = 0$ and $b_2 = 6 - 2 - 4 = 0$. The prepotential can still have a scale-dependent term involving only fixed masses. Such a term has zero Coulomb Hessian.

Finite mixing survives because the paired masses are unequal. Take a common mass unit and choose

$$a = 1, \qquad c = d = 3, \qquad m = 8, \qquad (\lambda_0, \lambda_1, \lambda_2) = (-3, 0, 3). \tag{XI.5.84}$$

The six bridge periods and three logarithmic differences are

$$\begin{aligned} (z_{-0}, z_{-1}, z_{-2}) &= (4, 7, 10), \qquad (z_{+0}, z_{+1}, z_{+2}) = (6, 9, 12), \\ (A_0, A_1, A_2) &= \left(\log \frac{9}{4}, \log \frac{81}{49}, \log \frac{36}{25} \right). \end{aligned} \tag{XI.5.85}$$

Inserting these values in (XI.5.78) gives

$$\begin{aligned} D_{ac} &= \frac{1}{3} \log \left[\left(\frac{4}{9} \right)^2 \frac{81}{49} \frac{36}{25} \right] \simeq -0.25152949, \\ D_{ad} &= \frac{1}{3} \log \left[\frac{4}{9} \frac{49}{81} \left(\frac{36}{25} \right)^2 \right] \simeq -0.19475762. \end{aligned} \tag{XI.5.86}$$

These numbers compare mass ratios and contain no μ. The end hypers and vectors cannot cancel them, since their periods each depend on only one gauge node. A vanishing beta coefficient has removed the common running, while the bifundamental still communicates a finite response between the two Coulomb sectors.

The same matrix identifies which photon combination responds when one bridge particle becomes light. For instance, keep $a = 1, c = 2, d = 5$ and set $m = 4 + h$, with $h > 0$. Then

$$(z_{-0}, z_{-1}, z_{-2}, z_{+0}, z_{+1}, z_{+2}) = (h, h + 2, h + 7, h + 2, h + 4, h + 9). \tag{XI.5.87}$$

Only the first period tends to zero. Its gradient is $w_* = (-1, -2/3, -1/3)^T$, so the singular contribution is

$$\tau_{\text{sing}}^{\text{br}} = \frac{w_* w_*^T}{4\pi i} \log \frac{h^2}{\mu^2}, \qquad w_* w_*^T = \begin{pmatrix} 1 & 2/3 & 1/3 \\ 2/3 & 4/9 & 2/9 \\ 1/3 & 2/9 & 1/9 \end{pmatrix}. \tag{XI.5.88}$$

This rank-one charge bilinear acts only on the combination $w_*^T \delta X$. The two independent tangent directions

$$\delta X_1 = (-2/3, 1, 0)^T, \qquad \delta X_2 = (-1/3, 0, 1)^T, \qquad w_*^T \delta X_1 = w_*^T \delta X_2 = 0 \tag{XI.5.89}$$

leave the light central charge unchanged to first order and have no logarithmically singular response from this particle. The bilinear is not normalized as an idempotent projector; its coefficient is fixed by the charged determinant. The formula describes the approach to a perturbative hyper threshold with the other charged masses separated. For the photon-only action along the approach, its external momentum must also obey $p_{\text{ext}} \ll h$. At $h = 0$ the light hyper must be retained as an additional field.

XI.5.9 Remove a massive bridge at fixed dynamical scales

We can now follow an actual mass-removal trajectory instead of comparing two flavor counts. Increase m while keeping a, c, d and all end masses finite. Both signs at every right weight then become heavy. Which bare couplings must change if the two remaining gauge theories are to have fixed low-energy scales?

Write $\delta_{sr} = sa + \lambda_r$ and take $m > 0$ much larger than all fixed splittings. The threshold expansion is

$$\log \frac{(m+\delta_{sr})^2}{\mu^2} = \log \frac{m^2}{\mu^2} + \frac{2\delta_{sr}}{m} - \frac{\delta_{sr}^2}{m^2} + O(m^{-3}). \tag{XI.5.90}$$

For the mixed row, summing the two signs first gives

$$\sum_s s = 0, \qquad \sum_s s\delta_{sr} = 2a, \qquad \sum_s s\delta_{sr}^2 = 4a\lambda_r. \tag{XI.5.91}$$

The common logarithm cancels by the first identity. The $1/m$ term is proportional to $\sum_r v_r = 0$. The next term therefore gives the leading communication between the nodes:

$$\begin{pmatrix} D_{ac} \\ D_{ad} \end{pmatrix} = -\frac{4a}{m^2} \sum_r \lambda_r v_r + O(m^{-3}) = -\frac{4a}{3m^2} \begin{pmatrix} 2c+d \\ c+2d \end{pmatrix} + O(m^{-3}). \tag{XI.5.92}$$

The finite mixed response thus vanishes as the bridge is removed. This limit holds at fixed roots. A correlated motion that keeps one $m + sa + \lambda_r$ finite would retain that charged field and give a different low-energy theory.

The diagonal logarithms remain as thresholds in the two separate gauge couplings. The relevant quadratic moment is

$$\sum_{s,r} \delta_{sr}^2 = 6a^2 + 2\sum_r \lambda_r^2, \qquad \sum_r \lambda_r^2 = \frac{2}{3}(c^2 + cd + d^2). \tag{XI.5.93}$$

It contains no mixed node term. The coefficients reproduce three lost fundamentals for $SU(2)$ and two for $SU(3)$. After removing the bridge, the remaining beta coefficients are

$$b_1^{\mathrm{IR}} = 2 \cdot 2 - 1 = 3, \qquad b_2^{\mathrm{IR}} = 2 \cdot 3 - 4 = 2. \tag{XI.5.94}$$

The two end sectors have stayed in place. They become the one-flavor $SU(2)$ and four-flavor $SU(3)$ theories, with vanishing bridge mixing at the renormalizable level.

To turn these coefficients into a scale trajectory, use $S_i = 8\pi^2/g_i^2$ and the one-loop equation already fixed in (XI.5.54). Differentiating S_i gives

$$\frac{dS_i}{d\log\mu} = -\frac{16\pi^2}{g_i^3}\frac{dg_i}{d\log\mu} = b_i^{\mathrm{IR}}, \qquad S_i(\mu) - S_i(m) = b_i^{\mathrm{IR}} \log\frac{\mu}{m}. \tag{XI.5.95}$$

Define a weak one-loop matching convention at the heavy mass and keep its phase fixed. For zero theta, exponentiating the last equation yields

$$q_i^{\mathrm{IR}}(\mu) = q_i^{\mathrm{UV}} \left(\frac{m}{\mu}\right)^{b_i^{\mathrm{IR}}}, \qquad \Lambda_i^{b_i^{\mathrm{IR}}} = \mu^{b_i^{\mathrm{IR}}} q_i^{\mathrm{IR}}(\mu) = m^{b_i^{\mathrm{IR}}} q_i^{\mathrm{UV}}. \tag{XI.5.96}$$

Here Λ_i denotes the scale defined by this convention. Finite threshold constants can be absorbed in its definition. In particular, retaining fixed finite scales requires

$$q_1^{\mathrm{UV}} = \frac{\Lambda_1^3}{m^3}, \qquad q_2^{\mathrm{UV}} = \frac{\Lambda_2^2}{m^2}, \qquad m \longrightarrow \infty. \tag{XI.5.97}$$

Keeping the bare q_i fixed instead gives $\Lambda_i = m(q_i^{\mathrm{UV}})^{1/b_i^{\mathrm{IR}}}$ and sends the inferred scales to infinity. It would not keep a fixed weak Coulomb theory. The powers three and two come from the screening change, not from a choice of how to name the scale.

There are two different energy uses in this argument. Choose a retained weak Coulomb point with all root and matter thresholds finite, nonzero and of order A, with $A \gg \Lambda_i$. Take $m \gg A$. A running-coupling matching scale can then lie above the retained thresholds, for example

$$\mu_{\mathrm{match}} = \sqrt{Am}, \qquad A \ll \mu_{\mathrm{match}} \ll m, \qquad p_{\mathrm{ext}} \ll \min\{|\text{retained charged periods}|\}. \tag{XI.5.98}$$

The last inequality instead specifies the momentum of the photon effective action. We keep the gauge couplings at that Coulomb point perturbative independently. Running below a further charged threshold changes the beta coefficient; the above-threshold b_i^{IR} is not used through every lower-energy interval.

The geometry distinguishes the same variables. The bridge period grows as $Z(G) = m - a + \lambda_0$, while the root periods stay fixed. The independent base actions implement the weak coupling path. At leading real weak matching they satisfy

$$\mathrm{Re}\, T_{B_1} = 3 \log \frac{m}{\Lambda_1} + \text{finite}, \qquad \mathrm{Re}\, T_{B_2} = 2 \log \frac{m}{\Lambda_2} + \text{finite}. \tag{XI.5.99}$$

These are local period and leading bare-action statements. They do not identify an exact geometric flat coordinate with a fully corrected field-theory coupling.

A simultaneous string limit keeps this large four-dimensional mass below the discarded string and base scales. For instance, with M_0 fixed and weak g_s fixed, choose

$$m = \sqrt{M_s M_0}, \qquad \epsilon = \frac{2\pi g_s}{M_s}, \qquad \epsilon m \longrightarrow 0, \qquad \frac{m}{M_s} \longrightarrow 0. \tag{XI.5.100}$$

The actions in (XI.5.99) grow only logarithmically. For the same controlled base shape as before,

$$M_{\mathrm{KK,B_i}} \sim \frac{M_s}{\sqrt{\log(M_s/M_0)}}, \qquad \frac{m}{M_{\mathrm{KK,B_i}}} \longrightarrow 0. \tag{XI.5.101}$$

Thus the bridge mass diverges in fixed four-dimensional units while its dimensionless fiber period collapses. The required isolation of other bulk sectors remains a premise of the local limit. This trajectory does not itself construct a toric transition to a smaller matter diagram.

XI.5.10 Freeze three finite flavor masses

A second operation turns off the right gauge interaction without making the bridge heavy. Send $q_2^{\mathrm{UV}} \to 0$ at fixed weak q_1^{UV}, keeping a, c, d, m and the end masses finite. What does the surviving $SU(2)$ gauge field see? It still couples to all three right weights, now held as flavor parameters. Their masses are

$$M_r = m + \lambda_r, \qquad r = 0, 1, 2, \qquad z_{sr} = M_r + sa. \tag{XI.5.102}$$

The middle hyper therefore becomes three full fundamentals of the retained node. Together with its one original end fundamental, they give $N_f = 4$ above their finite thresholds. The heavy-bridge limit instead left only that one end fundamental.

The complete mass polynomial exhibits how the two root splittings survive in the flavor data. With $u = x + m$, tracelessness gives

$$\sum_r \lambda_r = 0, \qquad \sum_{r<t} \lambda_r \lambda_t = -\frac{c^2 + cd + d^2}{3}, \qquad \prod_r \lambda_r = -\frac{(2c + d)(c - d)(c + 2d)}{27}. \tag{XI.5.103}$$

Hence the three threshold factors multiply to

$$\begin{aligned} P(x) &= \prod_r (x + M_r) \\ &= (x + m)^3 - \frac{c^2 + cd + d^2}{3}(x + m) - \frac{(2c + d)(c - d)(c + 2d)}{27}. \end{aligned} \tag{XI.5.104}$$

For an asymmetric example take $c = 2, d = 5, m = 8$. The frozen right eigenvalues and induced masses are

$$\begin{gathered} (\lambda_0, \lambda_1, \lambda_2) = (-3, -1, 4), \qquad (M_0, M_1, M_2) = (5, 7, 12), \\ P(x) = x^3 + 24x^2 + 179x + 420. \end{gathered} \tag{XI.5.105}$$

Both splittings are visible. Replacing the finite eigenvalues by zero would give $(x + 8)^3$, which has a different spectrum of charged thresholds. A vanishing gauge coupling has not required this replacement.

The same conclusion holds directly at the prepotential level. At fixed M_r the bridge expression is exactly a sum of three fundamental contributions,

$$\mathcal{F}_{\mathrm{br}}|_{c,d,m \text{ fixed}} = \frac{1}{8\pi i} \sum_{r=0}^{2} \sum_{s=\pm 1} f(M_r + sa), \qquad \tau_{aa}^{\mathrm{br}} = \frac{1}{4\pi i} \sum_{r,s} \log \frac{(M_r + sa)^2}{\mu^2}. \tag{XI.5.106}$$

Taking the a-derivative after fixing the background agrees with taking it first and then fixing c, d, m. No derivative of a frozen eigenvalue with respect to a is introduced. In the asymmetric example, at $a = 1$, erasing those splittings changes D_{aa} by

$$D_{aa}\big|_{M=(5,7,12)} - D_{aa}\big|_{M=(8,8,8)} = \log \frac{335036416}{771895089} \simeq -0.83460942. \tag{XI.5.107}$$

This difference is finite and independent of μ. The former mixed entries τ_{ac}, τ_{ad} now describe responses to background flavor parameters. They are not kinetic mixing between three retained interacting photons.

To see how the dynamical spectator fluctuations separate, keep its gauge coupling small and nonzero temporarily. In real photon variables write the local kinetic form as

$$K = \begin{pmatrix} A & B \\ B^T & C/g_2^2 + H \end{pmatrix}, \qquad A > 0, \qquad C > 0, \tag{XI.5.108}$$

where B is a finite 1×2 row and H a finite symmetric 2×2 matrix. The retained finite masses ensure that these loop terms do not diverge. The positive matrix C is the spectator tree form in its chosen Cartan coordinates. Pick a fixed matrix R with $R^T C R = I$. Rescaling the spectator fluctuations by $g_2 R$ gives

$$\begin{pmatrix} 1 & 0 \\ 0 & g_2 R \end{pmatrix}^T K \begin{pmatrix} 1 & 0 \\ 0 & g_2 R \end{pmatrix} = \begin{pmatrix} A & g_2 B R \\ g_2 R^T B^T & I + g_2^2 R^T H R \end{pmatrix}. \tag{XI.5.109}$$

The mixed kinetic term tends to zero in these normalized variables. Completing the kinetic square gives the same limit, since the finite correction to the retained block is

$$B(C/g_2^2 + H)^{-1} B^T = g_2^2 B C^{-1} B^T + O(g_2^4) \longrightarrow 0. \tag{XI.5.110}$$

This is a normalization of a kinetic form. It has not treated the spectator photons as massive particles to be removed from a Wilson action. When we choose a fixed background, the complementary free fields and fields neutral under the retained node are simply outside the interacting sector we are describing.

The geometry also retains the flavor splitting. Restrict the height sequence $(1, 2, 3, 4)$ to the first two strips, with heights $(1, 2, 3)$. The resulting open subfan has nine rays and eight smooth three-cones. Its divisor stars are

column point	full fan	retained subfan
$(1, 1)$	complete star	complete star
$(2, 1),\ (2, 2)$	complete stars	incomplete stars

(XI.5.111)

A complete quotient star makes the corresponding invariant surface compact. Thus only the $SU(2)$ divisor remains compact. Both cones next to the bridge wall $((1, 2), (2, 0))$ are retained, so the bridge periods and three flavor weights remain. The open fan realizes the chosen sector locally; it does not establish metric convergence of the full geometry along the weak-coupling trajectory.

The same rank-changing geometry has now supplied two controlled operations. Sending the bridge mass to infinity requires both bare couplings to change if both dynamical scales are held fixed. Turning off the right interaction at finite root periods instead keeps three flavor masses. We return next to the original $SU(2) \times SU(2)$ example, whose five-puncture description gives an independent comparison of its mass and Coulomb counts.

XI.5.11 Compare the mass and Coulomb counts at fixed poles

The balanced matter content also has a useful comparison at the massless point. At the massless origin the specific $SU(2) \times SU(2)$ Lagrangian in (XI.5.55) has two exactly marginal gauge couplings. This is a property of the four-dimensional conformal theory, in addition to the one-loop check. We can compare its parameter counts in a separate description without computing an effective period.

In that description the two gauge parameters are positions on a sphere with five distinct punctures. A fractional linear transformation places three of the punctures at $0, 1, \infty$, leaving the two positions s, t. In this paragraph s, t denote puncture positions. The mass and Coulomb data are encoded in a quadratic differential

$$\phi_2(z)\, dz^2 = \frac{P_6(z)}{D(z)^2}\, dz^2, \qquad D(z) = z(z-1)(z-s)(z-t), \qquad \deg P_6 \leq 6. \tag{XI.5.112}$$

For a finite puncture z_i the double-pole coefficient is $P_6(z_i)/D'(z_i)^2$. At infinity, set $w = 1/z$. If p_6 is the leading degree-six coefficient, the leading terms are $P_6/D^2 \sim p_6 z^{-2}$ and $dz^2 = w^{-4} dw^2$, so the double-pole coefficient there is p_6. These five coefficients encode squared masses in that presentation.

The infinity calculation is essential. A polynomial of degree six has seven coefficients, and four finite evaluations constrain only four linear combinations. The fifth parameter comes from the change of coordinate of the *quadratic differential*, including the dz^2 factor:

$$z = w^{-1}, \qquad dz^2 = w^{-4} dw^2, \qquad \frac{P_6(z)}{D(z)^2} dz^2 = \left(\frac{p_6}{w^2} + O(w^{-1}) \right) dw^2. \tag{XI.5.113}$$

Fixing just the rational function's behavior without transforming dz^2 would miscount the pole at infinity.

Hold all five coefficients fixed. Fixing the one at infinity requires $\deg(\Delta P_6) \leq 5$; fixing those at the four finite punctures forces a zero at each z_i. Hence

$$\Delta P_6 = D(z)(u + vz). \tag{XI.5.114}$$

Here u, v denote polynomial deformation coefficients, unrelated to the fiber coordinates in (XI.5.11). Divisibility by D fixes the four finite pole coefficients, and the degree bound removes the possible $z^2 D$ term. Each of the two surviving directions changes the simple-pole and regular terms while leaving all double poles fixed. For example, near a finite puncture t_α,

$$\frac{\Delta P_6}{D^2} dz^2 = \frac{u + vz}{D(z)} dz^2 = \left[\frac{u + v t_\alpha}{D'(t_\alpha)(z - t_\alpha)} + O(1) \right] dz^2. \tag{XI.5.115}$$

This local expansion shows how the differential can change without changing any of its mass data.

Take a changed set of finite punctures $(t_0, t_1, t_2, t_3) = (0, 1, 7/4, -2)$. All are distinct, and

$$D(z) = z^4 - \frac{3}{4}z^3 - \frac{15}{4}z^2 + \frac{7}{2}z, \tag{XI.5.116}$$

$$(D'(t_0), D'(t_1), D'(t_2), D'(t_3)) = \left(\frac{7}{2}, -\frac{9}{4}, \frac{315}{64}, -\frac{45}{2}\right). \tag{XI.5.117}$$

The nonzero derivatives make the finite pole evaluations well defined. An explicit fixed-pole motion is

$$\Delta P_6 = D(z)(2 - 3z) = -3z^5 + \frac{17}{4}z^4 + \frac{39}{4}z^3 - 18z^2 + 7z. \tag{XI.5.118}$$

It vanishes at all four finite punctures and has no degree-six coefficient. The pole masses therefore stay fixed while the differential changes.

One can also show directly that the five mass coefficients may be chosen independently. Let their finite values be c_α and their infinity value be c_∞. Introduce the four interpolation polynomials

$$L_\alpha(z) = \prod_{\beta \neq \alpha} \frac{z - t_\beta}{t_\alpha - t_\beta}, \qquad L_\alpha(t_\beta) = \delta_{\alpha\beta}. \tag{XI.5.119}$$

Then one representative with precisely these pole data is

$$P_6^{(0)}(z) = c_\infty z^6 + \sum_{\alpha=0}^{3} \left[c_\alpha D'(t_\alpha)^2 - c_\infty t_\alpha^6\right] L_\alpha(z). \tag{XI.5.120}$$

The added interpolation term has degree at most three and hence does not change c_∞. Its evaluation corrects the leading term at every finite puncture. All polynomials with these same five values are $P_6^{(0)} + D(u + vz)$. The space of P_6 has dimension seven and the kernel has dimension two. Thus the pole data are five independent parameters and the two fixed-pole variations supply the Coulomb data. This checks the same $2 + 5 + 2$ accounting as Figure XI.5.3. It does not equate the squared pole masses to our signed linear coordinates or the puncture positions to our base exponentials. To compare the two constructions at a weak boundary, we can instead follow the matter left by turning off one gauge coupling.

XI.5.12 Turn a gauge node into a flavor background

What remains of the bridge when the second gauge field stops interacting? We can send Q_{B_2} to zero at fixed weak Q_{B_1}. The two base periods are independent, and the limit puts no condition on the fixed fiber splitting of node 2. Keep a_2 and all five masses finite.

An explicit scale trajectory shows how weak coupling can coexist with a small physical base. For example, let $M_s \to \infty$ at fixed weak g_s and take

$$\operatorname{Re} T_{B_2} = c \log(M_s/M_0), \qquad c > 0, \qquad |Q_{B_2}| = (M_0/M_s)^c. \tag{XI.5.121}$$

Here M_0 is a fixed reference mass. The leading action in (XI.5.49) gives

$$g_2^2(M_s) \simeq \frac{8\pi^2}{c\log(M_s/M_0)} \longrightarrow 0. \tag{XI.5.122}$$

The dimensionless action grows, but the physical area shrinks: the same trajectory gives

$$A_2 = \frac{2\pi c\log(M_s/M_0)}{M_s^2} \longrightarrow 0, \qquad M_{\mathrm{KK},2} \sim \frac{M_s}{\sqrt{\log(M_s/M_0)}} \longrightarrow \infty \tag{XI.5.123}$$

up to fixed shape factors. The KK estimate uses a controlled base shape with a single area length scale. It does not give the spectrum of the noncompact threefold. As in the local limit of Chapter 2, other unwanted excitations must become heavy or have vanishing couplings to the retained sector.

We next follow the charged matter through this limit. The four signed central periods were $m \pm a_1 \pm a_2$. Once the gauge coupling of node 2 vanishes, its two eigenvalues become fixed flavor data for node 1. If x denotes a node-1 electric eigenvalue, the two masses that enter its threshold factors are read from

$$(x+m+a_2)(x+m-a_2) = (x+m)^2 - a_2^2. \tag{XI.5.124}$$

For example, take $m = 13$ and $a_2 = 3$ in the real chamber used above. The two pairs of node-1 masses are then

$$(m_L + a_0, m_L - a_0) = (12, 10), \qquad (m+a_2, m-a_2) = (16, 10). \tag{XI.5.125}$$

At $a_2 = 0$ the two induced masses coincide and the former $SU(2)_2$ acts on their flavor indices. A generic nonzero a_2 leaves only its Cartan unbroken by the background. In either case the two induced hypers count as two fundamentals:

$$N_{f,1} = 2 + 2 = 4, \qquad b_1 = 4 - 4 = 0, \tag{XI.5.126}$$

where b_1 is evaluated above the four finite thresholds. Setting a coupling to zero did not erase the corresponding scalar background, nor did it remove the fields charged under the surviving gauge group.

For a different input, take $m = 9/2$ and $a_2 = 5/4$. The two new bare masses and their threshold polynomial are

$$(m+a_2, m-a_2) = \left(\frac{23}{4}, \frac{13}{4}\right), \qquad (x+m)^2 - a_2^2 = x^2 + 9x + \frac{299}{16}. \tag{XI.5.127}$$

This is a change of flavor data at the same zero-coupling cusp, not a change in the number of induced doublets. It also distinguishes their two screening thresholds. More generally let $M_- = |m - a_2| \ll M_+ = |m + a_2|$, and choose the original left threshold magnitudes and retained Coulomb splitting much smaller than M_-. In weak energy windows separated from these thresholds, the light fundamental counts give

window above the left thresholds	$N_{f,1}$	b_1
$\mu \ll M_-$	2	2
$M_- \ll \mu \ll M_+$	3	1
$M_+ \ll \mu$	4	0

(XI.5.128)

The numerical example above separates two thresholds but does not provide a long logarithmic interval between them. The hierarchy just stated supplies such an interval when needed. The zero-coupling operation retains both finite masses, while an observation at sufficiently low energy can exclude one or both from its effective flavor count.

The same linear formula separates freezing from increasing an eigenvalue without bound. At fixed finite m, sending $|a_2|$ to infinity sends both induced threshold magnitudes to infinity. If instead one correlates the mass with the splitting, the algebra changes:

$$m = a_2 + \mu_* \quad \Longrightarrow \quad m - a_2 = \mu_*, \qquad m + a_2 = 2a_2 + \mu_*. \tag{XI.5.129}$$

This would retain only one finite induced threshold. Neither mass trajectory is forced by $Q_{B_2} \to 0$. A weak gauge coupling and a large scalar background control different terms in the Lagrangian, just as the base action and the fiber periods are independent in the geometry.

Returning to the limit with all masses fixed and finite, the interacting sector is $SU(2)$ with four flavors. A strict zero-coupling description can also retain the free gauge fields of node 2 and its matter neutral under node 1. We omit those complementary fields when we fix the background and describe only the first interacting sector; they were not sent to infinite mass.

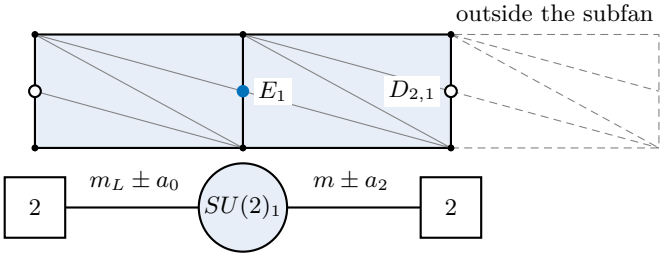


Figure XI.5.4: An open subfan for the retained gauge sector. The solid part keeps the first two strips, with E_1 still compact. The formerly interior point $D_{2,1}$ is now on the boundary, and its column supplies the right flavor background. The old bridge G_1 still lies in a retained strip and gives the two masses $m \pm a_2$. The dashed strip is excluded from this local comparison.

The retained gauge and flavor sectors can also be described by an open part of the original fan. Keep the first two strips of Figure XI.5.1 and omit the third. This is an open subfan, with heights $(2, 2, 2)$. The base curve C_2 has lost one of its two adjacent cones, so its retained part is noncompact. Likewise $D_{2,1}$ is now on the boundary of the rectangle and is noncompact; E_1 is the only compact gauge divisor. The intersection between C_1 and C_2 and its bridge curve are still present. Thus Figure XI.5.4 realizes the same right flavor data directly. The open fan is a local model for this sector. Its construction does not assert metric convergence of the original threefold along (XI.5.121).

In the two-node model, the two base actions control the bare interactions and the fiber periods control charged masses. At a weak cusp one can vary the former while

holding the latter fixed. The next chapter takes a different step: for a one-node model, it follows the periods that determine the *effective* coupling at a specified Coulomb vacuum.

Take-home message of this chapter

A split compact column supplies a gauge root and a base action. An adjacent bridge supplies matter charged under both columns. The signed midpoint of its periods is a bare mass. A column whose gauge dynamics is held fixed can still supply flavor weights to its neighbor. At each dynamical node the whole neighbor dimension contributes to the matter trace.

XI.5.13 Exercises

1. **Remove an end flavor.** One left end fundamental is heavy relative to the observation scale. The central bifundamental and the other end hypers are light at that scale. Compute the effective fundamental count and b at each node, in left-to-right order.

2. **Keep the scalar while switching off the coupling.** At the weak cusp of node 2 keep $a_2 = 3/2$ and the central bifundamental mass $m = 4$, in a common mass unit. Find the two induced masses at node 1 and its b above all four finite thresholds, including the two original left fundamentals.

3. **Recognize a pure Coulomb variation.** For this calculation measure all finite fiber and mass coordinates after multiplication by the same fixed ϵ. Thus every variation is dimensionless. Take the following coefficients of a common infinitesimal change:

$$\begin{aligned}(\delta T_{F_0}, \delta T_{F_1}, \delta T_{F_2}, \delta T_{F_3}) &= (0, 3, -2, 0),\\ (\delta T_{G_0}, \delta T_{G_1}, \delta T_{G_2}) &= (-3/2, -1/2, 1),\\ (\delta T_{B_1}, \delta T_{B_2}) &= (3, -2).\end{aligned}$$

   Find the two scaled Coulomb changes, the five scaled mass changes in the order (XI.5.35), and the two changes in T_K.

4. **Rebalance neighboring ranks.** Take $N_1 = 2, N_2 = 3$ with one bifundamental. Find the left and right fundamental multiplicities for zero running at both nodes. Give the Coulomb dimension and the total number of bare full-hyper masses, and explain how the heights $(1, 2, 3, 4)$ encode your counts.

5. **Separate the two area scales.** Explain how T_{B_2} can grow while the physical base area shrinks. Derive the base KK estimate for (XI.5.121), and state which additional assumptions are needed to isolate the four-dimensional theory.

Use `benchmark/tasks.json` to find the question IDs and `benchmark/PROTOCOL.md` for submission.

The last two exercises and the additional transfer exercises below are written work.

6. Starting with the characters S_i, T_i, derive both directions of (XI.5.14). Show which coordinate is invertible on the common-column chart, and verify that its transverse A_1 equation agrees when read from either adjoining strip.

7. Change only μ_{L-} by a small amount η, keeping all other masses, both Coulomb coordinates and both T_K fixed. Find the changes of $m_L, a_0, Z(F_0), Z(G_0)$. Explain why the bridge moves differently from the one-mass variation in the text.

8. For the heights $(1, 2, 3, 4)$, reproduce the six middle weights using the off-block roots of $\mathfrak{su}(5)$. Use those weights to compute both neighbor contributions to b, and recover the period midpoint from the six eigenvalue expressions.

9. For the punctures $(0, 1, 7/4, -2, \infty)$, choose finite double-pole coefficients $(1, 4, 9, 16)$ and infinity coefficient 25. Construct $P_6^{(0)}$ by interpolation. Explain why adding (XI.5.118) changes the differential without changing any of these coefficients.

10. Compare three trajectories at $Q_{B_2} \to 0$: fixed (m, a_2), fixed m with $a_2 \to \infty$, and $m - a_2 = \mu_*$ fixed with $a_2 \to \infty$. Identify which induced thresholds remain finite. State the energy window when assigning a light-flavor count.

11. In the $SU(2) \times SU(3)$ response, replace the third right eigenvalue b_2 temporarily by $2b_2$, leaving $(-b_1, b_1 - b_2)$ unchanged. Recompute the three right gradients. Show that the mixed common-scale logarithm still cancels, but that the coefficient of $1/m$ in the mixed response need not vanish. Explain where the $SU(3)$ trace constraint entered the unmodified calculation.

12. Freeze the right node at $c = 3, d = 6, m = 11$ and take $a = 1$. Find the three induced masses and their cubic $P(x)$. Use those finite masses in the retained a-Hessian and compare it with the result from replacing every induced mass by m. State separate conditions on a matching scale and on external photon momentum for interpreting these two expressions in the weak theory.

Status and sources

Geometry and charges. The fan and integral wall calculations (XI.5.1)–(XI.5.26) are [MATH]. The linear-column construction and product chart are adapted from Katz, Mayr, et al. (1997, §§2.1, 5.2, Fig. 7); the chosen phase has disjoint compact divisors. The ordinary transverse ALE dictionary uses ordinary unfrozen ALE enhancement [GEO-X]. The split genus-zero twist, fixed flavor ends and simple-collision full hyper use Katz, Mayr, et al. (1997, §§2.1, 6.1) and Katz and Vafa (1996, §4.1, Eq. (4.1)) [GEO-E].

Periods and couplings. The mass and boundary period combinations (XI.5.33)–(XI.5.40) are [MATH], as are the inverse map (XI.5.44) and simultaneous variation (XI.5.47). Their retained gauge-sector interpretation uses the protected D2 frame and local boundary choice [GEO-E]. The leading action (XI.5.49) uses Chapter 3 and Katz, Mayr, et al. (1997, Eq. (2.2)) [SUGRA]. The two weak bare coordinates use the same

source's §5.2, Eqs. (5.5)–(5.6) [GEO-E]. Sufficient isolation of the protected sector is [DEC].

Changed ranks. The finite height comparison $(1, 2, 3, 4)$ uses the same lower-hull and semigroup construction. Its charts (XI.5.64), weights (XI.5.66), centered periods and index arithmetic are [MATH]. The full-hyper and ordinary gauge-sector interpretations reuse the split-collision and genus-zero dictionaries above [GEO-E]. This comparison does not assert an arbitrary-rank classification.

The coupled Coulomb response. The weak one-loop charged determinant in (XI.5.73)–(XI.5.76) uses Ennes et al. (1999, Eq. (23), PDF pp. 6–7) for the product-group massless bridge and D'Hoker et al. (1997, Eq. (2.1), PDF pp. 4–5) for the massive full-hyper determinant and Wilson action. This is an imported perturbative protected prepotential in the stated electric patch [BPS:1/2|holo], with the finite quadratic scheme fixed in (XI.5.73). Its power here is the complete zero-instanton function of the three Coulomb coordinates and six bare masses; no instanton term is calculated. The nonzero bridge mass is inserted through the six displayed central charges. Neither source's asymptotically free spectral curve or instanton expansion is used for the balanced theory. The inverse-Cartan coordinate change, six response entries, complete second-moment cancellation, finite mixed example and isolated charge bilinear (XI.5.71)–(XI.5.89) are [MATH] conditional on that determinant.

Mass removal and a finite spectator background. The large-mass coefficient, screening change and integrated one-loop matching (XI.5.90)–(XI.5.97) are [MATH] under the stated weak matching definition and fixed-root hypotheses. They are not an exact geometric coupling-coordinate map. The controlled hierarchy and retention of the isolated four-dimensional sector remain [DEC]. The cubic, fixed-background Hessian, kinetic-form limit and retained divisor stars (XI.5.102)–(XI.5.111) are [MATH]. The interpretation as a flavor background reuses Katz, Mayr, et al. (1997, §§2.1, 6.1) [GEO-E]; complementary free fields are omitted by the stated sector choice. The calculation establishes no new exact spectral curve, global lattice or metric convergence.

Balance and the weak cusp. The index (XI.5.55), fixed-pole kernel (XI.5.114), and threshold product (XI.5.124) are [MATH] under their stated inputs. The changed-puncture interpolation (XI.5.118) and changed-mass product (XI.5.127) are algebraic consequences in those same frames [MATH]. The massless exact marginality, four-flavor weak cusp, and pole comparison are from Gaiotto (2009, §§2.1–2.2, Eqs. (2.13), (2.18)). Identification of the local IIA sector with the Lagrangian and its weak limit is [GEO-E]; the base scale trajectory is subject to [DEC]. Its Eq. (2.1) uses $\theta/\pi + 8\pi i/g^2$, twice our τ in (XI.5.50) for matched θ, g. No identification of the two exponents or of bare and effective couplings is made.

References

D'Hoker, E., I. M. Krichever, and D. H. Phong (1997). "The Effective Prepotential of N=2 Supersymmetric SU(Nc) Gauge Theories". In: *Nucl. Phys. B* 489, pp. 179–210. DOI: 10.1016/S0550-3213(97)00035-7. arXiv: hep-th/9609041.

Ennes, I. P. et al. (1999). "One-instanton predictions of Seiberg–Witten curves for product groups". In: *Phys. Lett. B* 452, pp. 260–264. DOI: 10.1016/S0370-2693(99)00301-9. arXiv: hep-th/9901124.

Gaiotto, D. (2009). "N=2 Dualities". In: arXiv: 0904.2715 [hep-th].

Katz, S., P. Mayr, and C. Vafa (1997). "Mirror Symmetry and Exact Solution of 4D N=2 Gauge Theories I". In: *Adv. Theor. Math. Phys.* 1, pp. 53–114. DOI: 10.4310/ATMP.1997.v1.n1.a2. arXiv: hep-th/9706110.

Katz, S. and C. Vafa (1996). "Matter from Geometry". In: arXiv: hep-th/9606086.

Chapter XI.6

Solving the engineered theory with its mirror

XI.6.1 A coupling that depends on the vacuum

A wrapped D2-brane on the fiber of local F_0 gives the W boson of a four-dimensional gauge theory. The local limit keeps its mass finite and sends the string scale to infinity. This establishes which electric degree of freedom the geometry is meant to retain. It leaves a different problem: how does the coupling of the remaining photon vary over the Coulomb branch? The photon feels the gauge instantons even after the base has become large in string units. The same limit that suppresses worldsheet wrapping of the base enhances the contributions of curves of large fiber degree.

We will compute the coupling on the mirror. The input is the local type IIA geometry $X = K_{F_0}$, with $F_0 = \mathbb{P}^1_b \times \mathbb{P}^1_f$. Its mirror $\widehat{X}$ contains a punctured curve. The three-form periods on $\widehat{X}$ reduce to integrals on that curve. Two combinations survive in field-theory units. Their electric and magnetic periods, a and a_D, determine the photon coupling through the derivative da_D/da. The finite singularities mark places where one combination of electric and magnetic charges can have zero central charge.

We use the base and fiber limit of Chapter 2, the mirror periods of Volume V, and the rank-one special geometry of Volume 0. Our main task is to identify the cycles before normalizing their integrals. In this example the compactified mirror curve in the limit and the original Seiberg–Witten cubic are related by a degree-two map. A loop around a cut of either curve need not represent a compact three-cycle of $\widehat{X}$. Keeping track of that difference will fix the relative normalization of the two gauge periods.

We then repeat the construction for an A_2 fibration. Its pure $SU(3)$ limit replaces the elliptic curve by a genus-two curve. We will compute all four local gauge periods, obtain the matrix of photon couplings, and follow a heavy-root limit back to the rank-one normalization just established.

XI.6.2 From the two rulings to the mirror

What information about the two rulings of F_0 enters the mirror equation? Label the five rays of X by their height-one projections. The central ray gives the compact divisor F_0. The other four rays come in two opposing pairs (Figure XI.6.1). In the order central, base pair, fiber pair the height and direction rows form the matrix

$$R = \begin{pmatrix} 1 & 1 & 1 & 1 & 1 \\ 0 & 1 & -1 & 0 & 0 \\ 0 & 0 & 0 & 1 & -1 \end{pmatrix}. \tag{XI.6.1}$$

The last two rows require equal entries within each pair of an integral relation. If those entries are m and n, the height row then requires the central entry to be $-2m-2n$. In particular the two primitive curve relations are

$$\ell_b = (-2,1,1,0,0), \qquad \ell_f = (-2,0,0,1,1). \tag{XI.6.2}$$

The same coefficient -2 can be read on F_0 itself. If b, f denote the base and fiber classes, $b^2 = f^2 = 0$ and $b \cdot f = 1$. The normal bundle of the zero section is K_{F_0}, so both intersections with the compact divisor have degree -2:

$$K_{F_0} = -2b - 2f, \qquad K_{F_0} \cdot b = K_{F_0} \cdot f = -2. \tag{XI.6.3}$$

We will return to the fiber intersection when we count the pairing of electric and magnetic cycles.

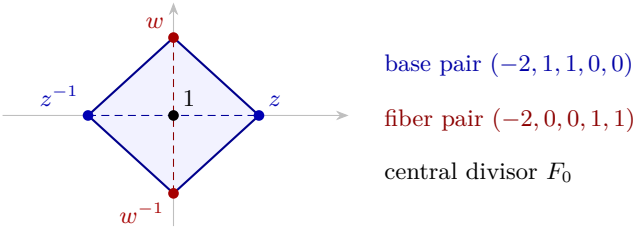


Figure XI.6.1: Height-one ray projections of local F_0 and the Laurent monomials at the corresponding points. In each pair, the sum of the two ray projections is twice the central projection. The height row in (XI.6.1) gives the central coefficient in each relation.

The local toric mirror rule assigns a multiplicative relation to each row of (XI.6.2). For monomials Y_i with their coefficients kept separate, these relations become

$$Y_{b,+}Y_{b,-} = Y_0^2, \qquad Y_{f,+}Y_{f,-} = Y_0^2. \tag{XI.6.4}$$

Divide out the common monomial Y_0. With $z = Y_{b,+}/Y_0$ and $w = Y_{f,+}/Y_0$, the other two ratios are z^{-1} and w^{-1}. Thus the mirror on the torus $T = (\mathbb{C}^*)^2$ is described by a Laurent polynomial with five coefficients. Its conic presentation and its degeneration locus are

$$\widehat{X} = \{UV = H(z,w)\}, \qquad \Sigma = \{H(z,w) = 0\} \subset T. \tag{XI.6.5}$$

Here $U, V \in \mathbb{C}$. Over $H \neq 0$ the conic is $\mathbb{C}^*$, parametrized by U. Over Σ it is the union of two axes. The phase circle in the generic fiber can shrink at their intersection. That circle will turn a surface bounded by a curve on Σ into a closed three-cycle.

The polynomial may be multiplied by a constant, and a constant rescaling of z or w changes the coefficients within its respective pair. The ratios invariant under these operations are

$$z_b = \frac{a_{b,+}a_{b,-}}{a_0^2}, \qquad z_f = \frac{a_{f,+}a_{f,-}}{a_0^2}. \tag{XI.6.6}$$

For example, the coefficient pair $(2, 8)$ can be made into $(4, 4)$ by setting $z = 2\widetilde{z}$. Neither the resulting product 16 nor the corresponding ratio in (XI.6.6) changes. Choose reciprocal pairs with equal coefficients and set the common magnitude in the fiber pair to one. In the real chart used below we write

$$H = K - w - w^{-1} - c(z + z^{-1}), \qquad z_f = \frac{1}{K^2}, \qquad z_b = \frac{c^2}{K^2}. \tag{XI.6.7}$$

The signs select the fiber degeneration near $w = +1$. They do not change the two products defining the algebraic coordinates.

This quotient of coefficients gives a useful way to compare mirror equations written in different charts. For positive coefficients A, B in a pair $Az + Bz^{-1}$, set

$$z = \sqrt{B/A}\,\widetilde{z}, \qquad Az + Bz^{-1} = \sqrt{AB}\,(\widetilde{z} + \widetilde{z}^{-1}). \tag{XI.6.8}$$

The ratio B/A selects a coordinate on the torus; the product AB survives as a complex structure parameter. For example, the two polynomials with base coefficients $(2, 8)$ and $(1, 16)$ give the same z_b at the same constant coefficient. Their critical equations look different before rescaling, but their critical values agree. With equal fiber coefficients of magnitude F, division of the whole polynomial by F gives

$$K = \frac{a_0}{F}, \qquad c = \frac{\sqrt{AB}}{F}, \qquad z_f = \frac{F^2}{a_0^2}, \qquad z_b = \frac{AB}{a_0^2}. \tag{XI.6.9}$$

Thus the curve calculation can be translated without guessing which individual coefficient is the base parameter. The remaining step is more than a coefficient rescaling: the physical mass is a flat period, whose relation to z_b, z_f contains the analytic correction computed below.

The protected mirror identification is the physical input at this step. In type IIA, the complexified Kähler parameters of X are vector multiplet parameters. On the type IIB mirror, their counterparts are complex structure parameters of $\widehat{X}$; the relevant integrals are periods of its holomorphic three-form. Changing the type while keeping the original X does not exchange these moduli. In particular, type IIB on X does not turn the original fiber Kähler period into a vector multiplet complex structure period. The calculation below uses both the change of type and the mirror map.

XI.6.3 Keep the two singularities at finite distance

Why does the base exponential have to vanish along with a particular displacement of the fiber coordinate? At a singular point of (XI.6.5), $U = V = 0$, $H = 0$, and the two

logarithmic derivatives of H vanish. In the chart with $c \neq 0$ these derivatives require

$$z - z^{-1} = 0, \qquad w - w^{-1} = 0. \tag{XI.6.10}$$

For $z = \sigma_b$ and $w = \sigma_f$, with $\sigma_b, \sigma_f = \pm 1$, the critical value is $K - 2\sigma_f - 2c\sigma_b$. Multiplying these four values gives the principal discriminant in the torus:

$$\frac{\prod_{\sigma_b,\sigma_f}(K - 2\sigma_f - 2c\sigma_b)}{K^4} = (1 - 4z_f - 4z_b)^2 - 64 z_f z_b. \tag{XI.6.11}$$

At $z_b = 0$ the expression on the right has a double zero at $z_f = 1/4$. A small nonzero z_b splits that zero. If z_b is of order ϵ^4, resolving the two nearby zeros requires probing the fiber coordinate on the scale ϵ^2.

Let $L = \Lambda_{\mathrm{SW}}^2$ and let u be the scaled displacement, both with dimensions of mass squared. Initially take $u > L > 0$ and $\epsilon > 0$. Choose

$$K = 2 + \epsilon^2 u, \qquad c = \frac{\epsilon^2 L}{2}, \qquad w = e^{\epsilon p}. \tag{XI.6.12}$$

The dimensionless logarithm of w becomes a variable p of mass dimension one. With this choice the critical product factors as

$$K^4 D_{\mathrm{tor}} = \epsilon^4 (u^2 - L^2)\big[(4 + \epsilon^2 u)^2 - \epsilon^4 L^2\big], \qquad D_{\mathrm{tor}} = (1 - 4z_f - 4z_b)^2 - 64 z_f z_b. \tag{XI.6.13}$$

The $w = +1$ critical values stay at $u = \pm L$; the $w = -1$ critical values move to $u = -4/\epsilon^2 \pm L$. Meanwhile $w + w^{-1} = 2 + \epsilon^2 p^2 + O(\epsilon^4 p^4)$. Consequently the limiting curve at finite p and fixed $z \neq 0$ is

$$p^2 = u - \frac{L}{2}(z + z^{-1}). \tag{XI.6.14}$$

This expansion is local to the scaling region. It does not approximate the curve uniformly at the punctures. Figure XI.6.2 shows why setting $z_b = 0$ before scaling would miss the two finite singularities.

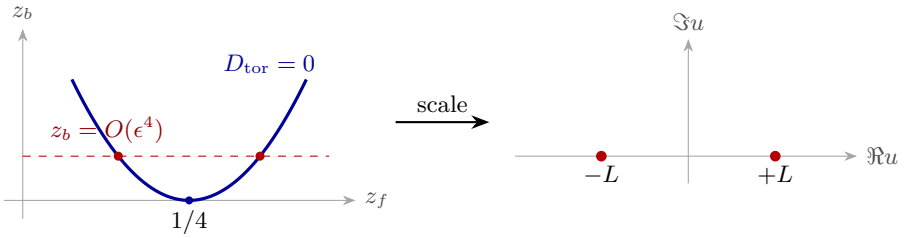
To connect (XI.6.12) to the IIA limit, we need the flat coordinates, rather than just the algebraic z_b, z_f. Recall $T_i = -2\pi i t_i$ and $Q_i = e^{-T_i}$. The protected wrapped-brane dictionary in the real fiber frame of Chapter 2 uses

$$\epsilon = \frac{2\pi g_s}{M_s}, \qquad T_f = \epsilon a_W, \qquad Q_b \sim C_{\mathrm{IIA}} e^{i\theta_b} (\epsilon \Lambda_{\mathrm{IIA}})^4. \tag{XI.6.15}$$

Here $a_W = M_W$ is a mass; no normalization of a has been used. The scale relation for Q_b includes the inherited matching across the base Kaluza–Klein threshold. It does not follow by extrapolating the pure gauge beta function above that threshold.

The local Picard–Fuchs system gives the correction from z_i to Q_i. With $\theta_i = z_i \partial_{z_i}$ and $\theta = \theta_b + \theta_f$, its two operators are

$$\mathcal{L}_i = \theta_i^2 - z_i (2\theta)(2\theta + 1), \qquad i = b, f. \tag{XI.6.16}$$



Algebraic coordinates Scaled Coulomb plane

Figure XI.6.2: The degenerations seen at two resolutions. At left the principal discriminant is tangent to the large-base boundary $z_b = 0$ at $z_f = 1/4$. At right the scaled u plane retains the two critical points of the limiting curve. The other pair, at $-4/\epsilon^2 \pm L$, leaves every fixed finite region. Axes and separations are schematic.

Both operators annihilate the constant solution. Applying $\mathcal{L}_i$ to either bare logarithm $\log z_j$ gives $-2z_i$. Thus the two single logarithmic solutions with the usual large-radius asymptotics have the same analytic correction g. Its first coefficients satisfy $g_{10} = g_{01} = 2$. At total degree $N = m + n > 1$, the equations read

$$m^2 g_{mn} = (2N-2)(2N-1) g_{m-1,n}, \qquad n^2 g_{mn} = (2N-2)(2N-1) g_{m,n-1} \quad \text{(XI.6.17)}$$

when the corresponding index is positive. For instance both equations give $g_{11} = 12$. Iterating from the first coefficients gives

$$g = 2 \sum_{m+n>0} \frac{(2m+2n-1)!}{(m!)^2 (n!)^2} z_b^m z_f^n, \qquad -T_i = \log z_i + g, \qquad Q_i = z_i e^g. \quad \text{(XI.6.18)}$$

The identification of these large-radius normalized periods with the closed flat Kähler coordinates is part of the mirror dictionary. Their analytic term is essential: as z_f tends to $1/4$, it is not small.

The sum can be evaluated on the chosen real ray. Let $\langle \cdot \rangle$ denote averaging on a unit circle, and write $z = e^{i\vartheta}$. On the two unit circles $K > 2 + 2c$, so the logarithm series is uniformly convergent. Its constant Laurent term gives

$$g = -2 \left\langle \left\langle \log \left(1 - \frac{w + w^{-1} + c(z + z^{-1})}{K} \right) \right\rangle_w \right\rangle_z . \quad \text{(XI.6.19)}$$

Only even powers within each reciprocal pair contribute to the constant term. At orders $2m$ and $2n$ the binomial factors cancel the pair factorials in the expansion, leaving the coefficients of (XI.6.18).

For each z on its unit circle let $r > 1$ solve $r + r^{-1} = K - c(z + z^{-1})$. The argument of the logarithm factors as

$$\frac{r}{K}(1 - w/r)(1 - w^{-1}/r). \quad \text{(XI.6.20)}$$

The two logarithms of the last factors average to zero. The logarithm of r/K therefore gives the full w average. Combining this with (XI.6.18) gives

$$T_f = 2\langle \log r \rangle_z, \qquad \frac{Q_b}{Q_f} = \frac{z_b}{z_f} = c^2, \qquad \log r = 2\,\operatorname{arsinh}\left(\frac{\epsilon\sqrt{u - L\cos\vartheta}}{2}\right). \tag{XI.6.21}$$

For example, at $c = 0$ the root is constant on the circle. The result reduces to $Q_f = r^{-2}$ and $z_f = Q_f/(1+Q_f)^2$. In the correlated limit the root varies around the circle. Its average gives a nontrivial function of the finite Coulomb parameter:

$$\lim_{\epsilon\to 0}\frac{T_f}{\epsilon} = 2\left\langle \sqrt{u - L\cos\vartheta}\right\rangle_z, \qquad \lim_{\epsilon\to 0}\frac{Q_b}{\epsilon^4} = \frac{L^2}{4}. \tag{XI.6.22}$$

The first limit behaves as $2\sqrt{u}$ for u/L large. At finite u/L the average is the mass coordinate, so u is not simply $a_W^2/4$. The second limit matches (XI.6.15) if

$$L^2 = 4C_{\mathrm{IIA}}e^{i\theta_b}\Lambda_{\mathrm{IIA}}^4. \tag{XI.6.23}$$

This relation uses the specified Laurent chart and includes one theta phase. The contour calculation begins on the positive real scale ray; a complex scale can be reached by analytic continuation with a chosen branch of L. The sign of that branch interchanges the two finite singularities. We next identify the cycle whose integral produces the first limit in (XI.6.22).

XI.6.4 How fast does the flat period converge?

Before identifying that cycle, we can ask how the exact flat coordinate approaches its limiting value. This tests the scaling using a quantity that will become the electric mass, rather than just the zeros of the discriminant. Keep $u > L > 0$ fixed and define the angular moments

$$A_j(u,L) = \frac{1}{\pi}\int_0^\pi (u - L\cos\vartheta)^{j/2}\,d\vartheta. \tag{XI.6.24}$$

Reflection about π makes this the same average as on the full unit circle. Each A_j has mass dimension j and is finite on this ray. The exact equation (XI.6.21) reads

$$\frac{T_f}{\epsilon} = \frac{4}{\pi\epsilon}\int_0^\pi \operatorname{arsinh}\left(\frac{\epsilon\sqrt{u - L\cos\vartheta}}{2}\right)d\vartheta. \tag{XI.6.25}$$

The small parameter for this integral is controlled by its largest argument, $\epsilon\sqrt{u+L}/2$. Expanding the inverse hyperbolic sine gives

$$\operatorname{arsinh} v = v - \frac{v^3}{6} + \frac{3v^5}{40} + O(v^7). \tag{XI.6.26}$$

For fixed u, L the argument is bounded uniformly in ϑ, so termwise averaging is justified for sufficiently small ϵ. The first correction to the limiting period is

$$\frac{T_f}{\epsilon} = 2A_1 - \frac{\epsilon^2}{12}A_3 + \frac{3\epsilon^4}{320}A_5 + O(\epsilon^6). \tag{XI.6.27}$$

All terms have mass dimension one. Since $A_3 > 0$, a small positive finite ϵ lowers this period relative to $2A_1$. The sign also follows without a series: for $v > 0$, $\operatorname{arsinh} v < v$.

There is a quantitative error estimate on the same ray. For $0 \le v \le 1$ the alternating series has decreasing terms. If $\epsilon\sqrt{u+L}/2 \le 1$, retaining through the cubic term therefore gives

$$0 \le \frac{T_f}{\epsilon} - \left(2A_1 - \frac{\epsilon^2}{12}A_3\right) \le \frac{3\epsilon^4}{320}A_5 \le \frac{3\epsilon^4}{320}(u+L)^{5/2}. \tag{XI.6.28}$$

This bound concerns the specified finite-ϵ mirror period. Interpreting it as a correction to a particular four-dimensional action at finite string scale would require the other sectors of that finite-scale compactification.

As a numerical example take $u = 3L$ and write $\eta = \epsilon\sqrt{L}$. The dimensionless moments are

$$\frac{A_1}{\sqrt{L}} = 1.7196932002\ldots, \qquad \frac{A_3}{L^{3/2}} = 5.3049853355\ldots. \tag{XI.6.29}$$

The limiting value of $T_f/(\epsilon\sqrt{L})$ is therefore $3.4393864004\ldots$. Direct integration of the inverse hyperbolic sine and the two-term expression give

η	$T_f/(\epsilon\sqrt{L})$	$2A_1/\sqrt{L} - \eta^2 A_3/(12L^{3/2})$
0.2	3.42195618	3.42170312
0.1	3.43498163	3.43496558

(XI.6.30)

Halving η reduces the difference between these columns from 2.53066×10^{-4} to 1.60531×10^{-5}, close to the factor of sixteen predicted for an order-η^4 remainder. The leading difference from the limiting period itself is instead of order η^2.

The condition on the largest argument also clarifies the order of limits. At finite ϵ, the weak-coupling region must still satisfy $\epsilon^2 u \ll 1$ for this expansion. In contrast, after taking $\epsilon \to 0$ at fixed u, L, the limiting periods can be continued to arbitrarily large finite u/L. This is why the large loop used later belongs to the scaled curve, with the other two critical values already removed to infinity.

XI.6.5 Which curve contours lift to compact three-cycles?

A one-cycle on Σ can carry a three-form period only if we can close the three-cycle above it. What does closure require? At a point of T write $d = |U|^2 - |V|^2$. Shrink d at fixed H and at fixed phases where they are defined. The squared radii along the deformation, with parameter $0 \le t \le 1$, are

$$|U_t|^2,\ |V_t|^2 = \frac{\sqrt{(1-t)^2 d^2 + 4|H|^2}\ \pm (1-t)d}{2}. \tag{XI.6.31}$$

This fixes the product. At $H = 0$ the nonzero coordinate on either axis shrinks to zero. The resulting space over T is $T \times S^1$ with the circle collapsed over each point of Σ. In

particular a two-chain D in T whose boundary lies on Σ carries a phase circle over its interior, and that circle closes at the boundary.

This construction captures the compact three-cycle homology of the affine mirror. To see the count, the circle of phase $\arg U$ has a continuous phase-zero section, including at the collapse. Projection to T splits off this section. After taking the quotient by the section, the collapsed-circle space becomes the reduced suspension of T/Σ. Since $H_3(T) = 0$, the ordinary integral homology is

$$H_3(\widehat{X};\mathbb{Z}) \simeq H_2(T,\Sigma;\mathbb{Z}). \tag{XI.6.32}$$

The punctured curve has $H_2(\Sigma) = 0$, so the exact sequence of the pair gives

$$0 \longrightarrow H_2(T) \longrightarrow H_2(T,\Sigma) \xrightarrow{\partial} \ker\big[H_1(\Sigma) \longrightarrow H_1(T)\big] \longrightarrow 0. \tag{XI.6.33}$$

We omit $\mathbb{Z}$ from the remaining homology notation. The map on the right records the two windings of a curve contour in the ambient torus. A contour whose windings do not both vanish cannot be the boundary of a two-chain in T.

We can find the windings at finite ϵ. Project Σ onto the z plane. The two reciprocal roots $w_\pm$ satisfy

$$w_+ + w_- = K - c(z + z^{-1}), \qquad w_+ w_- = 1. \tag{XI.6.34}$$

Set $x(z) = L(z + z^{-1})/2$. The sheets meet when $w_+ + w_- = \pm 2$, at the two reciprocal pairs determined by $x(z) = u$ and $x(z) = u + 4/\epsilon^2$. The compactified cover has four simple branch points, hence genus one. At each of $z = 0, \infty$ there are two punctures. The leading roots are

	small root	large root
$z \longrightarrow 0$	$-z/c$	$-c/z$
$z \longrightarrow \infty$	$-1/(cz)$	$-cz$

(XI.6.35)

where small and large refer to the magnitude of w. Let $\ell_{0,\pm}$ and $\ell_{\infty,\pm}$ be positively oriented loops about the ends where w has local winding ± 1. The local coordinate at infinity is $1/z$. Therefore

$$W(\ell_{0,\pm}) = (1, \pm 1), \qquad W(\ell_{\infty,\pm}) = (-1, \pm 1). \tag{XI.6.36}$$

Both components of every puncture winding have the same parity. This property will restrict the electric cycle.

For $u > L$ define $t_* = \operatorname{arcosh}(u/L)$. The first pair of branch points is $z_{\text{in}} = e^{-t_*}$, $z_{\text{out}} = e^{t_*}$. On the unit circle and between those two points along the positive real axis, w_+ is the larger real root. The following two cycles use these paths:

$$\begin{aligned} &A' : |z| = 1 \text{ counterclockwise on } w_+, \\ &B' : z_{\text{out}} \to z_{\text{in}} \text{ on } w_+, \quad z_{\text{in}} \to z_{\text{out}} \text{ on } w_-. \end{aligned} \tag{XI.6.37}$$

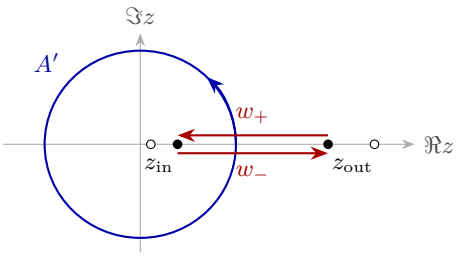
The two arcs of B' join at $w = 1$. In the complex z plane the tangent to A' at $z = 1$ points up, and the w_+ tangent to B' points left. They intersect once, positively. This gives a primitive basis A', B' on the compactified curve. Their ambient windings are

$$W(A') = (1, 0), \qquad W(B') = (0, 0), \qquad A' \cdot B' = 1. \tag{XI.6.38}$$

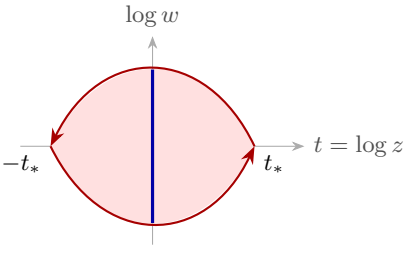
In particular A' winds once in z, even though w_+ is positive along the whole contour. The lower unit-circle lift A_- also has winding $(1, 0)$. Taking both lifts of the disk inside the unit circle, with small holes at $z = 0$, gives

$$A' + A_- = \ell_{0,+} + \ell_{0,-}. \tag{XI.6.39}$$

The compact electric boundary uses the two lifts with opposite signs; the magnetic contour already has zero winding.



Projections of A' and B'



Magnetic filling disk

Figure XI.6.3: Relative boundaries of the electric cylinder and the magnetic disk, drawn over the z plane. At left, the electric boundary takes the difference of the two unit-circle lifts, while the magnetic contour runs between the two positive turning points and changes sheets. The other pair of branch points is farther inside and outside. At right, the fiber coordinate $\log w$ between its two root values fills the magnetic disk. The blue segment is the slice of the electric cylinder at $z = 1$.

We can solve the integer closure condition explicitly. Use A', B' and three of the puncture loops $\ell_{0,+}, \ell_{0,-}, \ell_{\infty,+}$. The omitted loop is minus the sum of the other three. A contour with coefficients $(a_1, b_1, r_1, s_1, t_1)$ has zero winding exactly when

$$\begin{pmatrix} 1 & 0 & 1 & 1 & -1 \\ 0 & 0 & 1 & -1 & 1 \end{pmatrix} \begin{pmatrix} a_1 \\ b_1 \\ r_1 \\ s_1 \\ t_1 \end{pmatrix} = 0, \qquad a_1 = -2r_1, \quad t_1 = s_1 - r_1. \tag{XI.6.40}$$

For example, a single A' cannot be corrected with any integer combination of puncture loops. Two copies can be corrected by subtracting $\ell_{0,+} + \ell_{0,-}$. An integral basis of the kernel is

$$\begin{aligned} \gamma_e &= 2A' - \ell_{0,+} - \ell_{0,-} = A' - A_-, \\ \gamma_m &= B', \\ \gamma_{\text{bg}} &= \ell_{0,+} + \ell_{\infty,-}. \end{aligned} \tag{XI.6.41}$$

Filling the punctures removes only the last direction and the explicit puncture terms. The two gauge boundaries thus project onto $2\mathbb{Z}A' \oplus \mathbb{Z}B'$, an index-two sublattice of the compact curve homology.

The kernel calculation also tells us how to reduce a new contour to these three directions. For a zero-winding contour with coefficients $(a_1, b_1, r_1, s_1, t_1)$, the two equations above imply the integral decomposition

$$\gamma = -r_1\gamma_e + b_1\gamma_m + (r_1 - s_1)\gamma_{\mathrm{bg}}, \qquad a_1 = -2r_1, \quad t_1 = s_1 - r_1. \tag{XI.6.42}$$

For example, consider a contour whose windings cancel only after several puncture contributions are included:

$$\gamma = 6A' - B' - 3\ell_{0,+} + 2\ell_{0,-} + 5\ell_{\infty,+}, \tag{XI.6.43}$$

$$W(\gamma) = (6 - 3 + 2 - 5,\ -3 - 2 + 5) = (0, 0), \tag{XI.6.44}$$

$$\gamma = 3\gamma_e - \gamma_m - 5\gamma_{\mathrm{bg}}. \tag{XI.6.45}$$

Its compact projection is $6A' - B'$. Its relative period also contains a background component, which the compact projection forgets. Choosing a lift to $H_2(T, \Sigma)$ can in addition add the ambient torus class in (XI.6.33). Thus zero winding determines which contour can bound, while the chosen relative lift determines its full period. The projection alone cannot decide whether a class has a finite period in field-theory units.

For these boundaries, Figure XI.6.3 also gives the actual filling chains. The electric chain runs along the unit circle in z, with $\log w$ ranging from $-\log r$ to $+\log r$ over each z. The magnetic chain uses the positive real interval from z_{in} to z_{out}, again filling between the two logarithms; the interval in $\log w$ shrinks to a point at each end. A phase circle in the conic fiber then gives the compact electric and magnetic three-cycles. We orient their boundaries as in (XI.6.41).

There are two crossings on the punctured curve, one for each sheet at $z = 1$. On the lower sheet the orientations of both crossing arcs reverse, so the signs agree. To see how this count lifts, separate the interiors of the three-cycles at opposite values of $|U|^2 - |V|^2$, proportional to $|H|$ and vanishing at the boundary. Near a boundary crossing the two chain interiors can approach along distinct rays $H \in e^{i\alpha_j}\mathbb{R}_{\geq 0}$. In the normal coordinates (U, V) the real two-planes of the lifts then have the form

$$V = \rho_j e^{i\alpha_j}\overline{U}, \qquad \rho_j > 0. \tag{XI.6.46}$$

The difference of the two maps is anti-linear on $\mathbb{C}$. Its real determinant is $-|\rho_2 e^{i\alpha_2} - \rho_1 e^{i\alpha_1}|^2$. Each crossing contributes one transverse intersection with the same normal orientation factor. Hence the magnitude of the three-cycle pairing is two, in agreement with $|K_{F_0} \cdot f|$ in (XI.6.3). Below we use the signed particle pairing $+2$ in electric-then-magnetic order. The pairing gives charge information without presuming that a stable particle occupies every homology class.

To compute the periods, use $\Omega = dU/U \wedge d\log w \wedge d\log z$ and orient the phase circle first. Normalize the dimensionless three-period of the lift of D as

$$\Pi_D = \frac{1}{(2\pi i)^2}\int_{\Gamma_D}\Omega = \frac{1}{2\pi i}\int_D d\log w \wedge d\log z = \frac{1}{2\pi i}\int_{\partial D}\log w\,\frac{dz}{z}. \tag{XI.6.47}$$

The last equality holds on the explicit gauge chains, where $\log w$ is single valued. A common branch shift adds a multiple of the total z winding of the boundary, which is

zero. The two integrals give

$$\Pi_e = 2\langle \log r \rangle_z = T_f, \qquad \Pi_m = \frac{2i}{\pi} \int_0^{t_*} \log w_+(e^t)\, dt. \tag{XI.6.48}$$

In the second integral, the upper root is followed in the decreasing z direction. Both legs have the same contribution, and the integrand in $t = \log z$ is even. This gives the positive imaginary sign. As $\epsilon \to 0$ the integration paths stay at finite nonzero z. On the magnetic segment $\log w_+(e^t) = 2\,\mathrm{arsinh}(\epsilon\sqrt{u - L\cosh t}/2)$, so both periods in (XI.6.48) are of order ϵ. This time the first equality with T_f comes from a compact three-cycle, rather than only a flat-coordinate solution.

There are two further affine period directions. The winding map is onto, by (XI.6.36) and (XI.6.38). The punctured genus-one curve has first homology of rank five, and the kernel in (XI.6.33) has rank three. The remaining rank-one term $H_2(T)$ lifts the ambient torus. In the normalization of (XI.6.47), its period is $2\pi i$ for the torus ordered w, z.

For the third kernel direction in (XI.6.41), write $\zeta = w/z$. At the small-z, small-w puncture, $\zeta \to -1/c$; at the large-z, large-w puncture, $\zeta \to -c$. The two positive puncture loops have opposite z windings. Fill them with an annulus in the z plane, interpolating between their periodic logarithms of ζ. Since $d\log\zeta \wedge d\log z = d\log w \wedge d\log z$, the integral is the difference of the two log averages. Each average equals the logarithm of the corresponding asymptotic constant, by Taylor expansion in its local puncture coordinate. Consequently

$$\Pi_{\mathrm{bg}} = \log(-1/c) - \log(-c) = -2\log c = T_b - T_f \pmod{2\pi i}. \tag{XI.6.49}$$

The ambient torus accounts for the constant-period change between relative lifts. This is distinct from a common logarithm branch shift on one fixed gauge chain.

At fixed L the background logarithm is independent of u, and it grows as $\epsilon \to 0$. Dividing by ϵ makes it and the nonzero ambient constant divergent, while (XI.6.48) gives the two finite directions. No fixed integral combination with a nonzero background coefficient can cancel a logarithm against the constant or the order-ϵ periods. This accounts for all four directions of the affine model. Modes belonging to a compact completion or a different noncompact boundary condition are not counted by (XI.6.32). Their decoupling remains the separate condition of the local field-theory limit.

XI.6.6 The cubic and its normalized differential

How does the limiting curve (XI.6.14) give the original Seiberg–Witten periods? It is useful to keep the two curves distinct while comparing their cycles. On the compactification E' of the limiting curve, define

$$x = \frac{L}{2}(z + z^{-1}), \qquad s = \frac{L}{2}(z - z^{-1}), \qquad s^2 = x^2 - L^2, \qquad p^2 = u - x. \tag{XI.6.50}$$

Eliminating x and then solving for z gives

$$s^2 = (p^2 - u)^2 - L^2, \qquad z = \frac{x + s}{L}. \tag{XI.6.51}$$

This is a birational presentation of E' as the Toda quartic. To obtain the cubic, use instead $y = -ips$. Then

$$y^2 = (x^2 - L^2)(x - u). \tag{XI.6.52}$$

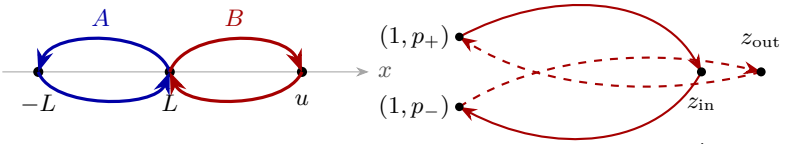
Let E be its smooth compactification. At a generic (x, y) the two preimages are (z, p) and $(z^{-1}, -p)$. They cannot coincide on a smooth fiber. A finite fixed point would require $z = \pm 1$ and $p = 0$, which gives $u = \pm L$. The points over $z = 0, \infty$ are exchanged. Thus on smooth fibers the map $\varphi : E' \to E$ is an unramified cover of degree two. With origins chosen compatibly it is an isogeny, rather than a change of birational coordinates.

We can detect the difference directly from the roots. The polynomial discriminants of the quartic and the monic cubic are

$$\operatorname{disc}_p\big[(p^2 - u)^2 - L^2\big] = 256L^4(u^2 - L^2), \qquad \operatorname{disc}_x\big[(x^2 - L^2)(x - u)\big] = 4L^2(u^2 - L^2)^2. \tag{XI.6.53}$$

For the cubic, the three root differences are $2L, u - L, u + L$. For the quartic, put $r_1^2 = u + L$ and $r_2^2 = u - L$. The pairs of opposite roots give squared differences $4r_1^2$ and $4r_2^2$, and the cross differences give $(r_1^2 - r_2^2)^4$. In the Weierstrass convention for y^2 equal to a monic cubic, the elliptic discriminant is 16 times the polynomial discriminant. The two finite zeros on the two presentations agree, but their orders differ. The j invariant distinguishes the smooth curves as well. Using $(pz)^2 = -(L/2)z(z^2 - 2uz/L + 1)$ to compute the invariant of E' gives, for instance,

$$j(E')\big|_{u=2L} = \frac{140608}{3}, \qquad j(E)\big|_{u=2L} = \frac{21952}{9}. \tag{XI.6.54}$$



Two-sheet cuts of the cubic E Two lifts of B on E'

Figure XI.6.4: Cycle transport under the degree-two map. The primitive A' on the cover runs once around the electric cut of the cubic. One cubic B traversal runs from $z = 1$ to an inner turning point and back to the other sheet over $z = 1$. A second traversal uses the outer turning point and closes the lifted contour. The compact electric boundary is a difference of lifts and projects to $2A$, even though A' itself maps to A.

Orient the electric cycle A of E along the two sheets over $[-L, L]$, and orient B out from $x = L$ to u on $y = +i\sqrt{u - x}\sqrt{x^2 - L^2}$ and back on the other sheet. On the A' unit circle we have

$$z = e^{i\vartheta}, \qquad x = L\cos\vartheta, \qquad y = Lp\sin\vartheta. \tag{XI.6.55}$$

For the first half of the circle x decreases from L to $-L$ with $y > 0$. In the second half x increases with $y < 0$. These two arcs trace A once. At $x = L$, y is a local coordinate:

A points along its positive real direction and B along its positive imaginary direction. Thus $A \cdot B = +1$.

Follow B from the preimage $z = 1, p > 0$. Since $y = -ips$, the outgoing arc has $z < 1$. At $x = u$ the square root p changes sign. The return arc reaches $z = 1, p < 0$, a different point over the initial endpoint. Another traversal of B passes through z_{out} and returns to $z = 1, p > 0$. Together these arcs trace the B' of (XI.6.37). Thus

$$\varphi_* A' = A, \qquad \varphi_* B' = 2B, \qquad \varphi_*(\gamma_e, \gamma_m) = (2A, 2B) \quad \text{after compact projection.} \tag{XI.6.56}$$

The last equality uses the relative winding constraint, not just the isogeny. The image of the gauge boundaries has intersection four on E, twice their intersection on E' as required by the degree of the map. Neither the curve alone nor the particle lattice selected here specifies a maximal Wilson–'t Hooft line lattice.

The three-form integrals in (XI.6.48) have a differential limit. In the scaling region $\epsilon^{-1} \log w \to p$. To match the orientation on E, use the Seiberg–Witten form

$$\lambda_{\text{SW}} = \frac{\sqrt{2}}{2\pi} \frac{(x-u)\,dx}{y}, \qquad \varphi^* \lambda_{\text{SW}} = \frac{\sqrt{2}}{2\pi i} p\, \frac{dz}{z}. \tag{XI.6.57}$$

The second equality follows from $dx = s\,dz/z$ and $(x-u)/y = p/(is)$. It fixes the relative sign of the forms, not just their absolute values. Put

$$a = \oint_A \lambda_{\text{SW}}, \qquad a_D = \oint_B \lambda_{\text{SW}}. \tag{XI.6.58}$$

On the two gauge contours, (XI.6.56) and (XI.6.57) now give

$$\lim_{\epsilon \to 0} \frac{(\Pi_e, \Pi_m)}{\epsilon} = \sqrt{2}\,(a, a_D). \tag{XI.6.59}$$

For the electric integral, one can also verify this directly: $\oint_{A'} p\,dz/(2\pi i z)$ is the average in (XI.6.22) before the factor of two. The magnetic cycle B' has no puncture term and gives two B integrals. The two factors of two have different geometric origins, but give the same conversion in (XI.6.59).

For the physical interpretation, choose the particle central-charge convention

$$Z = n_m a_D + n_e a, \qquad M_{\text{BPS}} = \sqrt{2}\,|Z|, \qquad (n_m, n_e)_W = (0, \pm 1). \tag{XI.6.60}$$

The protected mirror charge dictionary assigns a common conversion from three-periods to central charges. In the real weakly coupled chamber the electric period is T_f, and Chapter 2 gives $T_f/\epsilon = a_W = M_W$. Equations (XI.6.59) and (XI.6.60) therefore fix the common conversion to $\Pi/(\sqrt{2}\,\epsilon)$ in the limit, with

$$a_W = \sqrt{2}\,a \quad (u > L), \qquad M_W = \sqrt{2}\,|a| \tag{XI.6.61}$$

in the transported electric frame wherever the protected W state is present. This comparison fixes the units of the light vector sector. It does not set a graviphoton normalization in an unspecified compact model. Using A' alone would halve the electric period while leaving the magnetic one unchanged, and would give $da_D/d(a/2) = 2\,da_D/da$. That is the derivative ratio in the primitive cover coordinates, not the coupling for the fixed particle charges. We use the common pair (XI.6.59) to compute the coupling.

XI.6.7 Electric and magnetic periods at weak coupling

The point of the period calculation is to vary the vacuum with the strong scale held fixed. In the electric patch rigid special geometry gives

$$a_D = \frac{\partial \mathcal{F}}{\partial a}, \qquad \tau = \frac{\partial^2 \mathcal{F}}{\partial a^2} = \frac{da_D/du}{da/du}. \tag{XI.6.62}$$

The ratio of the periods themselves is not the response of the photon to a change of vacuum.

We can differentiate the form in (XI.6.57) at fixed x, L. Set $c_\lambda = \sqrt{2}/(2\pi)$. Since $y^2 = (x^2 - L^2)(x - u)$, the derivatives are

$$\partial_u \lambda_{\rm SW} = -\frac{c_\lambda}{2}\frac{dx}{y}, \qquad \partial_u^2 \lambda_{\rm SW} = -\frac{c_\lambda}{4}\frac{dx}{(x-u)y}. \tag{XI.6.63}$$

The first derivative is holomorphic on the compact smooth curve. The original form has a double pole and no residue at infinity, as follows by taking $x = v^{-2}$. The combination needed for a closed differential equation is exact along the fiber:

$$(u^2 - L^2)\partial_u^2 \lambda_{\rm SW} + \frac{1}{4}\lambda_{\rm SW} = \frac{c_\lambda}{2}\, d_x\left(\frac{x^2 - L^2}{y}\right). \tag{XI.6.64}$$

For example, putting the two terms on the left over the common denominator $(x-u)y$ gives the numerator $c_\lambda(x^2 - 2ux + L^2)/4$. Differentiating the primitive on the right gives the same expression. Integration over a closed transported cycle kills the exact form. Both periods $\Pi = a, a_D$ thus satisfy

$$(u^2 - L^2)\Pi'' + \frac{1}{4}\Pi = 0. \tag{XI.6.65}$$

The two indicial roots at infinity are both $1/2$ for powers of u. This explains why the magnetic period can have a logarithm multiplying the electric one.

To determine the two solutions in the selected frame, integrate along the two sides of each cut. The signs of y and of the path reverse together, giving equal contributions on the two sheets:

$$a = \frac{\sqrt{2}}{\pi}\int_{-L}^{L} \frac{\sqrt{u-x}\,dx}{\sqrt{L^2 - x^2}}, \tag{XI.6.66}$$

$$a_D = \frac{i\sqrt{2}}{\pi}\int_{L}^{u} \frac{\sqrt{u-x}\,dx}{\sqrt{x^2 - L^2}}. \tag{XI.6.67}$$

Let $m = 2L/(u+L)$ and define the complete elliptic integrals with parameter m,

$$K(m) = \int_0^{\pi/2} \frac{d\phi}{\sqrt{1 - m\sin^2\phi}}, \qquad E(m) = \int_0^{\pi/2} \sqrt{1 - m\sin^2\phi}\, d\phi. \tag{XI.6.68}$$

In (XI.6.66) take $x = -L + 2L\sin^2\phi$. The Jacobian cancels the root in the denominator. In (XI.6.67) take $x = u - (u-L)\sin^2\phi$. The remaining integrand is proportional to $\sin^2\phi/\sqrt{1-(1-m)\sin^2\phi}$. Its integral is $[K(1-m)-E(1-m)]/(1-m)$, by subtraction of the defining integrals. This yields

$$a = \frac{2\sqrt{2(u+L)}}{\pi}\,E(m), \tag{XI.6.69}$$

$$a_D = \frac{2i\sqrt{2(u+L)}}{\pi}[K(1-m) - E(1-m)]. \tag{XI.6.70}$$

The magnetic contour has positive imaginary period. For the derivative of (XI.6.67) the moving upper endpoint contributes zero because the numerator vanishes there. In the differentiated integrals, the same changes of variable give

$$a' = \frac{\sqrt{2}}{\pi\sqrt{u+L}}K(m), \qquad a'_D = \frac{i\sqrt{2}}{\pi\sqrt{u+L}}K(1-m), \qquad \tau = i\frac{K(1-m)}{K(m)}. \tag{XI.6.71}$$

In particular at $u = 3L$ one has $m = 1/2$ and $\tau = i$. In the same vacuum $a_D/a \simeq 0.373i$. The difference persists away from this example, as shown in Figure XI.6.5. Since $0 < m < 1$ on the real ray, both K integrals are positive and $\operatorname{Im}\tau > 0$.

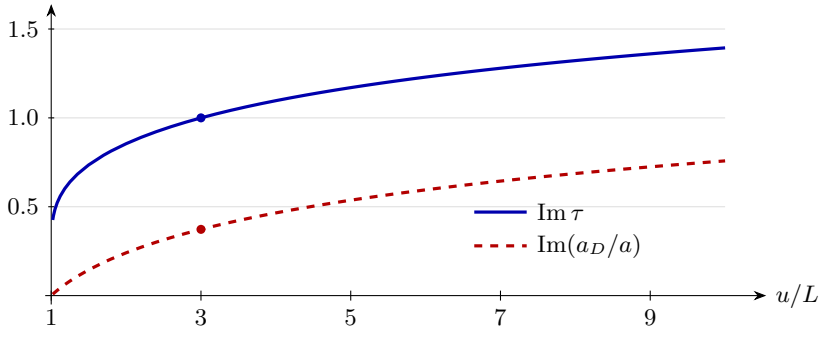


Figure XI.6.5: Two different ratios of the same periods on the real ray $u > L$. The solid curve is the photon coupling $\operatorname{Im}(da_D/da)$ from (XI.6.71). The dashed curve is $\operatorname{Im}(a_D/a)$. At $u/L = 3$ the two values are 1 and approximately 0.373. The plotted range begins at $u/L = 1.02$; both ratios tend to zero as $u/L \downarrow 1$.

For the weak-coupling expansion use $t = L^2/u^2$. The electric period is proportional to the angular average of $\sqrt{u - L\cos\vartheta}$. Odd powers of $\cos\vartheta$ average to zero. The first two even moments are $1/2$ and $3/8$. Multiplying by their binomial coefficients gives

$$a = \sqrt{2u}\left(1 - \frac{t}{16} - \frac{15t^2}{1024} + O(t^3)\right). \tag{XI.6.72}$$

The differential equation gives the same coefficients. If $a/\sqrt{2} = \sum_{n\geq 0} c_n L^{2n} u^{r_n}$ with $r_n = 1/2 - 2n$, the coefficient of $L^{2n}u^{r_n}$ in (XI.6.65) vanishes when

$$4n^2 c_n = r_{n-1}(r_{n-1} - 1)c_{n-1}. \tag{XI.6.73}$$

With $c_0 = 1$ this reproduces the two terms in (XI.6.72).

The leading magnetic logarithm and its finite constant follow from the actual contour. In (XI.6.70), the standard endpoint expansions of the elliptic integrals are $K(1-m) = \log(4/\sqrt{m}) + O(m \log m)$ and $E(1-m) = 1 + O(m \log m)$. They give the leading magnetic factor $\log(8u/L) - 2$. To find the first correction without reexpanding the elliptic integrals, let $h = \log(8u/L)$. For any solution a of (XI.6.65), applying the operator to ah gives

$$(u^2 - L^2)(2a'/u - a/u^2) = \sqrt{2}\, L^2 u^{-3/2}/4 + O(L^4 u^{-7/2}). \tag{XI.6.74}$$

At this order adding $\sqrt{2}\, bL^2 u^{-3/2}$ contributes $4\sqrt{2}\, bL^2 u^{-3/2}$. Thus $b = -1/16$, and the result is

$$a_D = \frac{i}{\pi}\sqrt{2u}\left[(1 - t/16)(h-2) - t/16 + O(t^2 \log(u/L))\right], \tag{XI.6.75}$$

$$\tau = \frac{i}{\pi}\left[h - \frac{5}{16}t + O(t^2)\right]. \tag{XI.6.76}$$

Here the second line comes from differentiating the first line and dividing by a'. The coefficient of the magnetic logarithm is proportional to a to all orders in the local expansion, as required by the repeated indicial root. The derivative ratio cancels the common factor.

Inverting (XI.6.72) gives $u = a^2/2 + L^2/(4a^2) + O(L^4/a^6)$. Hence the same coupling in the electric coordinate is

$$\frac{\pi}{i}\tau = \log\left(\frac{4a^2}{L}\right) - \frac{3L^2}{4a^4} + O(L^4/a^8). \tag{XI.6.77}$$

Using $\operatorname{Im}\tau = 4\pi/g^2$ on the real weakly coupled ray, this gives $8\pi^2/g^2 = 4\log(|a|/\Lambda_{\rm SW}) + O(1)$, the pure $SU(2)$ beta coefficient in Chapter 2. The first power correction becomes $-3L^2/a_W^4$. Inserting (XI.6.23) then gives $-12 C_{\rm IIA} e^{i\theta_b}(\Lambda_{\rm IIA}/a_W)^4$ in the displayed normalization of τ. It agrees with the one-instanton pole of Chapter 2 after matching the leading logarithm. Chapter 7 will approach the instanton terms from the worldsheet sums.

The specified contours and branch also delimit the freedom in $\mathcal{F}$. At fixed L an additive constant, including a background-only term, has no effect on its derivatives. A linear term in a would add a constant to a_D and spoil its selected vanishing at $u = L$. Adding $ka^2/2$ with integer k changes a_D to $a_D + ka$. This is an integral change of particle frame with corresponding charge and monodromy transformations. It is not a freedom to change the coupling while keeping the frame fixed. A change in the definition of the strong scale can shift a finite logarithm constant. Here the scale relation and the contours fix both that definition and the constant in (XI.6.75).

XI.6.8 The response carried by the two periods

The exact periods let us explain the difference between a_D/a and da_D/da throughout the real ray. This difference measures how much the magnetic response changes while the

electric coordinate varies. The second-order equation (XI.6.65) has no first-derivative term. Consequently its two solutions have a conserved Wronskian. In the present order of the periods, define

$$\mathcal{W} = a\,a_D' - a_D\,a', \qquad \mathcal{W}' = a\,a_D'' - a_D\,a'' = 0. \tag{XI.6.78}$$

The cancellation follows by inserting $a'' = -a/[4(u^2 - L^2)]$ and the same equation for a_D. It holds on every smooth patch reached by the specified continuation. We can determine the constant in a region where the periods are simple. Their weak limits give

$$a \sim \sqrt{2u}, \qquad a_D \sim \frac{i}{\pi} a(h-2), \qquad h' = \frac{1}{u}. \tag{XI.6.79}$$

Terms proportional to a' cancel in the determinant, leaving

$$\mathcal{W} = \lim_{u\to+\infty} \frac{i}{\pi}\frac{a^2}{u} = \frac{2i}{\pi}. \tag{XI.6.80}$$

The inverse-power corrections vanish in this limit. Since the Wronskian is constant, its leading weak value fixes it exactly. Its nonzero value also shows that the two periods are independent solutions, even though their leading powers of u coincide.

Divide (XI.6.80) by aa'. On the ray $u > L$, both factors are strictly positive by their defining integrals, and we obtain

$$\tau - \frac{a_D}{a} = \frac{2i}{\pi a a'}, \qquad \operatorname{Im}\tau > \operatorname{Im}\frac{a_D}{a} > 0. \tag{XI.6.81}$$

Thus the two curves in Figure XI.6.5 cannot coincide anywhere on this open ray. A quotient of periods compares the values already accumulated along two contours. The derivative quotient compares their responses to the same small variation of the vacuum. The constant Wronskian relates those comparisons without identifying them.

For example the elliptic formulas give the following values, independent of the positive choice of L:

u/L	$a/\sqrt{L}$	$\operatorname{Im}(a_D/a)$	$\operatorname{Im}\tau$
3	2.43201345	0.37273393	1.00000000
5	3.15429652	0.53678596	1.17015938

(XI.6.82)

Changing from $u/L = 3$ to 5 changes the elliptic parameter from $1/2$ to $1/3$. At the first point the equality $K(1-m) = K(m)$ fixes $\tau = i$. At the second point the complementary parameters differ, so this special value no longer holds. The ratio a_D/a is smaller at both points by the exact positive amount in (XI.6.81).

The same identity tells us how the two ratios change. Differentiating them and using the period equation yields

$$\frac{d}{du}\left(\frac{a_D}{a}\right) = \frac{\mathcal{W}}{a^2} = \frac{2i}{\pi a^2}, \tag{XI.6.83}$$

$$\frac{d\tau}{du} = \frac{a_D''a' - a_D'a''}{(a')^2} = \frac{\mathcal{W}}{4(u^2-L^2)(a')^2} = \frac{i}{2\pi(u^2-L^2)(a')^2}. \tag{XI.6.84}$$

Both imaginary parts increase strictly with u on the real ray. In the gauge kinetic normalization already chosen, $\operatorname{Im}\tau = 4\pi/g^2$, this means that the photon coupling decreases as the vacuum moves toward weak coupling. For complex u, these derivatives remain local analytic identities, but there is no corresponding ordering of their complex values.

Finally the scale dependence of this comparison is fixed by homogeneity. Substituting $x = L\xi$ into the period integrals gives, with $r = u/L$,

$$a(u,L) = \sqrt{L}\,\mathfrak{a}(r), \qquad a_D(u,L) = \sqrt{L}\,\mathfrak{a}_D(r), \qquad a' = L^{-1/2}\mathfrak{a}'(r). \tag{XI.6.85}$$

The product aa' in (XI.6.81) is therefore dimensionless and depends only on r. Raising L at fixed u/L rescales both particle central charges by $\sqrt{L}$ and leaves their dimensionless response unchanged. This separates a change of the physical mass scale from a change of vacuum within the same scaled family.

XI.6.9 The two finite monodromies

A logarithm at weak coupling gives the monodromy around both finite singularities. To distinguish the singularities we need a contour that shrinks at one of them. Let $u = L + \delta$ with $\delta > 0$ initially. In (XI.6.67) put $x = L + \delta v$. The length of the cut and the two square roots give

$$a_D = \frac{i\sqrt{2}}{\pi}\frac{\delta}{\sqrt{2L}}\int_0^1 \sqrt{\frac{1-v}{v}}\,dv + O(\delta^2) = \frac{i\delta}{2\sqrt{L}} + O(\delta^2). \tag{XI.6.86}$$

The integral is $\pi/2$. In contrast, the electric contour does not vanish. In (XI.6.66) at $u = L$ the factor $\sqrt{L-x}$ cancels, leaving

$$a(L) = \frac{\sqrt{2}}{\pi}\int_{-L}^{L}\frac{dx}{\sqrt{x+L}} = \frac{4\sqrt{L}}{\pi}. \tag{XI.6.87}$$

The shrinking contour gives a local magnetic coordinate.

The derivative of the electric integral is singular. Writing $q = L - x$, the endpoint contribution has the kernel $[q(q+\delta)]^{-1/2}/\sqrt{2L}$. For a cutoff q_0 fixed and small compared with L,

$$\int_0^{q_0}\frac{dq}{\sqrt{q(q+\delta)}} = 2\,\operatorname{arsinh}\sqrt{q_0/\delta} = -\log(\delta/L) + O(1). \tag{XI.6.88}$$

In a' this gives the coefficient $-1/(2\pi\sqrt{L})$ of $\log(\delta/L)$. By the local differential equation (XI.6.65), only the vanishing analytic solution can multiply the logarithm. Comparing its slope in (XI.6.86) gives

$$a = a_{\mathrm{an}} + \frac{i}{\pi}a_D\log(\delta/L) \tag{XI.6.89}$$

with a_{an} analytic at $\delta = 0$. A counterclockwise loop adds $2\pi i$ to the logarithm, and hence sends a to $a - 2a_D$.

For the complete based convention, let $\mathbf{\Pi} = (a_D, a)^{\mathsf{T}}$ at a real base point $u_0 > L$. Both small loops are counterclockwise. The stem to $+L$ is approached from the right. The stem to $-L$ passes below $+L$, as in Figure XI.6.6. Use a large counterclockwise loop enclosing both singularities in the finite, scaled u plane. This loop is taken after the limit in (XI.6.14); it does not surround the two displaced critical values of the finite-ϵ curve. The large loop changes $\sqrt{u}$ to $-\sqrt{u}$ and adds $2\pi i$ to $\log u$. Equations (XI.6.72) and (XI.6.75) then give

$$M_+ = \begin{pmatrix} 1 & 0 \\ -2 & 1 \end{pmatrix}, \qquad M_\infty = \begin{pmatrix} -1 & 2 \\ 0 & -1 \end{pmatrix}. \tag{XI.6.90}$$

A positively oriented loop in the local coordinate $1/u$ would give M_∞^{-1} instead.

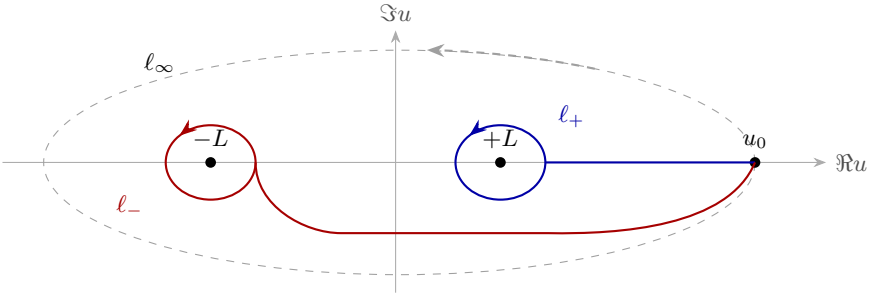


Figure XI.6.6: Based loops in the finite u plane, with base point $u_0 > L$. Each stem is traversed in both directions; the arrows on the circles indicate counterclockwise continuation. The lower stem fixes the meaning of the $-L$ matrix in the frame at u_0. The dashed outer loop is counterclockwise in u, not in $1/u$.

In this cut system the large loop is homotopic to traversing the $+$ loop and then the lower-stem $-$ loop. The counterclockwise boundary of a thin neighborhood of the stems runs along the horizontal stem to $+L$ and returns along its other edge to the lower stem for $-L$. The period matrices are written as left actions on a column. To continue the functions along the second path, continue the entries of $M_+\mathbf{\Pi}$; the constant M_+ stays on the left. Thus the based path order gives $M_\infty = M_+ M_-$. Solving for the second finite monodromy gives

$$M_- = M_+^{-1} M_\infty = \begin{pmatrix} -1 & 2 \\ -2 & 3 \end{pmatrix}. \tag{XI.6.91}$$

For example, reversing the order in the matrix product would give $\left(\begin{smallmatrix} -5 & 2 \\ -8 & 3 \end{smallmatrix}\right)$ instead of M_∞. Moving the minus stem across the other singularity changes its matrix by conjugation. The path is part of the specification.

A charge row $q = (n_m, n_e)$ with $qM = q$ gives an invariant combination $q\mathbf{\Pi}$. Here the primitive rows are

$$q_+ = (1, 0), \qquad q_- = (1, -1). \tag{XI.6.92}$$

At a finite singularity the local solutions have analytic and logarithmic parts. The invariant solution is the analytic one because the other picks up the nonzero log shift. For

any analytic solution (XI.6.65) at $u = \pm L$ forces its constant term to vanish. Hence the two invariant combinations really are the vanishing a_D and $a_D - a$, not just fixed charge labels. In the pure gauge theory the first is the monopole charge and the second the dyon charge, up to overall signs. This identification uses the light-particle interpretation of the Seiberg–Witten solution in the isolated protected sector. A vanishing period alone does not prove that a particle with that charge is present.

Why does the first matrix in (XI.6.90) have a shear of magnitude two if the primitive cover cycle has a single nodal twist? In the cover basis (B', A') the period vector for compact gauge boundaries is obtained by multiplying the second component by two. The two finite matrices in the primitive cover basis are therefore

$$\widetilde{M}_+ = \begin{pmatrix} 1 & 0 \\ -1 & 1 \end{pmatrix}, \qquad \widetilde{M}_- = \begin{pmatrix} -1 & 4 \\ -1 & 3 \end{pmatrix}. \tag{XI.6.93}$$

Here $M_\pm = S\widetilde{M}_\pm S^{-1}$ with $S = \mathrm{diag}(1, 2)$. This is the same index-two effect we found from the windings in Section XI.6.5. The differential and the lattice are needed together to recover the period monodromies.

It is useful to repeat the calculation after an integral change of magnetic frame. Keep the based paths fixed and let $k \in \mathbb{Z}$. The shear and its action are

$$T_k = \begin{pmatrix} 1 & k \\ 0 & 1 \end{pmatrix}, \qquad \mathbf{\Pi}^{(k)} = T_k \mathbf{\Pi} = \begin{pmatrix} a_D + ka \\ a \end{pmatrix}. \tag{XI.6.94}$$

Continuing this new column around the same loop gives $T_k M \mathbf{\Pi}$, so its matrix must be $M^{(k)} = T_k M T_k^{-1}$. Direct multiplication gives

$$M_+^{(k)} = \begin{pmatrix} 1 - 2k & 2k^2 \\ -2 & 1 + 2k \end{pmatrix}, \qquad M_-^{(k)} = \begin{pmatrix} -1 - 2k & 2(k+1)^2 \\ -2 & 3 + 2k \end{pmatrix}. \tag{XI.6.95}$$

The central charge must describe the same state in either frame. Its row therefore changes by the inverse matrix:

$$q^{(k)} = q T_k^{-1}, \qquad q_-^{(k)} = (1, -1 - k), \qquad q_-^{(k)} \mathbf{\Pi}^{(k)} = a_D - a. \tag{XI.6.96}$$

For a worked example take $k = -1$. Then $a_D^{(-1)} = a_D - a$ and

$$M_+^{(-1)} = \begin{pmatrix} 3 & 2 \\ -2 & -1 \end{pmatrix}, \qquad M_-^{(-1)} = \begin{pmatrix} 1 & 0 \\ -2 & 1 \end{pmatrix}, \qquad q_-^{(-1)} = (1, 0). \tag{XI.6.97}$$

The singularity at $-L$ now has the magnetic form of the shear, because its vanishing central charge is the first coordinate. The state and the singularity have not changed; the electric and magnetic labels have. By contrast, reversing a loop at a fixed frame replaces M by M^{-1}. Its fixed charge row stays the same, while the sign of the logarithmic continuation reverses. Conjugating a matrix and inverting it answer different questions.

XI.6.10 Two photons from an A_2 fibration

What changes when two independent fiber spheres can shrink? An A_2 surface fiber has two simple-root curves. Fibering that surface over a base $\mathbb{P}^1$ engineers the protected

sector of pure $SU(3)$ theory. A generic Coulomb vacuum retains two photons. We therefore need four gauge periods and a symmetric 2×2 response matrix. The rank-one method still starts from a Laurent polynomial, but its compact curve will have genus two. We will carry one example from that polynomial to its periods and then recover the rank-one sector by making one root heavy.

Use six monomials in the order $(z, z^{-1}, 1, t, t^2, t^3)$. Their height and exponent rows are

$$R_3 = \begin{pmatrix} 1 & 1 & 1 & 1 & 1 & 1 \\ 1 & -1 & 0 & 0 & 0 & 0 \\ 0 & 0 & 0 & 1 & 2 & 3 \end{pmatrix}. \tag{XI.6.98}$$

The three integral relations that describe the base and the two fiber classes are

$$\begin{aligned} \ell_b &= (1, 1, -2, 0, 0, 0), \\ \ell_1 &= (0, 0, 1, -2, 1, 0), \\ \ell_2 &= (0, 0, 0, 1, -2, 1). \end{aligned} \tag{XI.6.99}$$

Indeed, multiplying each row by R_3^t gives zero. The second difference in the last two rows is the A_2 chain. Its two compact surfaces supply the two magnetic gauge directions. The mirror equation is $UV = H$, where

$$H = a(z + z^{-1}) + b_0 + b_1 t + b_2 t^2 + b_3 t^3. \tag{XI.6.100}$$

The coefficient products invariant under rescaling the monomials are obtained directly from (XI.6.99),

$$z_b = \frac{a^2}{b_0^2}, \qquad z_{f_1} = \frac{b_0 b_2}{b_1^2}, \qquad z_{f_2} = \frac{b_1 b_3}{b_2^2}. \tag{XI.6.101}$$

As in the F_0 example, these are algebraic coordinates. A flat Kähler exponential requires the mirror map.

To retain two finite Coulomb parameters, bring the cubic close to a triple root at $t = 1$. Introduce an inverse-mass parameter η, a mass cubed $s \neq 0$, and parameters u, v of mass dimensions two and three. Choose the coefficient chart

$$\begin{aligned} a &= \frac{\eta^3 s}{2}, \qquad b_0 = 1 - \eta^2 u + \eta^3 v, \\ b_1 &= -3 + \eta^2 u, \qquad b_2 = 3, \qquad b_3 = -1. \end{aligned} \tag{XI.6.102}$$

The fiber polynomial has four monomials, $1, t, t^2, t^3$. At the triple root their coefficients are $(1, -3, 3, -1)$. The departures of b_0 and b_1 in the displayed chart carry the two distinct vacuum coordinates: u enters both at order η^2, while v enters b_0 at order η^3. In particular,

$$\begin{aligned} z_b &= \frac{\eta^6 s^2}{4}\big(1 + O(\eta^2)\big), \\ z_{f_1} &= \frac{1}{3} - \frac{\eta^2 u}{9} + \frac{\eta^3 v}{3} + O(\eta^4), \\ z_{f_2} &= \frac{1}{3} - \frac{\eta^2 u}{9}. \end{aligned} \tag{XI.6.103}$$

Thus u is resolved at order η^2, while the difference of the two fiber coordinates resolves v at order η^3. Setting both fiber coordinates to $1/3$ before this resolution would discard the Coulomb branch. The base exponent is six, as expected for pure $SU(3)$. No numerical identification of η with the F_0 parameter ϵ is needed here.

Set $t = 1 + \eta x$, keeping x finite. The complete polynomial in this chart becomes

$$\frac{H}{\eta^3} = \frac{s}{2}(z + z^{-1}) - P(x), \qquad P(x) = x^3 - ux - v. \tag{XI.6.104}$$

This equality is exact. The limiting operation is still needed for the differential and for the interpretation of the surviving periods. Define

$$y = \frac{s}{2}(z - z^{-1}), \qquad y^2 = P(x)^2 - s^2, \qquad z = \frac{P + y}{s}. \tag{XI.6.105}$$

The six simple roots of $(P - s)(P + s)$ are branch points of a double cover of the x-sphere. Riemann–Hurwitz gives $2g - 2 = 2(-2) + 6$, hence $g = 2$. We write $s = \Lambda_3^3$ and $q = s^2 = \Lambda_3^6$; the choice of sign of s exchanges the two cubic factors.

The logarithmic three-form reduction supplies $\log t\, d\log z$. In the zoomed chart,

$$\frac{\log t}{\eta}\frac{d\log z}{2\pi i} \longrightarrow \lambda_3 = \frac{x\, d\log z}{2\pi i} = \frac{x(3x^2 - u)}{2\pi i\, y}\, dx. \tag{XI.6.106}$$

All terms have mass dimension one. We fix the common period unit so that a small electric period tends to a root e_i of P at weak coupling. Denote these small electric periods by E_i; their contours and orientations are specified next. In this eigenvalue convention the W central charges and BPS masses are

$$Z_{ij} = E_i - E_j, \qquad M_{W_{ij}} = \sqrt{2}\,|E_i - E_j|. \tag{XI.6.107}$$

The protected mirror identification and the matching to the wrapped-brane mass fix this common physical unit. Polynomial algebra by itself fixes neither that identification nor isolation from bulk modes. The latter remains the local-limit assumption used in the preceding construction.

XI.6.11 Four periods and a matrix of couplings

Which genus-two cycles carry the gauge charges? Start in a real weak-coupling patch with three distinct real roots e_i of P. For sufficiently small positive s, each root splits into a pair of branch points. Let their increasing order be $b_1 < \cdots < b_6$, and place cuts on the three paired intervals. Orient A_i counterclockwise on the sheet defined near an enclosing circle by

$$y = P\sqrt{1 - \frac{s^2}{P^2}}, \qquad \sqrt{1 - \frac{s^2}{P^2}} \longrightarrow 1 \quad (s \longrightarrow 0). \tag{XI.6.108}$$

Then $E_i = \oint_{A_i} \lambda_3 \to e_i$, because the limiting integrand is xP'/P. Each contour has z winding $+1$. For example,

$$\frac{1}{2\pi i}\oint_{A_i} d\log z = \frac{1}{2\pi i}\oint_{A_i} \frac{P'}{y}\, dx = 1. \tag{XI.6.109}$$

This integer is fixed under a smooth deformation of the contour that avoids punctures. On the same small contour, $t = 1 + \eta x$ has zero winding for sufficiently small η.

An individual A_i therefore fails the zero-winding condition for a compact three-cycle boundary. To see which combinations can be corrected by puncture loops, first return to the finite η Laurent curve. At $t = 0$ there are two ordinary solutions for z, each with local winding $(n_z, n_t) = (0, 1)$. At infinity, balance z or z^{-1} against the cubic term. Writing a local parameter as $h = 1/t$ gives

end	leading relation	(n_z, n_t)
$t = 0$, first	$z \to z_0 \neq 0$	$(0, 1)$
$t = 0$, second	$z \to z_1 \neq 0$	$(0, 1)$
$t = \infty$, first	$z \sim t^{-3}$	$(3, -1)$
$t = \infty$, second	$z \sim t^{3}$	$(-3, -1)$

(XI.6.110)

Punctures can cancel electric z winding only in multiples of three. Differences of two A_i already have zero winding in both torus coordinates. They give the two simple-root electric boundaries

$$\alpha_1 = A_1 - A_2, \qquad \alpha_2 = A_2 - A_3. \tag{XI.6.111}$$

On the compactified curve $A_1 + A_2 + A_3 = 0$. Thus, in its primitive electric basis (A_1, A_2), the two root rows are

$$C_e = \begin{pmatrix} 1 & -1 \\ 1 & 2 \end{pmatrix}, \qquad \det C_e = 3. \tag{XI.6.112}$$

This index-three projection is the A_2 root lattice inside the primitive electric period lattice. It follows from this curve's punctures. The degree-two elliptic map used earlier has no role in this genus-two calculation.

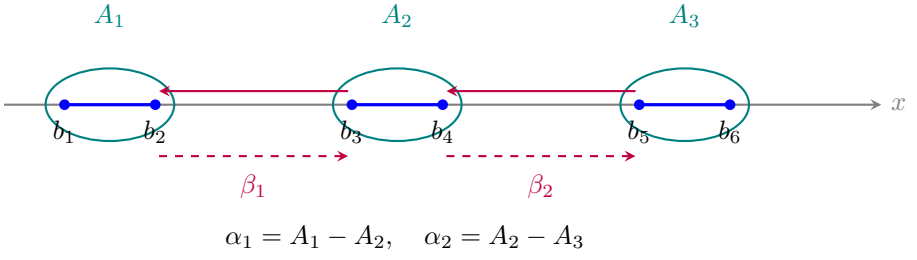


Figure XI.6.7: The three weak-coupling cuts of the genus-two curve, shown schematically rather than to scale. The contours A_i encircle individual cuts on the specified sheet. A solid gap arrow travels from right to left on that sheet; the dashed return is on the opposite sheet. These define β_1 and β_2. Electric differences cancel the common z winding. The canonical magnetic basis is $B_1 = \beta_1 + \beta_2$, $B_2 = \beta_2$.

For the magnetic directions use the gap cycles in Figure XI.6.7. The first goes from b_3 to b_2 on the specified sheet and returns on the other sheet; the second goes from b_5 to b_4 and returns. Between the first two cuts $P > s$, so the two lifts of z are on

the positive real ray. Between the next two cuts $P < -s$, so they are on the negative real ray. Each lift goes out and returns without winding around zero. With the stated orientations the intersections are

$$(A_i \cdot \beta_j) = \begin{pmatrix} 1 & 0 \\ -1 & 1 \\ 0 & -1 \end{pmatrix}, \qquad B_1 = \beta_1 + \beta_2, \quad B_2 = \beta_2. \tag{XI.6.113}$$

Consequently $A_i \cdot B_j = \delta_{ij}$ for $i, j = 1, 2$. The root electric boundaries paired with the two gap magnetic cycles have the expected Cartan form,

$$(\alpha_i \cdot \beta_j) = \begin{pmatrix} 2 & -1 \\ -1 & 2 \end{pmatrix}. \tag{XI.6.114}$$

These are local particle-charge statements. Specifying the maximal allowed Wilson–'t Hooft lines, or the absolute global form of a compact completion, requires more information than these gauge periods.

Define the four independent period coordinates by

$$\mathbf{E} = \begin{pmatrix} E_1 \\ E_2 \end{pmatrix}, \qquad \mathbf{b} = \begin{pmatrix} b_1^{\mathrm{mag}} \\ b_2^{\mathrm{mag}} \end{pmatrix}, \qquad b_i^{\mathrm{mag}} = \oint_{B_i} \lambda_3. \tag{XI.6.115}$$

The superscript distinguishes magnetic periods from branch points. The remaining electric period is $E_3 = -E_1 - E_2$. Indeed, at the two infinities $xP'/y = \pm(3 + O(x^{-2}))$. The differential has no residue, and the sum of the three small-cut contours has zero period.

There are two independent ways to change the vacuum. A ratio of two period components no longer even has the correct matrix type for their response. Use the two Jacobians, whose rows are cycles and whose columns are the coordinates (u, v),

$$J_{ik} = \frac{\partial E_i}{\partial m_k}, \qquad D_{ik} = \frac{\partial b_i^{\mathrm{mag}}}{\partial m_k}, \qquad (m_1, m_2) = (u, v). \tag{XI.6.116}$$

Where J is invertible, $d\mathbf{b} = D\, d\mathbf{m}$ and $d\mathbf{E} = J\, d\mathbf{m}$ give

$$\tau_3 = DJ^{-1}, \qquad db_i^{\mathrm{mag}} = (\tau_3)_{ij}\, dE_j. \tag{XI.6.117}$$

Special geometry identifies this symmetric matrix with the Hessian of the prepotential in the declared primitive period coordinates. Its imaginary part is positive in a physical patch. These coordinates retain the particle root sublattice in (XI.6.111); they do not replace it by all primitive electric cycles.

We can compute the Jacobians without differentiating moving branch endpoints. From $\log z$ and (XI.6.105),

$$\partial_u \log z = -\frac{x}{y}, \qquad \partial_v \log z = -\frac{1}{y}. \tag{XI.6.118}$$

For either parameter, differentiate $x\, d\log z$ and integrate by parts. This gives the complete identities

$$\begin{aligned} \partial_u \lambda_3 &= \frac{x\, dx}{2\pi i\, y} + d\left(-\frac{x^2}{2\pi i\, y}\right), \\ \partial_v \lambda_3 &= \frac{dx}{2\pi i\, y} + d\left(-\frac{x}{2\pi i\, y}\right). \end{aligned} \tag{XI.6.119}$$

The exact terms have single-valued meromorphic primitives on the smooth curve and integrate to zero on transported closed cycles. The two surviving forms, $x\,dx/y$ and dx/y, are a basis of holomorphic one-forms. The order in (XI.6.116) is therefore directly visible in the integrands.

Here is a complete numerical vacuum in units of an arbitrary reference mass. Take

$$u = 7, \qquad v = 6, \qquad s = 0.1, \qquad P = (x+2)(x+1)(x-3). \tag{XI.6.120}$$

The ordered branch points are

$$\begin{aligned} (b_1, b_2) &= (-2.019540319, -1.979497290),\\ (b_3, b_4) &= (-1.025491504, -0.975448386),\\ (b_5, b_6) &= (2.994988705, 3.004988794). \end{aligned} \tag{XI.6.121}$$

For the A integrals, circles $x = e_i + 0.2e^{i\theta}$ enclose one pair each and avoid the other cuts. On them use (XI.6.108). For a magnetic gap $[l, r]$, let $G(x)$ be the product of $x - b_k$ over the other four branch points and put $\sigma = \operatorname{sign} P((l+r)/2)$. The endpoint substitution

$$x = l + (r-l)\sin^2\frac{\theta}{2}, \qquad y = \sigma\sqrt{(x-l)(r-x)}\sqrt{-G(x)} \tag{XI.6.122}$$

cancels the square-root endpoints. For a numerator $N(x)$ this right-to-left gap cycle gives

$$\oint_\beta \frac{N(x)\,dx}{2\pi i\, y} = -\frac{1}{\pi i}\int_0^\pi \frac{N(x(\theta))}{\sigma\sqrt{-G(x(\theta))}}\,d\theta. \tag{XI.6.123}$$

Use $N = xP'$ for the period and $N = x, 1$ for its two derivatives. Thus the same smooth real integrals determine both $\mathbf{b}$ and D. Combining them with the three enclosing-circle integrals gives

$$\begin{aligned} (E_1, E_2, E_3) &= (-1.999759552, -1.000234823, 2.999994375),\\ \mathbf{b} &= -i\begin{pmatrix} 6.881015151\\ 6.086481413\end{pmatrix},\\ J &= \begin{pmatrix} -0.400501344 & 0.200322994\\ 0.250500191 & -0.250323659\end{pmatrix}. \end{aligned} \tag{XI.6.124}$$

The magnetic Jacobian obtained from the two gap integrals is

$$D = i\begin{pmatrix} -1.044322345 & 0.164634323\\ -0.097704191 & -0.474282433\end{pmatrix}. \tag{XI.6.125}$$

Its columns follow the same (u, v) order as J. Finally the matrix response is

$$\begin{aligned} \tau_3 &= i\begin{pmatrix} 4.397044385 & 2.861075031\\ 2.861075031 & 4.184269083\end{pmatrix},\\ \operatorname{eig}(\operatorname{Im}\tau_3) &= (1.427604400, 7.153709068). \end{aligned} \tag{XI.6.126}$$

The off-diagonal entry measures the response of one magnetic coordinate to the other electric coordinate. The positive eigenvalues give positive photon kinetic terms in this patch. Their symmetry is also a useful check on the independently evaluated A and B integrals. Changing the order to $J^{-1}D$ would not implement the chain rule in (XI.6.116).

XI.6.12 Weak coupling and the split discriminant

How does the genus-two solution resolve a classical gauge singularity? We can first approach weak coupling without crossing any discriminant. Choose a circle around one root e_i of P with $|s/P| < 1$ everywhere on it. The square root has the uniformly convergent binomial expansion

$$\frac{1}{y} = \frac{1}{P}\left(1 + \frac{s^2}{2P^2} + \frac{3s^4}{8P^4} + \cdots\right). \tag{XI.6.127}$$

Uniform convergence on this fixed circle permits termwise integration. The electric period becomes

$$E_i = e_i + \frac{s^2}{2}\operatorname*{Res}_{x=e_i}\frac{xP'}{P^3} + O(s^4). \tag{XI.6.128}$$

The correction is simple enough to derive without solving a system of differential equations. A total derivative gives

$$d\left(\frac{x}{P^2}\right) = \left(\frac{1}{P^2} - \frac{2xP'}{P^3}\right)dx, \qquad \operatorname*{Res}_{e_i}\frac{xP'}{P^3} = \frac{1}{2}\operatorname*{Res}_{e_i}\frac{1}{P^2}. \tag{XI.6.129}$$

Writing $x = e_i + \xi$ and $A = P'(e_i) \neq 0$ gives

$$\frac{1}{P^2} = \frac{1}{A^2\xi^2}\left(1 - \frac{P''(e_i)}{A}\xi + O(\xi^2)\right). \tag{XI.6.130}$$

It follows that the first instanton-order displacement is

$$E_i = e_i - \frac{s^2 P''(e_i)}{4P'(e_i)^3} + O(s^4) = e_i - \frac{3s^2 e_i}{2(3e_i^2 - u)^3} + O(s^4). \tag{XI.6.131}$$

The expansion parameter is $q = s^2 = \Lambda_3^6$. Its coefficient is singular when two classical roots approach each other, so a small q alone is not a uniform weak-coupling condition there. The enclosing-circle criterion states the actual local domain.

For the vacuum just calculated, the three first corrections are

$$(\Delta E_1, \Delta E_2, \Delta E_3) = (0.000240000, -0.000234375, -0.000005625). \tag{XI.6.132}$$

They sum to zero. Comparing with (XI.6.124), the omitted terms are approximately 4.48×10^{-7}, -4.48×10^{-7}, -8.04×10^{-11}, respectively. Halving s reduces these remainders by about sixteen, as the next power s^4 predicts. The corresponding W periods involve differences, for example

$$E_1 - E_2 = -0.999524729 + \cdots, \qquad E_2 - E_3 = -4.000229198 + \cdots. \tag{XI.6.133}$$

Together with (XI.6.107), this converts the curve calculation into protected particle masses. Chapter 7 compares such weak gauge quantities with the contributions of curves wrapping the base.

To locate the quantum singularities, factor the sextic into its two cubics. The cubic discriminants and their resultant are

$$\Delta_\pm = 4u^3 - 27(v \pm s)^2, \qquad \mathrm{Res}_x(P - s, P + s) = (2s)^3. \tag{XI.6.134}$$

The resultant is particularly transparent: at each of the three roots of $P - s$, the other factor has value $2s$. The discriminant of a product is the product of the two discriminants times the square of the resultant. Hence

$$\mathrm{Disc}_x(P^2 - s^2) = 64s^6\,[4u^3 - 27(v + s)^2]\,[4u^3 - 27(v - s)^2]. \tag{XI.6.135}$$

For $s \neq 0$, a generic zero comes from a collision of roots within one cubic. It does not come from the two members of an individual weak-coupling cut, which belong to opposite cubics. For example, at $u = 7, v = 6, s = 0.1$,

$$\Delta_+ = 367.33, \qquad \Delta_- = 432.13, \tag{XI.6.136}$$

so the period calculation lies on a smooth fiber. At fixed u, v, the reduced discriminant has the classical limit

$$\frac{\mathrm{Disc}_x(P^2 - s^2)}{64s^6} \longrightarrow (4u^3 - 27v^2)^2. \tag{XI.6.137}$$

The full sextic discriminant instead vanishes at $s = 0$, when $y^2 = P^2$ is singular for every vacuum. Dividing out its explicit scale factor is essential in comparing the classical loci.

We can now resolve one ordinary quantum singularity locally. For fixed $s \neq 0$, choose a double root at $x = r$ of $P - s$. The conditions $P'(r) = 0$ and $P(r) = s$ give

$$u_* = 3r^2, \qquad v_* = -2r^3 - s, \qquad P - s = (x - r)^2(x + 2r). \tag{XI.6.138}$$

An isolated ordinary node requires

$$r \neq 0, \qquad 2r^3 + s \neq 0. \tag{XI.6.139}$$

The first condition keeps a third root away; the second keeps the other cubic nonsingular, since at this vacuum $\Delta_- = -108s(2r^3 + s)$.

Move transversely by $v = v_* + \delta$ at fixed $u = u_*$, and write $x = r + \xi$. The local polynomial and its branch points are

$$\begin{aligned} P - s &= 3r\xi^2 + \xi^3 - \delta, \\ y^2 &= 2s(3r\xi^2 - \delta) + O(\xi^3, \delta\xi^2, \delta^2), \\ \xi_\pm &= \pm\sqrt{\frac{\delta}{3r}} + O(\delta). \end{aligned} \tag{XI.6.140}$$

Let ν enclose the two colliding points and choose the local sheet $y \sim \sqrt{6sr}\,\xi$ when $\delta = 0$. The period vanishes at the node because xP'/y is regular there. Its first derivative is fixed by the holomorphic form in (XI.6.119),

$$\left.\frac{\partial Z_\nu}{\partial \delta}\right|_{\delta=0} = \frac{1}{2\pi i}\oint_\nu \frac{d\xi}{\sqrt{6sr}\,\xi} = \frac{1}{\sqrt{6sr}}. \tag{XI.6.141}$$

Thus the protected vanishing central charge has the local behavior

$$Z_\nu = \oint_\nu \lambda_3 = \frac{\delta}{\sqrt{6sr}} + O(\delta^2). \tag{XI.6.142}$$

The dimensions agree: δ has mass dimension three and $\sqrt{sr}$ has dimension two. At $r = 1, s = 0.1$, the slope is $1/\sqrt{0.6} = 1.290994449$. Direct small-contour integration at $\delta = 10^{-4}$ gives $Z_\nu = 0.0001291077392$, consistent with the linear result and a quadratic remainder.

A dual cycle intersecting ν once has a logarithmic period. For an orientation in which its continuation adds Z_ν, its singular part is $Z_\nu \log\delta/(2\pi i)$. This is the local primitive Picard–Lefschetz action. The physical interpretation as a light charged hypermultiplet uses the protected gauge-theory dictionary, as it did for the rank-one monopole. At $r = 0$ the local equation is instead $y^2 = x^3(x^3 + 2s)$; the ordinary-node expansion no longer applies. We do not need that higher collision to compute the smooth periods or the generic singularities considered here.

XI.6.13 Recovering a rank-one sector

Can the rank-two curve reproduce the rank-one solution with its specific mass convention? Separate one classical eigenvalue from the other two. To avoid confusing the separation with the rank-one period a, call the heavy displacement a_h and factor the cubic as

$$P(x) = (x + 2a_h)\big[(x - a_h)^2 - U\big]. \tag{XI.6.143}$$

Its roots are $-2a_h, a_h \pm \sqrt{U}$, so the last pair remains at finite relative distance while the two other root differences grow like $3a_h$. Matching coefficients gives

$$u = 3a_h^2 + U, \qquad v = -2a_h^3 + 2a_h U. \tag{XI.6.144}$$

The divergent W masses remove the off-diagonal directions connecting the isolated eigenvalue to the nearby pair from the finite-energy sector. There remains an interacting rank-one sector and a spectator photon.

Set $x = a_h + X$, $s = 3a_h S$, and $y = 3a_h Y$, and take $a_h \to +\infty$ with X, U, S fixed. The full curve reads

$$Y^2 = \left(1 + \frac{X}{3a_h}\right)^2 (X^2 - U)^2 - S^2 \longrightarrow (X^2 - U)^2 - S^2. \tag{XI.6.145}$$

This gives the scale relation in the present polynomial chart,

$$\Lambda_2^4 = S^2 = \frac{\Lambda_3^6}{9a_h^2}. \tag{XI.6.146}$$

Here $\Lambda_2^2 = S$ names the scale of this limiting quartic. Although s grows in this trajectory, s/a_h^3 goes to zero. The heavy-root separation, rather than a requirement that Λ_3 stay fixed, controls the reduction. Equation (XI.6.146) is not an independently fixed worldsheet threshold constant for every finite fibration.

The differential also contains a potentially large term,

$$\lambda_3 = \frac{a_h\, d\log z}{2\pi i} + \frac{X\, d\log z}{2\pi i}. \tag{XI.6.147}$$

Each small electric contour in the nearby pair has z winding one. Their difference cancels the first term. The magnetic gap cycle has zero winding and cancels it as well. On these gauge boundaries the finite differential is therefore

$$\lambda_{\mathrm{eff}} = \frac{X\, d\log z}{2\pi i} = \frac{2X^2}{2\pi i\, Y}\, dX, \qquad \frac{S}{2}(z + z^{-1}) = X^2 - U. \tag{XI.6.148}$$

Taking only the curve limit and keeping the a_h term would miss why the light periods are finite.

We can compare this result with the original cubic in §XI.6.6 without changing its labels or units. Use a subscript "old" only within this comparison and set

$$p = \sqrt{2}X, \qquad u_{\mathrm{old}} = 2U, \qquad L_{\mathrm{old}} = 2S, \qquad z_{\mathrm{old}} = -z. \tag{XI.6.149}$$

Then $p^2 = u_{\mathrm{old}} - (L_{\mathrm{old}}/2)(z_{\mathrm{old}} + z_{\mathrm{old}}^{-1})$. The map to the old cubic is explicitly

$$x_{\mathrm{old}} = -2(X^2 - U), \qquad y_{\mathrm{old}} = 2i\sqrt{2}\, XY, \tag{XI.6.150}$$

and substitution gives

$$y_{\mathrm{old}}^2 = (x_{\mathrm{old}}^2 - L_{\mathrm{old}}^2)(x_{\mathrm{old}} - u_{\mathrm{old}}). \tag{XI.6.151}$$

Its normalized differential pulls back to

$$\frac{\sqrt{2}}{2\pi}\, \frac{(x_{\mathrm{old}} - u_{\mathrm{old}})\, dx_{\mathrm{old}}}{y_{\mathrm{old}}} = 2\lambda_{\mathrm{eff}}. \tag{XI.6.152}$$

This factor acts together with the cycle map. It cannot be inferred from the visual similarity of two quartics.

On the reference slice $U > S > 0$, let A_R be the counterclockwise small contour around the right-hand cut of the limiting quartic. The left contour becomes $-A_R$ in compact homology. Thus the root electric period is twice a primitive period. Let β_{gap} retain the right-to-left gap orientation used in the genus-two example. The old positive magnetic convention uses $-\beta_{\mathrm{gap}}$. The degree-two map and its period consequences are

$$\begin{aligned} A_R &\longmapsto A_{\mathrm{old}}, \qquad -\beta_{\mathrm{gap}} \longmapsto 2B_{\mathrm{old}}, \\ E_R - E_L &\longrightarrow 2\oint_{A_R} \lambda_{\mathrm{eff}} = a_{\mathrm{old}}, \\ -\oint_{\beta_{\mathrm{gap}}} \lambda_{\mathrm{eff}} &\longrightarrow a_{D,\mathrm{old}}. \end{aligned} \tag{XI.6.153}$$

In particular the physical root mass tends to $\sqrt{2}|a_{\mathrm{old}}|$, exactly the earlier W mass. The sign of the magnetic gap is part of the comparison, just as the stems were part of the rank-one monodromy calculation. The spectator photon and the heavy periods remain outside this rank-one pair. This reduction exhibits one finite interacting sector of the genus-two solution; it does not identify the entire rank-two theory with pure $SU(2)$.

XI.6.14 Exercises

Use the real reference branch of the chapter and the specified based paths. The first three exercises have bounded numerical or algebraic answers; the remaining exercises ask for written arguments.

1. **Change the Laurent chart.** Start from

$$H = 2 + 2\epsilon^2 u - w - w^{-1} - \frac{\epsilon^2 L}{2} z - \frac{2\epsilon^2 L}{z}, \qquad L > 0.$$

   Find the positive rescaling $z = \rho\widetilde{z}$ making the base coefficients equal. Determine the multiplier κ in $u' = \kappa u$ that puts the polynomial into (XI.6.12), and give the new scale L' in terms of L. Check by multiplying the four critical values and calculating the two coefficients of

$$\lim_{\epsilon \to 0} \frac{D_{\mathrm{tor}}}{\epsilon^4 L^2} = c_2 (u/L)^2 + c_0.$$

   Submit ρ, κ, c_2, c_0. Explain on paper why agreement of the zero set alone would leave one of the requested coefficients undetermined.

2. **Extract the logarithmic coupling.** Retain the first power correction in the weak periods. Differentiate with respect to u at fixed L and write $(\pi/i)\tau = c_h h + c_t L^2/u^2 + \cdots$, where $h = \log(8u/L)$. Then invert the electric period and find the coefficient c_a of L^2/a^4 in the expansion at fixed a. Using the gauge kinetic normalization of this chapter, find the coefficient b_0 multiplying $\log(|a|/\Lambda_{\mathrm{SW}})$ in $8\pi^2/g^2$. Submit c_h, c_t, c_a, b_0.

3. **Change the magnetic frame.** Keep the paths of Figure XI.6.6 and use $\mathbf{\Pi}' = T\mathbf{\Pi}$ with $T = \left(\begin{smallmatrix} 1 & 2 \\ 0 & 1 \end{smallmatrix}\right)$. Compute both matrices M'_+, M'_- in the new frame, as well as the new row q'_- for the same vanishing dyon, with first component $+1$. Verify directly that $q'_- \mathbf{\Pi}'$ equals $q_- \mathbf{\Pi}$. Submit both matrices and the row. On paper, explain why reversing a loop would be a different operation from this change of basis.

4. **Compare the three compactifications.** Identify the vector multiplet moduli in type IIA on X, type IIB on $\widehat{X}$, and type IIB on X. Track the shrinking fiber parameter through the actual mirror construction. Explain why type IIB on X does not substitute for the mirror period calculation. State one claim about additional bulk modes or line operators that the local calculation leaves open. This is a written exercise.

5. **Control a period limit.** On the real ray $u = 5L$, choose two values of $\eta = \epsilon\sqrt{L}$ differing by a factor of two and satisfying $\eta\sqrt{6}/2 \leq 1$. Compute the exact average for $T_f/(\epsilon\sqrt{L})$ and its two-term approximation in (XI.6.27). Bound the difference using (XI.6.28). Explain why this error estimate cannot be used for arbitrarily large u at fixed ϵ. This is a written transfer exercise.

6. **Separate a compact projection from its period.** Decompose the zero-winding contour $4A' + 2B' - 2\ell_{0,+} + \ell_{0,-} + 3\ell_{\infty,+}$ in the basis (XI.6.41). Determine its compact projection and the part of its relative period that diverges in field-theory units. State what remains ambiguous if only its boundary, rather than its relative lift, is specified. This is a written transfer exercise.

7. **Transfer the weak-period calculation to another vacuum.** Let $P = (x+3)(x+1)(x-4)$ and take a sufficiently small nonzero s. Determine u, v and all three coefficients of s^2 in the electric periods. Verify their sum vanishes. Choose a radius for each enclosing circle on which $|s/P| < 1$, and compare a contour evaluation with the first correction. State why the physical W central charges are differences of these periods. This is a written transfer exercise.

8. **Follow an ordinary genus-two degeneration.** Set $r = 2, s = 1$ in (XI.6.138). Find the singular vacuum, show that the other cubic remains nonsingular, and determine the leading branch-point splitting and vanishing period under $v = v_* + \delta$. Then identify which step fails at $r = 0$. Explain why this strong-coupling collision joins different branch points from the pair in a weak-coupling electric cut. This is a written transfer exercise.

Status and sources

§XI.6.2. The F_0 ray relations and invariant products in (XI.6.2) and (XI.6.6) are [MATH]. The local mirror hypersurface and use of its protected complex structure periods are [GEO-E], using the local mirror construction. See (S. H. Katz et al. 1997, arXiv:hep-th/9609239v2, Secs. 4.2–4.3, Eqs. (4.2)–(4.3), (4.11)) and (Aganagic et al. 2002, arXiv:hep-th/0105045v1, Sec. 2, Eqs. (2.4)–(2.6), and Sec. 6.2, pp. 31–32). The toric rays are taken in the lattice of one-parameter subgroups.

§XI.6.3. The discriminant, scaled curve and flat-coordinate evaluation are [MATH]. For (XI.6.16) and the closed mirror map, see (S. H. Katz et al. 1997, arXiv:hep-th/9609239v2, Eqs. (4.11), (5.6)) and (Aganagic et al. 2002, arXiv:hep-th/0105045v1, Eqs. (6.6)–(6.7)). The interpretation of the flat periods is [GEO-E], with the brane-action normalization and the period matching and wrapped-brane premise in (XI.6.15). Bulk isolation is [DEC]. The explicit curve in (S. H. Katz et al. 1997, arXiv:hep-th/9609239v2, Sec. 5.1) uses F_2; Sec. 5.2 treats F_0 periods. Here the Laurent calculation starts with F_0.

§XI.6.4. The moment expansion and its real-ray remainder bound in (XI.6.27)–(XI.6.28) are [MATH] consequences of the exact flat-period average in (XI.6.21). They estimate that period, without introducing a finite-string-scale effective action.

§XI.6.5. The relative homology, winding kernel, pairing and four affine period directions are [MATH], derived in (XI.6.32)–(XI.6.49) for the stated affine hypersurface. For

reduction to logarithmic periods, see (S. H. Katz et al. 1997, arXiv:hep-th/9609239v2, Eqs. (4.8)–(4.10)). Discarding the two background directions is a local period statement; bulk isolation remains [DEC]. The general contour decomposition in (XI.6.42) is [MATH] in the same winding kernel.

§XI.6.6. The degree-two map, pushforward of cycles and pullback of the differential are [MATH]. The Toda and cubic forms can be compared to (S. H. Katz et al. 1997, arXiv:hep-th/9609239v2, Eq. (5.3)) and (Seiberg and Witten 1994, arXiv:hep-th/9407087v1, Eqs. (6.6), (6.19)). For the distinction between isogenous presentations and their charge pairings, see (Closset and Magureanu 2024, arXiv:2308.10225v3, Sec. 2, Eqs. (2.46)–(2.53), (2.67)). The common physical period conversion from the protected mirror charge dictionary is [GEO-E]. Equation (XI.6.60) uses the central-charge normalization stated there; the unit W charge is in the text following Eq. (6.30) of (Seiberg and Witten 1994). For the joint limit of a curve and differential, see (S. Katz et al. 1997, arXiv:hep-th/9706110v2, Secs. 5.1–5.2).

§XI.6.7. The exact differential, elliptic integrals and weak series are [MATH]. Compare (Seiberg and Witten 1994, arXiv:hep-th/9407087v1, Eqs. (6.19)–(6.30)). The protected photon coupling in the engineered sector is [GEO-E]; the matching of the perturbative log and first power correction with the worldsheet calculation is supporting [BPS:1/2|holo], at the displayed weak order only. The source for the one-instanton comparison is (S. H. Katz et al. 1997, arXiv:hep-th/9609239v2, Sec. 5, pp. 12–15).

§XI.6.8. The conserved Wronskian, exact ratio difference, monotonicity on the real ray, and homogeneity are [MATH] consequences of the normalized periods and rigid equation in §XI.6.7. The physical coupling uses the same [GEO-E] identification and normalization already stated there. No additional statement about the populated particle spectrum is used.

§XI.6.9. The two based monodromies and their vanishing covectors are [MATH]. The identification of the light monopole and dyon of the engineered sector is [GEO-E], using the protected construction and the pure-gauge solution in (Seiberg and Witten 1994, arXiv:hep-th/9407087v1, Secs. 5.4–5.5, Fig. 1, Eqs. (5.12)–(5.16) and Sec. 6). The local scope leaves the full stable spectrum, absolute line lattice and compact embedding undetermined. The frame shears in (XI.6.95) are [MATH] conjugations of these same based monodromies; their charge rows transform contragrediently.

§XI.6.10. The A_2 fibration engineering pure $SU(3)$ and its protected local mirror interpretation are [GEO-E], using the higher-rank local mirror construction. The source is (S. H. Katz et al. 1997, arXiv:hep-th/9609239v2, Sec. 6.1, pp. 19–21, Eqs. (6.1)–(6.5)). The six-monomial coefficient chart, algebraic-coordinate scaling, genus and limiting differential in (XI.6.98)–(XI.6.106) are [MATH]. The eigenvalue period normalization and BPS mass dictionary are [GEO-E], in the convention of (Klemm et al. 1996, arXiv:hep-th/9505150v1, Secs. 4.1–4.2, Eqs. (4.4), (4.9)–(4.12)). Bulk isolation remains [DEC]. No exact finite-scale mirror map or common base threshold with F_0 is asserted.

§XI.6.11. The puncture windings, electric index-three projection, root/coroot intersections, derivative identities and explicit period integrals are [MATH] calculations in the stated local chart. The geometric charge interpretation and special-geometry identification of DJ^{-1} are [GEO-E], following (Klemm et al. 1996, arXiv:hep-th/9505150v1,

Secs. 4.1–4.2, Eqs. (4.7)–(4.10), (4.15)–(4.16)). The source's root/weight distinction does not select an absolute Wilson–'t Hooft line lattice for this local model. Numerical entries in (XI.6.124) and (XI.6.126) evaluate the displayed contours; they are not source quotations.

§XI.6.12. The contour expansion, residue coefficient, exact sextic resultant and generic-node normal form are [MATH]. The curve and its reduced discriminant agree with (Klemm et al. 1996, arXiv:hep-th/9505150v1, Sec. 4.1, Eqs. (4.4)–(4.5)); direct period asymptotics are developed in its Appendix A, pp. 46–47. The local Picard–Lefschetz action is [MATH], as in (Klemm et al. 1996, arXiv:hep-th/9505150v1, Sec. 4.2, Eq. (4.17)). The light-particle interpretation is [GEO-E]. No full stability spectrum, cusp fixed-point classification or globally based $Sp(4,\mathbb{Z})$ matrices are inferred.

§XI.6.13. The heavy-root curve, scale relation, differential cancellation and comparison to the original cubic and particle basis are [MATH]. The protected finite gauge-sector interpretation is [GEO-E] under the same local-isolation [DEC] premise. The old differential and degree-two map retain precisely the conventions and source associations of §XI.6.6; the right-to-left gap has the magnetic sign stated in (XI.6.153). These calculations do not identify the complete rank-two and rank-one theories.

References

Aganagic, M., A. Klemm, and C. Vafa (2002). "Disk instantons, mirror symmetry and the duality web". In: *Z. Naturforsch. A* 57, pp. 1–28. DOI: 10.1515/zna-2002-1-201. arXiv: hep-th/0105045.

Closset, C. and H. Magureanu (2024). "Reading between the rational sections: Global structures of 4d $\mathcal{N} = 2$ KK theories". In: *SciPost Phys.* 16, p. 137. DOI: 10.21468/SciPostPhys.16.5.137. arXiv: 2308.10225 [hep-th].

Katz, S., P. Mayr, and C. Vafa (1997). "Mirror Symmetry and Exact Solution of 4D N=2 Gauge Theories I". In: *Adv. Theor. Math. Phys.* 1, pp. 53–114. DOI: 10.4310/ATMP.1997.v1.n1.a2. arXiv: hep-th/9706110.

Katz, S. H., A. Klemm, and C. Vafa (1997). "Geometric engineering of quantum field theories". In: *Nucl. Phys. B* 497, pp. 173–195. DOI: 10.1016/S0550-3213(97)00282-4. arXiv: hep-th/9609239.

Klemm, A., W. Lerche, and S. Theisen (1996). "Nonperturbative effective actions of N=2 supersymmetric gauge theories". In: *Int. J. Mod. Phys. A* 11, pp. 1929–1974. DOI: 10.1142/S0217751X96001000. arXiv: hep-th/9505150.

Seiberg, N. and E. Witten (1994). "Electric-magnetic duality, monopole condensation, and confinement in N=2 supersymmetric Yang-Mills theory". In: *Nucl. Phys. B* 426. [Erratum: Nucl.Phys.B 430, 485–486 (1994)], pp. 19–52. DOI: 10.1016/0550-3213(94)90124-4. arXiv: hep-th/9407087.

Chapter XI.7

Worldsheet instantons become gauge instantons

XI.7.1 Which degree counts gauge instantons

A worldsheet in the local Calabi–Yau has two degrees. The instanton expansion of pure 4D $\mathcal{N}=2$ $SU(2)$ gauge theory has only one. To see how the two expansions are related, we will fix the degree along the base and sum over the degree along the fiber. A single worldsheet contribution then tends to zero in the field theory limit, while the sum at fixed base degree can remain finite. This chapter calculates that finite contribution at the first two instanton orders and compares it with the electric and magnetic periods of the preceding chapter. We then repeat the construction at one instanton order for an A_2 fibration, where two fiber sums determine the Coulomb dependence of a rank-two prepotential.

The geometry is still the total space of the canonical bundle of $F_0 = \mathbb{P}^1_b \times \mathbb{P}^1_f$. In its zero section choose the oriented holomorphic curves

$$B = \mathbb{P}^1_b \times \{\text{pt}\}, \qquad F = \{\text{pt}\} \times \mathbb{P}^1_f. \tag{XI.7.1}$$

The first sphere is the base. The second is the fiber whose wrapped D2-brane gives the electric W state. We use the flat coordinates from the local limit,

$$T_C = -2\pi i t_C = \frac{1}{2\pi\alpha'}\int_C (J - iB_{\text{NS}}), \qquad Q_C = e^{-T_C}, \qquad C = B, F. \tag{XI.7.2}$$

These dimensionless coordinates enter the worldsheet weight. Their real parts measure area in string units and their imaginary parts fix the phase. The area determines the suppression of a term; the phase identifies the topological sector in which it occurs. These are different uses of the same complex coordinate. In particular Q_b and Q_f are the exponentials of flat coordinates, rather than the algebraic coefficients of the Laurent mirror curve. Subscripts b, f will denote the two curves; B_{NS} is the two-form.

Projection to $\mathbb{P}^1_b$ sends B to the fundamental class and contracts F. For a contribution with class $dB + mF$ and cover order $r \geq 1$, the total class, worldsheet weight and base

phase are therefore

$$[\Sigma] = rdB + rmF, \tag{XI.7.3}$$

$$e^{-r(dT_b+mT_f)} = Q_b^{rd} Q_f^{rm}, \tag{XI.7.4}$$

$$Q_b^{rd} = e^{-rd\,\mathrm{Re}\,T_b}\, e^{ird\theta_b}, \qquad \theta_b = \frac{1}{2\pi\alpha'}\int_B B_{\mathrm{NS}}. \tag{XI.7.5}$$

In the local engineering limit, the unit-base phase is the positive Yang–Mills instanton phase. The spacetime argument for this identification uses the field equation for the NS two-form. A worldsheet wrapping the base is a point source in 4D, and the flux measured on a linking three-sphere records the number of base wrappings. In the reduction of the ALE gauge sector, the Yang–Mills instanton density sources the same flux. We use this identification with the background curvature contribution separated, and assume the isolated protected sector of the field theory limit. In the unit phase convention of the reduction, the Fourier mode $e^{ik\theta_b}$ then has

$$k = rd. \tag{XI.7.6}$$

This argument labels terms in a protected expansion. It requires no correspondence between individual worldsheet maps and individual gauge field configurations.

One can check the degree assignment without the spacetime reduction. Write $\pi_b : F_0 \to \mathbb{P}^1_b$ for the projection. Applying its pushforward before and after covering gives

$$(\pi_b)_*(dB + mF) = d[\mathbb{P}^1_b], \qquad (\pi_b)_*\big(r(dB + mF)\big) = rd[\mathbb{P}^1_b]. \tag{XI.7.7}$$

The fiber coefficient disappears in this operation because the fiber maps to a point. The physical identification then uses this integer as the Fourier exponent of the gauge instanton weight. For example, a cover with $(d, m, r) = (2, 1, 2)$ gives total degree $(4, 2)$ and phase $e^{4i\theta_b}$. A different fiber degree changes the Coulomb dependence of its contribution, while leaving this phase unchanged. This is why the entire row at fixed total base degree must be collected before comparing with one coefficient of the gauge expansion.

In making that collection, Q_b and Q_f are initially independent formal variables. A coefficient of Q_b^k is therefore a function of Q_f, rather than a single curve invariant. Only after determining that function do we impose the field theory trajectory relating the two variables. This order keeps track of which infinite fiber sum accompanies each instanton order.

Figure XI.7.1 separates the two roles. Moving to the right leaves k fixed when r is fixed. A double cover, however, multiplies both degrees. For example, the two distinct inputs

$$(d, m, r) = (1, 3, 2) \qquad \text{and} \qquad (2, 6, 1) \tag{XI.7.8}$$

both contribute at $Q_b^2 Q_f^6$. They have different weights in the prepotential. In particular, knowing the total bidegree does not determine whether a term arose by covering. Nor does a single contribution require a primitive vector in $H_2(F_0, \mathbb{Z})$: a coefficient of class $2B + 2F$ can appear before taking any covers. To distinguish these terms, we need the connected amplitude.

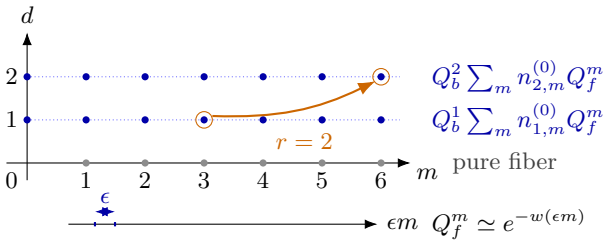


Figure XI.7.1: Base degree d is vertical and fiber degree m is horizontal. The blue rows are the sums of single genus-zero contributions before covering. The orange arrow shows a double cover from $(1,3)$ to the total degree $(2,6)$. The gray row has no base wrapping. The lower axis shows the scaled fiber degree used in the local limit. The dots locate possible degrees, including degrees whose invariant vanishes.

XI.7.2 Connected amplitudes and the fiber factor

The 4D prepotential comes from the connected genus-zero amplitude. To extract it, we use the closed A-model expansion recalled in Volume IV. Let λ denote the topological expansion parameter, independent of the physical string coupling. With $n_{d,m}^{(g)}$ the signed Gopakumar–Vafa coefficient of class $dB + mF$ and index label g, the positive-curve part is

$$\log Z_{\text{curve}} = \sum_{\substack{d,m\geq 0\\ (d,m)\neq(0,0)}} \sum_{r\geq 1,\, g\geq 0} \frac{n_{d,m}^{(g)}}{r} \left[2\sin\left(\frac{r\lambda}{2}\right)\right]^{2g-2} Q_b^{rd} Q_f^{rm}. \tag{XI.7.9}$$

At fixed curve class the term of order λ^{-2} comes from $g = 0$. To see which terms can mix at the next order, expand the inverse sine kernel itself:

$$\frac{1}{[2\sin(r\lambda/2)]^2} = \frac{1}{r^2\lambda^2} + \frac{1}{12} + O(\lambda^2), \qquad [2\sin(r\lambda/2)]^0 = 1. \tag{XI.7.10}$$

Both a genus-zero label and a genus-one label can therefore contribute to a term of order λ^0. The coefficient of λ^{-2} is distinguished because no higher label can enter it. Its factor r^{-3} combines r^{-1} in the cover sum with $(r\lambda)^{-2}$ from the kernel. Thus the coefficient of λ^{-2} in the connected curve contribution is

$$F_0^{\text{curve}} = \sum_{(d,m)\neq(0,0)} n_{d,m}^{(0)}\, \mathrm{Li}_3(Q_b^d Q_f^m), \qquad \mathrm{Li}_3(y) = \sum_{r\geq 1} \frac{y^r}{r^3}. \tag{XI.7.11}$$

The cover of $B + 3F$ in the previous example carries $1/8$ of its single contribution's coefficient. The term from $2B + 6F$ carries the coefficient of that class itself. This distinction holds at finite string scale.

To use the local partition product, set

$$x = Q_f, \qquad q = e^{i\lambda}, \qquad S_r = (q^{r/2} - q^{-r/2})^2 = -[2\sin(r\lambda/2)]^2. \tag{XI.7.12}$$

A hat will indicate the coefficient in the S_r kernel. Changing from the sine kernel to this kernel leaves the amplitude unchanged if

$$\widehat{n}^{(g)}_{d,m} = (-1)^{g-1} n^{(g)}_{d,m}, \qquad \widehat{f}_{dg}(x) = \sum_m \widehat{n}^{(g)}_{d,m} x^m, \qquad G_d(q,x) = \sum_g S_1^{g-1} \widehat{f}_{dg}(x). \tag{XI.7.13}$$

For a fixed positive power k of Q_b, the integer equation $rd = k$ gives the coefficient

$$[Q_b^k] \log Z_{\text{curve}} = \sum_{r|k} \frac{G_{k/r}(q^r, x^r)}{r}. \tag{XI.7.14}$$

The change of sign at $g = 0$ comes from the kernel and applies at both base degrees. It is useful to write out the first two instances of the divisor relation:

$$[Q_b] \log Z_{\text{curve}} = G_1(q,x), \qquad [Q_b^2] \log Z_{\text{curve}} = G_2(q,x) + \frac{1}{2} G_1(q^2, x^2). \tag{XI.7.15}$$

The doubled arguments encode the doubled fiber degree and the doubled topological parameter in the same cover. Replacing $G_1(q^2, x^2)$ by $G_1(q,x)$ would preserve neither of these operations. In particular the factor $1/2$ in this formula becomes $1/8$ at genus zero, since the small-λ part of $G_1(q^2, x^2)$ supplies another factor $1/4$.

There are two separate normalizations to perform. First, we extract the positive-base part at fixed x, q. For this operation all invertible factors that are independent of Q_b cancel:

$$Z_{\text{red}} = \frac{Z(Q_b, x; q)}{Z(0, x; q)} = 1 + Q_b Z_1 + Q_b^2 Z_2 + \cdots . \tag{XI.7.16}$$

Here Z is the curve partition product, with any separately specified degree-zero normalization. This division removes a constant-map factor, if present, and the pure-fiber factor. A constant-map factor independent of a has no gauge derivative at fixed background. The pure-fiber factor does have a gauge derivative: the fiber modulus is precisely the one we vary. It is removed to define an instanton contribution, and retained when computing the perturbative coupling. A factor with a nonzero positive-base connected coefficient would change the quantity in (XI.7.16) if divided out. The separately specified classical polynomial is likewise kept distinct from the positive-degree curve expansion.

The logarithm in this prescription has a direct role. If c_1, c_2 are the connected coefficients at orders one and two, exponentiating them produces

$$\exp(Q_b c_1 + Q_b^2 c_2 + \cdots) = 1 + Q_b c_1 + Q_b^2 \left(c_2 + \frac{1}{2} c_1^2 \right) + \cdots , \tag{XI.7.17}$$

$$c_1 = Z_1, \qquad c_2 = Z_2 - \frac{1}{2} Z_1^2. \tag{XI.7.18}$$

The square of the order-one term describes two disconnected contributions whose total degree is two. A cover, in contrast, is already a connected map. It remains in c_2 and is removed only if the aim is to recover G_2 rather than the full connected amplitude.

There is a similarly direct way to test a proposed division. Suppose $A(x,q)$ is independent of Q_b, whereas $H = \exp[Q_b b_1(x,q) + O(Q_b^2)]$. Then

$$\frac{AZ}{(AZ)|_{Q_b=0}} = \frac{Z}{Z|_{Q_b=0}}, \qquad [Q_b] \log(Z_{\text{red}}/H) = Z_1 - b_1(x,q). \tag{XI.7.19}$$

The first equality explains the cancellation of a base-zero factor. The second shows exactly how a positive-base division would change an instanton coefficient. Neither equality says that A has a vanishing electric derivative: that requires A to be independent of the electric variable as well. In the actual fiber factor this extra condition fails.

Second, we fix the overall unit of the 4D prepotential before computing any positive-base term. We can do this with the perturbative contribution we just separated. The empty pair of partitions in the local product gives

$$\log Z_{\text{fiber}} = 2\sum_{r\geq 1}\frac{x^r}{rS_r}, \qquad F_0^{\text{fiber}} = -2\,\mathrm{Li}_3(x). \tag{XI.7.20}$$

The plus sign in the S_r expression and the minus sign in F_0^{fiber} follow from (XI.7.12). To compare with the periods, work first on the real electric patch $u > L > 0$ of the preceding chapter. Use $L = \Lambda_{\text{SW}}^2$, the electric period $a > 0$, the electric separation $w = \sqrt{2}a$, and the length $\epsilon = 2\pi g_s/M_s$, with $M_s = 1/\sqrt{\alpha'}$. Then $T_f = \epsilon w + O(\epsilon^3)$ on a smooth weak patch. These asymptotics can be differentiated there at fixed L. The derivative can be taken directly from the convergent fiber sum on $0 < x < 1$. With $x = e^{-\epsilon\sqrt{2}a}$ to leading order,

$$\partial_a\,\mathrm{Li}_s(x) = -\epsilon\sqrt{2}\,\mathrm{Li}_{s-1}(x), \qquad \partial_a^2\,\mathrm{Li}_3(x) = 2\epsilon^2\,\mathrm{Li}_1(x). \tag{XI.7.21}$$

Each derivative lowers the polylogarithm index because it multiplies the term of fiber degree m by m. Two derivatives expose the logarithmic singularity at $x = 1$. The protected geometric identification relates $\epsilon^{-2}F_0$ to a mass-dimension-two prepotential.

At leading order ∂_a^2 brings down two factors of $\epsilon\sqrt{2}$ from the fiber weight. Using $\mathrm{Li}_1(x) = -\log(1-x)$ gives

$$\partial_a^2\big[\epsilon^{-2}F_0^{\text{fiber}}\big] = -4\,\mathrm{Li}_1(e^{-\epsilon\sqrt{2}a}) + o(1) \tag{XI.7.22}$$

$$= 4\log(1 - e^{-\epsilon\sqrt{2}a}) + o(1) \tag{XI.7.23}$$

$$= 4\log(\epsilon\sqrt{2}a) + o(1). \tag{XI.7.24}$$

The argument of the last logarithm is dimensionless. For the comparison, write it as the sum of $\log(a/\mu)$ and $\log(\epsilon\sqrt{2}\mu)$ with fixed reference mass μ. Only the first term has a slope in $\log a$. A polynomial in the large-radius T_b, T_f, whose leading variation in this limit is affine in a, does not supply this logarithmic slope. It can affect the subtraction of terms analytic in a. In particular, matching the log does not fix the perturbative additive constant in the coupling.

The signed period frame has $a_D = \partial_a\mathcal{F}_{\text{SW}}$. At weak coupling its curvature is

$$\tau = \partial_a^2\mathcal{F}_{\text{SW}} \;\sim\; \frac{i}{\pi}\log\!\left(\frac{4a^2}{L}\right). \tag{XI.7.25}$$

The two slopes are 4 and $2i/\pi$. Equivalently, taking $a\partial_a$ of the curvature removes any additive perturbative constant and gives

$$\lim_{\epsilon\to 0} a\partial_a\partial_a^2[\epsilon^{-2}F_0^{\text{fiber}}] = 4, \qquad a\partial_a\tau_{\text{pert}} = \frac{2i}{\pi}. \tag{XI.7.26}$$

The ratio of these numbers fixes a multiplicative unit, whereas an additive shift in τ belongs to a separate choice. Therefore the conversion factor multiplying the scaled sine coefficient is $i/(2\pi)$, under the common protected prepotential identification. The comparison below keeps the fixed period frame and its perturbative subtraction. It does not remove further functions of a from the instanton series.

XI.7.3 Enumerating the first two base sectors

At first sight the fiber sum at fixed base degree requires an infinite collection of curve invariants. The local F_0 partition product instead gives a finite sum of rational functions of x at each base degree. Here we import that product and evaluate it explicitly through total size two. For a pair of Young diagrams R, U, with total size $|R| + |U| = k$, it gives

$$Z_k = \sum_{|R|+|U|=k} \frac{W_R^2 W_U^2}{\prod_\ell (1 - q^\ell x)^{2C_\ell(R,U)}}. \tag{XI.7.27}$$

Only three nonempty diagrams occur here. A box (i, j) has content $j - i$, and its hook length H counts that box, the boxes to its right and the boxes below it. Figure XI.7.2 shows both quantities for the diagrams needed in the sum. The weights and the cross factors in (XI.7.27) are

$$\kappa_R = 2 \sum_{(i,j)\in R} (j - i), \qquad W_R^2 = \frac{q^{\kappa_R/2}}{\prod_{(i,j)\in R} S_{H(i,j)}}, \tag{XI.7.28}$$

$$f_R(q) = \sum_{(i,j)\in R} q^{j-i}, \qquad \sum_\ell C_\ell(R, U) q^\ell = f_R + f_U + (q - 2 + q^{-1}) f_R f_U. \tag{XI.7.29}$$

For the empty diagram take $W_\varnothing = 1$ and $f_\varnothing = 0$.

The low-order product can now be reconstructed one diagram at a time. A row of length two has contents $0, 1$, hooks $2, 1$ and $\kappa = 2$. Its square weight is $q/(S_1 S_2)$; an empty partner gives one cross exponent at each of $\ell = 0, 1$. The column reverses the nonzero content and replaces q by q^{-1}. A single box in each diagram has no nonzero content, but the cross term in (XI.7.29) changes its two zero shifts to one positive and one negative shift. The contributions are listed below; each summand is for one ordering.

Pair family	Number	Summand
$(\square, \varnothing)$	2	$[S_1(1 - x)^2]^{-1}$
$([2], \varnothing)$	2	$q[S_1 S_2(1 - x)^2(1 - qx)^2]^{-1}$
$([1, 1], \varnothing)$	2	$q^{-1}[S_1 S_2(1 - x)^2(1 - q^{-1}x)^2]^{-1}$
$(\square, \square)$	1	$[S_1^2(1 - qx)^2(1 - q^{-1}x)^2]^{-1}$

In the first three rows the number includes exchanging the two diagrams. The last row has only one ordering. Thus there are two ordered pairs at size one and five at size two, with no extra factor for the split pair.

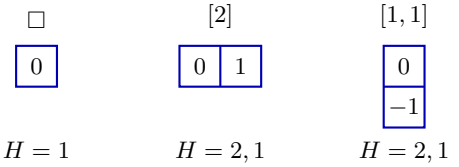


Figure XI.7.2: The nonempty diagrams through size two. The numbers inside the boxes are the contents, with the upper left box at $(1,1)$. The hook lengths below each diagram are read starting with that box. The row and column have the same hooks and opposite sums of contents.

For the split pair, the cross polynomial is explicitly

$$f_\square + f_\square + (q - 2 + q^{-1}) f_\square^2 = q + q^{-1}. \tag{XI.7.30}$$

The two diagrams in this pair both have hook length one. Adding the contributions gives

$$Z_1 = \frac{2}{S_1(1-x)^2}, \tag{XI.7.31}$$

$$Z_2 = \frac{2}{S_1 S_2 (1-x)^2}\left[\frac{q}{(1-qx)^2} + \frac{q^{-1}}{(1-q^{-1}x)^2}\right] + \frac{1}{S_1^2(1-qx)^2(1-q^{-1}x)^2}. \tag{XI.7.32}$$

The dependence on x is already summed in these expressions. In particular the single box gives $(1-x)^{-2}$ and includes every fiber degree even though its base degree is one.

We now separate the two operations that affect order two. Expanding the logarithm removes the disconnected product of two order-one terms. In the result the cover of the order-one contribution still occurs. Applying (XI.7.14) after taking the logarithm gives

$$[Q_b^2] \log Z_{\mathrm{red}} = Z_2 - \tfrac{1}{2} Z_1^2, \tag{XI.7.33}$$

$$G_1 = Z_1, \qquad G_2 = Z_2 - \tfrac{1}{2} Z_1^2 - \tfrac{1}{2} Z_1(q^2, x^2). \tag{XI.7.34}$$

Thus the disconnected subtraction belongs to the connected partition function, and the cover subtraction belongs to the reconstruction of the single GV labels. At $x = 0$, the connected sine genus-zero coefficient of Q_b^2 is $-1/4$ from the double cover of the base. Assigning it to G_2 would give a spurious fractional invariant for class $2B$. This example can be checked before any genus expansion. Put $s = S_1$, so that $q + q^{-1} = 2 + s$ and $S_2 = s(4+s)$. Setting $x = 0$ in the product gives

$$Z_1(q,0) = \frac{2}{s}, \qquad Z_2(q,0) = \frac{2(2+s)}{s^2(4+s)} + \frac{1}{s^2}, \tag{XI.7.35}$$

$$Z_2(q,0) - \frac{1}{2} Z_1(q,0)^2 = \frac{1}{s(4+s)} = \frac{1}{S_2}, \tag{XI.7.36}$$

$$\frac{1}{2} Z_1(q^2,0) = \frac{1}{S_2}, \qquad G_2(q,0) = 0. \tag{XI.7.37}$$

The complete connected order-two term at this fiber degree is exactly a cover. Its s^{-2} terms cancel when the disconnected product is removed. Its remaining S_2^{-1} term cancels only in the single-contribution function. This calculation gives a practical way to distinguish the two subtractions without relying on the value of any particular enumerative invariant.

For completeness, both required GV coefficients at base two can be read without expanding in fiber degree. Write $D = 1-x$ and $s = S_1$. The product and the symmetric sum appearing in (XI.7.32) satisfy

$$(1-qx)(1-q^{-1}x) = D^2 - xs, \qquad S_2 = s(4+s), \tag{XI.7.38}$$

$$\frac{q}{(1-qx)^2} + \frac{q^{-1}}{(1-q^{-1}x)^2} = \frac{2D^2 + (1+x^2)s}{(D^2-xs)^2}. \tag{XI.7.39}$$

The first identity follows by writing $q + q^{-1} = 2 + s$. For the numerator in the second, combine the two terms over the common denominator and use the same sum. Substituting gives an expression regular at $s = 0$ for fixed x away from its poles:

$$sG_2 = \frac{1}{s}\left[1 + \frac{2[2D^2 + (1+x^2)s]}{(4+s)D^2} - \frac{2}{D^4}\right] - \frac{1}{(4+s)(1-x^2)^2}. \tag{XI.7.40}$$

In fact the term in square brackets vanishes at $s = 0$, the cancellation due to connectedness. To expand it, put $\alpha = x/D^2$ and use $(1 - xs/D^2)^{-2} = 1 + 2\alpha s + 3\alpha^2 s^2 + \cdots$. The bracket becomes

$$\frac{1}{D^4}\left[\left(5\alpha + \frac{1}{4}\right)s + \left(8\alpha^2 + \frac{\alpha}{4} - \frac{1}{16}\right)s^2 + O(s^3)\right]. \tag{XI.7.41}$$

The last term in (XI.7.40) then subtracts the cover. The constant and linear coefficients of sG_2, together with the single-box result, are

$$\widehat{f}_{10}(x) = \frac{2}{(1-x)^2}, \qquad \widehat{f}_{11}(x) = 0, \tag{XI.7.42}$$

$$\widehat{f}_{20}(x) = \frac{6x + 8x^2 + 6x^3}{(1-x)^6(1+x)^2}, \tag{XI.7.43}$$

$$\widehat{f}_{21}(x) = \frac{9x^2 + 14x^3 + 9x^4}{(1-x)^8(1+x)^2}. \tag{XI.7.44}$$

For example, the first terms of $-\widehat{f}_{20}(x)$ are $-6x - 32x^2 - 110x^3$. These are the signed genus-zero invariants at base degree two and fiber degrees one, two and three. The three coefficients agree with those from the local mirror calculation at large radius. For the 4D limit, what matters instead is the pole at $x = 1$.

XI.7.4 The field theory limit of the fiber sums

Why can the connected result survive when the base weight goes to zero? The answer is already visible in $\widehat{f}_{10}$. As Q_f tends to one, the weights of fibers with increasingly

large degree cease to be small. We need the pole of the entire sum, and its order must compensate for the vanishing base weight.

Fix a, L in the weak electric frame and take $\epsilon \to 0$. Introduce a dimension-four parameter P, the coefficient of the leading base weight. The flat-coordinate relation of the preceding chapter gives

$$T_f = \epsilon w + O(\epsilon^3), \qquad w = \sqrt{2}a, \tag{XI.7.45}$$

$$\frac{Q_b}{Q_f} = \epsilon^4 P, \qquad P = \frac{L^2}{4}, \tag{XI.7.46}$$

$$Q_b = \epsilon^4 P\,[1 + O(\epsilon)], \qquad 1 - Q_f = \epsilon w + O(\epsilon^2). \tag{XI.7.47}$$

In the physical IIA normalization this is $P = C_{\mathrm{IIA}} e^{i\theta_b} \Lambda_{\mathrm{IIA}}^4$, with a fixed finite matching constant C_{IIA}. Thus L^2 already includes the phase if continued to complex scale. We take the positive real branch for the limiting argument. The electric separation w is holomorphic under local continuation, while the mass is $\sqrt{2}|a|$ in the chamber of the W state.

The partition product is often expressed with length β, Coulomb variable a_{IKP} and scale Λ_{IKP}. With $Q_F = e^{-2\beta a_{\mathrm{IKP}}}$ and $Q_B = (\beta \Lambda_{\mathrm{IKP}}/2)^4$, the limiting map is

$$\beta = \epsilon, \qquad a_{\mathrm{IKP}} = \frac{a}{\sqrt{2}}, \qquad \Lambda_{\mathrm{IKP}}^4 = 16P = 4L^2. \tag{XI.7.48}$$

The paths in the two flat coordinates agree to the leading orders in (XI.7.47); they need not agree at finite length. For the continued genus parameter we write $q = e^{\epsilon h}$, so $\lambda = -i\epsilon h$. The parameters $a, w, h, \Lambda_{\mathrm{SW}}$ have mass dimension one and L, u have dimension two. This conversion of genus parameter is independent of the physical ten-dimensional string coupling in ϵ.

Consider a finite truncation of the base-one fiber sum. For each fixed upper limit M, and fixed $w > 0$,

$$\lim_{\epsilon \to 0} \epsilon^2 \sum_{m=0}^{M} 2(m+1) e^{-\epsilon w m} = 0. \tag{XI.7.49}$$

The ϵ^2 here is ϵ^{-2} from converting the prepotential times ϵ^4 from the base. With the entire sum present, the limit instead gives

$$\lim_{\epsilon \to 0} \epsilon^2 \sum_{m \geq 0} 2(m+1) e^{-\epsilon w m} = \lim_{\epsilon \to 0} \frac{2\epsilon^2}{(1 - e^{-\epsilon w})^2} = \frac{2}{w^2}. \tag{XI.7.50}$$

The difference can be seen in the scaled degree of Fig. XI.7.1. The distance between adjacent values of ϵm is ϵ. For a polynomial weight with leading growth m^p the corresponding Riemann sum is

$$\epsilon \sum_{m \geq 0} (\epsilon m)^p e^{-w\epsilon m} \;\longrightarrow\; \int_0^\infty s^p e^{-ws}\, ds = \frac{\Gamma(p+1)}{w^{p+1}}. \tag{XI.7.51}$$

The exponential bounds the large-s tail for $w > 0$. Thus a range of fiber degrees of order ϵ^{-1} contributes even though every fixed finite list of such degrees would miss the pole.

Base two illustrates the same mechanism with a stronger pole. The leading numerator of $\widehat{f}_{20}$ at $x = 1$ is 5 after pulling out $(1-x)^{-6}$. Because $[x^m](1-x)^{-6} = \binom{m+5}{5}$, the signed genus-zero growth is $-m^5/24$. The pole at $x = -1$ gives only an alternating term of order at most m, which does not affect this leading estimate.

It remains to see what happens to the covers. The three nonzero pole orders from (XI.7.44) are

$$p_{10} = 2, \qquad p_{20} = 6, \qquad p_{21} = 8, \qquad p_{dg} = 4d + 2g - 2 \quad \text{for these three labels.} \tag{XI.7.52}$$

Define $\widehat{A}_{dg} = \lim_{x\to 1}(1-x)^{p_{dg}}\widehat{f}_{dg}(x)$. For a fixed positive base degree d and cover r in this calculation, $S_r \simeq (r\epsilon h)^2$ and $1 - x^r \simeq r\epsilon w$. The covered term of the continued logarithm scales as

$$\frac{Q_b^{rd}}{r} S_r^{g-1}\widehat{f}_{dg}(x^r) \;\sim\; \frac{P^{rd}\widehat{A}_{dg}}{r}\frac{(rh)^{2g-2}}{(rw)^{p_{dg}}}\epsilon^{4d(r-1)}. \tag{XI.7.53}$$

The double cover at total base degree two has $d = 1, r = 2$. For its genus-zero piece this expression is $\epsilon^4 P^2/(16h^2w^2)$ to leading order. So it contributes at finite scale but disappears from the 4D coefficient. This power counting concerns fixed labels at positive base degree. The pure-fiber covers at $d = 0$ were instead responsible for the perturbative log.

We can now extract the two prepotential terms. For the sine coefficient the two surviving numerators are $-2, -5$. The field theory result for the rescaled positive-base genus-zero coefficient through order two is

$$\lim_{\epsilon\to 0}\epsilon^{-2}F_0^{+} = -\frac{2P}{w^2} - \frac{5P^2}{w^6} \qquad \text{through } P^2, \tag{XI.7.54}$$

where F_0^{+} means the positive-base part of F_0^{curve}. The limit is taken coefficient by coefficient. We have used (XI.7.47) after extracting the coefficients in the independent flat variables. On the chosen trajectory the extra factor Q_f in Q_b tends to one and cannot change the two leading coefficients.

Multiplying by the common factor fixed from the one-loop log, then inserting $w = \sqrt{2}a$, gives

$$\frac{\pi}{i}\mathcal{F}_{\text{inst}}(a) = -\frac{P}{2a^2} - \frac{5P^2}{16a^6} = -\frac{L^2}{8a^2} - \frac{5L^4}{256a^6}, \tag{XI.7.55}$$

$$\frac{\pi}{i}\tau_{\text{inst}}(a) = -\frac{3L^2}{4a^4} - \frac{105L^4}{128a^8}. \tag{XI.7.56}$$

Here and below these expressions omit orders above two. Each term in $\mathcal{F}_{\text{inst}}$ has mass dimension two and is even in a. Two derivatives at fixed L give the dimensionless coupling terms. In the equivalent continued calculation $\lambda^{-2} = -\epsilon^{-2}h^{-2}$, so one multiplies the h^{-2} coefficient of the connected 4D instanton expansion by $-i/(2\pi)$. The scale and sign are now fixed. The two numbers can be tested against the periods without using them to fix a new parameter.

XI.7.5 How much of the fiber tower survives?

A fixed number of fiber degrees misses the field theory limit. How fast must a cutoff grow to retain a specified part of the result? This question makes the resummation mechanism quantitative. We keep $w > 0$ on the real electric slice and use $x = e^{-\epsilon w}$ for the leading limit. The smooth higher corrections to T_f in (XI.7.47) do not change the limits below. The cutoff is a way to approximate the fiber sum, without interpreting the truncated list as a separate gauge theory.

For base one the finite sum is elementary but instructive. Differentiate the finite geometric series once, or subtract its infinite tail, to obtain

$$\sum_{m=0}^{M} 2(m+1)x^m = \frac{2\{1-(M+2)x^{M+1}+(M+1)x^{M+2}\}}{(1-x)^2}. \tag{XI.7.57}$$

For fixed M, the numerator cancels the pole as $x \to 1$. To retain part of the pole, instead keep a fixed maximum scaled degree. Let $c > 0$ be dimensionless and take

$$M_\epsilon = \left\lfloor \frac{c}{\epsilon w} \right\rfloor, \qquad \epsilon w M_\epsilon \longrightarrow c. \tag{XI.7.58}$$

There are now order ϵ^{-1} terms. Writing the numerator of (XI.7.57) as $1 - x^{M+1}[1 + (M+1)(1-x)]$ makes its limit transparent. Since $x^{M_\epsilon+1} \to e^{-c}$ and $(M_\epsilon+1)(1-x) \to c$, we find

$$\lim_{\epsilon\to 0} \epsilon^2 \sum_{m=0}^{M_\epsilon} 2(m+1)e^{-\epsilon w m} = \frac{2}{w^2}\, R_1(c), \qquad R_1(c) = 1-(1+c)e^{-c}. \tag{XI.7.59}$$

The fraction R_1 tends to zero at $c = 0$ and to one at $c = \infty$. For example, a cutoff at twice the inverse exponential decay scale captures about 59.4% of the base-one limit. It is already much better than a fixed degree cutoff, but it has not saturated the sum.

Base two weights the large degrees more heavily. We can extract this fact exactly from the rational function, rather than estimating a few of its coefficients. With $D = 1 - x$, partial fractions give

$$\widehat{f}_{20}(x) = \frac{5}{D^6} - \frac{5}{D^5} + \frac{1}{4D^4} - \frac{1}{16D^2} - \frac{1}{16D} - \frac{1}{16(1+x)^2} - \frac{1}{16(1+x)}. \tag{XI.7.60}$$

The two poles have different jobs. The pole at $x = 1$ produces an ordinary polynomial in m; the pole at $x = -1$ produces an alternating one. Using the binomial-series coefficients of each term yields the exact expression, for $m \geq 0$,

$$A_m := [x^m]\widehat{f}_{20}(x) = \frac{(m+2)(2m^4+16m^3+40m^2+32m+3)}{48} - \frac{(-1)^m(m+2)}{16}, \tag{XI.7.61}$$

$$A_m = \frac{m^5}{24} + O(m^4). \tag{XI.7.62}$$

For $m = 0, 1, 2$ this gives $0, 6, 32$, as in the direct series. The leading coefficient is $5/5! = 1/24$. Its sine counterpart has the opposite sign. In particular the leading

power is fixed by a sixth-order pole, while its coefficient requires the factorial from the binomial expansion.

Rescale the sum by the base-two genus-zero power ϵ^6. Terms growing as m^4 or less vanish in this limit, and the alternating term vanishes even under an absolute-value bound. For the leading term put $t = \epsilon w m$ in the Riemann sum. The same moving cutoff then gives

$$\lim_{\epsilon\to 0} \epsilon^6 \sum_{m=0}^{M_\epsilon} A_m e^{-\epsilon w m} = \frac{1}{24 w^6} \int_0^c t^5 e^{-t}\, dt = \frac{5}{w^6}\, R_5(c), \tag{XI.7.63}$$

$$R_5(c) = 1 - e^{-c} \sum_{j=0}^{5} \frac{c^j}{j!}. \tag{XI.7.64}$$

Integrating by parts five times gives the last expression. The normalization agrees with the pole numerator 5 because the full integral is $5! = 120$. This verifies the fiber-growth argument independently of taking the rational function directly to $x = 1$.

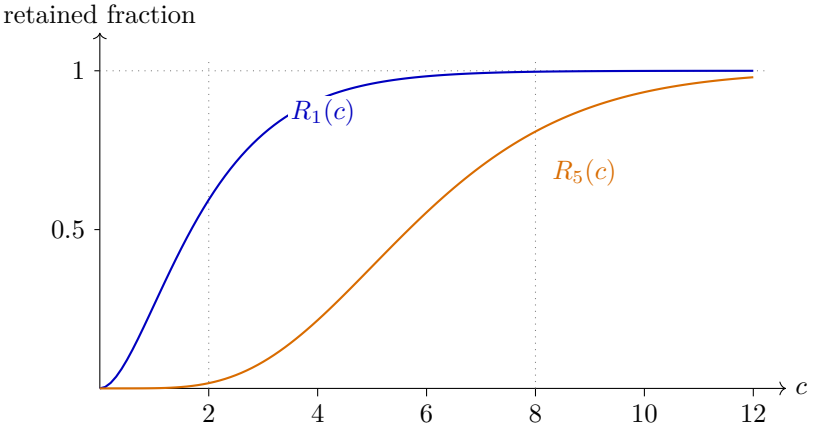


Figure XI.7.3: Fraction of the leading resummed fiber contribution retained by a cutoff $m \le c/(\epsilon w)$ on the positive real slice. The blue curve is the base-one fraction $R_1(c)$ and the orange curve is the base-two fraction $R_5(c)$. The vertical dotted lines mark $c = 2$ and $c = 8$. The stronger degree growth at base two moves the contributing range to larger scaled fiber degree. These are fractions of the continued positive coefficients; the common sine sign cancels in each fraction.

The changed base degree matters even though the same exponential $e^{-\epsilon w m}$ suppresses each term. At $c = 2$ the base-two sum retains only about 1.66%, compared with 59.4% at base one. At $c = 8$ the two fractions are approximately 80.9% and 99.7%, respectively. The dominant densities are te^{-t} and $t^5 e^{-t}$; their maxima occur at $t = 1$ and $t = 5$. A degree range sufficient for one instanton order can therefore be inadequate for the next.

Changing the Coulomb separation also changes the necessary cutoff. Doubling w at fixed ϵ, c halves M_ϵ up to integer rounding while retaining the same limiting fraction. It

simultaneously changes the full coefficients by w^{-2} and w^{-6}. The scaled range and the size of the contribution thus have separate roles. Taking $c \to \infty$ after the moving-cutoff limit recovers the full fiber sums used in the prepotential. Keeping M fixed instead collapses the scaled range to zero and gives the vanishing limits found earlier.

XI.7.6 Checking both orders from the periods

The instanton terms in the prepotential are sensitive to the physical period normalization. A useful comparison is to reconstruct them from the cubic with no worldsheet input. Recall from the preceding chapter the signed electric and magnetic periods of

$$y^2 = (x_{\mathrm{SW}}^2 - L^2)(x_{\mathrm{SW}} - u). \tag{XI.7.65}$$

Here x_{SW} is a cubic coordinate, distinct from the fiber fugacity x used above. The electric period is the integral around the cut $[-L, L]$. Changing variables from x_{SW} to $L\cos\vartheta$ gives

$$a = \sqrt{2u}\left\langle \left(1 - \frac{L}{u}\cos\vartheta\right)^{1/2} \right\rangle, \qquad \langle f \rangle = \frac{1}{2\pi}\int_0^{2\pi} f(\vartheta)\, d\vartheta. \tag{XI.7.66}$$

The normalization here includes both sides of the cut. The average of each odd power of $\cos\vartheta$ vanishes. For the even powers, the constant term of $(e^{i\vartheta} + e^{-i\vartheta})^{2j}/2^{2j}$ gives

$$\langle \cos^{2j}\vartheta \rangle = \frac{1}{4^j}\binom{2j}{j}. \tag{XI.7.67}$$

For $t = L^2/u^2$ the binomial series then yields

$$a = \sqrt{2u}\left(1 - \frac{t}{16} - \frac{15t^2}{1024} + O(t^3)\right). \tag{XI.7.68}$$

In particular, keeping the classical formula $u = a^2/2$ beyond leading order would remove exactly the information needed for the instanton calculation.

To invert the series, put $\xi = L^2/a^4$ and $u = (a^2/2)(1 + b\xi + c\xi^2 + \cdots)$. Then $t = 4\xi - 8b\xi^2 + O(\xi^3)$. Substitution in (XI.7.68) gives

$$1 = 1 + \left(\frac{b}{2} - \frac{1}{4}\right)\xi + \left(\frac{c}{2} - \frac{b^2}{8} + \frac{3b}{8} - \frac{15}{64}\right)\xi^2 + O(\xi^3). \tag{XI.7.69}$$

Thus $b = 1/2$ and $c = 5/32$, giving the electric inverse

$$u = \frac{a^2}{2} + \frac{L^2}{4a^2} + \frac{5L^4}{64a^6} + O(a^2\xi^3). \tag{XI.7.70}$$

To recover the magnetic information we use the same differential equation for both periods. With primes denoting derivatives in u at fixed L, it is

$$(u^2 - L^2)y''_{\mathrm{per}} + \frac{1}{4}y_{\mathrm{per}} = 0, \qquad y_{\mathrm{per}} = a,\ a_D. \tag{XI.7.71}$$

There is no first-derivative term. Consequently the Wronskian $W = aa'_D - a'a_D$ has $W' = aa''_D - a''a_D = 0$. Its constant is determined by the large-u behavior of the signed periods,

$$a \sim \sqrt{2u}, \qquad \frac{a_D}{a} \sim \frac{i}{\pi}\left[\log(8u/L) - 2\right], \qquad W = a^2 \frac{d}{du}(a_D/a) = \frac{2i}{\pi}. \tag{XI.7.72}$$

This is the one place where the ratio of periods is useful. The physical coupling itself is the derivative ratio a'_D/a', since the derivative follows a change of the electric period.

Converting the Wronskian to an a derivative gives the prepotential directly. Use $a_D = \partial_a \mathcal{F}_{\rm SW}$ to obtain

$$a\,\partial_a a_D - a_D = W\,\partial_a u, \tag{XI.7.73}$$

$$\frac{d}{da}\big(a\partial_a \mathcal{F}_{\rm SW} - 2\mathcal{F}_{\rm SW}\big) = \frac{2i}{\pi}\,\partial_a u. \tag{XI.7.74}$$

After integration, the Euler derivative of $\mathcal{F}_{\rm SW}$ is $(2i/\pi)u$ up to an a-independent constant. The homogeneous quadratic term is part of the separately fixed perturbative frame. At order k, the Euler operator acts as

$$(a\partial_a - 2)a^{2-4k} = -4k\,a^{2-4k}. \tag{XI.7.75}$$

Using (XI.7.70), we find the two reduced prepotential coefficients

$$\frac{2(1/4)}{-4} = -\frac{1}{8}, \qquad \frac{2(5/64)}{-8} = -\frac{5}{256}. \tag{XI.7.76}$$

These multiply L^2/a^2 and L^4/a^6 in units i/π. This reconstruction uses two different kinds of information. The electric inverse gives the coefficients of $u(a)$, while the Wronskian fixes how u enters the Euler derivative. If the electric inverse is known but the period normalization is not fixed, the same two coefficients alone do not set the overall prepotential unit.

The integration constants also have distinct effects. Define $\widetilde{\mathcal{F}} = (\pi/i)\mathcal{F}_{\rm SW}$. The integrated equation reads

$$(a\partial_a - 2)\widetilde{\mathcal{F}} = 2u + C(L). \tag{XI.7.77}$$

An a-independent term $-C(L)/2$ is a particular solution for the last term and has no electric derivative. The homogeneous solution is $c(L)a^2$, which changes both a_D and the constant part of τ. Its coefficient is already determined by choosing the signed period frame and perturbative subtraction. At the inverse powers a^{-2}, a^{-6} used here the Euler eigenvalues are nonzero, so neither ambiguity changes the instanton coefficients. The reconstructed coefficients agree with (XI.7.55), including the relative and overall signs. As a check on the perturbative part, the leading $u = a^2/2$ gives $(i/\pi)a^2\log(a/\mu)$ plus a quadratic term, with the logarithmic slope used in (XI.7.25). The agreement concerns the first two orders of the protected weak-coupling expansion in this frame.

The parameter controlling the relative size of the two terms is $\xi = L^2/a^4$. It is useful to compare this suppression before and after taking electric derivatives. Denote the displayed one- and two-instanton parts by subscripts $1, 2$. Their ratios are

$$\frac{\mathcal{F}_2}{\mathcal{F}_1} = \frac{5}{32}\xi, \qquad \frac{\tau_2}{\tau_1} = \frac{35}{32}\xi. \tag{XI.7.78}$$

The second ratio is seven times larger: two derivatives weight the higher inverse power of a more strongly. For a changed input, choose a reference mass μ, $L = 2\mu^2$ and $a = 2\mu$. Then $\xi = 1/4$, and the magnitudes of the two ratios are $5/128$ and $35/128$. These numbers compare the retained terms, rather than estimating the uncomputed remainder. Moving to $a = 4\mu$ at the same scale divides both ratios by sixteen. This change gives a direct weak-coupling test of the Coulomb dependence on which the comparison rests.

XI.7.7 Higher genus and the GV trace

The connected partition function contains coefficients besides the prepotential. To see one explicitly, keep the continued parameter h finite while taking the field theory limit of the Young-diagram product. This reverses the order of the small-genus-parameter expansion and the limit used above. At either base order considered here, a diagram pair of total size k has k hooks. Each hook contributes a factor proportional to ϵ^{-2}. In the cross factors,

$$S_j \sim (j\epsilon h)^2, \qquad 1 - q^\ell x \sim \epsilon(w - \ell h), \qquad \sum_\ell C_\ell(R,U) = |R| + |U| = k. \quad \text{(XI.7.79)}$$

The last equality follows from the content polynomial at $q = 1$. The cross factors give another ϵ^{-2k}, and together the two factors cancel $Q_b^k \sim \epsilon^{4k} P^k$. We exclude the poles $h = 0, w = \pm h$ when evaluating the order-two rational functions. The later Laurent expansion is around $h = 0$ at fixed $w \neq 0$.

Write the reduced limit as $1 + Pz_1 + P^2 z_2 + \cdots$. Applying (XI.7.79) to the two terms of (XI.7.32) gives

$$z_1 = \frac{2}{h^2 w^2}, \quad \text{(XI.7.80)}$$

$$z_2 = \frac{1}{2h^4 w^2}\left[\frac{1}{(w-h)^2} + \frac{1}{(w+h)^2}\right] + \frac{1}{h^4(w^2-h^2)^2}. \quad \text{(XI.7.81)}$$

For instance, the factor $1/2$ in the first term is the product of the two equivalent orderings and the inverse square of the hook length two. The two signs of the shift come from the row and column. Without the logarithm, the h^{-4} term would be the leading singularity of z_2. Taking the connected coefficient gives instead

$$z_2 - \frac{1}{2}z_1^2 = \frac{5w^2 - 2h^2}{h^2 w^4 (w^2 - h^2)^2} \quad \text{(XI.7.82)}$$

$$= \frac{5}{h^2 w^6} + \frac{8}{w^8} + O(h^2). \quad \text{(XI.7.83)}$$

After restoring P^2, the pole is the continued prepotential coefficient from (XI.7.54). The constant agrees with the leading numerator 8 of $\widehat{f}_{21}$, divided by w^8. The cancellation can also be displayed as an expansion in $v = h^2/w^2$:

$$z_2 - \frac{1}{2}z_1^2 = \frac{1}{h^2 w^6}\frac{5 - 2v}{(1-v)^2}, \qquad (5-2v)(1 + 2v + O(v^2)) = 5 + 8v + O(v^2). \quad \text{(XI.7.84)}$$

The h^{-4} behavior of the unconnected product has disappeared before the coefficients are interpreted. For example, changing w from 2 to 3 in a common mass unit changes the h^{-2} coefficient from $5/64$ to $5/729$, while the constant changes from $1/32$ to $8/6561$. The two changes follow different powers of w and cannot be absorbed in a common shift of the rigid coupling.

This agreement of the constant terms requires the limit. At finite ϵ the continued genus-zero kernel itself has an h^0 term,

$$\frac{1}{S_1} = \frac{1}{\epsilon^2 h^2} - \frac{1}{12} + O(\epsilon^2 h^2). \tag{XI.7.85}$$

It contributes to the genus expansion but is not a genus-one GV label. At positive base degree two this particular constant, multiplied by Q_b^2 and the genus-zero fiber pole, is $O(\epsilon^2)$ and drops out. In the resulting protected amplitude the h^0 term belongs to the genus-one sector. With the gravitational background included it contributes to a curvature-squared coupling. It does not alter the two-derivative prepotential of the flat rigid theory. The distinction is between two coefficients of one connected function, with different physical uses.

The fact that GV invariants are protected also limits the spectral information they retain. Consider a massive short sector at fixed charge in the wrapped-brane interpretation. Its 5D little group has two spin labels, j_L, j_R. Strip the universal left short factor $I_1 = 2[0] + [1/2]$, of ordinary dimension four. The GV trace retains the left representation after weighting each right spin by its signed dimension:

$$\sum_{j_L, j_R} N_{j_L, j_R}(j_L, j_R) \;\longmapsto\; \sum_{j_L, j_R} (-1)^{2j_R}(2j_R + 1) N_{j_L, j_R}[j_L]. \tag{XI.7.86}$$

For example, the reduced representation $2(0,0) \oplus (0, \frac{1}{2})$ has two right singlets and one right doublet. Their contributions to the trace cancel,

$$\mathrm{ind}_R = 2[0] - 2[0] = 0, \qquad \dim_{\mathrm{red}} = 2 + 2 = 4, \qquad \dim(I_1 \otimes \mathrm{red}) = 16. \tag{XI.7.87}$$

This is a representation example, not an assertion that this collection occurs in the local geometry. It shows why a signed invariant cannot recover all the multiplicities even within a short sector. In fact one can add any number of copies of this trace-zero reduced representation without changing the left representation retained by the trace. Even a nonzero index therefore has the same ambiguity. The two inventories

$$(0,0), \qquad 3(0,0) \oplus (0, \tfrac{1}{2}) \tag{XI.7.88}$$

both give [0] after the right-spin trace, while their ordinary reduced dimensions are 1 and 5. Restoring I_1 gives 4 and 20 states. The difference is already invisible at fixed charge before addressing any change of stability chamber. The example concerns representations, rather than an asserted inventory of this geometry. Nor does the trace determine which 4D particles are stable in a chamber. In this chapter it organizes a definite protected calculation. The finite-radius theory and general instanton localization require further input.

XI.7.8 A single base wrapping with two fibers

What changes when the shrinking fiber has two simple roots? The rank-one calculation suggests summing the fiber degrees at fixed base wrapping. For an A_2 fibration, however, there are three positive roots. The sphere associated with the sum of the simple roots must contribute along with the two simple-root spheres. We will calculate one base wrapping for this geometry and follow it to a prepotential with two independent electric variables.

Take the resolved A_2 surface fibered over the base sphere in the triangular toric geometry with compact divisors F_2, F_4. Denote the fiber classes by F_1, F_2 and their flat fugacities by x_f, y_f. The three positive-root classes and their weights are

$$F_1, \quad F_2, \quad F_1 + F_2, \qquad Q_{12} = x_f, \quad Q_{23} = y_f, \quad Q_{13} = x_f y_f. \tag{XI.7.89}$$

Here F_2 as a curve class is distinguished from the Hirzebruch surface by context. Write $Q_B = e^{-T_B}$ for the flat base fugacity. The protected engineering dictionary identifies its exponent with instanton order in the rigid pure-$SU(3)$ sector. The isolation of this sector is still an assumption about the full compactification.

Use $q_{\rm top} = e^{i\lambda}$ for the topological fugacity, reserving q below for the scale in the genus-two curve. For the empty pair of partitions define

$$K_{\varnothing\varnothing}(Q; q_{\rm top}) = \exp\left(\sum_{r\geq 1} \frac{Q^r}{r S_r}\right), \qquad S_r = (q_{\rm top}^{r/2} - q_{\rm top}^{-r/2})^2. \tag{XI.7.90}$$

The partition function separates into a pure-fiber factor and a base expansion,

$$\begin{aligned} Z &= Z_{\rm fib}\widehat{Z}, \qquad \widehat{Z} = 1 + Q_B Z_1 + O(Q_B^2), \\ Z_{\rm fib} &= K_{\varnothing\varnothing}(x_f; q_{\rm top})^2 K_{\varnothing\varnothing}(y_f; q_{\rm top})^2 K_{\varnothing\varnothing}(x_f y_f; q_{\rm top})^2. \end{aligned} \tag{XI.7.91}$$

The three factors correspond to the three roots in (XI.7.89). They depend on the Coulomb variables even though they have no base degree. Consequently $[Q_B]\log Z = Z_1$, but removing $Z_{\rm fib}$ also removes a perturbative coupling.

The fiber-resummed product is a sum over three partitions. Using the hook weights W_R and content coefficients C_ℓ defined in the rank-one calculation, and writing R^T for the transposed Young diagram, its form is

$$\widehat{Z} = \sum_{R_1,R_2,R_3} \frac{\displaystyle\prod_{i=1}^{3} Q_{b_i}^{|R_i|} W_{R_i}(q_{\rm top})^2\, (-1)^{\sum_i \alpha_i |R_i|} q_{\rm top}^{\frac{1}{2}\sum_i \alpha_i \kappa_{R_i}}}{\displaystyle\prod_{i<j}\prod_{\ell} (1 - q_{\rm top}^{\ell} Q_{ij})^{2C_\ell(R_i, R_j^T)}}, \quad (\alpha_1,\alpha_2,\alpha_3) = (4,2,0). \tag{XI.7.92}$$

The base classes in this fibration are

$$Q_{b_1} = Q_B x_f^4 y_f^2, \qquad Q_{b_2} = Q_B y_f^2, \qquad Q_{b_3} = Q_B. \tag{XI.7.93}$$

These are the geometric input to the calculation, including the indicated framing. We use the resummed product rather than deriving the general topological vertex. Its dependence on all fiber wrappings is essential to the limit.

At total size one there are just three terms. A single box has one hook of length one, zero content and zero κ, hence

$$W_{\square}^2 = \frac{1}{S_1}, \qquad S_1 = (q_{\mathrm{top}}^{1/2} - q_{\mathrm{top}}^{-1/2})^2, \qquad C_\ell(\square, \varnothing) = \delta_{\ell 0}, \qquad C_\ell(\varnothing, \varnothing) = 0. \tag{XI.7.94}$$

An occupied position i couples to the other two positions through the two corresponding root curves. Figure XI.7.4 displays these pairings. All three framing signs are positive. Substituting the box in turn at each position gives

$$S_1 Z_1 = f_3(x_f, y_f) = \frac{x_f^4 y_f^2}{(1-x_f)^2(1-x_f y_f)^2} + \frac{y_f^2}{(1-x_f)^2(1-y_f)^2} \tag{XI.7.95}$$

$$+ \frac{1}{(1-y_f)^2(1-x_f y_f)^2}. \tag{XI.7.96}$$

For example, the first term sees both F_1 and $F_1 + F_2$, while the middle term sees the two simple-root curves. Dropping the third positive root would change the first and third denominators. It would change the Coulomb function, rather than merely its constant normalization.

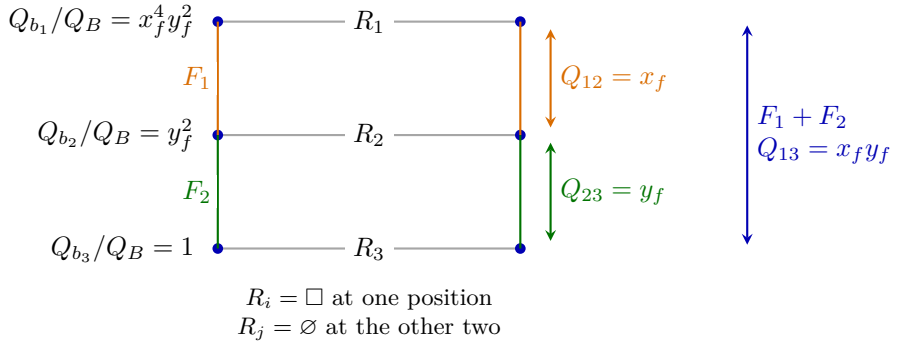


Figure XI.7.4: Three partition positions in the normalized A_2-fibration product. A single box at position i couples to each other position j through the root class shown at the right. The weights at the left are the corresponding base classes divided by Q_B. Only one box is placed at a time. The drawing records the root pairings; the external slopes of the full toric web are omitted.

There is no positive-base covering subtraction at this order: $rd = 1$ forces $r = d = 1$. There is also no disconnected subtraction, since the linear coefficient of the logarithm is Z_1. In the sine convention the genus-zero fiber function is therefore $-f_3$. The box product has no additional dependence on q_{top} after multiplication by S_1, so the primitive functions with higher genus label vanish at this base order. The higher powers in the sine kernel itself remain distinct from such labels.

XI.7.9 The higher-rank rational function

How do two infinite fiber sums become one instanton coefficient? Work first in a real weak electric patch with $E_1 < E_2 < E_3$ and $E_1 + E_2 + E_3 = 0$. The two simple-root gaps are $d_1 = E_2 - E_1$ and $d_2 = E_3 - E_2$. Along the rigid trajectory set

$$x_f = e^{-\beta d_1}, \qquad y_f = e^{-\beta d_2}, \qquad Q_B = \beta^6 K_{\mathrm{geo}} + o(\beta^6), \qquad q_{\mathrm{top}} = e^{\beta h}. \tag{XI.7.97}$$

The parameter β has inverse-mass dimension. It need not be identified numerically with the ϵ of the earlier local-F_0 chart. Here $[E_i] = [h] = 1$ and $[K_{\mathrm{geo}}] = 6$. The flat base coordinate is still independent of the algebraic coefficient z_b of a mirror polynomial.

Each denominator $1 - e^{-\beta d}$ gives βd at leading order. The fiber monomials in the numerators of (XI.7.96) tend to one. Thus

$$\lim_{\beta\to 0} \beta^4 f_3(e^{-\beta d_1}, e^{-\beta d_2}) = \frac{1}{d_1^2 d_2^2} + \frac{1}{d_2^2 (d_1+d_2)^2} + \frac{1}{d_1^2 (d_1+d_2)^2} \equiv R. \tag{XI.7.98}$$

A change of fibration gives a useful second example. The F_0, F_2 fibration has instead

$$f_1(x_f, y_f) = \frac{1}{(1-x_f)^2(1-y_f)^2} + \frac{1}{(1-y_f)^2(1-x_f y_f)^2} + \frac{x_f^2}{(1-x_f)^2(1-x_f y_f)^2}. \tag{XI.7.99}$$

Its finite fiber series differs from f_3, but its scaled limit is the same R. We can see which fiber degrees make this possible without expanding a long list of classes.

Write $c_{nm} = [x_f^n y_f^m] f_1$. Expanding each squared geometric denominator gives the exact expression

$$c_{nm} = (n+1)(m+1) + \mathbf{1}_{m\geq n}(n+1)(m-n+1) + \mathbf{1}_{n\geq m+2}(m+1)(n-m-1). \tag{XI.7.100}$$

For instance $c_{0,0} = 2$, $c_{1,0} = 2$, and $c_{0,1} = 4$. The finite expression is sensitive to the chosen simple-root chart and the shifts in the base classes. Put $N = \beta n$, $M = \beta m$. Away from the separating diagonal the leading degree growth becomes

$$\beta^2 c_{nm} \;\longrightarrow\; \rho(N,M) = NM + \mathbf{1}_{M\geq N} N(M-N) + \mathbf{1}_{N\geq M} M(N-M). \tag{XI.7.101}$$

The finite shifts in f_3 have the same leading density. The two sums provide another β^{-2} from their mesh, explaining the fourth-order fiber pole.

The three terms in this density have separate geometric origins. On the first triangular region use $M = N + t$; on the second use $N = M + t$. Their Laplace integrals are

$$\int_0^\infty dN \int_0^\infty dM\, NM e^{-d_1 N - d_2 M} = \frac{1}{d_1^2 d_2^2}, \tag{XI.7.102}$$

$$\int_0^\infty dN \int_0^\infty dt\, N t e^{-(d_1+d_2)N - d_2 t} = \frac{1}{(d_1+d_2)^2 d_2^2}, \tag{XI.7.103}$$

$$\int_0^\infty dM \int_0^\infty dt\, M t e^{-(d_1+d_2)M - d_1 t} = \frac{1}{(d_1+d_2)^2 d_1^2}. \tag{XI.7.104}$$

Each integral factors into two copies of $\int_0^\infty te^{-dt}\,dt = d^{-2}$. Their sum reproduces (XI.7.98). In particular, the two triangular regions retain the mixed-root gap $d_1 + d_2$ even though there are only two independent fiber degrees.

There is a simpler way to express the answer after the limit. Introduce the invariants of the exact electric periods,

$$u_E = \frac{1}{2}\sum_i E_i^2, \qquad v_E = E_1E_2E_3, \qquad \Delta_E = \prod_{i<j}(E_i - E_j)^2 = 4u_E^3 - 27v_E^2. \tag{XI.7.105}$$

Putting the three terms over this common denominator, their numerators sum to $\sum_{i<j}(E_i - E_j)^2 = 6u_E$. Therefore

$$R(E) = \sum_{i=1}^{3} \frac{1}{\prod_{j\neq i}(E_i - E_j)^2} = \frac{6u_E}{\Delta_E}. \tag{XI.7.106}$$

The result is Weyl invariant and has mass degree -4. At the prescribed electric input $E = (-2, -1, 3)\mu$, one has $u_E = 7\mu^2$, $v_E = 6\mu^3$ and $\Delta_E = 400\mu^6$, hence $R = 21/(200\mu^4)$. The polynomial Δ_E is an electric Vandermonde, not the quantum discriminant of the genus-two curve. Its poles indicate the failure of the weak expansion as electric gaps close.

Since $S_1 \sim \beta^2 h^2$, the factors in the one-base term combine as

$$Q_B Z_1 \longrightarrow \frac{K_{\mathrm{geo}}}{h^2} R(E), \qquad \beta^{-2} F_{0,\mathrm{inst}}^{\mathrm{sine}} \longrightarrow -K_{\mathrm{geo}} R(E). \tag{XI.7.107}$$

To fix the physical prepotential unit, return to the pure-fiber factor. One root contributes $G_\beta(d) = -2\beta^{-2}\,\mathrm{Li}_3(e^{-\beta d})$. Its raw limit diverges. At the level of the coupling, the perturbative subtraction is explicit,

$$G_\beta''(d) = 2\log(1 - e^{-\beta d}), \qquad G_\beta''(d) - 2\log(\beta\mu) \longrightarrow 2\log(d/\mu). \tag{XI.7.108}$$

A third derivative removes this quadratic ambiguity before taking the limit,

$$G_\beta'''(d) = \frac{2\beta}{e^{\beta d} - 1} \longrightarrow \frac{2}{d}, \qquad \frac{d^3}{dd^3}\left[\frac{i}{4\pi} d^2 \log\frac{d^2}{\mu^2}\right] = \frac{i}{\pi d}. \tag{XI.7.109}$$

The sourced positive-root one-loop prepotential fixes the common conversion to $i/(2\pi)$ times the rescaled sine amplitude. Applying it to (XI.7.107), before any scale comparison with periods, gives

$$\mathcal{F}_{\mathrm{geo},1} = \frac{K_{\mathrm{geo}}}{2\pi i} R(E). \tag{XI.7.110}$$

The perturbative quadratic frame must still be fixed by the periods. It cannot change this inverse-power term at a fixed instanton scale.

XI.7.10 Reconstructing the coefficient from genus-two periods

Can the Coulomb function be found without the fiber product? Recall the genus-two family and eigenvalue-period convention of the preceding chapter,

$$P(X) = X^3 - uX - v, \qquad y^2 = P(X)^2 - q, \qquad \lambda = \frac{XP'(X)}{2\pi i y}\,dX, \qquad q = \Lambda_3^6. \tag{XI.7.111}$$

The spectral coordinate X is distinct from x_f. Let e_i be the three distinct roots of P and orient the small electric contours so that $E_i \to e_i$ as $q \to 0$. On a contour where $|q/P^2| < 1$, the expansion of the differential is

$$\lambda = \frac{XP'}{2\pi i P}\,dX + \frac{q}{4\pi i}\frac{XP'}{P^3}\,dX + O(q^2). \tag{XI.7.112}$$

The leading residue is e_i. For the correction, integration of $d(X/P^2)$ around the contour vanishes, so

$$\delta_i \equiv [q]E_i = \frac{1}{2}\,\mathrm{Res}_{e_i}\,\frac{XP'}{P^3} = \frac{1}{4}\,\mathrm{Res}_{e_i}\,\frac{1}{P^2} = -\frac{P''(e_i)}{4P'(e_i)^3}. \tag{XI.7.113}$$

The last step follows by putting $X = e_i + \xi$ and expanding $P = P'(e_i)\xi + P''(e_i)\xi^2/2 + \cdots$. The residue of P^{-2} is $-P''(e_i)/P'(e_i)^3$.

To invert the invariant u, two residue identities suffice. At infinity, P^{-2} has no X^{-1} coefficient, so the sum of its finite residues vanishes. Similarly X/P^2 has no residue at infinity. Expressing its residue near e_i gives

$$\sum_i \delta_i = 0, \qquad \sum_i \left[\frac{1}{P'(e_i)^2} - \frac{e_i P''(e_i)}{P'(e_i)^3}\right] = 0, \qquad \sum_i e_i\delta_i = -\frac{1}{4}R(e). \tag{XI.7.114}$$

Since $u = \frac{1}{2}\sum_i e_i^2$, the quadratic invariant of the exact electric periods is $u_E = u - qR(e)/4 + O(q^2)$. Replacing e by E inside the already order-q term therefore yields

$$u = u_E + \frac{q}{4}R(E) + O(q^2). \tag{XI.7.115}$$

For example, with $(u, v) = (7, 6)$ in common mass units, the classical roots are $(-2, -1, 3)$. The correction vector is

$$E = e + q\left(\frac{3}{125}, -\frac{3}{128}, -\frac{9}{16000}\right) + O(q^2). \tag{XI.7.116}$$

At $q = .01$, direct integration gives $E = (-1.9997595521, -1.0002348229, 2.9999943749)$. The sum stays zero. Substituting these periods in (XI.7.115) reconstructs $u = 7$ with an error of order q^2, rather than treating the classical roots as exact electric coordinates.

Recovering the prepotential also requires magnetic information. A higher-rank replacement for the rank-one Wronskian is the special-geometry residue identity at the two infinities. Let $\lambda_{\mathrm{n}} = 2\pi i\lambda = X\,d\log(P + y)$ be the native differential, and write

$$\mathcal{D} = E_1\partial_{E_1} + E_2\partial_{E_2} - 2. \tag{XI.7.117}$$

In the canonical period frame this identity is

$$\mathcal{D}\mathcal{F} = -\frac{1}{2\pi i}\sum_{\sigma=\pm}\mathrm{Res}_{\infty_\sigma}(\zeta_\sigma\lambda_{\mathrm{n}})\,\mathrm{Res}_{\infty_\sigma}(\zeta_\sigma^{-1}\lambda_{\mathrm{n}}). \tag{XI.7.118}$$

We use the special-geometry identity as an input and evaluate its residues in this family. It supplies information about the prepotential beyond the electric inversion alone.

Set $w = P + y$, so the exact curve relation is $2P = w + q/w$. At the two infinities take $w = \zeta_+^{-3}$ and $w = \zeta_-^3$, respectively. To invert X, insert $X = c/\zeta + d\zeta + \cdots$. The coefficients of ζ^{-3} and ζ^{-1} give

$$2c_+^3 = 1, \qquad 2c_-^3 = q, \qquad 6c_\pm^2 d_\pm - 2uc_\pm = 0, \qquad d_\pm = \frac{u}{3c_\pm}. \tag{XI.7.119}$$

On the first sheet $\lambda_{\mathrm{n}} = -3X\,d\zeta_+/\zeta_+$, while on the second it is $+3X\,d\zeta_-/\zeta_-$. Each product of residues is consequently $9c_\pm d_\pm = 3u$, with the two signs canceling within the product. Thus

$$\mathcal{D}\mathcal{F} = -\frac{6u}{2\pi i} = \frac{3i}{\pi}u. \tag{XI.7.120}$$

The formal instanton expansion has $\mathcal{F}_{\mathrm{inst}} = \sum_{k\geq 1} q^k f_k(E)$ with total mass degree two. Because $[q] = 6$, f_1 has degree -4 in E, and $\mathcal{D}f_1 = -6f_1$. Inserting (XI.7.115) then determines the first instanton term,

$$-6\mathcal{F}_{\mathrm{curve},1} = \frac{3iq}{4\pi}R(E), \qquad \mathcal{F}_{\mathrm{curve},1} = \frac{q}{8\pi i}R(E) = \frac{3qu_E}{4\pi i\Delta_E}. \tag{XI.7.121}$$

The dimensional and formal-expansion hypotheses exclude a quadratic homogeneous term from this instanton coefficient. Such a term belongs to the separately specified perturbative frame.

Equations (XI.7.110) and (XI.7.121) give the same function of both electric periods. Their overall scale agrees if we choose

$$q = 4K_{\mathrm{geo}}. \tag{XI.7.122}$$

This is one instanton-scale matching choice made using the computed coefficient. The resulting scalar agreement is not an additional independent test. The functional Coulomb dependence, its derivatives and its heavy-root reduction remain nontrivial comparisons. In particular (XI.7.122) is not derived from an exact flat mirror map or from identifying Q_B with the algebraic z_b. The finite physical threshold relating the local sector to a chosen ultraviolet completion remains to be fixed in that completion.

XI.7.11 Two coupling responses and a heavy eigenvalue

The rank-two prepotential predicts a matrix rather than a single coupling. Take the independent electric coordinates to be $a = E_1$, $b = E_2$, with $E_3 = -a - b$, and differentiate at fixed q. The instanton correction is

$$\delta\tau_{ij} = \frac{q}{8\pi i}\,\partial_{E_i}\partial_{E_j}R(E_1, E_2, -E_1 - E_2), \qquad i, j = 1, 2. \tag{XI.7.123}$$

At $E = (-2, -1, 3)\mu$ this yields the explicit response

$$\mathrm{Hess}_{a,b} R = \frac{1}{\mu^6} \begin{pmatrix} 37407/40000 & -10257/20000 \\ -10257/20000 & 4107/10000 \end{pmatrix}. \tag{XI.7.124}$$

The mixed response is nonzero. It expresses the fact that changing one independent electric period also changes the third eigenvalue and the mixed-root gap. At fixed q, doubling all three electric periods divides R by sixteen and the response matrix by sixty-four. A value of R at a single point would not determine this response; derivatives must be taken before substituting the chosen input. Nor should positivity of the complete kinetic term be tested on its isolated instanton correction.

There is a direct magnetic check of this matrix. Recall that the moduli derivatives of the differential, modulo exact forms, are

$$\partial_u \lambda \simeq \frac{X\, dX}{2\pi i y}, \qquad \partial_v \lambda \simeq \frac{dX}{2\pi i y}. \tag{XI.7.125}$$

Integrating these two holomorphic forms along both electric and both canonical magnetic cycles gives the Jacobians J and D, hence $\tau_{\mathrm{ex}} = DJ^{-1}$. These integrals use neither the fiber product nor the residue identity (XI.7.118). To compare inverse-power terms without fitting a constant coupling, subtract the known one-loop Hessian in the same frame. On a positive real q patch define

$$\mathcal{F}_{1-\mathrm{loop}}(E; q) = \frac{i}{4\pi} \sum_{i<j} (E_i - E_j)^2 \log \frac{(E_i - E_j)^2}{q^{1/3}}, \tag{XI.7.126}$$

$$T(q) = \tau_{\mathrm{ex}}(u, v; q) - \mathrm{Hess}_{E_1, E_2} \mathcal{F}_{1-\mathrm{loop}}(E(q); q). \tag{XI.7.127}$$

The unspecified constant quadratic frame contributes the same constant matrix C to $T(q)$. The predicted difference between two values is therefore

$$T(q_1) - T(q_2) = \frac{1}{8\pi i} \left[q_1 \,\mathrm{Hess}\, R(E(q_1)) - q_2 \,\mathrm{Hess}\, R(E(q_2)) \right] + O(q_1^2) + O(q_2^2). \tag{XI.7.128}$$

The exact electric coordinates change with q even when u, v are kept fixed; the right hand side uses their actual values.

For an observed matrix difference $\mathcal{O} = T(q_1) - T(q_2)$ and its leading prediction $\mathcal{P}$ in (XI.7.128), the relative error is $\|\mathcal{O} - \mathcal{P}\|_{\mathrm{F}} / \|\mathcal{P}\|_{\mathrm{F}}$. We use the Frobenius norm $\|M\|_{\mathrm{F}}^2 = \sum_{ij} |M_{ij}|^2$; the absolute remainder is the numerator $\|\mathcal{O} - \mathcal{P}\|_{\mathrm{F}}$.

For the example $(u, v) = (7, 6)$, integrate around the three small cuts and through the two intervening gaps, then form J, D in the canonical frame. At $q = 0.01$, 0.0025 and 0.000625, the successive matrix differences agree with the displayed first-instanton prediction to relative errors 0.0026853 and 0.00066885. The absolute remainder decreases by a factor 16.0871 when both q values are divided by four. This is the expected quadratic remainder, while reversing the predicted sign fails already at leading order. It tests the response normalization within the curve convention independently of the geometric scale choice.

Finally make one eigenvalue heavy while retaining a pair. To avoid changing the meaning of the independent a, b above, write this new parametrization as

$$(E_1, E_2, E_3) = (A + \mathfrak{b}, A - \mathfrak{b}, -2A), \qquad |A| \longrightarrow \infty, \qquad \mathfrak{b} \neq 0 \text{ fixed}. \tag{XI.7.129}$$

The root function becomes

$$R_3 = \frac{1}{4\mathfrak{b}^2(3A+\mathfrak{b})^2} + \frac{1}{4\mathfrak{b}^2(3A-\mathfrak{b})^2} + \frac{1}{(3A+\mathfrak{b})^2(3A-\mathfrak{b})^2} \tag{XI.7.130}$$

$$= \frac{3(3A^2+\mathfrak{b}^2)}{2\mathfrak{b}^2(9A^2-\mathfrak{b}^2)^2}, \qquad 9A^2R_3 \longrightarrow R_2 = \frac{1}{2\mathfrak{b}^2}. \tag{XI.7.131}$$

The last summand, involving only the heavy gaps, vanishes faster than the two terms coupling the retained pair to the heavy eigenvalue. Their leading contributions add to the rank-one root function.

The scale that must accompany this limit follows from the curve. Write

$$P(X) = (X+2A)\big((X-A)^2-U\big), \qquad X = A+Z, \quad y = 3AY, \quad q_3 = 9A^2q_2. \tag{XI.7.132}$$

Its equation becomes

$$Y^2 = \left(1+\frac{Z}{3A}\right)^2 (Z^2-U)^2 - q_2 \longrightarrow (Z^2-U)^2 - q_2. \tag{XI.7.133}$$

The retained primitive rank-one electric period is $\mathfrak{b}$, with $\mathfrak{b} \to \sqrt{U}$ at weak coupling; U is not set to its classical value beyond leading order. Write $K_3 = K_{\mathrm{geo}}$ for the rank-two flat-base scale coefficient and K_2 for the retained rank-one flat-base scale coefficient. Combining the scale and root-function limits gives

$$\mathcal{F}_{3,1} = \frac{q_3R_3}{8\pi i} \longrightarrow \frac{q_2}{16\pi i\mathfrak{b}^2}, \qquad K_2 = \frac{K_3}{9A^2}, \qquad \mathcal{F}_{\mathrm{geo},2,1} = \frac{K_2}{4\pi i\mathfrak{b}^2}. \tag{XI.7.134}$$

Thus the single scale choice $q = 4K_{\mathrm{geo}}$ is preserved by the reduction. The spectator photon remains separate from this rank-one sector. The primitive period $\mathfrak{b}$ is not the original cubic period a used earlier in the chapter. The preceding chapter derives the differential and cycle conversion, with the electric root difference $2\mathfrak{b}$ tending to that original a and the right-to-left gap carrying the opposite original magnetic orientation. Keeping the primitive frame here makes the rank-two to rank-one comparison explicit without changing the earlier local-F_0 formulas. The limit concerns this protected local sector; isolation from the remaining compactification modes is the additional assumption already stated.

Exercises

Give the requested entries as exact integers or fractions, in the specified order. Explain your reasoning separately.

1. An order-three cover is applied to class $2B + 5F$. Find its total base and fiber degrees. Now consider the separate term with $d = 1, r = 2, g = 0$. What power of ϵ suppresses it in the local limit? Finally, for fixed positive w, evaluate $\lim_{\epsilon\to 0} \epsilon^2 \sum_{m=0}^{3} 2(m+1)e^{-\epsilon w m}$. Report the four answers in that order. Explain why the last answer changes if the full fiber sum is performed first, and why knowing the total base degree does not determine how the contribution arose.

2. Let $Z = 7e^{5x}(1+3y+7y^2)$ with independent variables x, y and y the base fugacity. Find the y, y^2 coefficients of $\log(Z/Z|_{y=0})$, then compute $\partial_x \log Z|_{y=0}$. Finally, divide the normalized Z by e^{2y} and find the new linear coefficient of its logarithm. Report those four entries in order. Explain why a factor can be removable for the instanton calculation and still contribute to a derivative with respect to the fiber variable.

3. Strip P^2 from the continued 4D base-two connected term and set $w = 2$ in a fixed mass unit. Find the coefficients of h^{-2} and h^0, in that order. Explain which coefficient enters the rigid prepotential and why a finite-ϵ term of order h^0 need not have genus-one GV label.

4. Compare two reduced short representations at fixed charge, $A = (0,0)$ and $B = 3(0,0) \oplus (0,\frac{1}{2})$, with left spin written first. Compute the two coefficients of $[0]$ in the right-spin trace, the two ordinary reduced dimensions, and the two ordinary dimensions after restoring I_1. Report the six entries in that order, taking A first in each pair. Explain what information the trace loses and why it does not determine a 4D stability chamber.

5. Use $P = L^2/4$ as the expansion variable and evaluate at $a = 2$ in a fixed mass unit. Find the coefficients of P, P^2 in $(\pi/i)\mathcal{F}_{\text{inst}}$, followed by the coefficients of P, P^2 in $(\pi/i)\tau_{\text{inst}}$. Differentiate before setting $a = 2$, keeping P fixed. Explain why using a_D/a in place of the coupling, or using $w = a$ without changing the rest of the parameter map, would change the comparison.

Written transfer practice. These questions ask for derivations and explanations; they add no entries to the numerical submissions above.

1. At fixed $w > 0$, choose $M_\epsilon = \lfloor c/(\epsilon w) \rfloor$. Derive $R_1(c)$ from the finite sum and $R_5(c)$ from the exact degree growth. Compare the errors for $c = 2$ and $c = 8$, then explain how M_ϵ should change when w is doubled. Identify which step fails for a fixed cutoff.

2. Starting from $(a\partial_a - 2)\widetilde{\mathcal{F}} = 2u + C(L)$, separate the particular constant solution, the quadratic homogeneous solution and the inverse-power terms. Explain which choices affect a_D, which affect τ, and why a common factor must be fixed before

comparing either instanton coefficient. Derive the two ratios in (XI.7.78) without setting a to a number before differentiation.

Further written transfer practice.

1. Derive the shifted coefficient formula for $[x_f^n y_f^m] f_3$ directly from its three denominators. Compare it with (XI.7.100) at $(n, m) = (0, 0), (1, 0), (0, 1)$ and explain why the finite differences disappear from the leading cone density. At fixed $d_2 > 0$, find the leading behavior of R as $d_1 \to 0$ and identify the weak-expansion hypothesis that is lost.

2. Reconstruct (XI.7.121) from the two infinity expansions and the electric inverse without using the topological-string coefficient. Explain which step imports special geometry and which fixes a coordinate convention. If a geometric calculation used $Q_B = \beta^6 \widetilde{K}$, state the single scale relation needed to compare its coefficient with the curve, and distinguish that choice from an independent test of its dependence on E.

3. Differentiate $R(a, b, -a - b)$ before evaluating it at a nonzero electric input with three distinct eigenvalues. Determine how the Hessian transforms under a constant change from (E_1, E_2) to simple-root electric coordinates. Then take the heavy-root limit with $q_3 = 9A^2 q_2$ and explain why keeping q_3 fixed would remove the retained instanton correction.

Status and sources

§XI.7.1. Projection, cover bidegree and phase in (XI.7.2)–(XI.7.6) are [MATH]. The base phase measures instanton charge [GEO-E] with the brane-action normalization and base-period convention used above. See (Katz et al. 1997, hep-th/9609239v2, Eqs. (2.1), (3.1)); the trace there is schematic and the curvature source is separated. Isolation remains [DEC].

§XI.7.2. The sine expansion (XI.7.9) is [WS-T] in the stated domain of the topological string expansion; see (Gopakumar and Vafa 1998, hep-th/9812127v1, Eqs. (3.1)–(3.3)). The divisor expansion, base-zero normalization and curvature (XI.7.24) are [MATH] given the sine kernel and (Iqbal and Kashani-Poor 2003a, hep-th/0212279v4, Eqs. (31), (39)–(46), Sec. 5.4). The rigid normalization is [GEO-E], using the Kähler-period normalization and weak period slope, with the classical polynomial and coupling subtraction fixed separately.

§XI.7.3. The imported product (XI.7.27) is [WS-T]; its size-two evaluation and both subtractions are [MATH]. See (Iqbal and Kashani-Poor 2003a, Eqs. (27), (35)–(39), (47)–(48)). The signed sine coefficients agree with (Katz et al. 1997, Sec. 5, Table 1). Iqbal and Kashani-Poor's (50) gives the sine sign at base one; the product and the display preceding (61) give the positive continued sign, related by (XI.7.12). Covers start at one per (40)–(41), despite (58).

§XI.7.4. The flat trajectory and masses use the complexified Kähler periods and local engineering in the weak period frame. Compare (Katz et al. 1997, Sec. 5, Eq. (5.2))

and (Iqbal and Kashani-Poor 2003a, Eq. (1), Sec. 5.2). The resummation, cover powers and limits through base order two are [MATH] conditional on the product and map.

§XI.7.6. The inversion and Wronskian are [MATH] in the weak period frame of Chapter 6, using (Seiberg and Witten 1994, hep-th/9407087v1, Eqs. (6.14)–(6.26)). The match of (XI.7.76) and (XI.7.55) is [BPS:1/2|holo] through order two, on the stated weak electric patch with the given background and subtraction. It leaves the full spectrum, global line lattice and finite-radius theory open.

§XI.7.7. The fixed-h coefficient and the finite trace example are [MATH]. See (Iqbal and Kashani-Poor 2003a, Secs. 5.2–5.4, Eqs. (66)–(69)). Their $q = e^{-\beta h}$ reverses the shift in (XI.7.79); transposing both diagrams interchanges the signs. The genus-one background interpretation is [WS-T] in the stated background for the topological amplitude. The right-spin trace uses (Gopakumar and Vafa 1998, Eq. (3.1)).

Additional mathematical consequences. The finite-sum, degree-growth and moving-cutoff calculations in §XI.7.5, including (XI.7.60)–(XI.7.64), are [MATH] consequences of the same rational functions on $w > 0$. The Euler-constant and relative-order calculations, and the further finite spin-inventory examples, use the same hypotheses as their parent sections. They introduce no new physical premise or extension beyond base order two.

§XI.7.8. The A_2-fibration engineering dictionary is [GEO-E], with isolation [DEC], from (Katz et al. 1997, Sec. 6.1, Eqs. (6.1)–(6.5)). The normalized product (XI.7.92) is the imported [WS-T] input of (Iqbal and Kashani-Poor 2003b, hep-th/0306032v2, Eqs. (37), (49)–(56), Appendix, Fig. 16); its fiber resummation uses the source's assumption (52). The single-box evaluation through (XI.7.96) is [MATH], matching its (58). Only base order one is used.

§XI.7.9. The second fibration uses (Iqbal and Kashani-Poor 2003b, Eq. (60)). The finite coefficients, cone density, exact scaled pole and invariant form (XI.7.106) are [MATH]. The common physical prepotential unit is [GEO-E], fixed by the sourced positive-root one-loop expression (Katz et al. 1997, Eq. (6.2)) and the finite third derivative (XI.7.109); its raw unsubtracted polylogarithm has no finite limit. The flat scale K_{geo} is not identified with an algebraic mirror coefficient.

§XI.7.10. The primitive curve, differential and cycle frame are those of Chapter 6; compare (D'Hoker et al. 1996a, hep-th/9609041v1, Eqs. (2.2)–(2.7)). The electric residue and invariant inversion are [MATH]. The special-geometry RG identity is imported from (D'Hoker et al. 1996b, Eqs. (3.1)–(3.10)). Its infinity specialization and Euler reconstruction are [MATH] under the stated dimensional and formal-expansion hypotheses, agreeing with (D'Hoker et al. 1996a, Eq. (4.33b), Sec. V(b)) in its unredefined curve scale. The comparison is [BPS:1/2|holo] only at order one and conditional on (XI.7.122). That scalar scale choice is not independent evidence for a flat-coordinate threshold; the functional Coulomb dependence is calculated on both sides.

§XI.7.11. The Hessian, direct magnetic-response comparison and protected heavy-root limit are [MATH] in the same primitive period frame. The magnetic quadrature uses the holomorphic Jacobians of Chapter 6 independently of the RG identity and worldsheet coefficients. The heavy curve and the conversion to the original cubic frame also use Chapter 6. The spectator sector, environmental isolation and absolute ultraviolet

threshold are not determined by these comparisons. Any all-orders or finite-scale identity remains outside these comparisons.

References

D'Hoker, E., I. M. Krichever, and D. H. Phong (1996a). *The Effective Prepotential of N=2 Supersymmetric SU(Nc) Gauge Theories*. Version 1. arXiv: hep-th/9609041.

D'Hoker, E., I. M. Krichever, and D. H. Phong (1996b). *The Renormalization Group Equation in N=2 Supersymmetric Gauge Theories*. arXiv: hep-th/9610156.

Gopakumar, R. and C. Vafa (1998). *M-Theory and Topological Strings–II*. DOI: 10.48550/arXiv.hep-th/9812127. arXiv: hep-th/9812127 [hep-th].

Iqbal, A. and A.-K. Kashani-Poor (2003a). "Instanton Counting and Chern–Simons Theory". In: *Adv. Theor. Math. Phys.* 7.3, pp. 457–497. DOI: 10.4310/ATMP.2003.v7.n3.a4. arXiv: hep-th/0212279.

Iqbal, A. and A.-K. Kashani-Poor (2003b). *SU(N) Geometries and Topological String Amplitudes*. Version 2. arXiv: hep-th/0306032.

Katz, S. H., A. Klemm, and C. Vafa (1997). "Geometric engineering of quantum field theories". In: *Nucl. Phys. B* 497, pp. 173–195. DOI: 10.1016/S0550-3213(97)00282-4. arXiv: hep-th/9609239.

Seiberg, N. and E. Witten (1994). "Electric-magnetic duality, monopole condensation, and confinement in N=2 supersymmetric Yang-Mills theory". In: *Nucl. Phys. B* 426. [Erratum: Nucl.Phys.B 430, 485–486 (1994)], pp. 19–52. DOI: 10.1016/0550-3213(94)90124-4. arXiv: hep-th/9407087.

Chapter XI.8

Atlas of local IIA gauge engineering

XI.8.1 What belongs in a construction record?

Suppose we are given a pure four-dimensional gauge algebra and asked to recover the curves whose wrapped branes produce its particles. There can be several answers. Even when two compact surfaces give the same light gauge sector, the curves we call the section and the fiber need not have the same intersections. Conversely, two fibrations with the same transverse ADE type can give different matter. We need to know what was held fixed when we kept the light particles and discarded other modes.

We will assemble a construction record from the calculations of the preceding chapters. The input is a marked geometry, including the compact cycles, the fibration, and the background periods. The limit specifies the physical masses and couplings we keep and which other sectors can be omitted. The output gives the local gauge algebra, matter, and a quantitative test in a stated frame. The gauge algebra and any absolute gauge or line data occupy separate fields. If only the former is determined, the latter stays open.

The comparison to keep in mind is local F_0 versus local F_2. We will build both records from their section and fiber, then calculate which term of the first instanton contribution survives. This example shows how to ask two distinct questions: whether two realizations have a common local gauge description, and whether a specified observable agrees in matched coordinates. We will use the same separation of input, limit and output when comparing matter and thresholds.

The reader should be able to use a record in both directions. Starting from geometry, one follows the curve periods to masses, fixes the backgrounds, and takes the stated limit. Starting from a desired light sector, one asks which rows actually contain the required matter and which quantitative comparison has been performed. We will practice this by changing one input at a time. This avoids confusing a new value of a parameter with a new choice of what that parameter means.

XI.8.2 Two marked geometries for a pure gauge sector

What compact information must we retain to compare two realizations of a pure rank-one sector? For $X_n = \mathrm{Tot}(K_{F_n})$, the compact surface is F_n. Mark its effective section S and ruling fiber F. The fiber is the vanishing sphere of the split A_1 construction; the section measures the base. Two distinct fibers do not meet, and a section meets each fiber once. The normal degree of the marked section supplies the last entry in the intersection form,

$$I_n = \begin{pmatrix} S^2 & S\cdot F \\ S\cdot F & F^2 \end{pmatrix} = \begin{pmatrix} -n & 1 \\ 1 & 0 \end{pmatrix}. \tag{XI.8.1}$$

These are intersections within the compact surface. The periods we will compare are $A_s = J\cdot S$ and $A_f = J\cdot F$, with J the Kähler class restricted to the surface. The period over F fixes the coefficient of S in J. The period over S then fixes the coefficient of F:

$$J = A_f S + (A_s + nA_f)F, \tag{XI.8.2}$$

$$\frac{1}{2}J^2 = A_s A_f + \frac{n}{2}A_f^2. \tag{XI.8.3}$$

At the same values of the two marked periods, the second term is absent on F_0 and present on F_2. The integral lattice alone would miss the distinction. In the F_0 lattice the change from (S, F) to $(S - F, F)$ gives

$$\begin{pmatrix} 1 & -1 \\ 0 & 1 \end{pmatrix} I_0 \begin{pmatrix} 1 & 0 \\ -1 & 1 \end{pmatrix} = I_2. \tag{XI.8.4}$$

The class $S - F$ is not the marked effective section on F_0. For example, its area in the old marked periods is $A_s - A_f$, not A_s. Thus the congruence is an isometry of abstract forms, not an identification of the effective curve data.

A numerical area comparison makes the marking visible. Choose a common area unit $A_* > 0$, and set $A_s = 3A_*$, $A_f = A_*$. The two surface volumes are

$$\frac{\mathrm{Vol}(F_0)}{A_*^2} = 3, \qquad \frac{\mathrm{Vol}(F_2)}{A_*^2} = 4. \tag{XI.8.5}$$

The units matter here. These volumes have dimension length to the fourth power, whereas the periods have dimension length squared. Their unequal values do not obstruct the later gauge-sector comparison, which uses a scaling trajectory. They say that equal marked periods do not make the compact surfaces identical.

One can instead rewrite the same F_0 Kähler class in the basis $\widetilde{S} = S - F$, $\widetilde{F} = F$. Its periods become $\widetilde{A}_s = A_s - A_f$, $\widetilde{A}_f = A_f$. The volume is unchanged when periods and basis are transformed together:

$$\widetilde{A}_s\widetilde{A}_f + \widetilde{A}_f^2 = (A_s - A_f)A_f + A_f^2 = A_s A_f. \tag{XI.8.6}$$

For the numerical choice this gives $2 + 1 = 3$, rather than 4. The comparison therefore has two distinct operations. Rewriting a single geometry changes the coordinate values

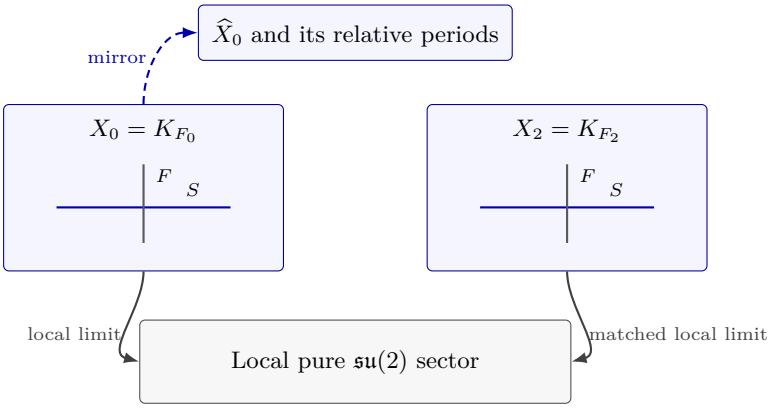


Figure XI.8.1: The two local Hirzebruch geometries are marked by their effective section S and fiber F, shown as crossing curves. The dashed arrow selects the worked mirror of X_0. The solid arrows take local limits with the light scales matched. The common light sector does not identify the two marked surfaces or supply a period comparison for X_2.

assigned to a fixed Kähler class. Comparing F_0 and F_2 at common marked period values compares different geometric inputs. A row must say which operation is intended before its volume can be used.

To follow the solid arrows in Fig. XI.8.1, one must match physical scales, not just set A_f to zero. In the F_0 frame take zero fiber B period. The wrapped D2 tension gives $M_W = A_f/((2\pi)^2 g_s \alpha'^{3/2})$. In units with $M_s = 1/\sqrt{\alpha'}$, define the dimensionless complex action $T_C = (\int_C J - i\int_C B)/(2\pi\alpha')$, the fugacity $Q_C = e^{-T_C}$, and the length $\epsilon = 2\pi g_s/M_s$. The retained pure gauge trajectory is

$$T_f = \epsilon M_W, \qquad \epsilon \longrightarrow 0, \tag{XI.8.7}$$

$$Q_b = C_b e^{i\theta} (\epsilon\Lambda)^4. \tag{XI.8.8}$$

Here M_W and the weak matching scale Λ are held finite as M_s grows at fixed g_s; C_b is a finite positive matching factor. Both sides of each action relation are dimensionless. The base carries the phase once. Its leading logarithmic growth is compatible with the pure vector coefficient. The matching of the bare base action to the gauge scale is a premise across the base KK threshold, not a use of four-dimensional running up to the string scale. For F_2 we compare the same scaling class after matching the base and fiber coordinates and the phase.

A controlled base metric gives a separate check. If the base radius squared is of order $\alpha' \operatorname{Re} T_b$, then

$$M_{\mathrm{KK},b} \sim \frac{M_s}{\sqrt{\operatorname{Re} T_b}} \sim \frac{M_s}{\sqrt{\log(M_s/M_0)}} \longrightarrow \infty, \tag{XI.8.9}$$

where M_0 is a fixed reference mass and order-one geometric factors have been suppressed. This uses the base metric, not a radius estimate for the sub-stringy fiber. The wrapped D2 mass uses the ordinary protected continuation to the shrinking fiber.

The calculation of a base gap does not constrain an unrelated bulk radius. To see the distinction, compare independent scales at fixed g_s and positive dimensionless compact volume v_6:

$$M_{\mathrm{Pl},4}^2 \;\propto\; \frac{v_6 M_s^2}{g_s^2} \;\longrightarrow\; \infty, \qquad M_{\mathrm{KK,bulk}} \sim R_{\mathrm{bulk}}^{-1} \quad \text{if } R_{\mathrm{bulk}} \text{ is fixed.} \tag{XI.8.10}$$

This is a comparison of scale estimates, not an example of a compact family realizing both simultaneously. An unwanted finite-mass mode would still matter if it coupled to the local sector. To claim the local theory, we require divergent gaps or vanishing couplings for such modes. With the ordinary split A_1 dictionary, the matched trajectory and sufficient isolation, the two geometries describe the same local pure $\mathfrak{su}(2)$ sector. The next step is to compare something more precise than that algebra.

XI.8.3 Matching one instanton coefficient

Which part of the first instanton term survives the limit? At base degree one there is no positive-base multicover subtraction. Write $q = Q_f$ for the flat fiber fugacity and let m be the fiber degree. The two explicit genus-zero sequences have the terms

$$d_{1,m}^{(0)} = -2(m+1), \qquad d_{1,m}^{(2)} = -2m, \qquad m \geq 1. \tag{XI.8.11}$$

A term with $m = 0$ drops out of the calculation below. These inputs are from the two marked degree conventions of the comparison. We need no general shift rule relating higher degrees.

Since $q = e^{-T_f}$, differentiating with respect to T_f acts as $-D = -q\,d/dq$. The second derivative therefore weights the m-th term by m^2 in the same conversion on each side. Apply D to the geometric series. For $0 < q < 1$,

$$\sum_{m\geq 1} q^m = \frac{q}{1-q}, \tag{XI.8.12}$$

$$D^2 \frac{q}{1-q} = \frac{q(1+q)}{(1-q)^3}, \tag{XI.8.13}$$

$$D^3 \frac{q}{1-q} = \frac{q(1+4q+q^2)}{(1-q)^4}. \tag{XI.8.14}$$

The extra constant in $d_{1,m}^{(0)}$ adds a term proportional to the second sum. Therefore the two weighted functions are

$$W_0(q) = -\frac{4q(1+2q)}{(1-q)^4}, \tag{XI.8.15}$$

$$W_2(q) = -\frac{2q(1+4q+q^2)}{(1-q)^4}. \tag{XI.8.16}$$

Setting $q = 1$ in the two numerators gives the same fourth-order coefficient. But the difference retains the extra m^2 sum:

$$W_0(q) - W_2(q) = -\frac{2q(1+q)}{(1-q)^3}. \tag{XI.8.17}$$

The coefficient of the difference is negative in the distance $1-q$, the positive coordinate on this approach to the limit.

Let the two trajectories have the same matching factor, phase and finite scales in Eqs. (XI.8.7) and (XI.8.8). Since $1-q = 1-e^{-T_f} \sim \epsilon M_W$, the leading terms and their difference scale as

$$Q_b W_n(q) \longrightarrow C_b e^{i\theta} \left(\frac{\Lambda}{M_W}\right)^4 \lim_{q\to 1^-} (1-q)^4 W_n(q), \tag{XI.8.18}$$

$$Q_b(W_0 - W_2) = O(\epsilon) \quad \text{at fixed } M_W, \Lambda. \tag{XI.8.19}$$

This explains why the two finite functions differ even though their leading terms agree after the limit. The sum over fiber degrees must be performed before taking this limit. With finitely many terms the sum would stay finite as $q \to 1$, and multiplication by Q_b would send it to zero.

We can also determine the first size of the discrepancy without introducing another geometric model. Hold the matching factor and phase fixed and approach along the exact trajectory $q = e^{-\epsilon M_W}$. The leading Laurent coefficients give

$$W_n(e^{-\epsilon M_W}) = -\frac{12}{\epsilon^4 M_W^4} + O(\epsilon^{-3}), \tag{XI.8.20}$$

$$Q_b(W_0 - W_2) = -4C_b e^{i\theta} \epsilon \frac{\Lambda^4}{M_W^3} + O(\epsilon^2). \tag{XI.8.21}$$

The second equation is a finite-cutoff diagnostic in the stated coordinates. It does not provide the first correction to an arbitrary compact completion, whose omitted sectors have not been specified. It tells us why a numerical comparison at small nonzero ϵ should show a discrepancy even when the limiting coefficient agrees.

Now change the retained mass from M_W to $2M_W$, leaving Λ, C_b, and θ fixed in this comparison. The common surviving term and the leading difference respond differently:

$$\frac{[Q_b W_n]_{2M_W}}{[Q_b W_n]_{M_W}} \longrightarrow \frac{1}{16}, \qquad \frac{[Q_b(W_0 - W_2)]_{2M_W}}{[Q_b(W_0 - W_2)]_{M_W}} \longrightarrow \frac{1}{8}. \tag{XI.8.22}$$

The brackets mean evaluation on the respective trajectories; the second ratio compares their nonzero leading discrepancies before they vanish. This is a useful use of the atlas. A reader can test the predicted mass power of the selected observable while keeping its scale and phase matching explicit. Merely comparing two numbers without their retained mass would miss this dependence.

To see the truncation problem directly, keep a finite largest fiber degree $m_{\max}$ independent of ϵ. The same operation gives

$$\lim_{\epsilon\to 0} \epsilon^4 \sum_{m=1}^{m_{\max}} m^2 d_{1,m}^{(n)} e^{-m\epsilon M_W} = 0, \qquad \lim_{\epsilon\to 0} \epsilon^4 W_n(e^{-\epsilon M_W}) = -\frac{12}{M_W^4}. \tag{XI.8.23}$$

The fiber degrees that grow as $1/(\epsilon M_W)$ contribute to the resummed pole. A finite list of enumerative coefficients therefore cannot replace the exact rational function for this

limit. This is a failure of interchanging the sum and limit, within the fixed base-degree calculation already at hand.

We have matched one specified observable in a common scale and phase. The common local gauge description of the previous section uses the ordinary physical construction and sufficient isolation in addition to this result. Nor does this computation compare all instanton orders. To record more than the leading term we need, among other things, a common period frame.

XI.8.4 The mirror record and its particle frame

What makes a curve calculation part of the record? We need the mirror, the scale limit, and the cycles that give the gauge periods. The dashed arrow in Fig. XI.8.1 denotes the worked mirror of X_0. It changes the description of the geometry. The local limit is a different operation.

The selected mirror $\widehat{X}_0$ is a conic bundle over the algebraic torus with multiplicative coordinates z, w. Use the chart and scaling

$$UV = G(z,w) = K - w - w^{-1} - C(z + z^{-1}), \tag{XI.8.24}$$

$$K = 2 + \epsilon^2 u, \qquad C = \tfrac{1}{2}\epsilon^2 L, \qquad L = \Lambda_{\mathrm{SW}}^2. \tag{XI.8.25}$$

Here u is the scaled Coulomb coordinate and L has the same mass dimension two. The torus variable z is not the flat fiber fugacity q of the previous section. At nonzero C, a critical point on the discriminant has $G = 0$ and

$$z\partial_z G = -C(z - z^{-1}) = 0, \qquad w\partial_w G = -(w - w^{-1}) = 0. \tag{XI.8.26}$$

Thus z, w each take the values ± 1. Substituting them in $G = 0$ gives $K = 2w + 2Cz$. For $w = +1$ the constant term matches that in Eq. (XI.8.25), and the finite critical values are $u = \pm L$. For $w = -1$ the mismatch in the constant term sends u to infinity. The scaled record therefore keeps two of the four torus critical values.

The compact curve by itself does not fix the period units. Let A', B' be the primitive compact cycles of the curve in their given order with $A' \cdot B' = +1$. A relative boundary with compact projection $rA' + sB'$ can also contain puncture loops. In the three-loop basis of the worked mirror, write their coefficients as p_+, p_-, p_∞. The two torus windings are

$$r + p_+ + p_- - p_\infty = 0, \qquad p_+ - p_- + p_\infty = 0. \tag{XI.8.27}$$

The equations impose that the boundary be trivial in the two ambient winding directions. Adding them yields $r = -2p_+$, with s unrestricted. The compact projection is therefore generated by $2A'$ and B', with the first lifted, for example, by $p_+ = p_- = -1, p_\infty = 0$. The projection matrix and its pairing in this order are

$$P = \begin{pmatrix} 2 & 0 \\ 0 & 1 \end{pmatrix}, \qquad P^{\mathsf{T}} \begin{pmatrix} 0 & 1 \\ -1 & 0 \end{pmatrix} P = \begin{pmatrix} 0 & 2 \\ -2 & 0 \end{pmatrix}. \tag{XI.8.28}$$

The determinant gives the index of the projected particle lattice. The record specifies the signed particle frame (a_D, a) and its based loops, with $M_+ M_- = M_\infty$. These are

local relative charges. They do not select the genuine line operators of an absolute theory.

For a concrete comparison, take the electric projection to be $\gamma_e = 2A'$ and the magnetic projection to be $\gamma_m = B'$. Then

$$\gamma_e \cdot \gamma_m = 2, \qquad [H_1(\overline{\Sigma}, \mathbb{Z}) : \langle \gamma_e, \gamma_m \rangle] = 2, \tag{XI.8.29}$$

where $\overline{\Sigma}$ denotes the compact curve. A proposed comparison using $\widetilde{\gamma}_e = A'$ would give pairing one. It is not a unimodular change of the same projected particle basis. If its period were nevertheless used as the electric unit at fixed magnetic period, the resulting quantities would satisfy

$$\widetilde{a} = \tfrac{1}{2} a, \qquad \widetilde{\tau} = \frac{\partial_u a_D}{\partial_u \widetilde{a}} = 2\tau. \tag{XI.8.30}$$

This locates a possible factor of two before any instanton coefficient is compared. It would change a physical normalization, even though the unmarked algebraic curve and its two critical values were unchanged. A matched mirror identifier alone is therefore insufficient. The comparison needs the cycle lift, ordering, normalization and continuation paths that turn that curve into the periods in the record.

A comparison of prepotentials also requires a normalization. On the positive electric patch $u > L > 0$, write the leading physical W scale as $w_{\mathrm{mass}} = \sqrt{2}a$. To see how the normalization is fixed before any instanton comparison, take the pure-fiber term $-2\,\mathrm{Li}_3(e^{-\epsilon\sqrt{2}a})$ in the sine convention. Its rescaled second derivative is

$$\partial_a^2 \left[-2\epsilon^{-2}\,\mathrm{Li}_3(e^{-\epsilon\sqrt{2}a}) \right] = 4\log(1 - e^{-\epsilon\sqrt{2}a}). \tag{XI.8.31}$$

The coefficient of $\log a$ is 4. In the signed period frame the weak derivative ratio has slope $2i/\pi$ in $\log a$. Their comparison fixes the conversion $i/(2\pi)$ from the rescaled sine amplitude to the period prepotential.

Let $P_b = L^2/4$ be the fixed coefficient of ϵ^4 in the matched flat ratio Q_b/Q_f. The connected positive-base amplitudes, resummed in the fiber and then taken to the limit, give the two terms

$$-\frac{2P_b}{w_{\mathrm{mass}}^2} - \frac{5P_b^2}{w_{\mathrm{mass}}^6}. \tag{XI.8.32}$$

The logarithm removes the disconnected terms. Its finite-scale degree-two coefficient still contains the double cover of a base-degree-one term. Subtract that cover to read the primitive coefficient. It belongs in the connected amplitude, but its contribution at this order is suppressed in the limit. With the fixed conversion and $w_{\mathrm{mass}} = \sqrt{2}a$, Eq. (XI.8.32) gives the genus-zero answer in the signed frame,

$$\frac{\pi}{i}\,\mathcal{F}_{\mathrm{inst}} = -\frac{L^2}{8a^2} - \frac{5L^4}{256a^6} \quad \text{through base degree two.} \tag{XI.8.33}$$

We can check these signs without the worldsheet sum. Use the independent inversion of the electric period through the same order:

$$u = \tfrac{1}{2}a^2 + \frac{L^2}{4a^2} + \frac{5L^4}{64a^6} + O(L^6/a^{10}). \tag{XI.8.34}$$

With $a_D = \partial_a \mathcal{F}$, the chain rule gives the first equality below. The independent signed-period calculation fixes the Wronskian on the right to $2i/\pi$. Integration then gives the second line.

$$\partial_u(a a_D - 2\mathcal{F}) = a\,\partial_u a_D - a_D\,\partial_u a = \frac{2i}{\pi}, \tag{XI.8.35}$$

$$(a\partial_a - 2)\mathcal{F} = \frac{2i}{\pi}u + \text{constant}. \tag{XI.8.36}$$

At positive base degree k, the operator on the left multiplies $L^{2k}a^{2-4k}$ by $-4k$. Inserting the two positive-base coefficients of u reproduces Eq. (XI.8.33). The relation between the two positive-base coefficients also offers a quick internal check on a proposed normalization. If $c_k L^{2k}a^{2-4k}$ is a term in $(\pi/i)\mathcal{F}$, its contribution to the period inversion is

$$[u]_{L^{2k}a^{2-4k}} = -2kc_k, \qquad -2\Big(-\frac{1}{8}\Big) = \frac{1}{4}, \qquad -4\Big(-\frac{5}{256}\Big) = \frac{5}{64}. \tag{XI.8.37}$$

Here square brackets denote the numerical coefficient of the indicated monomial. The factor $-2k$ follows from the Euler operator and the fixed Wronskian; it is not an adjustable sign for each order. This check uses an independently normalized period inversion as input. It does not extend the worldsheet calculation beyond the two displayed base orders.

The genus-one coefficient tabulated below is a separate protected background coupling. It is neither part of this rigid genus-zero prepotential nor a count of all particles.

This is the amount of information recorded for the F_0 mirror. A mirror chart for F_2 exists in the literature, but the comparison here does not work out its normalized relative periods. The agreement of the leading weighted poles gives no replacement for that calculation.

XI.8.5 Matter, thresholds and parameter roles

A transverse root diagram fixes neither the number of four-dimensional adjoint hypers nor the roles of their parameters. In a split A_2 fibration over a compact curve Σ_g, use the prescribed twist and trivial adjoint local system. The vector mode is counted by $H^0(\Sigma_g, \mathcal{O})$; the adjoint hyper modes by $H^0(\Sigma_g, K_{\Sigma_g})$. Connectedness and Riemann–Roch give

$$h^0(\mathcal{O}) = 1, \qquad h^0(K_{\Sigma_g}) = h^0(\mathcal{O}) + g - 1 = g. \tag{XI.8.38}$$

Thus the rational example has no adjoint hyper. The flat elliptic product with periodic spinors and trivial gauge and R holonomies has one massless adjoint hyper in four-dimensional $\mathcal{N} = 2$ language and preserves sixteen supercharges. In fundamental index units an adjoint hyper contributes $2N$, so

$$b_0 = 2N(1 - g) \tag{XI.8.39}$$

for the vector and adjoint sector in these examples, with $N = 3$ for A_2. The zeros and matter counts depend on the mode problem, not just on the transverse diagram. In particular a general elliptic fibration need not share the product holonomies or kernel.

A different change adds a localized fundamental. In the selected ordinary split A_2-to-A_3 example, a simple enhancement gives one full fundamental hyper in the local dictionary. We can compute its signed periods from the three wall periods. Write $a_1 = \lambda_1 - \lambda_2$ and $a_2 = \lambda_2 - \lambda_3$ for the root periods, and c for the third signed wall period. The tracelessness of the Coulomb eigenvalues gives

$$\lambda_3 = -\tfrac{1}{3}(a_1 + 2a_2), \tag{XI.8.40}$$

$$(\lambda_1, \lambda_2, \lambda_3) = (\lambda_3 + a_1 + a_2,\ \lambda_3 + a_2,\ \lambda_3). \tag{XI.8.41}$$

Because $c = \lambda_3 + m$ in the fixed flavor lift, the mass parameter and the weight periods are

$$m = c + \tfrac{1}{3}(a_1 + 2a_2), \tag{XI.8.42}$$

$$(\lambda_i + m)_{i=1}^{3} = (c + a_1 + a_2,\ c + a_2,\ c). \tag{XI.8.43}$$

The signed sums on the right are the suffix sums of the wall periods. The three entries are the components of one hyper. Changing the Coulomb periods at fixed m changes c. Therefore fixing the third wall period is not the same boundary condition as fixing the flavor mass. The magnitude for a physical threshold is taken only after forming a signed weight period.

In the worked matter record the two root periods are $a_1 = a_2 = 3$ and the third wall period is $c = 2$. The eigenvalues are then evenly spaced about zero. The lowest is minus the common root period, so the fixed mass is the third wall period plus that spacing. Add one and two spacings to the third wall period to obtain the higher two signed weights. This recovers the mass and periods in the table.

Explicitly, that row gives

$$(\lambda_1, \lambda_2, \lambda_3) = (3, 0, -3), \qquad m = 5, \qquad (\lambda_i + m) = (8, 5, 2). \tag{XI.8.44}$$

Use it to compare two possible changes of input. Increase a_1 from 3 to 6, hold $a_2 = 3$, and first keep the flavor mass fixed at 5. Tracelessness now requires

$$(\lambda_1, \lambda_2, \lambda_3) = (5, -1, -4), \qquad c = 1, \qquad (\lambda_i + m) = (10, 4, 1). \tag{XI.8.45}$$

The third wall period changes because it contains the lowest Coulomb eigenvalue. If we instead keep $c = 2$ under the same change of root period, we obtain

$$m = 6, \qquad (\lambda_i + m) = (11, 5, 2). \tag{XI.8.46}$$

These are two paths through the parameter space, with different flavor backgrounds. Both have the same new root periods. The record's mass field tells us which path is relevant to a comparison at fixed flavor source. The full hyper count remains one on these paths within the stated local description; its three weights have changed, not its multiplicity.

Take $M = |m|$ large compared with the Coulomb splittings, so the three components give one leading heavy threshold. In the weak region take both the high and low descriptions in the same leading real matching scheme. Above M the full fundamental

is active; below M it drops out. In the positive asymptotically free convention $b_0 = 2N - N_f$, match the inverse couplings at M:

$$(b_{\rm hi}, b_{\rm lo}) = (2N-1, 2N) \quad (N=3), \tag{XI.8.47}$$

$$b_{\rm hi} \log \frac{M}{\Lambda_{\rm hi}} = b_{\rm lo} \log \frac{M}{\Lambda_{\rm lo}}, \tag{XI.8.48}$$

$$\Lambda_{\rm lo}^{b_{\rm lo}} = M^{b_{\rm lo}-b_{\rm hi}} \Lambda_{\rm hi}^{b_{\rm hi}}. \tag{XI.8.49}$$

The powers give the same mass dimension on both sides. This is a relation between two energy windows. It does not identify the two geometries or the exact complex scales.

For the selected $N = 3$ threshold the relation can be written as a dimensionless response to the heavy mass:

$$\frac{\Lambda_{\rm lo}}{\Lambda_{\rm hi}} = \left(\frac{M}{\Lambda_{\rm hi}}\right)^{1/6}, \qquad \frac{\Lambda_{\rm lo}(2M)}{\Lambda_{\rm lo}(M)} = 2^{1/6} \quad (\Lambda_{\rm hi} \text{ fixed}). \tag{XI.8.50}$$

The two evaluations must both remain in the overlap region where the mass is much larger than the Coulomb splittings and the matching is weak. This comparison changes an energy threshold. It does not require a change of the compact intersection matrix. The mass field and the energy-window field are the relevant entries to consult.

For a product sector, the dimensions of the representations matter as well as the number of edges. Label the two fundamental dimensions n_1, n_2 and the end fundamental counts f_1, f_2. The open two-node strip of Fig. XI.8.2 has one full bifundamental between the compact gauge nodes and fixed flavor sectors at the noncompact ends.

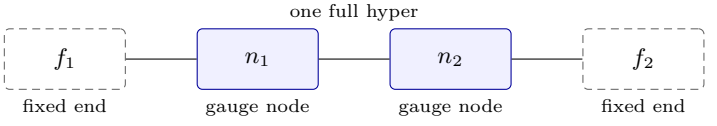


Figure XI.8.2: Matter of the selected open strip. The solid boxes are gauge nodes with fundamental dimensions n_1, n_2. The dashed boxes give the numbers f_1, f_2 of full fundamentals supported by the fixed flavor ends. The central edge is one full bifundamental. Its index at either gauge node is multiplied by the dimension at the other node.

Take a trace with two generators at node i on the bifundamental. The other tensor factor gives the trace of the identity, namely n_j. Hence

$$T_i(\mathbf{n}_i \otimes \overline{\mathbf{n}}_j) = n_j T_i(\mathbf{n}_i), \tag{XI.8.51}$$

$$b_i = 2n_i - f_i - n_j, \qquad j \neq i. \tag{XI.8.52}$$

With $n_1 = n_2 = 2$, two full fundamentals per end give zero at both nodes. If the second gauge factor has $n_2 = 3$ instead, keeping the same end matter no longer cancels the coefficients. Instead one solves $f_i = 2n_i - n_j$ separately at each node. This accounts for the neighboring-rank comparison in the atlas.

The ordered values make the change easy to diagnose:

$$(n_1, n_2; f_1, f_2) = (2, 2; 2, 2): \quad (b_1, b_2) = (4 - 2 - 2, 4 - 2 - 2) = (0, 0), \tag{XI.8.53}$$

$$(n_1, n_2; f_1, f_2) = (2, 3; 1, 4): \quad (b_1, b_2) = (4 - 1 - 3, 6 - 4 - 2) = (0, 0), \tag{XI.8.54}$$

$$(n_1, n_2; f_1, f_2) = (2, 3; 2, 2): \quad (b_1, b_2) = (-1, 2). \tag{XI.8.55}$$

Increasing the right rank increases its vector contribution and the matter contribution seen at the left node. Thus both end counts must be reconsidered, even though only one rank changed. An edge count alone cannot perform this comparison. A vanishing one-loop coefficient is an arithmetic check; the exact marginal couplings of the massless two-A_1 theory are a separate field-theory input.

The two-A_1 period chart distinguishes the dynamical and fixed parameters. Denote the internal fibers by F_i and their compact section lifts by B_i. The combinations $K_i = B_i - F_i$ have zero compact gauge-divisor pairings in the chosen frame. They can be held fixed as bare coupling coordinates while the Coulomb periods vary. The five fixed mass directions are the two left masses, the bridge mass, and the two right masses. The puncture count gives a separate check of the number of parameters; it supplies no equality between a puncture coordinate and an exact toric coupling.

Finally send the second bare fugacity to zero while keeping the second eigenvalues $\pm a_2$ finite as background values. For a fixed weight x of the first node, the bifundamental contributes the two factors

$$(x + m + a_2)(x + m - a_2), \tag{XI.8.56}$$

where m is the bridge mass in this example. The frozen node supplies two induced fundamentals to the retained node. The neighborhood subfan has one compact gauge divisor, and the surviving interacting sector has four full fundamentals. With sufficient isolation this is the stated local limit. Free fields can remain outside that interacting sector; the fan calculation does not assert that all omitted states become heavy.

The frozen row in the output panel uses $m = 4$, $a_2 = 3/2$. At fixed m, increasing the finite frozen eigenvalue to $5/2$ changes the two induced signed masses to

$$(m - a_2, m + a_2): \quad \left(\frac{5}{2}, \frac{11}{2}\right) \longmapsto \left(\frac{3}{2}, \frac{13}{2}\right). \tag{XI.8.57}$$

Their sum remains $2m = 8$, while their separation $2a_2$ increases. Both are finite background masses. Together with the two original end fundamentals they still give the same four-flavor count above all these thresholds:

$$b_{\text{retained}} = 2 \cdot 2 - (2 + 2) = 0. \tag{XI.8.58}$$

Sending a mass to infinity would require a different threshold comparison and scale matching. Freezing a coupling at finite eigenvalues has not performed that operation. This is why the frozen row keeps its induced masses in the parameter field as well as its surviving gauge node in the algebra field.

XI.8.6 Read the atlas

Start with the gauge sector of interest and follow its row back to the geometric input. The first row is the unfibered six-dimensional $(1,1)$ gauge EFT, so the four-dimensional running column does not apply to it. All the four-dimensional coefficients refer to the stated light matter and energy window. A zero in that column is a one-loop statement.

To select a row, first choose the observable and the regime in which you want to use it. For example, a pure rank-one weak coupling directs us to the Hirzebruch records. A fundamental threshold directs us to the simple A_2-enhancement record and its rational-base comparison. A background obtained by freezing a neighboring gauge node directs us to the strip pair. These choices use different operations on the input. The index below places them together so that the operation can be read before its output is compared.

Read an individual row from geometry through limit to output. Then check the unresolved field before exporting the conclusion to another row. The six-dimensional ALE row illustrates the need for this order. Its compact intersection and kinetic Gram are valid input for the higher-dimensional gauge EFT. They are not a four-dimensional beta function, and the missing beta entry has no numerical value to compare with the zeros in the four-dimensional rows.

Geometry	Retained algebra and one-loop coefficient
Ordinary A2 ALE	Ordinary su(3) gauge EFT at enhancement, with (1,1) supersymmetry.
Local F0	Local pure su(2) with eight supercharges under the ordinary wrapped-D2 continuation and limit. $b = 4$
Local F2	The source identifies the same local pure su(2) gauge limit under the stated matching. $b = 4$
Split A2 over a rational base	Pure local su(3) under the specified twist and trivial adjoint local system. $b = 6$
A2 times an elliptic curve	Local su(3); the product under the stated assumptions preserves sixteen supercharges. $b = 0$
Split A2 with one A3 enhancement	Local su(3) with the rational-base twist and a fixed flavor background. $b = 5$
Two gauged A1 nodes	Local su(2) plus su(2); in the separate field theory the massless Lagrangian has sourced exact marginal couplings. $b = \big(0, 0\big)$
One active node after freezing its neighbor	Local su(2) acting at the retained interacting node. $b = 0$
A1 and A2 neighboring gauge nodes	The selected neighboring gauge algebra is su(2) plus su(3) conditional on the ordinary local matter and twist dictionaries. $b = \big(0, 0\big)$

XI.8.7 The two Hirzebruch records

For the two Hirzebruch geometries, read the full record before looking at the matched pole. The fiber and base entries specify which parameters vary and which remain fixed. *Conditional* marks a result that needs the adjacent physical hypotheses. *Open* means that the stated result has not been established for that field. An explicit source chart can therefore coexist with an open period field. The abbreviation KKV refers to Katz, Klemm and Vafa.

Local F0	Input or assumption
Geometry and dimension	*Computed.* Total space of the canonical line bundle over the product of two projective lines; complex threefold with a four-dimensional target.
Compact curves and divisors	*Computed.* Base section S and fiber F on the compact zero section F_0.
Fibration	*Computed.* Split A1 over the rational base. The fiber is the transverse root curve.
Background periods	*Conditional.* Set B_f=0 in the W-mass calculation; retain the base theta phase once in Q_b. Use a chosen zero-flux local lift.
Limit and isolation	*Conditional.* Keep the W mass and strong scale finite in the matched fiber and base trajectory. Sufficient isolation, controlled base metric and cross-threshold matching remain premises.
Gauge algebra	*Sourced.* Local pure su(2) with eight supercharges under the ordinary wrapped-D2 continuation and limit.
Absolute gauge and line data	*Open.* Global gauge form, boundary polarization and genuine line lattice are not selected by these local data.
Matter	*Sourced.* No charged hypermultiplets in this pure gauge sector.
Parameters and their roles	*Conditional.* One Coulomb mass scale from the fiber; the base sets the leading bare coupling and theta. The signed period normalization uses a separate matching to the geometric W unit.
Four-dimensional beta	*Conditional.* Pure vector count in the stated four-dimensional running convention. $b = 4$
Mirror or period frame	*Sourced.* Affine chart $UV = G$ and protected identification with the signed cubic periods. *Computed.* The finite scaled critical values are $u = \pm L$; the compact projection has index 2. See §XI.8.4.
Remaining physical limits	*Open.* No proof of a suitable compact embedding or full bulk gap, all-instanton convergence or full BPS spectrum.

Local F2	Input or assumption
Geometry and dimension	*Computed.* Total space of the canonical line bundle over the second Hirzebruch surface; complex threefold with a four-dimensional target.
Compact curves and divisors	*Computed.* Negative section S and ruling fiber F on the compact zero section F_2.
Fibration	*Computed.* Split A1 over the rational base, in the stated ruled-surface phase.
Background periods	*Conditional.* Compare zero fiber B-field and a fixed base phase after matching the source-to-house coupling coordinates.
Limit and isolation	*Conditional.* Compare the same pure rank-one scaling class after a suitable base/fiber coordinate choice and scale matching; impose ordinary protected continuation and decoupling assumptions.
Gauge algebra	*Sourced.* The source identifies the same local pure su(2) gauge limit under the stated matching.
Absolute gauge and line data	*Open.* Global gauge form, boundary polarization and genuine line lattice are not selected by these local data.
Matter	*Sourced.* No charged hypers in this sourced pure local sector.
Parameters and their roles	*Conditional.* Fiber controls the W scale and base action controls the bare scale in the compared limit. No finite-geometry bare-to-effective map is computed.
Four-dimensional beta	*Conditional.* Pure vector count. $b = 4$
Mirror or period frame	*Open.* KKV gives a mirror chart in (5.4)–(5.5); no normalized periods, relative lattice or comparison map to F0 are replayed here.
Remaining physical limits	*Open.* Finite geometry differs; the broad printed fiber-degree shift is not used, and higher-base equality has not been checked for F2 here.

The selected outputs below record the marked surface volumes, the weighted pole, and the protected information that was worked out for F_0. The volume uses the periods A_s, A_f of Eq. (XI.8.3). The signs of the prepotential coefficients use the convention of Eq. (XI.8.33). The Laurent polynomial on the right of the mirror equation uses torus variables, whereas the weighted generating function in the F_2 panel uses z for the flat fugacity denoted by q in the derivation.

To use the two panels, first compare the marked curve field. It tells us why the same symbols A_s, A_f enter different volume polynomials. Next compare the retained-scale field. It identifies the common mass, weak scale and phase needed in Eq. (XI.8.18). Only then compare the weighted poles. The result is the finite observable retained by that particular limiting operation.

The mirror field answers a further question. For F_0 it points to a chart, a compact

projection and a signed-period normalization, so its finite-order prepotential coefficients can be read in that frame. For F_2, a source chart is available but the normalized comparison has not been carried out here. An open entry tells the reader exactly where to resume a calculation. Copying the F_0 coefficients into it would replace a missing period calculation by an assumption.

Local F0	Selected outputs
Section/fiber intersection	$\begin{pmatrix} 0 & 1 \\ 1 & 0 \end{pmatrix}$
Coefficient of the fourth-order weighted pole	-12
Compact boundary projection index	2
Signed prepotential coefficients at base orders one and two	$\left(-\frac{1}{8}, -\frac{5}{256}\right)$
Continued connected genus-one coefficient at base degree two (base weight stripped)	$8/w_{\mathrm{mass}}^8$, with $w_{\mathrm{mass}} = \sqrt{2}a$ on the weak positive patch. The torus coordinate w is dimensionless.
Volume in the marked section and fiber period coordinates	$A_f A_s$
Right side of the affine mirror equation UV = G	$-\frac{L\epsilon^2 z}{2} - \frac{L\epsilon^2}{2z} + \epsilon^2 u - w + 2 - \frac{1}{w}$
Fiber action at zero B-field	$M_W \epsilon$
Base fugacity divided by the finite matching factor and theta phase	$\Lambda^4 \epsilon^4$

Local F2	Selected outputs
Section/fiber intersection	$\begin{pmatrix} -2 & 1 \\ 1 & 0 \end{pmatrix}$
Coefficient of the fourth-order weighted pole	-12
Weighted degree-one generating function	$-\frac{2z\left(z^2+4z+1\right)}{(z-1)^4}$
Volume in the marked section and fiber period coordinates	$A_f\,(A_f + A_s)$

XI.8.8 Four ways to compare records

The comparison panels answer different questions. The first retains one leading coefficient and records the finite difference. The second records the sourced common gauge sector under the matched local limit. The threshold relation instead changes the active matter as the observation scale crosses a fixed mass. The scale control tests an inference about decoupling; it is not a second geometric construction.

A useful comparison therefore begins with a sentence of the form "we hold these backgrounds fixed, take this limit, and compare this quantity." For the first panel, the quantity is the leading weighted base-degree-one coupling contribution in the common flat frame. For the second, the conclusion is the local pure gauge sector under the ordinary construction and isolation hypotheses. The first panel's arithmetic can test a consequence of that sector assignment, but it does not supply the physical dictionary used by the second panel.

For the third panel, the observation energy passes through a fixed heavy threshold. One compares the running coupling above and below that energy, in one matching scheme. For the fourth panel, the purpose is to test whether a scale estimate is sufficient. A fixed bulk radius has a finite inverse-radius gap even when a Planck-mass estimate grows. It identifies a missing isolation argument without constructing an alternative compact model. Matching, changing an energy window and testing an implication are different uses of the same record format.

Matched observable	*Computed.* One leading fiber-weighted degree-one coupling term in matched scale and phase. Their unscaled rational functions differ; the source-supported pure local gauge-sector comparison is separate from the calculation.
Difference of weighted series $W_0 - W_2$	$-\dfrac{2q(1+q)}{(1-q)^3}$, with $q = Q_f$ the flat fiber fugacity.
Order of the difference pole	3
Coefficient of $(1-q)^{-3}$ in $W_0 - W_2$	-4

Same local gauge sector	*Sourced.* KKV identifies the ordinary pure rank-one gauge sector after scale and phase matching in the local limit. The compact effective section and finite marked geometry differ. This makes no statement about absolute gauge or line data or all-order equality.
Pure-vector one-loop coefficient for each geometry	$(4, 4)$

Threshold relation	*Conditional.* Common real weak one-loop matching scheme, |m| much greater than Coulomb splittings, above the strong scale. No geometric limit or absolute scale equality follows.
One-loop coefficients above and below	$(5, 6)$
Matching powers of threshold, high scale and low scale	$(1, 5, 6)$

Scale control	*Computed.* Fixed bulk radius and fixed positive dimensionless compact volume at fixed g_s are an independent-scale control, not an example of a constructed compact family.
Power of the string scale in the bulk KK mass	0
Power of the string scale in the Planck mass squared	2

XI.8.9 Other local sectors

For the other rows, the following quantitative fingerprints identify the calculation to reproduce. In the ALE entry the negative compact intersection I pairs the exceptional spheres. The positive kinetic Gram $-I^{-1}$ pairs the normalizable forms dual to their unit periods. The two matrices refer to different bases and uses. For the fibrations the ordered counts refer to vector multiplets, adjoint hypers and Weyl species per adjoint, respectively. In the split fundamental entry the last charge column is the relative flavor unit. The strip vertex pairs are lattice coordinates; the end fundamental counts are multiplicities. The two-node puncture kernel dimension refers to the separate description at fixed double poles. The complete record of defining rays, cone and relation data, periods, and remaining assumptions is supplied with the atlas.

The genus pair is a useful first comparison in this panel. Keep the transverse A_2 diagram and the stated trivial local system, then change from the rational base to the flat elliptic product with its specified holonomies. The adjoint-hyper count changes from zero to one, and its contribution cancels the vector coefficient. The zero follows from that matter count; reading only the unchanged diagram would miss the cancellation. Altering the holonomies would require solving the mode problem again rather than retaining the same row.

The two strip entries teach a different comparison. The compact-divisor vertices identify which gauge nodes remain dynamical; the induced masses identify which former Coulomb values have become background parameters. The separate puncture-kernel dimension is a check on the number of couplings in the two-node setting. Equal parameter counts can guide a proposed map, but a map also has to identify the periods

and their boundary conditions. The panel intentionally supplies the count without assigning a puncture coordinate to an exact toric coupling.

Ordinary A2 ALE	Selected outputs
Compact curve intersection	$\begin{pmatrix} -2 & 1 \\ 1 & -2 \end{pmatrix}$
Unit-period kinetic form	$\begin{pmatrix} \frac{2}{3} & \frac{1}{3} \\ \frac{1}{3} & \frac{2}{3} \end{pmatrix}$
Signed roots	6
Leading g6 squared divided by alpha prime	$16\pi^3$

Split A2 over a rational base	Selected outputs
Ordered wall normal degrees	$\begin{pmatrix} -2 & 0 \\ -4 & 2 \\ -6 & 4 \end{pmatrix}$
Vector, adjoint hyper, Weyl species counts per adjoint	$\big(1, 0, 2\big)$

A2 times an elliptic curve	Selected outputs
Vector, adjoint hyper, Weyl species counts per adjoint	$\big(1, 1, 4\big)$

Split A2 with one A3 enhancement	Selected outputs
Fundamental weights with primitive flavor charge	$\begin{pmatrix} 1 & 0 & 1 \\ -1 & 1 & 1 \\ 0 & -1 & 1 \end{pmatrix}$
Worked background mass	5
Worked signed central charges	$\big(8, 5, 2\big)$
Mass as a combination of signed periods	$\frac{a_1}{3} + \frac{2a_2}{3} + c$

Two gauged A1 nodes	Selected outputs
Column heights	$\begin{pmatrix}2,2,2,2\end{pmatrix}$
Bridge weights	$\begin{pmatrix}-1 & -1\\ -1 & 1\\ 1 & -1\\ 1 & 1\end{pmatrix}$
Coulomb, mass, coupling counts	$\begin{pmatrix}2,5,2\end{pmatrix}$
Fixed double-pole kernel dimension	2

One active node after freezing its neighbor	Selected outputs
Retained subfan column heights	$\begin{pmatrix}2,2,2\end{pmatrix}$
Retained compact divisor vertices	$\begin{pmatrix}1 & 1\end{pmatrix}$
Two induced masses	$\left(\frac{5}{2},\frac{11}{2}\right)$ for $m=4,\ a_2=3/2$, ordered as $m-a_2,\ m+a_2$; see Eq. (XI.8.56).

A1 and A2 neighboring gauge nodes	Selected outputs
Column heights	$\begin{pmatrix}1,2,3,4\end{pmatrix}$
Compact gauge divisor vertices	$\begin{pmatrix}1 & 1\\ 2 & 1\\ 2 & 2\end{pmatrix}$
Full fundamental counts	$\begin{pmatrix}1,4\end{pmatrix}$
Counterfactual beta with two fundamentals at each end	$\begin{pmatrix}-1,2\end{pmatrix}$

XI.8.10 Choose a higher-rank calculation

Suppose the required observable is a photon response rather than a one-loop flavor count. We must keep the independent Coulomb coordinates and differentiate before substituting their values. A rank-two sector has a matrix of responses, while a product of ranks one and two has three photon coordinates. The two beta coefficients of a product theory do not replace that three-by-three matrix. The following guide selects the calculations developed in Chapters XI.4–7. The algebra names specify local sectors; they do not add absolute gauge or line data.

For the pure rank-two row, $q=s^2$ is a curve parameter of mass dimension six, distinct from the earlier dimensionless fiber fugacity $q=Q_f$. Write $(t_1,t_2)=(u,v)$, and

let E_i and b_i^{mag}, $i = 1, 2$, be the electric and magnetic periods. The period Jacobians are $J_{ij} = \partial E_i/\partial t_j|_q$ and $D_{ij} = \partial b_i^{\mathrm{mag}}/\partial t_j|_q$. Where J is invertible, their response is $\tau = DJ^{-1}$.

Question and chapter	Input, computed response and scope
One fundamental threshold, XI.4	Two Coulomb coordinates and one fixed flavor mass in the split $\mathfrak{su}(3)$ construction. The full hyper gives a weak-electric 2×2 Hessian, a single-light-component limit and a common-heavy threshold. This is a perturbative matter contribution.
Coupled photons, XI.5	The balanced $\mathfrak{su}(2) \oplus \mathfrak{su}(3)$ strip, with one full bridge and the stated end matter. Its 3×3 weak response keeps finite mixing. Heavy bridge removal and freezing the right node at finite background eigenvalues are different limits.
Pure rank-two periods, XI.6	The explicit A_2 fibration, local six-monomial mirror and genus-two curve. Two electric and two magnetic periods give $\tau = DJ^{-1}$, with the exact curve discriminant and a protected heavy-root reduction in the declared frame.
One-base protected term, XI.7	The actual one-box product resummed in two fiber variables, compared with independently reconstructed pure rank-two periods. The output is one instanton order and its two-coordinate response, conditional on one scalar instanton-scale match.

Table XI.8.1: Select the observable before selecting a comparison. Weak matter determinants, a full curve response and a single protected instanton coefficient answer different questions. Each entry retains the physical engineering and isolation conditions of its chapter.

For the product example, vanishing common-scale running coexists with finite off-diagonal Coulomb response. To test independence of the photons, use the finite Hessian, including its coordinate transformation. Its rational gradients in simple-root coordinates are not a replacement for the integral compact-divisor charges. To remove the bridge, follow the heavy-mass scale matching of Chapter XI.5. To keep a flavor source, freeze the neighboring coupling while retaining its finite eigenvalues. The latter operation preserves finite induced masses and a response to background parameters; it has not integrated out those flavors.

For a pure rank-two protected comparison, start with the period frame of Chapter XI.6. In its normalization the curve and differential are

$$y^2 = P(x)^2 - q, \qquad P(x) = x^3 - ux - v, \qquad \lambda = \frac{xP'(x)}{2\pi i y}\, dx. \tag{XI.8.59}$$

The electric root-charge projection has index three in the specified compact basis. This index belongs to the root-charge sublattice, not to the primitive eigenvalue-period coordinates. It is not obtained by applying the rank-one index-two replacement of §XI.8.4. The ordered cycle integrals, their Jacobian and their magnetic partners determine the response.

Chapter XI.7 uses exact electric eigenvalue periods E_i, with $\sum_i E_i = 0$. Let $K_{\rm geo}$ be the geometric instanton-scale coefficient, also of mass dimension six. The leading protected function and the two coefficients are

$$R(E) = \sum_{i=1}^{3} \frac{1}{\prod_{j\neq i}(E_i - E_j)^2}, \qquad \mathcal{F}_{\rm geo,1} = \frac{K_{\rm geo}}{2\pi i} R(E), \qquad \mathcal{F}_{\rm curve,1} = \frac{q}{8\pi i} R(E). \tag{XI.8.60}$$

The periods must be distinct on this weak patch. Their electric Vandermonde denominator is not the exact quantum discriminant of the curve. Choosing $q = 4K_{\rm geo}$ makes the two scalar coefficients agree. This is one chosen scale match using the calculated coefficient, so the resulting scalar equality is not an independent normalization test. The dependence on both Coulomb periods, direct magnetic-response checks and the heavy-root reduction give distinct comparisons. No exact flat-coordinate or ultraviolet threshold identification follows.

The original panels retain their declared inputs and finite scope. Table XI.8.1 points to the additional complete calculations; it does not fill an open field in an earlier record by analogy or change the numerical Hirzebruch comparisons.

XI.8.11 Where a record stops

When a proposed row is missing information, first ask which inference needs it. The local gauge algebra does not fix boundary conditions for line charges. The equality of a protected coefficient does not fix a common period frame. The scaling of the Planck mass does not decide whether a coupled bulk mode survives. A stronger statement would require, respectively, absolute charge and boundary data, a matched relative period calculation, or a gap or coupling argument for the unwanted modes. This is why those fields are kept visible in the record.

Three directions remain for further reading. Other Hirzebruch geometries would need a separately worked phase and scale matching. Outer twists and coincident enhancements need a compact fibration and a determination of the light charged modes. Further unworked ranks, alternative chambers and compact completions require explicit geometry and boundary, period and scale data. These are reading leads; they do not supply the inputs and reproduced outputs needed for new rows.

Take-home message of this chapter

Start with a marked geometry and specify the retained scales and fixed backgrounds. State exactly which observable agrees and in which frame. This lets the reader reproduce the match and see which further comparisons still require data.

Exercises

For E1–E4, give exact values in the indicated order. Use `benchmark/tasks.json` to find the question IDs and `benchmark/PROTOCOL.md` for submission. Include the requested

explanations and the reasoning for E5.

E1. Recover a flavor mass. In the signed A_2 wall-period frame take $a_1 = 1$, $a_2 = 3$, and $c = -1$. This is a signed period exercise, without a claim about the stability of effective curves outside the original chamber. Compute the ordered traceless eigenvalues $(\lambda_1, \lambda_2, \lambda_3)$, the fixed flavor mass m, and the ordered signed periods $\lambda_i + m$. Explain why taking an absolute value before forming the sum would change a physical threshold. Submit `eigenvalues`, `mass`, and `signed_periods`.

E2. Compare an equal residue with unequal functions. Start from the two explicit degree-one sequences and apply the two fiber derivatives in the flat coordinate q. Give the two fourth-order pole coefficients in the order F_0, F_2, then give the order and coefficient of the difference $W_0 - W_2$ in the distance $1 - q$. Explain what survives multiplication by the common matched Q_b. Submit `leading`, `difference_order`, and `difference_coefficient`.

E3. Match a heavy threshold. Use the common leading real scheme with threshold $M = 8$ and $\Lambda_{\mathrm{hi}} = 1/4$ in the same mass units. Assume the Coulomb splittings are small relative to M. Give the two one-loop coefficients in the order above, below, and calculate the dimensionless ratio $\Lambda_{\mathrm{lo}}^{b_{\mathrm{lo}}}/\Lambda_{\mathrm{hi}}^{b_{\mathrm{lo}}}$. Check the mass dimensions in the matching equation. Submit `beta_above_below` and `scale_power_ratio`.

E4. Change the neighboring rank. Use the strip with gauge fundamental dimensions $(2, 3)$. Find the two full end fundamental counts that cancel the one-loop coefficients and check their beta vector. Then test the alternative of two fundamentals per end. Give all pairs in left-to-right order and explain the neighbor dimension in the bifundamental contribution. Submit `fundamentals`, `matched_beta`, and `two_each_beta`.

E5. Reject an insufficient record. A proposed F_0/F_2 record gives a pure gauge algebra, a matched fourth-order pole coefficient and a divergent Planck mass. It concludes that the normalized mirror periods and the absolute line spectra agree. It gives neither a coupled bulk KK gap nor a vanishing coupling argument. State what the pole calculation permits, use an independent fixed radius to test the bulk claim, and say what additional information would make a mirror or line comparison possible.

Written transfer practice. These questions use the same records with changed inputs and have no numerical submission contract.

1. At $A_s = 4A_*$, $A_f = 2A_*$, compare the two marked surface volumes. Then transform the F_0 basis to $(S - F, F)$ and carry its periods along. Explain why the transformed volume is still that of the original F_0 Kähler class.

2. In the matter example increase a_2 from 3 to 6 at fixed $a_1 = 3$ and $m = 5$. Find the new third wall period and signed weights. Compare with the path keeping $c = 2$ fixed. State which background changed on the latter path.

3. Keep the frozen-node bridge mass at $m = 4$ and set $a_2 = 2$. Identify the two induced masses, the interacting node, and an energy window in which all four fundamentals are active. Explain which part of the record would have to change before one could integrate out an induced flavor.

Status and sources

The source notes below describe the table entries. The conventions are those of XI.1–7.

Ordinary ALE input. The compact pairing and unit-period Gram are MATH in the stated complete ALE setting. Douglas and Moore, §§2.1–2.3, give the closed-string modes Douglas and Moore 1996; the ALE normalizable-cohomology locator is Hausel, Hunsicker and Mazzeo, Theorem 1 and §7.1.1 Hausel et al. 2004. The ordinary gauge enhancement uses the unfrozen ALE construction GEO-X, with the root-cycle application in S. Katz, Morrison, et al. 1996, §2.1. The leading RR coefficient uses the SUGRA normalization of XI.1 and Polchinski 1995, Eqs. (10), (12)–(15). The little-string scale trajectory uses the separate input of Giveon and Kutasov 1999, §1.

Marked surfaces and local limits. Equations (XI.8.1)–(XI.8.4) and the pole arithmetic (XI.8.11)–(XI.8.19) are MATH in the stated frames, using S. H. Katz et al. 1997, §§4.1, 4.3 and §5, printed p. 14. The common local gauge description is GEO-E, with the matched limit in S. H. Katz et al. 1997, §§2, 4.3 and 5–5.2. The exact bare scale matching and sufficient local isolation remain premises of the trajectory; the latter is DEC. Equation (XI.8.10) is a scale control.

Relative mirror and fixed instanton orders. The explicit critical points, compact projection, monodromies and coefficient arithmetic are MATH. The local mirror dictionary and the selected background coupling are GEO-E. The protected pure-gauge mirror input is Aganagic et al. 2002, §§2, 6.2 and S. H. Katz et al. 1997, §§4.2–4.3, 5.2; §5.1 of the latter gives the separate F_2 chart. The relative period comparison uses Seiberg and Witten 1994a, §§5–6. Equations (XI.8.31)–(XI.8.36) use the finite-order product and signed period match of XI.7, with Iqbal and Kashani-Poor 2003a, §§4–5.2 and Gopakumar and Vafa 1998, §§2–3. No absolute line lattice follows.

Using and changing records. The marked-period examples (XI.8.5)–(XI.8.6) are MATH. The same status applies to the exact-function consequences (XI.8.20)–(XI.8.23). The frame checks (XI.8.29)–(XI.8.30) and (XI.8.37) are MATH consequences of the preceding signed-frame inputs. Equations (XI.8.44)–(XI.8.46), (XI.8.50), and (XI.8.53)–(XI.8.58) are MATH parameter and one-loop comparisons within those same inputs and their energy windows. They supply no new geometric family, period identification or physical dictionary.

Higher-rank selection guide. Table XI.8.1 reuses the scoped calculations of XI.4–7. The weak full-hyper response is QFT-E, with its Hessian arithmetic MATH, using D'Hoker et al. 1997, Eq. (2.1) and the bounded product-theory input of Ennes

et al. 1999, Eq. (23). The pure rank-two geometric identification remains GEO-E, with isolation separate as DEC. Equation (XI.8.59), its cycles and response reuse S. H. Katz et al. 1997, §6.1 and Klemm et al. 1996, §§4.1–4.2. Equation (XI.8.60) recalls the MATH base-one calculation under the sourced product and resummation input Iqbal and Kashani-Poor 2003b, Eqs. (49)–(60), and the separately sourced residue-RG identity D'Hoker et al. 1996, §III. The single scalar scale match is a condition of comparison, not independent absolute normalization evidence. No original table status or absolute charge boundary is promoted.

Twists and matter. The mode counts, charge and mass arithmetic, threshold powers, and strip indices are MATH under their declared inputs. The four-dimensional matter identifications are GEO-E, with isolation kept separate. The twist uses S. Katz, Morrison, et al. 1996, §§2.1–2.3; the localized matter and compact chamber use S. Katz and Vafa 1997, §§2–4.1 and S. H. Katz et al. 1997, §§6.1–6.2. The threshold method is compared with Seiberg and Witten 1994b, §12.2. The strip and its spectator limit use S. Katz, Mayr, et al. 1997, §§2, 5.2, 6. The separate massless two-node field theory and puncture count use Gaiotto 2009, §§2.1–2.2.

References

Aganagic, M., A. Klemm, and C. Vafa (2002). "Disk instantons, mirror symmetry and the duality web". In: *Z. Naturforsch. A* 57, pp. 1–28. DOI: 10.1515/zna-2002-1-201. arXiv: hep-th/0105045.

D'Hoker, E., I. M. Krichever, and D. H. Phong (1997). "The Effective Prepotential of N=2 Supersymmetric SU(Nc) Gauge Theories". In: *Nucl. Phys. B* 489, pp. 179–210. DOI: 10.1016/S0550-3213(97)00035-7. arXiv: hep-th/9609041.

D'Hoker, E., I. M. Krichever, and D. H. Phong (1996). *The Renormalization Group Equation in N=2 Supersymmetric Gauge Theories*. arXiv: hep-th/9610156.

Douglas, M. R. and G. W. Moore (1996). "D-branes, quivers, and ALE instantons". In: arXiv preprint; not published in a journal. arXiv: hep-th/9603167.

Ennes, I. P. et al. (1999). "One-instanton predictions of Seiberg–Witten curves for product groups". In: *Phys. Lett. B* 452, pp. 260–264. DOI: 10.1016/S0370-2693(99)00301-9. arXiv: hep-th/9901124.

Gaiotto, D. (2009). "N=2 Dualities". In: arXiv: 0904.2715 [hep-th].

Giveon, A. and D. Kutasov (1999). "Little string theory in a double scaling limit". In: *JHEP* 10, p. 034. DOI: 10.1088/1126-6708/1999/10/034. arXiv: hep-th/9909110.

Gopakumar, R. and C. Vafa (1998). *M-Theory and Topological Strings–II*. DOI: 10.48550/arXiv.hep-th/9812127. arXiv: hep-th/9812127 [hep-th].

Hausel, T., E. Hunsicker, and R. Mazzeo (2004). "Hodge cohomology of gravitational instantons". In: *Duke Math. J.* 122.3, pp. 485–548. DOI: 10.1215/S0012-7094-04-12233-X. arXiv: math/0207169.

Iqbal, A. and A.-K. Kashani-Poor (2003a). "Instanton Counting and Chern–Simons Theory". In: *Adv. Theor. Math. Phys.* 7.3, pp. 457–497. DOI: 10.4310/ATMP.2003.v7.n3.a4. arXiv: hep-th/0212279.

Iqbal, A. and A.-K. Kashani-Poor (2003b). *SU(N) Geometries and Topological String Amplitudes*. Version 2. arXiv: hep-th/0306032.

Katz, S., P. Mayr, and C. Vafa (1997). "Mirror Symmetry and Exact Solution of 4D N=2 Gauge Theories I". In: *Adv. Theor. Math. Phys.* 1, pp. 53–114. DOI: 10.4310/ATMP.1997.v1.n1.a2. arXiv: hep-th/9706110.

Katz, S., D. R. Morrison, and M. R. Plesser (1996). "Enhanced gauge symmetry in Type II string theory". In: *Nucl. Phys. B* 477, pp. 105–140. DOI: 10.1016/0550-3213(96)00331-8. arXiv: hep-th/9601108.

Katz, S. and C. Vafa (1997). "Matter from geometry". In: *Nucl. Phys. B* 497, pp. 146–154. DOI: 10.1016/S0550-3213(97)00280-0. arXiv: hep-th/9606086.

Katz, S. H., A. Klemm, and C. Vafa (1997). "Geometric engineering of quantum field theories". In: *Nucl. Phys. B* 497, pp. 173–195. DOI: 10.1016/S0550-3213(97)00282-4. arXiv: hep-th/9609239.

Klemm, A., W. Lerche, and S. Theisen (1996). "Nonperturbative effective actions of N=2 supersymmetric gauge theories". In: *Int. J. Mod. Phys. A* 11, pp. 1929–1974. DOI: 10.1142/S0217751X96001000. arXiv: hep-th/9505150.

Polchinski, J. (1995). "Dirichlet branes and Ramond–Ramond charges". In: *Phys. Rev. Lett.* 75, pp. 4724–4727. DOI: 10.1103/PhysRevLett.75.4724. arXiv: hep-th/9510017.

Seiberg, N. and E. Witten (1994a). "Electric-magnetic duality, monopole condensation, and confinement in N=2 supersymmetric Yang-Mills theory". In: *Nucl. Phys. B* 426. [Erratum: Nucl.Phys.B 430, 485–486 (1994)], pp. 19–52. DOI: 10.1016/0550-3213(94)90124-4. arXiv: hep-th/9407087.

Seiberg, N. and E. Witten (1994b). "Monopoles, duality and chiral symmetry breaking in N=2 supersymmetric QCD". In: *Nucl. Phys. B* 431, pp. 484–550. DOI: 10.1016/0550-3213(94)90214-3. arXiv: hep-th/9408099.